TECHNICKÁ UNIVERZITA V LIBERCI

FAKULTA TEXTILNÍ

Soft Computing and Computer Vision for the Characterization and Evaluation of Fibrous Structures

HABILITAČNÍ PRÁCE

Souhrn uveřejněných vědeckých a odborných prací doplněný komentářem

Ing. Mohamed Eldessouki, PhD

Department of Materials Engineering

Květen 2015

Abstract

The evaluation of fibrous structures under certain operation parameters allows the understanding of the relations between the behavior of these structures and the controlled conditions. Ultimately, this provides an opportunity to control the material's performance by adjusting its processing conditions. This work presents a collection of research articles that focus on the evaluation of one-dimensional (yarns) and two-dimensional (fabrics) fibrous structures. At the first level, studying the yarn geometry and the internal structure was presented in two papers that considered the ring-spun as well as the air-jet spun yarns as main scope of study. One paper covers the calculation of the yarn diameter and its variation through experimental and analytical methods with a comparison to the available laboratory methods. The percentage of fibers and their radial distribution in the yarn's cross-section were evaluated in the other paper with case studies of cellulosic fibers that have different cross-sections.

Fabrics, as two-dimensional fibrous structures, were investigated at their production stage, as well as at their end-use stage. The quality of fabrics is mainly determined during their production, and the inspection of the fabric for faults is an essential process in any weaving mill. The automation of the fabric fault detection process is a challenging research topic and a development of a machine prototype that performs this task as well as the development of the analytical algorithms were presented in the current work. The algorithms of analysis were enhanced and presented in another research article that describes the implementation of the principle component analysis (PCA) for boosting the performance of the fault classification algorithm.

As fabrics are used and subjected to different forms of strains (especially of abrasion and friction) their wear performance becomes crucial, and the evaluation of the fabric pilling emerges as an important test that needs to be more characterized objectively. This was the main goal of the selected two papers on the objective evaluation of the pilling resistance in knitted and woven fabrics, as two production technologies that affect the fabric's surface properties. The evaluation algorithms were introduced in the form of an integrated system that built upon the best literature practices at the four stages of pilling evaluation. The high correlation between the objective evaluations obtained from the developed "smart" system and the subjective evaluations obtained from experts, suggests a promising technique for standardization.

It might be "unfortunate fact" that; textile industry has many parameters that are characterized *subjectively* based on *human operators*. Therefore, the main tools implemented in this collection of research articles for evaluating the fibrous structures were the image analysis (IA), the computer vision (CV), and the soft-computing (SC). These tools provide contemporary solutions for automating the tasks performed by human workers without sacrificing the "human intellect";

that is mimicked in these algorithms in the form of "artificial intelligence". Computer vision, with the aid of the soft-computing techniques, is capable of *perceiving* the fibrous materials and *reconstructing* them in a digital form that can be *segmented* and *understood* automatically which significantly facilitates the evaluation of these fibrous structures.

Although research in computer vision and soft-computing in the textile industry began long time ago, there are many reasons for these fields to be currently attractive for researchers. To name some of these reasons we should refer to: the diversity of problems in textiles, the recent advances in computational methods and algorithms, as well as the developments in hardware that expanded the computation power. Therefore, the significance of the algorithms presented in this work arises from the fact that these algorithms aim at *improving*, *simplifying*, *automating*, and *reducing* the time required for the current evaluation methods. This will, ultimately, result in revealing some properties of the fibrous structures that are not clearly understood because of their tedious and laborious measuring methods. To give one example for this point; this work presented a methodology for digitizing fibrous materials in three-dimensional models using the x-ray computed tomography (CT) without interfering with the structure by chemicals as it is traditionally done. It is encouraging to implement the automated characterization techniques developed in this work to help in studying the internal structure of the yarn with their *massive amount* of data that can be obtained from these CT yarn digital models.

Given the *limited amount* of data that we have nowadays on yarns (due to the limitations of the current laborious methods), the reader can imagine the major change that might occur in our current state of understanding for yarn structures by automating these methods with objective characterization. Having said that, the work presented here allows only a few steps in the direction of solving some of the textile related problems and there is, still, a plenty of room for further development.

Acknowledgment

I thank Allah, the Almighty God, for His guidance and the path He has led me on. Allah's words in the Quran were inspiring and encouraging for me to continuously seek knowledge.

This work is devoted to my family (especially my parents) and my little family (especially my lovely kids; Gehad, Omar, and Nada). On the professional level, I would like to thank those whose ideas and results were the topics of investigation in this work (the space is not be enough for them here, but their names appear in the citation inside this work). This work might not be possible without the collaboration and the support I received from many people around me. Although I could not name all of them, I would like to specially thank: Prof. Sayed Ibrahim for his continuous support and constructive discussions. Prof. Jiří Militky for his openness and his continuous willing to help in any matter. Prof. Bohuslav Neckář for the detailed discussions and setting the example of how scientific work should go. I would like also to thank the faculty, the staff, and the students at the Technical University of Liberec, Czech Republic; namely the members of the Department of Materials Engineering and the Department of Textile Technology. Thanks must be extended also to the faculty, the staff, and the students at the Department of Textile Engineering, Mansoura University, Egypt. Finally, I appreciate the role of everybody who contributed with any sort of help at any time, especially Dr. Adnan Mazari who offered the help within my tight time in preparing this work. Special thanks for the financial support I receive from the ESF operational program "Education for Competitiveness" in the Czech Republic in the framework of the project "Support of engineering of excellent research and development teams at the Technical University of Liberec".

Table of Contents

Abstract … i

Acknowledgment iii

Table of contents v

Table of figures viii

Part I Theory

Chapter 1: Thesis Orientation and Introduction 1

1.1. Introduction 3

1.2. The problem statement 4

1.3. The goal 4

1.4. The objectives 4

1.5. Scope of the study 5

1.5.1. Materials 5

1.5.2. Technologies 5

1.5.3. Computation methods 5

1.6. Thesis format and organization 5

Chapter 2: Computer Vision & Image Analysis 9

2.1. Introduction 11

2.2. Object digitization technologies 11

2.2.1. Sensing elements within the visible range 11

2.2.2. X-ray sensing elements 15

2.3. Digital image representation 18

2.4. Image understanding 22

2.5. Closing remarks on CV challenges 26

References 28

Chapter 3: Soft Computing 29

3.1. Introduction 31

3.2. Artificial Neural Networks (ANN) 32

3.2.1. Neuron model 33

3.2.2. Network structures 35

3.2.3. Back-propagation learning 37

3.2.4. Closing remarks on ANN 39

3.3. Modeling human judgment (fuzzy logic) 40

3.3.1. Crisp and fuzzy sets 40

3.3.2. Operations on Fuzzy Sets 42

3.3.3. Cotton grading 45

References 49

Part II Applications

Chapter 4: Chan-Vese Segmentation Model For Faster And Accurate Evaluation of Yarn Packing Density 51

Summary Sheet 53

The Paper 55

Snapshots of the paper as it appears in the journal 75

Chapter 5: A Dynamic and Robust Image Processing Based Method for Measuring The Yarn Diameter and Its Variation 79

Summary Sheet 81

The Paper 83

Snapshots of the paper as it appears in the journal 100

Chapter 6: An Automated Fabric Fault Detection and Classification System Based on Computer Vision and Soft Computing 105

Summary Sheet 107

The Paper ……..……. 109

Snapshots of the paper as it appears in the journal ...…….. 117

Chapter 7: The Application of Principal Component Analysis to Boost The Performance of The Automated Fabric Fault Detector And Classifier …… 121

Summary Sheet ……. 123

The Paper ……..……. 125

Snapshots of the paper as it appears in the journal ...…….. 143

Chapter 8: Integrated Computer Vision and Soft Computing System For Classifying The Pilling Resistance of Knitted Fabrics ………… 145

Summary Sheet ……. 147

The Paper ……..……. 149

Snapshots of the paper as it appears in the journal ...…….. 164

Chapter 9: Adaptive Neuro-Fuzzy System For Quantitative Evaluation of Woven Fabrics' Pilling Resistance ………… 167

Summary Sheet ……. 169

The Paper ……..……. 171

Snapshots of the paper as it appears in the journal ...…….. 200

Part III Closing

Chapter 10: Conclusion …...…… 205

Appendices

Appendix I: The author's list of publications

Table of Figures
(Part I ONLY)

Chapter 1

Figure 1. An overview of the author's main research interests and contributions (dotted circle highlights the topics that will be addressed in this work) 3

Figure 2. The application of computer vision and the computing & the soft computing algorithms in fibrous structures 6

Chapter 2

Figure 1. Arrangements of sensors for image acquisition: Single imaging sensor (top), Line sensor (middle), Array sensor (bottom) (Reproduced from Ref. [1]) 12

Figure 2. Fabric surface as digitized using an in-line arrangement of sensors in a flatbed scanner 13

Figure 3. An example of the digital image acquisition process with a 2D array of sensors 14

Figure 4. A high speed camera acquiring the images of yarn at 100 m/min 14

Figure 5. Schematic representation for the principle of CT scanning 16

Figure 6. Reconstructed digital model of the yarn (left) that allows its visualization with a higher magnification, as the dotted rectangle (middle), and with cross-sectional slicing (right) 18

Figure 7. Coordinate convention used in representing digital images (Reproduced from Ref. [1]) 19

Figure 8. 2D image of a woven fabric (top) with two different representations of the same image as expressed by the gray levels (bottom left) and the Fourier transformed image (bottom right) (Note; the main peak at the center of the FFT image was suppressed to present the other peaks) 21

Figure 9. Different image representation (shaded rectangles) suitable for image analysis problems in which objects have to be detected and classified (Reproduced from Ref. [5]) 22

Figure 10. Basic steps in image recognition and interpretation 23

Figure 11. Low and medium level processing of digital yarn image 24

Chapter 3

Figure 1. The parts of a nerve cell (or neuron). The length of the axon is usually about 100 times the diameter of the cell body (image reproduced from ref. [2]) 33

Figure 2. Simple computing unit (Node) 34

Figure 3. Three different activation (transfer) functions for neuron computational units... 35

Figure 4. Layered feed-forward network..... 36

Figure 5. Membership representation to the set X={1, 2, 3, 4, 5} (left), and the set Y=[1, 5] (right)..... 41

Figure 6. Membership function for the age-set of "young" people..... 42

Figure 7. Membership functions for the fuzzy sets A=[5, 8] (left) and B=4 (right) 43

Figure 8. The AND operator applied on the two fuzzy sets A and B..... 44

Figure 9. The OR operator applied on the two fuzzy sets A and B..... 44

Figure 10. . The NOT operator applied on the fuzzy set A..... 44

Figure 11. Crisp set–middle cotton grade (Reproduced from Ref. [3]) 46

Figure 12. Fuzzy set–middle cotton grade (Reproduced from Ref. [3]) 47

Figure 13. Fuzzy sets for cotton grade categories (Reproduced from Ref. [3])..... 48

PART I

Chapter 1

Thesis Orientation and Introduction

Thesis Orientation and Introduction

1.1. Introduction:

Over the past few years, the author of this work has been engaged in an intensive research with multi-disciplinary research groups and worked on different projects that covered: the applications of nanotechnology in developing efficient biological and chemical protective materials, enhancing the mechanical and interfacial properties of nanocomposites, developing biocomposite materials for tissue engineering applications, and the utilization of computational methods to solve problems related to the evaluation of fibrous structures. This offered a great chance for an experience in three main research fields that are shown in Figure 1 and cover the study of structure-and-properties of polymeric materials, their modeling and simulation, as well as some programming tools. These fields of research are intertwined in a way that the programming methods are used as ***tools*** for helping in the implementation of the simulation methods in ***understanding*** the ***performance*** of polymeric materials and their ***properties as connected to their structures***, which was applied in different application fields. The complete list of the author's contributions in these fields can be found in Appendix I at the end of this work.

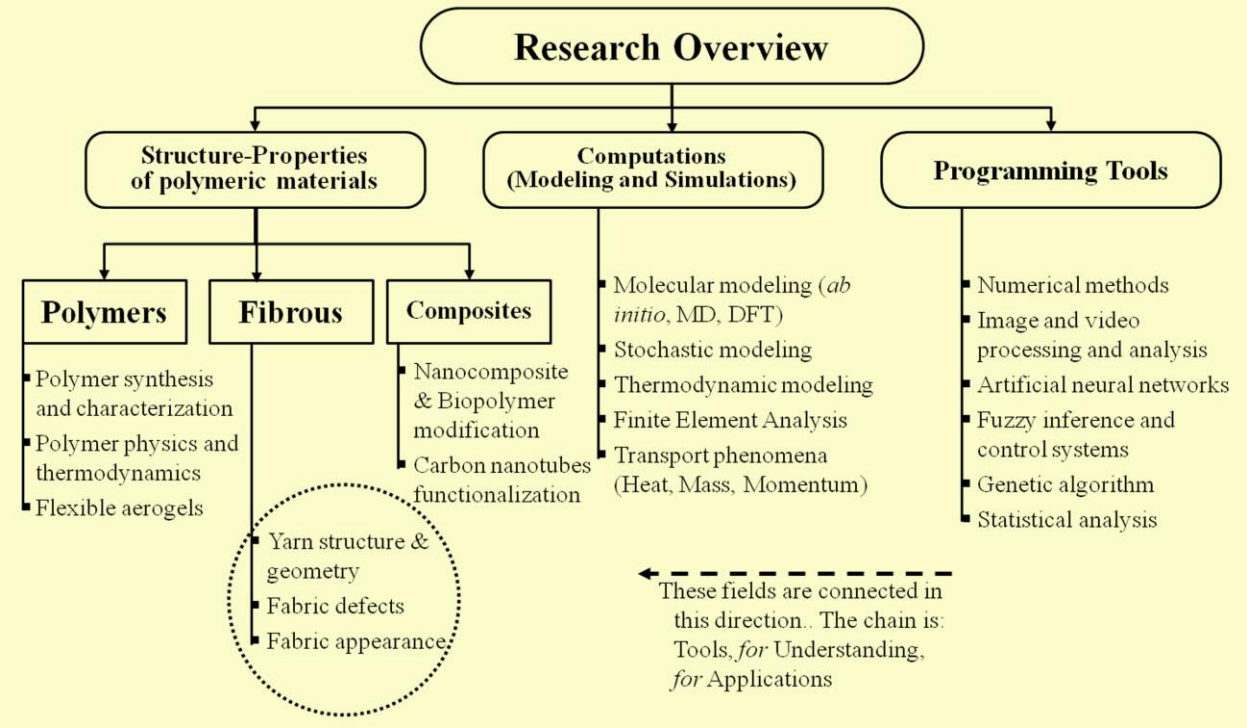

Figure 1. An overview of the author's main research interests and contributions (dotted circle highlights the topics that will be addressed in this work)

The latest research experiences of the author were developed at the Department of Textile Engineering, Mansoura University, Egypt and at the Department of Materials Engineering, Faculty of Textiles, Technical University of Liberec, Czech Republic. This research was more oriented towards the study of fibrous materials and their evaluation; where the author tried to contribute to the working environment by solving some of the problems emerged with the quality of fibrous structures, as presented below.

Fibrous structures and textile products have to conform to specific quality standards that determine their prices and the expected profit. Many tests on textile products are evaluated subjectively, where many criteria interact together to govern the final decision on the material's property. This subjective evaluation is usually carried out by human operators whose performance is susceptible to high degrees of uncertainty, because of the variability in experience among workers, work fatigue, change in mood…, etc. Most of these human-operated subjective evaluations are also dependent on the "observation" and the "visual alertness" of the worker. Therefore, methods were developed in this study to encounter these challenges that can be highlighted as follows:

1.2. The problem statement:

Many parameters that are considered in the evaluation of fibrous structures are performed ***manually*** through the ***observation*** of ***human operators*** who make their judgment based on ***subjective criteria***

1.3. The goal:

Replace the ***visual inspection*** and ***measurement*** processes during the evaluation of some fibrous structures with ***objective*** and ***smart systems*** that can work ***automatically***

1.4. The objectives:

To achieve the above goal, the presented work aims at:

- Developing objective evaluation criteria for the evaluation parameters
- Developing some algorithms that help to expedite the implementation of the selected criteria
- Developing computer vision techniques suitable for the final application
- Developing some "understanding" algorithms that imitate the human intelligence during the evaluation processes

1.5. Scope of the study:

1.5.1. Materials:

Although fibrous structures can extend to cover many materials, this study focuses the application on specific structures that are one-dimensional (yarns) and two dimensional (fabrics). The study covers the evaluation of fabric's faults during the production process and the fabric's pilling during the end-use application.

1.5.2. Technologies:

Yarns that were presented in this work were produced using ring-spinning, air-jet spinning, and some modifications on the ring-spinning frames to produce slub-yarns. This work also presented fabrics produced using the weaving as well as the knitting technologies.

1.5.3. Computation methods:

Image analysis, computer vision, and soft-computing are very wide fields that expand with the time due to the active research in these fields and results in new techniques from time to time. The scope of this study is the image analysis of binary and gray-scale images that were acquired through fixed frame images (still-images) or through the dynamic analysis of the image frames acquired with a video camera (high speed camera). The image segmentation was emphasized in this work as an essential prerequisite for image understanding. On the other hand, the artificial neural networks (ANN), and the adaptive neuro-fuzzy inference systems (ANFIS) were selected among the soft-computing techniques to be frequently implemented in this work.

1.6. Thesis format and organization:

This work is presented in ten chapters that are divided in three parts. Part I of this study presents the theory behind the work and consists of: this chapter on the work introduction and orientation, and two other chapters that cover the fundamentals of computer vision (chapter 2) and soft-computing (chapter 3). The aim of chapters 2 and 3 is not to discuss all the details behind the theory of compute vision (CV) and soft-computing (SC), but to touch very quickly on the basic knowledge that might be required for a reader without enough background in these fields. They also highlight some points that were not discussed in details in the published papers with special emphasis on the connection between these principles and their application in the textile field. Chapter 2 presents some image acquisition techniques relevant to the current work with more detailed description of the computed tomography (CT) as a promising technology that might solve some problems of the current imaging techniques. This chapter also discussed the digital representation of images which, once being digitized, allows the application of most traditional mathematical operations and algorithms for analyzing the images. The different stages required in image processing and computer vision for understanding the image content were presented, then the chapter concluded with listing the challenges facing the current state of computer vision and how these challenges directed the author through this work.

The difference between the soft-computing (SC) and the traditional hard-computing as well as the motivations behind the SC were presented in chapter 3 of this work. Only two SC algorithms were selected for presentation in this chapter; because they were used and implemented heavily in this study. The analogy of the artificial neural networks (ANN) to the biological nervous system was introduced in this chapter and the simplest neuron model was detailed. The ANN structures were presented and the feed-forward structure with back-propagation learning algorithm was emphasized, then the challenges and the critique of ANN were presented in the closing remarks of that section. Principles of the fuzzy logic and its controllers were introduced at the end of chapter 3 and the practical aspects were demonstrated with an example for replacing the subjective classing of cotton grades.

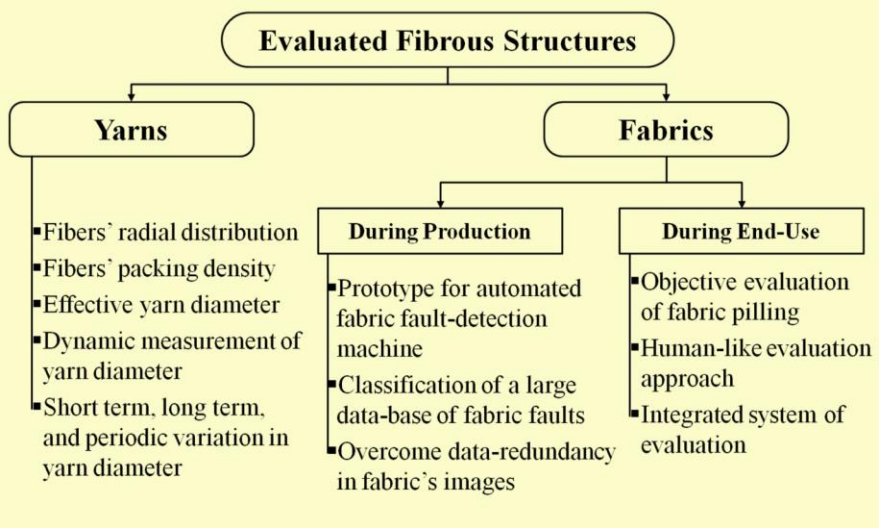

Figure 2. The application of computer vision and the computing & the soft computing algorithms in fibrous structures

An overview for Part II of this study is shown in Figure 2. This part presents a selected set of publications produced by the author with some applications of the image analysis (IA), computer vision (CV), and soft-computing (SC) in the evaluation of fibrous structures. To make it more readable and to have a unified style of this thesis, all papers were presented in the same format and font style regardless of the final formatting and type-setting of the journal. At the beginning of each chapter, a summary sheet of the paper was presented which briefly highlights: the paper's citation, the targeted problem, the objective(s), the scope, the computation algorithm, and the significance of the work. Finally, the summary sheet refers the reader to the demonstration of the software developed for the paper, if available. Also, at the end of each chapter (except chapter 4), minimized snapshots of the original paper as it appears in the final formatting of the journal were included.

The study of yarn geometry and its internal structure was presented in two chapters (chapter 4 and chapter 5) where chapter 4 presents the measurement of the packing density of fibers inside the yarn, the fibers radial distribution, the effective yarn diameter. This paper implements the Chan-Vese segmentation model for automatically allocating the contours of the yarn as well as the fibers inside. This segmentation algorithm allows the automation of the process which reduces the time required for the analysis and makes it independent from the subjective judgment of the human element. The method also avoids the approximations involved in the traditional methods by calculating the actual areas of the fibers and the yarn which makes it more accurate in determining the yarn packing density.

A dynamic and robust method for measuring the yarn diameter and its variation was introduced in chapter 5. The paper discussed in this chapter introduced a new effective image analysis method that reduces the time required for analyzing the yarn images; which becomes very essential when dealing with massive amount of yarn images captured by a high speed camera. The yarn diameter was measured at fixed intervals that assigned by the user which provides some degree of measuring flexibility that is missing with the commercial instruments for measuring the yarn diameter. The developed system was assigned the name DiaLib® with the advantage of being a “transparent system” for producing data that are usually obtained from expensive instruments with “black-box systems”.

The evaluation of two-dimensional fibrous structures at the production stage was presented in chapter 6 and chapter 7. The algorithms for detecting and classifying the fabric faults during their production were presented in chapter 6. The work behind this chapter resulted in a machine prototype for automatic fabric fault detection and classification that was developed at Mansoura University, Egypt and a video demonstration for this prototype is included on the companion CD. During the fabric image analysis, a huge set of spatial as well as spectral features was extracted which requires a dimensionality reduction for this set of features by selecting the most representing ones. This was achieved by analyzing the features using the principle component analysis (PCA), as presented in chapter 7. PCA application on the combined (spatial and spectral) features set led to a 36% reduction of the original data size, while preserving 99% of the information in the original dataset. PCA application not only reduced the data size, but also enhanced the performance of the used soft-computing classifiers. Results of this work with high classification rate and short processing times are promising to apply these techniques for real time fabric inspection systems.

The last two chapters of Part II discuss the objective evaluation of fabric pilling, as an important appearance and aesthetic property. Chapter 8 presented a study on the pilling resistance evaluation of knitted fabrics while chapter 9 presented another study on woven fabrics. The algorithms developed in both chapters were also different where the image features used in each study as well as the implemented soft-computing classifiers were different. A simple set of the first-order statistical features was used in the study of the knitted fabrics and the classification was performed using an ANN system. The second-order textural features were used, for the first

time, to analyze the pilling in woven fabrics, as presented in chapter 9. An algorithm for creating a features dataset required for the training and testing of the soft-computing classifier was described in this work; where a random noise was added to the limited number of fabric's standard images. The objective pilling classification of the woven fabric samples was performed using an adaptive neuro-fuzzy system (ANFIS) which showed a high performance in classifying the noised standard images as well as the actual fabric samples. Results of these studies showed high efficiency of the system that is independent of the fabric's structure or color. This suggests the system's validity in replacing the currently applied subjective pilling evaluation.

A final comment on the organization of this work is to inform the reader that this thesis is organized in a way that allows its handling from any point; because each chapter is written to be a stand-alone and does not have a direct dependency on other parts of the work. The theoretical part of this work (Part I) might be useful as a reference material that might be required for readers with limited background in the discussed fields, and can be skimmed (or skipped) by experienced readers. It is also important to point out that, there is a compact disc (CD) that was prepared as a companion material with this thesis. The CD allows an easy access in a digital form for the contents which includes:

- An electronic copy of this thesis; in a single file as well as in separate chapters for easier browsing
- A short video of the "fabric fault detection machine" prototype presented in this work
- The software programs developed during the work of each paper, if any, with some examples that allow the reader to test and use the programs
- Demonstrative videos for the developed software programs
- Other materials supporting the author's application for this habilitation work

PART I

Chapter 2

Computer Vision
&
Image Analysis

Computer Vision & Image Analysis

2.1. Introduction:

The current state of evaluation in textile fibrous structures depends on different tests and many of these tests require subjective evaluation by trained personnel. Therefore, modeling the fibrous structures in digitized form allows more objective study and evaluation. It also reveals some of the subtle properties that might be tedious for human operators to find systematically without mistakes. There are different systems for acquiring the physical fibrous structures to the digital world and some of these methods depend only on the projections of the structures or reconstruct a digital three-dimensional (3D) model for them. In this chapter, we will present some of the image acquisition techniques relevant to the current work, discuss the digital representation of images, and go over the stages required in image processing and computer vision (CV) to allow understanding the image content, then conclude with the challenges facing the current state of computer vision.

2.2. Object digitization technologies:

The types of images in which we are interested are generated by the combination of an "*illumination*" source and the *reflection* or *absorption* of energy from that source by the elements of the "*scene*" being imaged. We enclose *illumination* and *scene* in quotes to emphasize the fact that they are considerably more general than the familiar situation in which a visible light source illuminates a common everyday 3-D (three-dimensional) scene. For example, the illumination may originate from a source of electromagnetic (EM) energy such as radar, infrared, or X-ray source, or from less traditional sources such as ultrasound or even a computer-generated illumination patterns. Similarly, the scene elements could be familiar objects or being fibers, yarns, and fabric surface & structure, as emphasized in this study. Depending on the nature of the source, illumination energy is reflected from, or transmitted through, the objects. In some applications, such as Scanning Electron Microscopy (SEM), the reflected or transmitted energy is focused onto a photoconverter (*e.g.* a phosphor screen), which converts the energy into visible light.

2.2.1. Sensing elements within the visible range

Electromagnetic waves can be conceptualized as propagating sinusoidal waves of varying wavelengths and energies. If spectral bands are grouped according to their energy, we obtain a spectrum that ranges from gamma rays (highest energy) at one end to radio waves (lowest energy) at the other end. It is very common in many imaging applications to use illumination sources within the visual bands of the electromagnetic spectrum.

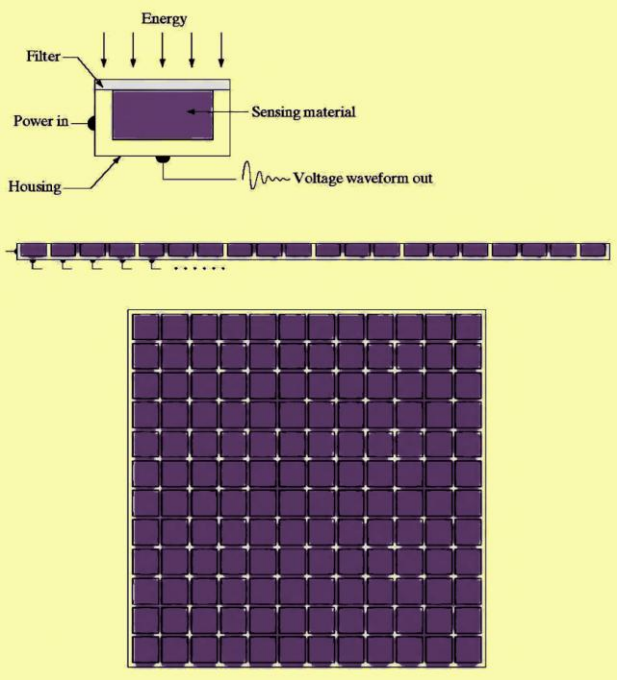

Figure 1. Arrangements of sensors for image acquisition: Single imaging sensor (top), Line sensor (middle), Array sensor (bottom) (Reproduced from Ref. [1])

The three principal sensor arrangements used to transform illumination energy into digital images are shown in Figure 1. The idea for a single sensor is that the incoming energy is transformed into a voltage by the combination of input electrical power and sensor material (e.g. silicon photodiode) that is responsive to the particular type of energy being detected. The output voltage waveform is the response of the sensor(s), and a digital quantity is obtained from each sensor by digitizing its response. The use of a filter in front of the sensor improves its selectivity; for example, a green (pass) filter in front of a light sensor favors light in the green band of the color spectrum results in a stronger output for green light than for other components in the visible spectrum.

The in-line arrangement of sensors in the form of a sensor strip provides imaging elements in one direction. The imaging strip gives one line of an image at a time, and this strip is implemented in two ways. Firstly, the object can move in front of the sensor strip and the obtained signal is accumulated and processed to build the global picture of the image. This technique is implemented in instruments for measuring yarn irregularity and yarn diameter such as the optical module on the recent versions of Uster Evenness Tester, and the Constant Tension Transport (CTT) tester produced by Lawson-Hemphill. Secondly, the object is static and the sensor strip moves perpendicular to its direction to complete the other dimension of the two-dimensional image. This is the type of arrangement used in most flatbed scanners and sensing devices with 4000 or more in-line sensors are possible. Some of our fabric surface images were digitized

using this technique which allows a uniform distribution of lighting on the fabric surface and high resolutions of the fabric's images are possible, an example of such image is shown in Figure 2.

Figure 2. Fabric surface as digitized using an in-line arrangement of sensors in a flatbed scanner

Numerous electromagnetic and some ultrasonic sensing devices are frequently arranged in an array format, such as the 2D array shown in Figure 1. This is also the predominant arrangement found in digital cameras such as the charge-coupled device (CCD) arrays, which can be manufactured with a broad range of sensing properties and can be packaged in rugged arrays of 4000 x 4000 elements or more. Since the sensor array shown in Figure 1 is two dimensional, its key advantage is that a complete image can be obtained by focusing the energy pattern onto the surface of the array. The principal manner in which array sensors are used is shown in Figure 3 where the energy from an illumination source being reflected from a scene object, but the energy also could be transmitted through the object. The first function performed by the imaging system is to collect the incoming energy and focus it onto an image plane. If the illumination is light, the front end of the imaging system is a lens, which projects the viewed scene onto the lens focal plane, as shown in Figure 3. The sensor array, which is coincident with the focal plane, produces outputs proportional to the integral of the light received at each sensor. Digital and analog circuitries sweep these outputs and convert them to a signal, which is then digitized by another section of the imaging system as diagrammatically shown in Figure 3.

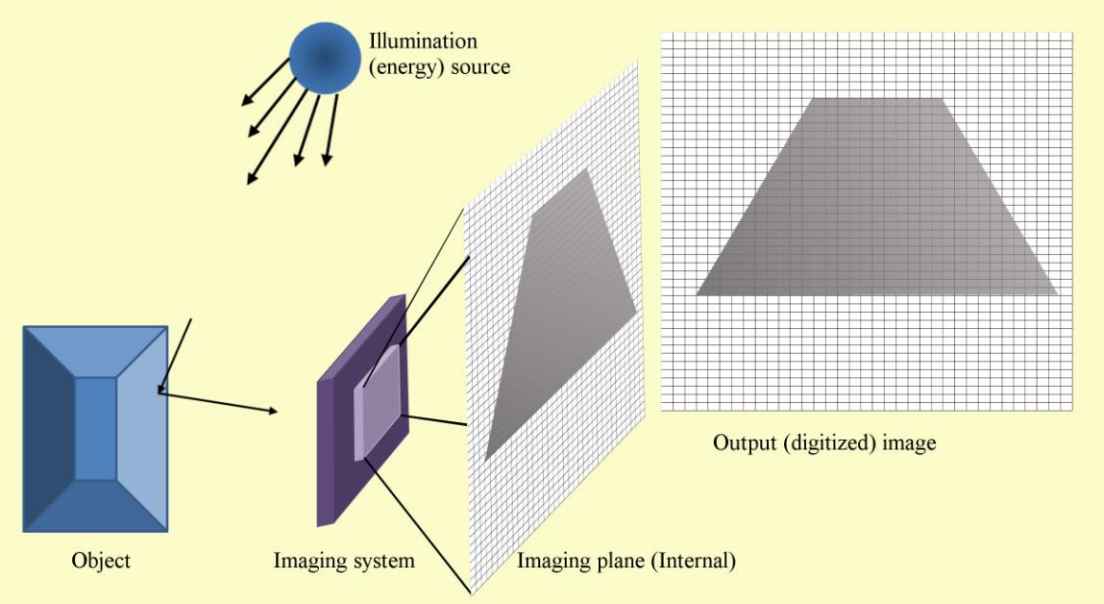

Figure 3. An example of the digital image acquisition process with a 2D array of sensors

In our work, we used this type of image acquisition many times where, for instance, a high speed CCD cameras was used to shoot the images of yarns running at a speed of 100 m/min as shown in Figure 4. In this work, four different instruments were synchronized to test the yarn properties simultaneously. The CCD camera was also installed on a microscope to digitize the microscopic images of fibers and yarns. This type of camera with the 2D arrays of sensors was also used during the evaluation of the fabric structures, fabric faults, and fabric appearance (especially for its pilling), as will be shown in the second part of this work that covers the applications.

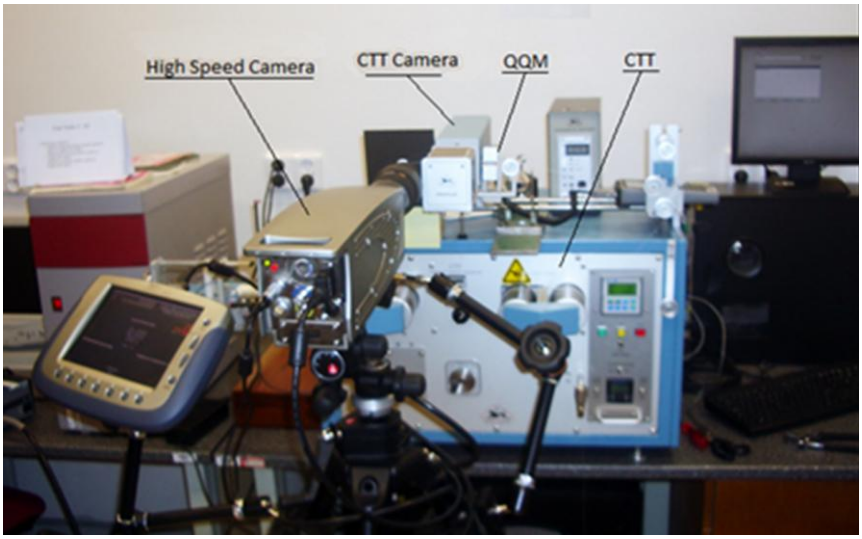

Figure 4. A high speed camera acquiring the images of yarn at 100 m/min

2.2.2. X-ray sensing elements

The previous methods of image acquisition and digitization mainly utilize illumination sources within the visible region of electromagnetic (EM) spectrum. In this section we will switch the focus to a more powerful technique in acquiring images by using the x-rays. X-rays are among the oldest sources of EM radiation used for imaging and best known use of x-rays is medical diagnostics, but they also are used extensively in industry and other areas, like astronomy. In our work, we recently utilize this technology to reconstruct digital models of fibrous structures and study the geometry and the internal structure of yarns with a neither destruction to the studied sample, nor the application of any chemicals that might affect its physical properties.

Computed Tomography (CT) is an imaging method that employs the tomography (from Greek words *tomos* means "*slice*" and *graphein* means "*to write*") where "digital geometry processing" is used to generate a three-dimensional image of the internals of an object from a large series of two-dimensional X-ray images taken around a single axis of rotation. The conception of the CT idea started at the end of the 1960s and the first commercially viable CT scanner was invented in 1972 by Hounsfield who won the 1979 Nobel Prize in medicine for this work. The CT technology was basically implemented in medical imaging and the clinical CT became the radiology's powerhouse as the first method to non-invasively acquire images of the inside of the human body. The method has evolved rapidly and was implemented in industrial fields by the end of the 1980s as one of the favorite Non Destructive Testing (NDT) techniques. The diversity of CT applications, with objects of different sizes, shifted the interest from large objects (as human bodies) to smaller ones and the need for the "higher spatial resolution" scanners started to emerge. The higher spatial resolution is obtained by either using clinical flat-panel imaging systems that achieve resolutions in the order of 150–200 µm or by using dedicated micro-CT (µ-CT) scanners, such as the one used in this study, which can usually achieve a spatial resolution less than 0.5 µm.

The principle of CT scanning stems from the fact that the information available from a single projection of an object in engineering drawing is limited and another projection is necessary to obtain the third projection and ultimately reconstructing the 3D perspective of the object. This explanation in engineering drawing applies also to CT scanning, where a single x-ray projection shows a superimposition of all objects in the path of the X-ray and therefore hard to understand the volumetric structure of the object. The information can be increased by taking two (and more) projections, however, increasing the number of projection directions (views) is of little help because the observer is not able to mentally solve the superposition problem and to "reconstruct" the internal information of the object. Fortunately it can be shown that a complete "*computed*" reconstruction of the object's interior is mathematically possible as long as a large number of views "*tomos*" have been acquired "*graphein*" over an angular range that covers an angle of at least 180˚. This acquisition scheme is implemented in CT scanners by using an X-ray tube together with a detector while the object is rotating within path of the X-ray beams as demonstrated in Figure 5.

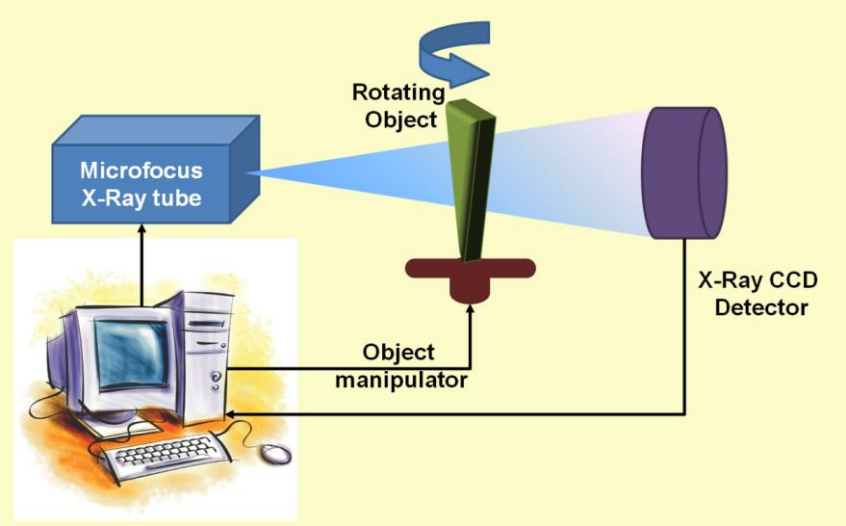

Figure 5. Schematic representation for the principle of CT scanning

Each x-ray projected image is a representation of the object's X-ray absorption along straight lines in a specific direction. For an incident x-ray with initial intensity I_0, an object of thickness d, and attenuation coefficient μ, the number I of quanta reaching the detector is given by the exponential attenuation law:

$$I = I_0 e^{-\mu d} \qquad (1)$$

The negative logarithm $p = -\ln I/I_0$ of each intensity measurement I gives information about the product of the object attenuation μ and its thickness d and proportionate to the tube current I (given a constant incident intensity I_0). For nonhomogeneous objects, the attenuation coefficient is a function of x, y, and z and the projection value p corresponds to the line integral along line L of the object's linear attenuation coefficient distribution $\mu(x, y, z)$:

$$p(L) = -ln\frac{I(L)}{I_0} = \int_L \mu(x,y,z)dL \qquad (2)$$

For flat-panel CT, the line L can be parameterized by the rotation angle α and the detector coordinates (u, v). We are interested in gaining knowledge of $\mu(x, y, z)$ by reconstructing the acquired data $p(L)$ and the CT "*image reconstruction*" process is defined as the process of computing the image $f(x, y, z)$ as an accurate approximation to $\mu(x, y, z)$ from the set of measured projection values $p(L)$.

To simplify the mathematics behind the image reconstruction process, assume a single-slice CT scanner whose detector consists of one detector-row only. The raw data would be given by setting the longitudinal detector coordinate v to zero: $p(\alpha, u, 0)$. The easiest way to perform image reconstruction of these mid-plane data is to make a *change of variables* to obtain raw data

in parallel-beam geometry and replace the source position α and the detector position u by other variables: θ that represents the ray angle with respect to the coordinate system, and ξ that represents the rays distance to the center of rotation. This allows the formulation of $\hat{p}(\theta, \xi) = p(\theta, u, 0)$ and the new two variables are related according to the relation

$$x \,.\, cos(\theta) + y \,.\, sin(\theta) = \xi \qquad (3)$$

The process of changing the variables to parallel geometry is known as *rebinning* and the parallel beam image reconstruction consists of a filtering of the projection data with the reconstruction kernel followed by a back-projection into image domain. This can be formulated mathematically as:

$$f(x, y) = \int_0^{\pi} d\theta \; \hat{p}(\theta, \xi) * k(\xi) \,|_{\xi = x \,.\, cos(\theta) + y \,.\, sin(\theta)} \qquad (4)$$

Where $k(\xi)$ is the reconstruction kernel and there are different convolution kernels available (e.g. smooth, standard, and sharp…,etc) to allow modifying the image sharpness (spatial resolution) and the image noise characteristics. This process is called filtered back-projection (FBP) where the projection data are to be convolved with the reconstruction kernel $k(\xi)$. The filtered data are then back-projected into the image along the original ray direction for all ray angles θ.

The extension to cone-beam data, where $v \neq 0$ in general, is straight forward and known as Feldkamp-type image reconstruction and today's micro-CT image reconstruction algorithms are mainly of this type. In Feldkamp-type reconstruction, the variable v is ignored during the filtering step (as done above) but accounted for the true ray geometry during the back-projection by using a three-dimensional back-projection. The achievable spatial resolution of a given micro-CT scanner is mainly determined by the magnification factor, by the detector pixel size and by the size of the focal spot. A certain spatial resolution can only be achieved when it is not limited by the voxel (the volume element) size. Ideally, the voxel size should be half of the spatial resolution value or less. On the other hand, the reconstruction times can range from some minutes up to hours, depending on the number of voxels used. The time for image reconstruction is in the order of $O(N^4)$ when N projections are back-projected into a volume of size N^3. Other techniques that cut down this effort to the order $O(N^3 logN)$ are described in the literature, but still need more improvement to be included in the product implementation for µ-CT cone-beam reconstruction [2].

In one of our recent studies on the utilization of CT [3], an air-jet yarn sample was scanned and the obtained projected images were used to reconstruct the 3D digital model of the yarn as demonstrated in Figure 6. The digital model of the yarn was manipulated in different ways where the yarn was magnified without losing the resolution and details, as shown also in Figure 6. The details of the 3D model depend mainly on the resolution of the CT scanner during the image acquisition stage not just on the resolution of the image that is magnified. The presence of the 3D digital model allows some treatments such as clipping and cutting certain parts of the structure as

well as slicing the yarn structure at any required plane direction. It is, therefore, very useful to use this model and obtain cross-sectional images along the yarn length, as demonstrated in Figure 6, without the need to apply any additional chemicals such as the ones required for hardening the yarn before its physical slicing using sharp edges and the microtome.

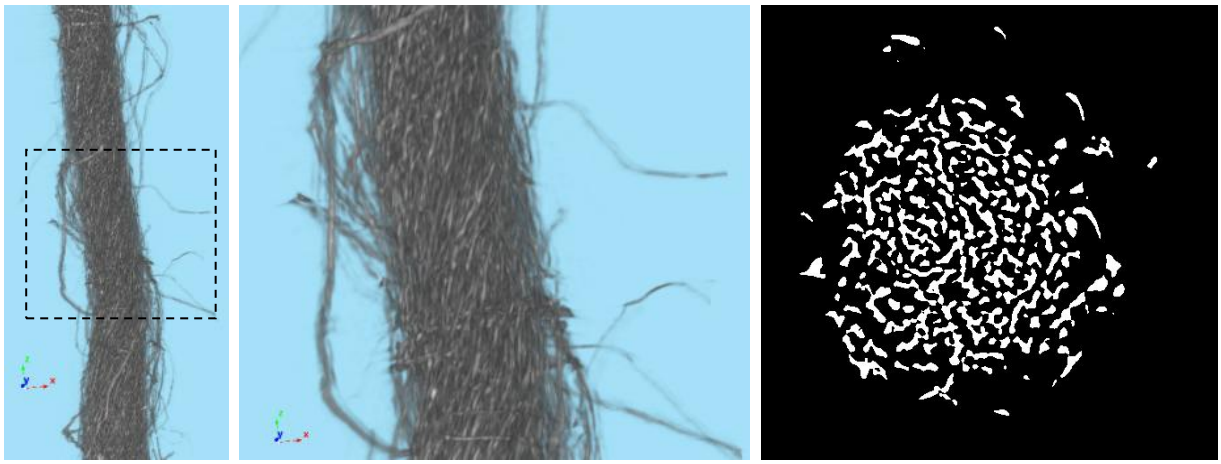

Figure 6. Reconstructed digital model of the yarn (left) that allows its visualization with a higher magnification, as the dotted rectangle (middle), and with cross-sectional slicing (right)

2.3. Digital image representation:

After the acquisition of images, they are represented in a digital form by two-dimensional functions of the form $f(x, y)$. The value or amplitude of f at spatial coordinates (x, y) is a positive scalar quantity whose physical meaning is determined by the source of the image. Most of the images in which we are interested in our studies are monochromatic images, whose values are said to span the gray-scale. Images can be also represented in color-space which "usually" means three channels for the same image that carry information on the red, the green and the blue levels in the image. For grayscale image that is generated from a physical process, its values are proportional to energy radiated by a physical source (e.g., electromagnetic waves). As a consequence, $f(x, y)$ must be nonzero and finite; that is,

$$0 < f(x, y) < \infty \qquad (5)$$

The function $f(x, y)$ may be characterized by two components; the amount of source illumination *incident* on the scene being viewed, and the amount of illumination *reflected* by the objects in the scene. Appropriately, these are called the illumination and reflectance components and are

denoted by $i(x, y)$ and $r(x, y)$, respectively. The two functions combine as a product to form $f(x, y)$:

$$f(x,y) = i(x,y)r(x,y) \quad (6)$$

where

$$0 < i(x,y) < \infty \quad (7)$$

and

$$0 < r(x,y) < 1 \quad (8)$$

Equation (8) indicates that reflectance is bounded by 0 (total absorption) and 1 (total reflectance). The nature of $i(x, y)$ is determined by the illumination source, and $r(x, y)$ is determined by the characteristics of the imaged objects. It is noted that these expressions also are applicable to images formed via transmission of the illumination through a medium, such as x-rays. In this case, we would deal with a *transmissivity* instead of a *reflectivity* function, but the limits would be the same as in equation (8), and the image function formed would be modeled as the product in equation (6).

After the image $f(x, y)$ is *sampled* and *quantized* so that the resulting digital image has M rows and N columns and the values of the coordinates (x, y) become discrete quantities. Integer values are used for these discrete coordinates and the values of the coordinates at the origin, for example, are $(x, y) = (0, 0)$. The next coordinate values along the first row of the image are represented as $(x, y) = (0, 1)$. It is important to keep in mind that the notation (0, 1) is used to signify the second sample along the first row and it does not mean that these are the actual values of physical coordinates when the image was sampled. Figure 7 demonstrates this coordinate convention.

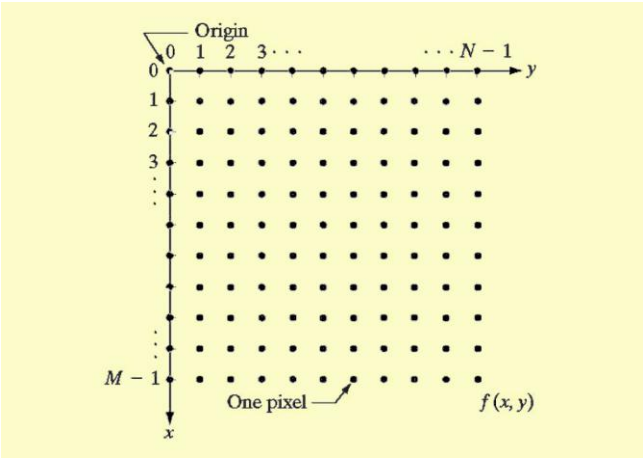

Figure 7. Coordinate convention used in representing digital images (Reproduced from Ref. [1])

The notation introduced in the preceding paragraph allows us to write the complete *M* x *N* digital image in the following compact matrix form:

$$f(x,y) = \begin{bmatrix} f(0,0) & f(0,1) & \dots & f(0,N-1) \\ f(1,0) & f(1,1) & \dots & f(1,N-1) \\ \vdots & \vdots & & \vdots \\ f(M-1,0) & f(M-1,1) & \dots & f(M-1,N-1) \end{bmatrix} \quad (9)$$

The right side of this equation is the digital image and each element of this matrix array is called an image element, picture element, pixel, or pet. In some discussions, it is advantageous to use a more traditional matrix notation to denote a digital image and its elements:

$$A = \begin{bmatrix} a_{0,0} & a_{0,1} & \dots & a_{0,N-1} \\ a_{1,0} & a_{1,1} & \dots & a_{1,N-1} \\ \vdots & \vdots & & \vdots \\ a_{M-1,0} & a_{M-1,1} & \dots & a_{M-1,N-1} \end{bmatrix} \quad (10)$$

It is clear that, $a_{i,j} = f(x = i, y = j) = f(i, j)$, so equations (9) and (10) are identical matrices.

Once the image is represented in a matrix form as expressed in equation (10), most of the mathematical rules and operations of linear algebra can be performed on the image. One of the very attractive features that drove me to work with images analysis is the possibility to make a sense of some mathematical calculations that can be performed in multi-dimensional space. For example, we start learning the rules of calculus in two-dimensional space with a single independent variable then generalize that to multi-variable calculus in multi-dimensional space. The advantage of the 2D space is that it allows us to graphically visualize different definitions such as the meaning of a tangent or the meaning of the integration of the curve...,etc. The generalization of these rules to multi-variables is challenging because of the lack of the graphical interpretation of the mathematical calculations. Digital imaging analysis in its 2D representation presents the intermediate step between the one dimensional and the multi-dimensional data where the rules can be applied and visualized at the same time. An example of this is the Fast Fourier Transform (FFT) which is usually introduced in lD and it becomes familiar and easy to be understood with a lD set of data, but 2D FFT is possible to be understood in treating the digital images. Another example is the application of the variational methods and the optimization of multi-variable functions that are necessary in most of the quantum mechanics applications. It is easier to understand these variational methods and their mathematical complexity when you deal with a 2D set of data (in the form of an image) such as our work on Chan-Vese segmentation model [4].

It is also important to note that the digital representation of an image might be deceiving for the human eye and might be hard to understand. Let us look at Figure 8, for example, which shows in its upper part an image of a woven fabric that is very familiar to the human eye and can be recognized easily, however it is more difficult for human to interpret the other two representations for the same image of the woven fabric that are shown at the bottom of Figure 8. The other two images in the bottom of Figure 8 are just two representations of the same fabric image by two different ways; one representation of the brightness (gray-scale) values of the picture and the other as a representation of the fabric image in the frequency domain after the application of the Fast Fourier Transform (FFT). It is clear from Figure 8 that; although all representations contain exactly the same information, it is very difficult for a human observer to find a correspondence between them, and without the prior knowledge of the image presented in the top of the figure, it is unlikely that one would recognize the fabric structure from the other two representations.

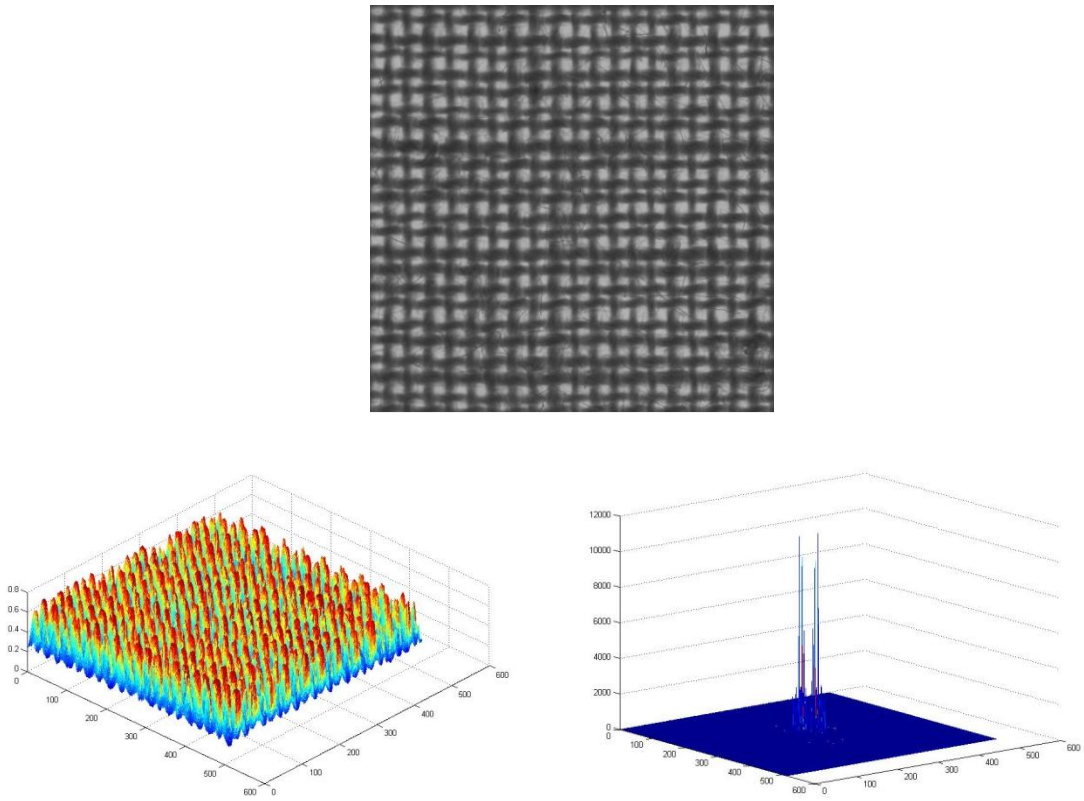

Figure 8. 2D image of a woven fabric (top) with two different representations of the same image as expressed by the gray levels (bottom left) and the Fourier transformed image (bottom right) (Note; the main peak at the center of the FFT image was suppressed to present the other peaks)

2.4. Image understanding:

Humans (and other living animals) use different senses to interact with their environment and one of the most important senses is the vision as it allows humans to *perceive* and *understand* the world surrounding them. Computer vision is the technology that aims at duplicating the effect of human vision by electronically *perceiving* and *understanding* that digital image. Image understanding by a machine can be seen as an attempt to find a relation between input image(s) and previously established models of the observed world. Transition from the input image(s) to the model reduces the information contained in the image to relevant information for the application domain. This process is usually divided into several steps and levels where the bottom layer contains raw image data and the higher levels interpret the data. Computer vision designs the intermediate representations and algorithms serving to establish and maintain relations between entities within and between the layers.

Image representation can be roughly divided according to data organization into four levels, as shown in Figure 9. The boundaries between individual levels are inexact, and more detailed divisions are also proposed in the literature. Figure 9 suggests a bottom-up way of information processing, from signals with almost no abstraction, to the highly abstract description needed for image understanding. Note that the flow of information does not need to be unidirectional; often feedback loops are introduced which allow the modification of algorithms according to intermediate results.

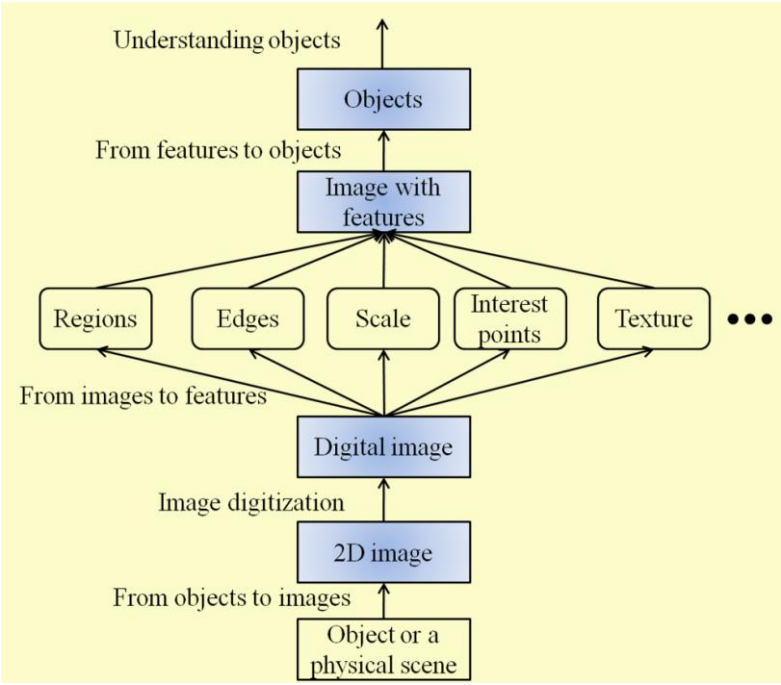

Figure 9. Different image representation (shaded rectangles) suitable for image analysis problems in which objects have to be detected and classified (Reproduced from Ref. [5])

This hierarchy of image representation and related algorithms is frequently categorized in a simpler way with *low*, *medium*, and *high level* image processing and understanding, as shown in Figure 10. Although the boarders between these levels are vague (especially the low and medium levels) and some techniques might be categorized in one or another, the low-level processing methods are usually distinguished by using very little knowledge about the content of images. In the case of image components' recognition by a computer, it is usually provided by high-level algorithms or directly by a human who understands the problem domain. The *Low* and *medium* level methods often include image compression, pre-processing methods for noise filtering, edge extraction, and image sharpening. *Low* and *medium* level image processing uses data which resemble the input image; for example, an input image captured by a camera is 2D in nature, being described by an image function $f(x, y)$ whose value, at simplest, is usually brightness depending on two parameters x and y the coordinates of the location in the image.

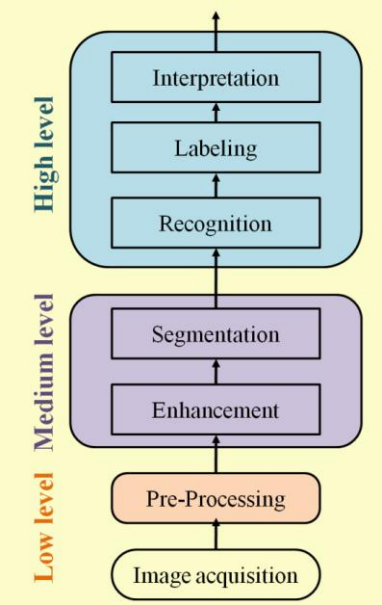

Figure 10. Basic steps in image recognition and interpretation

Low and medium level computer vision techniques overlap almost completely with digital image processing, which has been practiced for decades. The following sequence of processing steps is commonly seen: An image is captured by a sensor (such as a CCD camera) and digitized; then the computer suppresses noise (image pre-processing) and maybe enhances some object features which are relevant to understanding the image. Edge extraction is an example of processing carried out at this stage. Image segmentation is the next step, in which the computer tries to separate objects from the image background and from each other. Total and partial segmentation may be distinguished: total segmentation is possible only for very simple tasks, an example being the recognition of dark non-touching objects from a light background. In more complicated problems (the general case), medium-level image processing techniques handle the partial

segmentation tasks, in which only the cues which will aid further high-level processing are extracted. Often, finding parts of object boundaries is an example of low-level partial segmentation. Object description and classification in a totally segmented image are also understood as part of the medium-level image processing. Other medium-level operations are image compression, and techniques to extract information from (but not understand) moving scenes. An example of the low and medium levels processing of the longitudinal view of a yarn as well as its cross-sectional view is shown in Figure 11.

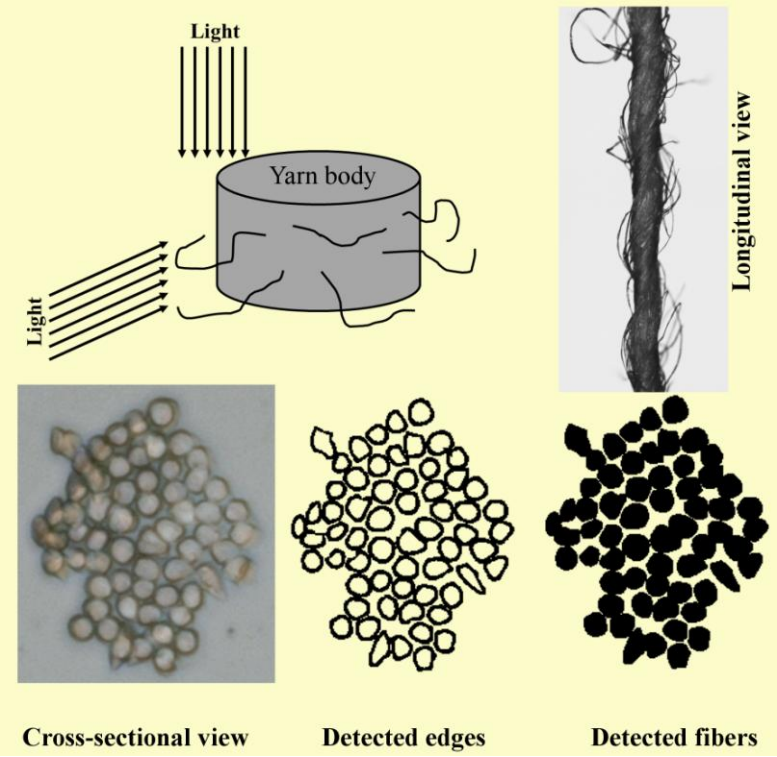

Figure 11. Low and medium level processing of digital yarn image

Most current low-level image processing methods were proposed in the 1970s or earlier. Recent research is trying to find more efficient and more general algorithms and is implementing them on more technologically sophisticated equipment; in particular, parallel machines are being used to ease the enormous computational load of operations conducted on image data sets. The requirement for better and faster algorithms is fuelled by technology delivering larger images (better spatial resolution), and color. A complicated and so far unsolved problem is how to order low-level steps to solve a specific task, and the aim of automating this problem has not yet been achieved. It is usually still a human operator who finds a sequence of relevant operations, and domain-specific knowledge and uncertainty cause much to depend on this operator's intuition and previous experience.

Low-level data are comprised of original images represented by matrices composed of brightness (or similar) values, while *high-level* data originate in images as well, but only those data which are relevant to high-level goals are extracted, reducing the data quantity considerably. High-level data represent knowledge about the image content; for example, object size, shape, and mutual relations between objects in the image. The high-level vision system includes three steps: recognition of the objects from the segmented image, labeling of the image and interpretation of the scene. Most of the artificial intelligence tools and techniques are required in high level vision systems. Recognition of objects from the image can be carried out through a process of pattern classification, which at present is realized by supervised learning algorithms (e.g. artificial neural networks). The interpretation process, on the other hand, requires knowledge-based computation (e.g. fuzzy logic controllers). Therefore, high-level processing is based on knowledge, goals, and plans of how to achieve those goals which tries to imitate human cognition and the ability to make decisions according to the information contained in the image. High-level vision begins with some form of formal model of the world, and then the 'reality' perceived in the form of digitized images is compared to the model. A match is attempted, and when differences emerge, partial matches (or sub-goals) are sought that overcome the mismatches; the computer switches to low-level image processing to find information needed to update the model. This process is then repeated iteratively, and 'understanding' an image thereby becomes cooperation between top-down and bottom-up processes. A feedback loop is introduced in which high-level partial results create tasks for low-level image processing, and the iterative image understanding process should eventually converge to the global goal.

Although the task of understanding the objects in an image is challenging in computer vision, the digital representation of an image in the form of a numerical matrix might also be challenging for human to understand the image. An example of this is the representation of the fabric image and its other two derivatives shown in Figure 8 and having the same amount of information. Therefore, understanding the digital image requires a lot of a priori knowledge by humans to interpret the images; while, on the other hand, the machine only begins with an array of numbers and will be attempting to make identifications and draw conclusions from data. Internal image representations are not directly understandable, while the computer is able to process local parts of the image, it is difficult for it to locate global knowledge. General knowledge, domain-specific knowledge, and information extracted from the image will be essential in attempting to 'understand' these arrays of numbers.

2.5. Closing remarks on CV challenges:

Computer vision involves sequence of operations that are characteristic of image understanding; such as: image capturing, early processing, segmentation, model fitting, motion prediction, qualitative / quantitative conclusions. Giving computers the ability to see is a challenging task and research in the field faces many obstacles. Examples of the computer vision challenges are:

- The ***loss of information*** where we live in a three-dimensional (3D) world and the available electronic visual sensors (*e.g.* cameras) used to digitize this 3D world usually give two- dimensional (2D) images. This projection to a lower number of dimensions is associated with an enormous loss of information where the projected images (in 2D) are capable of *mapping* points along rays but does not preserve angles and collinearity. Therefore, it is not enough to have a picture of an object to figure-out its dimensions and a *reference scale* is needed to differentiate between large and small objects in the acquired image. This challenge directed us to use some of the advanced techniques such as the computed tomography scanning to reconstruct a reliable model of our fibrous structures.

- The image ***interpretation*** is another challenge because humans bring their previous knowledge and *experience* to the current observation when they try to understand an image. Human ability to *reason* allows representation of long-gathered knowledge and its use to solve *new* problems. From the mathematical logic and/or linguistics point of view, interpretation of images can be seen as a mapping:

  Interpretation: image data → model

  The (logical) model means some specific world in which the observed objects make sense and there are several possible interpretations of the same image(s). An example might be: nuclei of cells in a biological sample, rivers in a satellite image, or parts in all industrial process being checked for quality. Introducing interpretation to computer vision allows us to use concepts from mathematical logic, linguistics as *syntax* (rules describing con'ectly formed expression), and *semantics* (study of meaning). Considering observations (images) as an instance of formal expressions, semantics studies relations between expressions and their meanings. The interpretation of image(s) in computer vision can be understood as an instance of semantics. Artificial intelligence (AI) has invested several decades in attempts to endow computers with the capability to understand observations; while progress has been tremendous, the practical ability of a machine to understand observations remains very limited.

- Another challenge is the ***noise*** that is inherently present in all measurements in the real world, but its existence in images requires different mathematical tools which are able to filter out the noise and deal with the uncertainty in the acquired images. Complex mathematical tools make the image analysis more challenging compared to the standard (deterministic) methods. It is also useful to use fuzzy logic controllers in such problems which allow some degree of uncertainty during the decision making about the presented data.

- The ***redundancy of data*** (too much data) is a challenge in computer vision due to the nature of huge data collected from images and video sequences. To get a sense of the data acquired, an example of non-compressed A4 sheet of paper scanned monochromatically at 300 dots per inch (dpi) at 8 bits per pixel will correspond to about 8.5 mega bytes (MB). Non-interlaced RGB 24 bit color video 512 x 768 pixels, 25 frames per second, makes a data stream of 225 Mb per second. If the image and video processing we perform is not very simple, then it is hard to achieve a real-time performance (i. e. to process 25 or 30 images per second) with traditional poor hardware. Therefore, it is very encouraging to apply new methods that reduces the amount required calculations such as our introduced method [6] to analyze the tremendous amount of ictures produced from the high speed camera imaging.

- The physics involved in image formation interferes with the ***measured brightness*** in images to form another challenge in computer vision. The radiance (brightness, image intensity) depends on the irradiance (light source type, intensity and position), the observer's position, the surface local geometry, and the surface reflectance properties. This is the reason why image capturing physics is often avoided in practical attempts aiming at image understanding, and a direct link between the appearance of objects in scenes and their interpretation is sought.

- The ***scope*** of the image is another challenge where a big difference can be observed by viewing an image through local window or through global view. Image analysis algorithms commonly analyze a particular storage bin in an operational memory (*e.g.* a pixel in the image) and its local neighborhood; the computer sees the image through a keyhole. Seeing the world through a keyhole makes it very difficult to understand more global context of the image.

- ***Dynamic scenes*** such as those to which we are accustomed, with moving objects or a moving camera, are increasingly common and represent another way of making computer vision more challenging.

References:

[1] R. C. González and R. E. Woods, *Digital image processing*. Prentice Hall, 2002.

[2] W. Semmler and M. Schwaiger, *Molecular Imaging I*. Springer, 2008.

[3] M. Eldessouki and S. Ibrahim, "Computed Tomography Application For investigating The Internal Structure Of Air-Jet Yarns," in *the 20th International Conference: Structure and Structural Mechanics of Textiles*, 2014.

[4] M. Eldessouki and S. Ibrahim, "Chan-Vese Segmentation Model For Faster And Accurate Evaluation of Yarn Packing Density," *(In Press. Text. Res. J.*

[5] T. Svoboda, J. Kybic, and V. Hlavac, *Image Processing, Analysis & and Machine Vision-A MATLAB Companion*. Thomson Learning, 2007.

[6] M. Eldessouki, S. Ibrahim, and J. Militky, "A Dynamic and Robust Image Processing Based Method for Measuring Yarn Diameter and Its Variation," *Text. Res. J.*, vol. 84, no. 18, pp. 1948–1960, 2014.

PART I

Chapter 3

Soft Computing

Soft Computing

3.1. Introduction:

A simple example that might draw the line between our way of thinking and doing the calculations in our minds in a *soft way* and how computers and machines think and do the computations in a *hard way* is to demonstrate the different algorithms used in both ways. Let us say, you are now reading this work in electronic format and you want to find the beginning of "chapter 5", for example, and you expect that chapter to start with the word "chapter 5". Searching for the word "chapter 5" using the *search algorithm* embedded in the software you are using for reading this document, and using your *human intelligent algorithm* in finding the required word demonstrates the difference between the *hard computing* and the *soft computing*, respectively. If you observe the search algorithm embedded in the software you use, you will find it comparing each word in the document with the required words and it usually starts from where you are and compares each word in the following text to the required words. If you start, for instance, from a page that is just next to the page that includes the required word, the search algorithm will do the *hard computing* and compares all the words until the end of the file then starts again from the beginning until reaching the required page. Human minds, on the other hand, think in a different way and perform *intelligent search* where they can change the starting point at any time and skip pages with thousands of words if they have the doubt that this is not the probable place for the required word. To find the beginning of "chapter 5" in a book of ten chapters, for example, human will decide to start at the middle of the book or to start at a *random* page then go backward or forward from that point according to how the words in that page *match* or *fit* the *search criterion*. It is the *soft computing* embedded in our intelligent brains that saves us the work of reading and comparing each word (the *hard computing* that followed by the traditional computing algorithms) and going directly to our required target based on a *fitness* criterion. We should notice that, computers can find the required word faster than the human being assigned the same task and this has nothing to do with advances in the *computation algorithms* itself but might be the advances in the *speed* of doing the tedious calculations. In fact, computers reach results faster, not because they are smarter or more intelligent but because they are doing the calculations *faster*, with the speed of the used electronics and hardware, and in a *systematic* way that does not affect with the *fatigue* that might affect humans in repeating the same task many times.

In our contemporary times, scientists are not content with the available resources and usually think of improving and advancing techniques to serve the human needs. In the middle of the 1950s, scientists decided to combine the advantages of computers (e.g. artificial, fast, systematic…, etc) and the advantages of human minds (e.g. intelligent, rational, interacting with uncertainty…, etc) and initiated a new science of that time which is called "***Artificial Intelligent***", usually abbreviated as **AI**. The name itself implies the two main advantages of the required systems of being *intelligent* as human and *artificial* as machines and computers and AI

can be defined as "the branch of computer science that is concerned with the automation of intelligent behavior" [1]. Therefore, the field of artificial intelligent attempts to understand intelligent entities (human) and implements this understanding in building intelligent entities. AI addresses one of the ultimate puzzles, "how is it possible for a slow, tiny brain, whether biological or electronic, to perceive, understand, predict, and manipulate a world far larger and more complicated than itself?", "how do we go about *creating* something with those properties?". Therefore, AI deals with the problem of creating an "*intelligent agent*" [2].

An agent is an object that is able to *perceive* its environment through *sensors* and acting upon that environment through *effectors*. Human "agents" use their eyes, ears, skins…,etc as sensors and their hands, legs…,etc as effectors. On the other hands, robotic agents use cameras, infra-red detectors…, etc as sensors and motors, mechanical arms…,etc as effectors. While the brain is used in human agents to respond to the sensor's signal with an appropriate effectors signal, the software (*program*) embedded in the robotic processor (architecture) performs a similar task in connecting the robot's sensors with its effectors, and the main goal of AI is to elevate the interaction of robots to their environment to reach the level of the *rational* human interaction. It is also a part of the AI to make the agent more *autonomous*; i.e. behaving according to its *own experience* rather than on knowledge of the environment that has been built-in by the designer. Achieving these goals of AI requires the *design* of the "agent program" that runs on the computing device, that is called "architecture" and *learning* becomes an important design stage, and the process equation turns to be: *agent = architecture + program*.

The following sections will focus on two "*soft-computing program*" designs that are built in our agents to imitate the human agent's *mapping*. This mapping refers to the processing of the received *percepts* from the sensorial inputs (in our case, images represent the inputs that are captured using the computer vision systems described in the last chapter) and *generating actions* through the effectors (in our case, evaluation decisions on input materials represented in the form of an alarm signal or a signal that is directed to a mechanical arm that remove defective parts…, etc). The task of the soft-computing program is to replace the procedure of "looking-up table of actions" corresponding to a set of percepts; because the *table-driven-agents* are not intelligent enough to deal with different situations that pop-up in daily life's judgments.

3.2. Artificial Neural Networks (ANN):

It is believed for long time that the brain is the center of intelligence and thinking in human beings. Therefore a mathematical model for the operation of the brain is very important and will be introduced here after understanding the biological system and its simplest computing elements. The fundamental functional unit of the nervous system (including the brain as the center of thinking) is the neuron (nerve cell). Each neuron consists of a cell body that contains the nucleus and there is a number of fibers branching out from the cell body and called *dendrites* and a single long fiber called the *axon*. Dendrites branch around the cell in a network form and the axon stretches out for a long distance compared to the cell body. Eventually, the axon also

branches into strands and substrands that connect to the dendrites and cell bodies of other neurons. The connecting junction is called a *synapse* and each neuron forms synapses with anywhere from a dozen to a hundred thousand other neurons, as demonstrated in Figure 1.

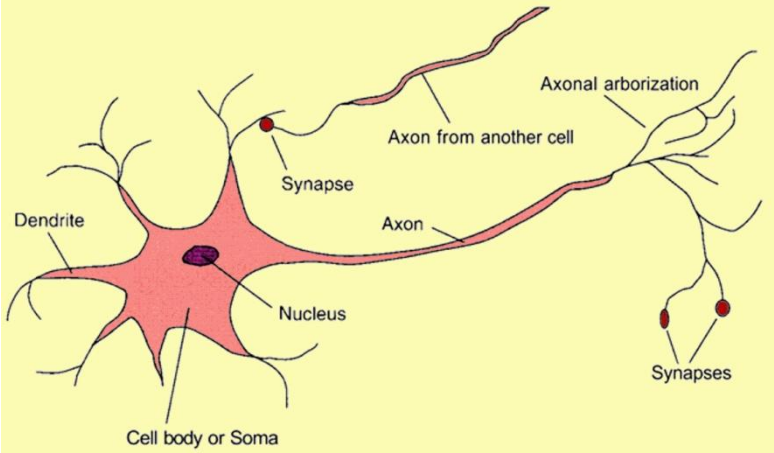

Figure 1. The parts of a nerve cell (or neuron). The length of the axon is usually about 100 times the diameter of the cell body (image reproduced from ref. [2])

Signals propagate from neuron to anther through electrochemical reactions where chemical transmitter substances are released from the synapses and enter the dendrite, raising or lowering the electrical potential of the cell body. When the potential reaches a *threshold*, an electrical pulse or *action potential* is sent down the axon. The pulse spreads out along the branches of the axon, eventually reaching synapses and releasing transmitters into the bodies of other cells. Synapses that increase the potential are called *excitatory*, and those that decrease it are called *inhibitory*. Neurons also form new connections with other neurons, and sometimes entire collections of neurons can migrate from one place to another and these mechanisms are thought to form the basis for learning in the brain and a collection of those neurons can lead to thought, action, and consciousness.

3.2.1. Neuron model

In biomimicry of the nervous system, the artificial neural network (ANN) appears as a mathematical representation for the neuron model. ANN is composed of a number of *nodes*, or *units*, connected by *links* and each link has a numeric *weight* associated with it. Weights are the primary means of long-term storage in neural networks, and *learning stage* usually takes place by updating these weights. Some of the units are connected to the external environment, and can be designated as *input* or *output* units. As demonstrated in Figure 2, each unit has: a set of *input links* from other units, a set of *output links* to other units, a current *activation level*, and a *means of computing* the activation level at the next step in time given its inputs and weights. Therefore, each unit does a local computation based on inputs from its neighbors, but without the need for any global control over the other units in the neural network. The design of a neural network for a specific task requires decisions on: how many units to be used, what kind of units are appropriate, and how the units are to be connected to form a network. After designing the

network architecture based on these questions, the weights of the network are *initialized* and a *learning algorithm* is used to *train* the *weights* based on a set of data for the task. It is also important to decide how to encode the data in terms of numeric inputs and outputs of the network.

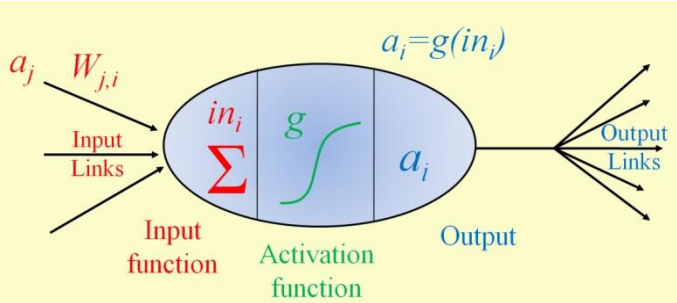

Figure 2. Simple computing unit (Node)

In artificial neurons, each unit performs a simple computation by receiving signals from its input links and computing a new activation level that is sent along each of the output links. The computation of the activation level is based on the values of each input signal received from the neighboring node and the weights on each input link. The computation in the neuron has a *linear component*, called the *input function* (in_i) that computes the *weighted sum* of the unit's input values. The neuron also has a *nonlinear component* called the *activation function* (g) that transforms the weighted sum into the final value that serves as the unit's *activation value* (a_i) and it is common to use the same activation function for all units in the network.

The total weighted input (in_i) is the sum of the input activations times their respective weights:

$$in_i = \sum_j W_{j,i} a_j = \boldsymbol{W_i} \cdot \boldsymbol{a_i} \qquad (1)$$

Where $\boldsymbol{W_i}$ denotes the weights on links into node *i*, and $\boldsymbol{a_i}$ refers to the set of input values for the i^{th} node, and the dot product denotes the sum of the pairwise products. The elementary computation step in each unit computes the new activation value for the unit by applying the activation function (g) to the result of the input function:

$$a_i = g(in_i) = g(\sum_j W_{j,i}\, a_j) \qquad (2)$$

There are different mathematical forms for the activation function (g), also called the *transfer function*, such as the step, sign, and sigmoid functions, as demonstrated Figure 3. The step function has a threshold *t* such that it outputs a 1 when the input is greater than its threshold, and outputs a 0 otherwise. The biological motivation is that a 1 represents the firing of a pulse down the axon, and a 0 represents no firing where the threshold represents the minimum total weighted input necessary to cause the neuron to fire.

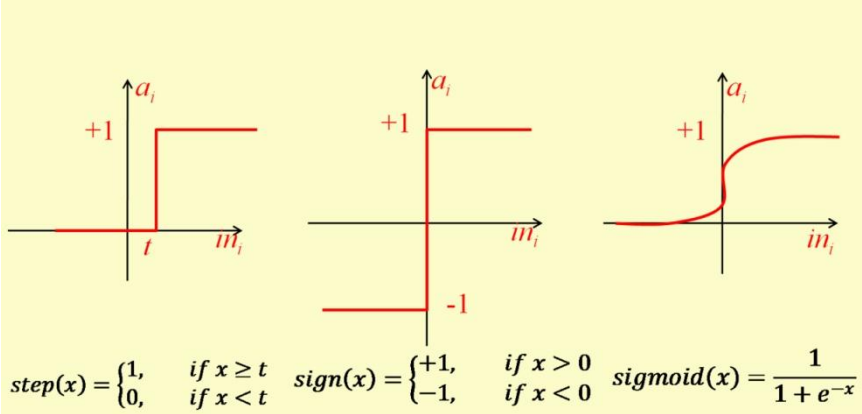

Figure 3. Three different activation (transfer) functions for neuron computational units

It is mathematically more convenient to replace the threshold with an extra input weight which allows for a simpler learning element because it needs only to worry about adjusting weights, rather than adjusting both weights and thresholds. Thus, instead of having a threshold t for each unit, we add an extra input whose activation a_0 is fixed at -1. The extra weight $W_{0,i}$ associated with a_0 serves the function of a threshold at t, provided that $W_{0,i}\ a_0 = -t$. Then all units can have a fixed threshold at 0. These two representations for thresholds are mathematically equivalent:

$$a_i = step_t\left(\sum_{j=1}^{n} W_{j,i}\ a_j\right) = step_0\left(\sum_{j=0}^{n} W_{j,i}\ a_j\right) \qquad (3)$$

Where $W_{0,i}=t$ and $a_0=-1$.

3.2.2. Network structures

There are different kinds of network structures that result in very different computational properties, and the most important structures that need to be distinguished are the *feed-forward* and the *recurrent* networks. In a feed-forward network, links are unidirectional, and there are no cycles, while in a recurrent network, the links can form any arbitrary topology. We usually deal with networks that are arranged in *layers*, and in a *layered feed-forward network*, each unit is linked only to units in the next layer; there are no links between units in the same layer, no links backward to a previous layer, and no links that skip a layer. The significance of the lack of cycles is that computation can proceed uniformly from input units to output units. The activation from the previous time step plays no part in the computation, because it is not fed back to an earlier unit. Hence, a feed-forward network simply computes a function of the input values that depends on the weight settings and it has no internal state other than the weights themselves. Figure 4 shows a simple example of a layered feed-forward network with two layers where the input units (square nodes) serve to pass activation to the next layer and may not be considered as an individual layer because no computations take place at these nodes.

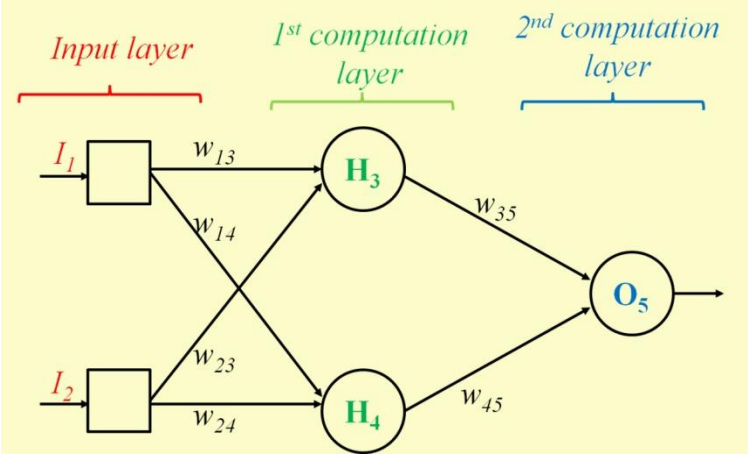

Figure 4. Layered feed-forward network

The activation value of each of the units in the input layer in Figure 4 is determined by the environment, and at the right-hand end of the network is the output unit that represents the effectors from the network model. In between, the nodes labelled H_3 and H_4, have no direct connection to the outside world and are called *hidden units*, because they cannot be directly observed by noting the input/output behavior of the network. Some networks, called *perceptrons*, have no hidden units and this simplifies their learning process, but it also means that perceptrons are very limited in what they can represent. Networks with one or more layers of hidden units are called *multilayer networks* and with one layer of sufficient number of hidden units it is possible to represent any continuous function of the inputs; while with two hidden layers it is also possible to represent discontinuous functions. The numbers of hidden layers and the units per layer are of great importance in the design of the ANN where too small network might be incapable of representing the desired function. On the other hand, too big networks tempt to *overfit* the data because there are too many parameters (i.e., weights) in the model and the ANN will memorize all the examples by forming a large lookup table and will not be able to generalize well to inputs that have not been seen before.

With a fixed structure and fixed activation functions g, the models represented by a feed-forward network are restricted to have a specific parameterized structure. The weights chosen for the network determine which of these models is actually represented. For example, the network in Figure 19.7 calculates the following function:

$$\begin{aligned} a_5 &= g\left(W_{3,5}\, a_3 + W_{4,5}\, a_4\right) \\ &= g\left(W_{3,5} g\left(W_{1,3} a_1 + W_{2,3} a_2\right) + W_{4,5} g\left(W_{1,4} a_1 + W_{2,4} a_2\right)\right) \end{aligned} \quad (4)$$

Where g is the activation function and a_i is the output of the i^{th} node.

It should be noticed that; because the activation functions *g* are nonlinear, the whole network represents a model of complex *nonlinear function* and if you think of the weights as *parameters* or *coefficients* of this nonlinear function, then the learning stage becomes a process of tuning these parameters to fit the data in the training set, analogically to the *nonlinear regression* modeling commonly used in statistics, and that is what ANN perform.

Although the biological neurons in our brains are not feed-forward networks, some regions of the brain are largely feed-forward and somewhat layered, but there are widespread back-connections and, therefore, the brain forms recurrent networks. Because activation is fed back to the units that caused it, recurrent networks have internal state stored in the activation levels of the units which means that computation can be less orderly than in feed-forward networks. Recurrent networks can become unstable, or oscillate, or exhibit chaotic behaviors and with a given set of inputs, it can take a long time to compute a stable output, and learning is made more difficult. On the other hand, recurrent networks can implement and model more complex designs and the *Hopfield networks* as well as the *Boltzmann machines* are two common examples of the recurrent networks that are used in such modeling.

3.2.3. Back-propagation learning

Learning in a feed-forward network with one computation layer (e.g. perceptrons) is a straight-forward process where the error (the difference between the network output and required target) is fed back to the network and the weights are adjusted to reduce this error. The problem, however, is to assess the blame for an error and divide it among the contributing weights and this is an easy task in perceptrons because there is only one weight between each input and the output. But in multilayer networks, there are many weights connecting each input to an output, and each of these weights contributes to more than one output. The back-propagation algorithm is a sensible approach to dividing the contribution of each weight where it provides a way of dividing the calculation of the gradient among the units, so the change in each weight can be calculated by the unit to which the weight is attached using only local information. Similar to the learning algorithm in the perceptron, back-propagation tries to minimize the error (*E*) between each target output (*T*) and the output actually computed by the network (*O*), that is:

$$E = \frac{1}{2}\sum_i (T_i - O_i)^2 \qquad (5)$$

This error function represents the *sum square error* which is selected because it allows easier differentiation in the next calculation steps. This error function can be expressed as a function of the weights by substituting the output value (*O*) in the previous equation, which can be expressed for a two-layer network as:

$$E = \frac{1}{2}\sum_i (T_i - g(\sum_j W_{j,i}\, a_j))^2$$
$$= \frac{1}{2}\sum_i (T_i - g(\sum_j W_{j,i}\, g(\sum_k W_{k,j}\, I_k)))^2 \quad (6)$$

Where I_k represent the k^{th} input to the network.

Notice that although the a_j term in the first line represents a complex expression, it does not depend on $W_{j,i}$. Also, only one of the terms in the summation over i and j depends on a particular $W_{j,i}$, so all the other terms are treated as constants with respect to $W_{j,i}$ and will disappear when differentiated. Hence, when we differentiate the first line with respect to $W_{j,i}$ we obtain:

$$\frac{\partial E}{\partial W_{j,i}} = -a_j (T_i - O_i) g'(\sum_j W_{j,i}\, a_j)$$
$$= -a_j (T_i - O_i) g'(in_i) = -a_j \Delta_i \quad (7)$$

With:

$$\Delta_i = (T_i - O_i) g'(in_i) = Err_i\, g'(in_i) \quad (8)$$

Therefore, the update rule for the weights in the output layer becomes:

$$W_{j,i}^{new} = W_{j,i}^{old} + \eta\, a_j\, \Delta_i \quad (9)$$

Where η is an arbitrary value that is called *the learning rate* and controls the speed of the network learning. For updating the connections between the input units and the hidden units, we need to define a quantity analogous to the error term for output nodes. Here is where we need the error back-propagation where the idea is that; hidden node j is "responsible" for some fraction of the error Δ_i in each of the output nodes to which it connects. Thus, the Δ_i values are divided according to the strength of the connection between the hidden node and the output node, and propagated back to provide the Δ_i values for the hidden layer. The propagation rule for the Δ_i values is the following:

$$\Delta_j = g'(in_j) \sum_i W_{j,i} \Delta_i \quad (10)$$

And the update rule for the weights leading into the layer becomes:

$$W_{k,j}^{new} = W_{k,j}^{old} + \eta\, I_k\, \Delta_j \quad (11)$$

Similar to the calculation of $W_{j,i}$, the derivation of the gradient error with respect to $W_{k,j}$ is slightly more mathematically involved, but has a similar result where:

$$\frac{\partial E}{\partial W_{k,j}} = -I_k \Delta_j \quad (12)$$

To obtain the update rules for the weights, we have to remember that the object is to *minimize* the error, so we need to take a small step in the direction opposite to the gradient.

As can be observed from this derivation, the derivative of the activation function *g* is required during the computation, so the *sign* and the *step* functions are not used in back-propagation networks. Back-propagation networks usually use the sigmoid function or some other variants that are easily differentiable. The *sigmoid* also has the convenient property that the derivative $g' = g(1 - g)$, so that little extra calculation is needed to find $g'(in_j)$.

3.2.4. Closing remarks on ANN

Although their popularity, artificial neural networks (ANN) still questionable as an optimum soft-computing method for machine learning and producing the required artificial intelligence. ANN can be evaluated from different points of view such as their:

- **Expressiveness**: Neural networks are attribute-based representations (i.e. most suitable for mapping continuous inputs and outputs), and do not have the expressive power of other logical representations (e.g. decision tree systems).
- **Computational efficiency**: Computational efficiency depends on the amount of computation time required to train the network to fit a given set of examples. If there are *m* examples, and $|W|$ weights, each training epoch takes $O(m|W|)$ time. However, work in computational learning theory has shown that the worst case number of epochs can be exponential in *n*, the number of inputs. In practice, time to convergence is highly variable, and vast arrays of techniques have been developed to try to speed up the process using tunable parameters. Local minima in the error surface are also a problem and at the cost of some additional computation, other techniques (e.g. simulated annealing method) can be used to assure convergence to a global optimum.
- **Generalization**: Neural networks can do a good job of generalization especially on functions for which they are well-suited. These seem to be functions in which the interactions between inputs are not too complicated, and for which the output varies smoothly with the input. There is no theorem to be proved here, but it does seem that neural networks have had reasonable success in a number of real-world problems.
- **Sensitivity to noise**: Because neural networks are essentially doing nonlinear regression, they are tolerant of noise in the input data. They simply find the best fit given the constraints of the network topology. On the other hand, it is often useful to have some idea of the degree of certainty of the output values and ANN do not provide probability distributions on the output values.
- **Transparency**: Neural networks are essentially black boxes, even if the network does a good job of predicting new cases, many users will still be dissatisfied because they will have no idea why a given output value is reasonable. If the output value represents, for example, a decision to perform open heart surgery, then an explanation is clearly in order. With decision trees and other logical representations, the output can be explained as a logical derivation and by appeal to a specific set of cases that supports the decision. This is not currently possible with neural networks.

- **Prior knowledge**: Learning systems can often benefit from prior knowledge that is available to the user or expert and prior knowledge can mean the difference between learning from a few well-chosen examples and failing to learn anything at all. Unfortunately, because of the lack of transparency, it is quite hard to use one's knowledge to "lead" a network to learn better.

All these considerations suggest that simple feed-forward networks, although very promising as construction tools for learning complex input/output mappings, do not fulfill our needs for a comprehensive theory of learning in their present form. Researchers in AI, psychology, theoretical computer science, statistics, physics, and biology are working hard to overcome these difficulties.

3.3. Modeling human judgment (fuzzy logic):

In situations where a great deal of human judgment must be made about a product or a system, most traditional models fail to fully characterize the nature of human judgment. In this case, a method of rule-based decision making should be used in conjunction with artificial intelligence systems and process control. The objective of this would be to emulate the thought process used by human beings. Such a method is now commonly known as 'fuzzy logic', a revolutionary approach to system identification and control pioneered by Lotfi Zadeh in 1965. Fuzzy Logic is a multivalued logic that allows intermediate values to be defined between conventional evaluations like yes/no, true/false, black/white…, etc. Notions like "rather warm" or "pretty cold" can be formulated mathematically and processed by computers. In this way an attempt is made to apply a more human-like way of thinking in the programming of computers. To realize the importance of the fuzzy logic and getting started with its terminology, it is important at the beginning to distinguish between the *crisp set* and the *fuzzy set* which will be defined in the following section.

3.3.1. Crisp and fuzzy sets

In classical mathematics we are familiar with what we call *crisp sets* which usually have "sharp" edges that identify the starting and ending points of a group (set) of points. The idea of crisp sets even consumes a lot of work with calculus beginners who start with learning the "limit" of a function and its continuity. A set of discrete points X for the first five integers is defined in mathematics as $X=\{1, 2, 3, 4, 5\}$ and any point does not belong to this group is outside the set X. The continuous set of numbers $Y = [1, 5]$ represents the same period and includes the natural numbers. These two sets are *crisp* in a way that the number 1.3 is not part of the set X (that is $1.3 \notin X$) while it belongs to Y ($1.3 \in Y$). Since Y is a "crisp" set, any value with any slightly lower value than 1 or slightly higher value than 5 will not belong to the set Y (therefore, $0.999 \notin Y$ and $5.001 \notin Y$). The two sets X and Y are graphically represented in Figure 5, where the vertical axes

in this figure represent the "membership (μ)" of a point on the horizontal axis to the required set. Any point that belongs to ($\in$) a set has a "full membership" with μ=1, and any point that does not belong to ($\notin$) a set has "no membership" with μ=0. Therefore, a "crisp set" can be defined as a set that has a "*binary membership*"; either μ=0 (no membership) or μ=1 (full membership). The principle of membership helps to define the set *X* mathematically as:

$$X = [x \mid P(x)] \tag{13}$$

That statement read as, the set *X* consists of all points *x* as long as the property *P*(*x*) holds true, and in this case the property *P*(*x*) is true when the membership $\mu(x)$=1.

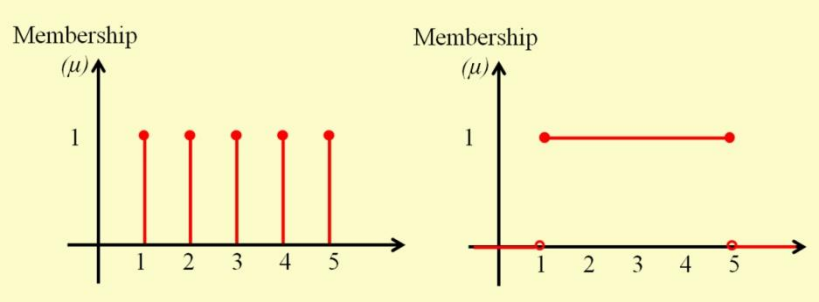

Figure 5. Membership representation to the set X={1, 2, 3, 4, 5} (left), and the set Y=[1, 5] (right)

The application of this crisp set in real life will be more complicated, because human have different sets that do not have such crisp edge; for example sets of: hot vs. cold, tall vs. short, young vs. old…, etc. Let us consider the age-set for "young" vs. "old" and consider the age of 20 years as a limit for a person to be consider as a "young". The representation of this set mathematically will be *Young* = [0, 20]; because the age starts at zero and we decided the limit for it to be 20 years old. The question for a person whose age is 15 years old will be very simple, and the answer definitely will be yes, this person belongs to the group of "young" people and his membership to this group will be μ=1. Similarly, a person with 20 years old will have membership μ=1 to the group of the "young" people. But in reality, it does not make sense for human to decide that a person on the day of being exactly 20 years old to be "young" and "not young" the next day. Human decisions about this problem tend to consider a person of even 21 years old to be "still young" or for someone of 25 years as "young enough". Therefore, the limit within the age-set between the "young" and the "old" is "*fuzzy*", not "crisp", and the membership to each set is "*continuous*", not "*binary*". The continuity of the membership suggests a "*membership function*" and any point *A* can take a value from zero to one; *i.e.* $\mu_A = [0, 1]$.

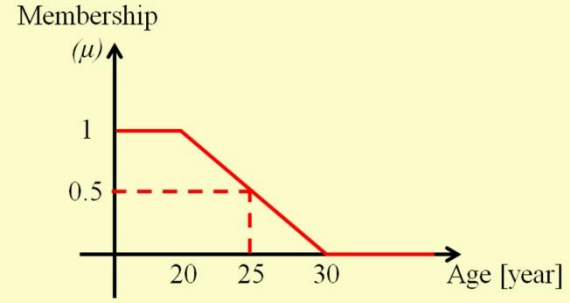

Figure 6. Membership function for the age-set of "young" people

A graphical representation for the principle of the "*fuzzy set*" of age-set and the membership function to the group of "young" people is demonstrated in Figure 6. Based on this figure, a person of age 25 years will be considered 50% belonging to the group of "young" people; and to describe this mathematically, we set the point A=25 and its membership $\mu(A) = \mu_A = 0.5$. Similarly, for a person of age 21 years: A=21 and $\mu(A) = \mu_A = 0.9$ that is he/she is 90% belonging to the group of "young" people. It is clear that, the membership function does not have to be linear as we considered in this example. In fact, membership function takes different shapes such as Gaussian, sigmoid, trapezoid, triangular…, etc. Setting the parameters of these membership functions allows the final decision for a point to resemble the human judgment about that point.

The concept of membership function is often confused with the probability concept. There is an obvious similarity between the two where both membership values and probability values exhibit a range from 0 to 1. However, the interpretation of this range of values is substantially different in the two cases. Fuzzy membership provides a measure of judgment, whereas the probability indicates the proportion of times the result is true or false in the long run. It is also crucial to understand that the fuzzy set theory is a means of specifying how well an object satisfies a *vague description*, not uncertainty about external world. For example, consider the proposition "Alex is tall", and the question: "Is this true, given that Alex is 175 cm?" Most people would hesitate to answer "true" or "false," preferring to say, "sort of." This is not a question of uncertainty about the external world, as we are sure of Alex's height, but it is a case of *vagueness* or *uncertainty* about the *meaning* of the *linguistic term* "tall".

3.3.2. Operations on Fuzzy Sets

Human used to apply some logical rules during their decision making and daily life judgments. We face many situations where our decisions should be made based on a "*logical sense*"; consider the tipping at a restaurant, for example, as a problem where you decide the amount of a tip based on the quality of food you eat. The logical rule for such problem will be: "if the food is

good, then tip is *high*". Notice the two "vague" and "fuzzy" terms used in this statement "good" and "high", and the questions "how good is good?" and "how high is high?" reflects back to the fuzzy logic. The application of fuzzy sets for this problem will make it easier to deal with this "uncertainty" of the limits and the vagueness of these terms.

This simple problem becomes more complicated as we consider other criteria in our judgment. For the same tipping problem, the logical rule in the human mind will consider not only the quality of food, but also the quality of service at the restaurant to determine the total amount of tip. The logical rule for the problem in this case will be: "if the food is *good* AND the service is *good*, then the tip is *high*". Notice the AND operator that is used to connect the two statements in our judgment, which poses the question of how to perform the "*logical operations*" (AND, OR, NOT) on fuzzy sets? In fuzzy logic terminology, these logical operations are defined as the "*fuzzy intersection*" or "*conjunction*" (AND), the "*fuzzy union*" or "*disjunction*" (OR), and the "*fuzzy complement*" (NOT). To perform these operations on fuzzy sets, the membership functions are subjected to some functions that replace the logical operators where: AND = *min* function, OR = *max*, and NOT = *additive complement*. This principle can be represented graphically for a two fuzzy intervals *A* and *B* where *A*= [5, 8] with a trapezoid membership function shown in Figure 7, and *B* = 4 with a triangular membership function shown in the same figure.

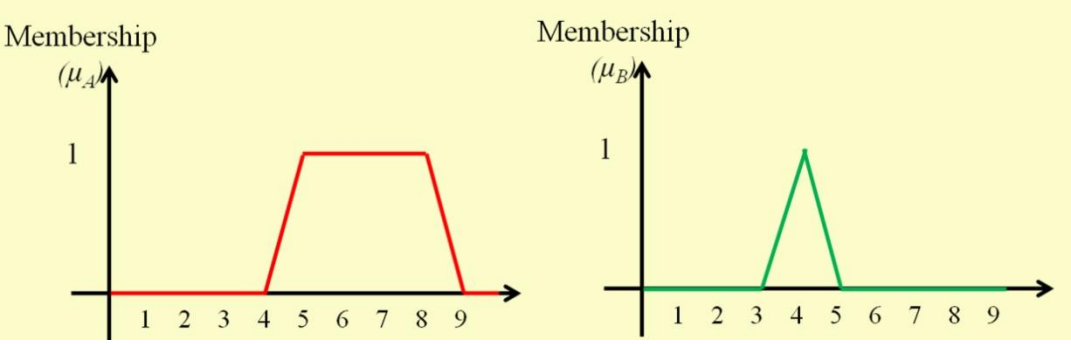

Figure 7. Membership functions for the fuzzy sets A=[5, 8] (left) and B=4 (right)

The application of the AND operator on both membership functions μ_A AND μ_B gives their intersection ($\mu_A \cap \mu_B$) and results in the can be obtained by applying the *minimum* function as shown in blue color at Figure 8.

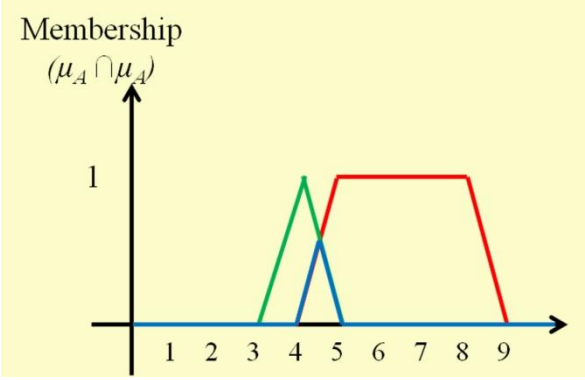

Figure 8. The AND operator applied on the two fuzzy sets A and B

The OR operator can be replaced with the *maximum* function and its application on the two fuzzy sets gives their union ($\mu_A \cup \mu_B$) as shown in blue color at Figure 9.

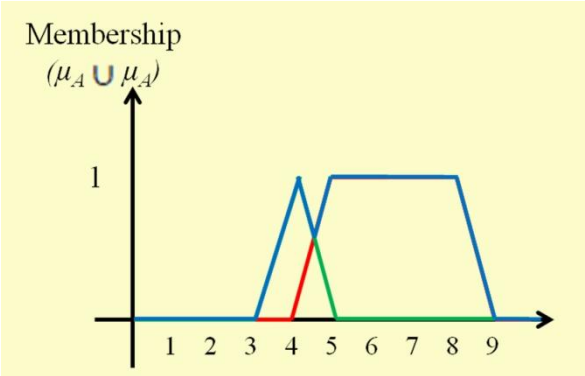

Figure 9. The OR operator applied on the two fuzzy sets A and B

Finally, the negation of the membership function μ_A can be seen as the blue curve in .

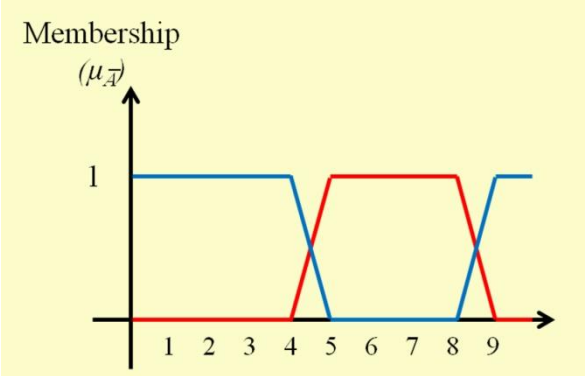

Figure 10. . The NOT operator applied on the fuzzy set A

The application of these principles and the fuzzy logic controller can be demonstrated with a practical textile example for a quantitative grading of cotton fibers using the fuzzy membership functions, based on the work presented by Elmoghazy [3] and explained in the following section.

3.3.3. Cotton grading

Cotton fiber is traditionally graded by subjective classing; in which a classer observes the appearance and the color of fibers and touches the fibers to determine their smoothness or roughness to the hand. Quantitatively, the color appearance is measured using color reflectance, *Rd*, and fiber roughness can be evaluated through testing a combination of parameters including fiber friction, bulk resiliency under cyclic pressing and un-pressing of the fibers, and the energy consumed to open the fiber bulk. This simple case illustrates the superiority of expert human judgment of certain phenomena to laboratory testing, as it takes many quantitative parameters and a significant amount of time to make a judgment of cotton grade that a classer can make in a few seconds. When a cotton classer observes, touches and handles the cotton sample, all these quantitative parameters come into play in a very complex interactive fashion that only the human brain supported by experience can comprehend. In recent years, efforts were made to convert subjective grading of cotton into instrumental grading. These efforts involved comparative analysis between subjective measures and instrumental measures, with expert classer opinion being one of the main references for calibrating the objective measures. This is a case where fuzzy logic analysis can be very useful as it can result in characterizing human judgment on the basis of a combination of expert opinion supported by instrumental grading.

To demonstrate the above point, let us take one of the quantitative parameters, say color reflectance, *Rd*, and assume that it is the only quantitative parameter required to make a judgment on the cotton grade. The traditional approach to relating the quantitative value (*Rd* values) to human judgment has been based on the discrete classification of the parameter of interest. For example, experts in the field may come together and establish the following criteria:

• Poor grade < 75 *Rd*, • Middle grade 75–80 *Rd*, • Good grade > 80 *Rd*

These criteria may be represented by the crisp set shown in Figure 11. The number zero is given for both poor and good grades, and the number 1.0 is given for middle grade cotton. This approach is very common in many human judgments owing to its simplicity. Indeed, people often use terms such as ‘good or bad’, and ‘true or false’ to characterize their judgments. The problem with this approach, however, is that it often masks a great deal of information and judgment resolution. A cotton classer being a human may easily judge extreme conditions such as extremely dark or extremely light color. As colors deviates from these extremes, human judgment may become progressively fuzzy. In this case, the crisp set with binary scoring may not be accurate.

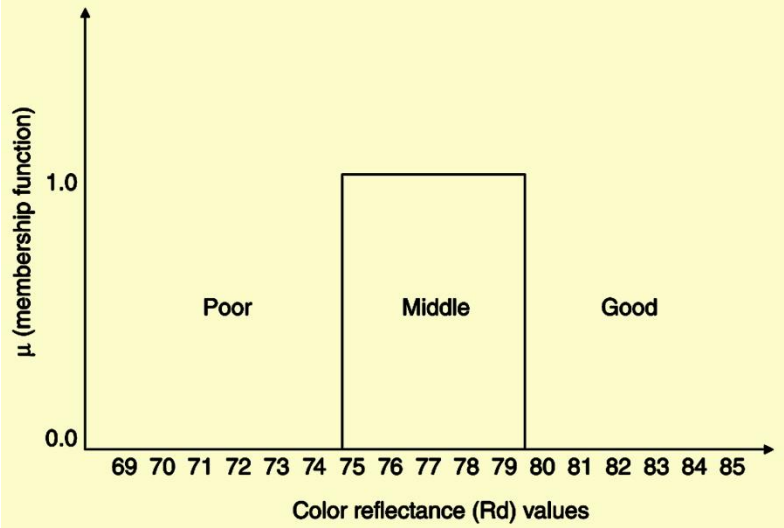

Figure 11. Crisp set–middle cotton grade (Reproduced from Ref. [3])

If the grading criteria of *Rd* listed above are accepted by experts, we will find that the classer's judgment of very poor and very good grades represent a clear cut. As we approach the middle grade from the low or the high value, different classers may have different opinions about whether the cotton is 'poor to middle', 'definitely middle' or 'middle to good'. This fuzziness can be resolved by the use of the fuzzy logic membership function. This is developed based on asking a panel of classing experts to vote on the matter. The fraction of the panel that regards cotton with a given *Rd* value as 'middle grade' will give a number from 0 and 1, which will indicate the strength of their judgment. An expert who examines a cotton sample of, say, 77 *Rd* value, may determine that it is too close to the poor category, but not close enough to be judged poor. In this case, he/she may give a number close to zero (say 0.3). This number implies the uncertainty of his/her judgment about how to consider this cotton sample, a 'middle' or 'poor grade'. Similarly, an expert who examines a cotton sample of, say, 79 *Rd* value, may determine that it is too close to the good category. As a result, he/she may again give a number close to zero; say 0.2 which implies a judgment uncertainty of middle grade. Finally, an expert who examines a cotton sample of, say, 78 *Rd* value, may determine that it is definitely middle-grade cotton and gives a number 1 or close to 1 (say, 0.8) to imply judgment certainty.

The above example illustrates one way in which fuzzy logic handles the extent of certainty of human judgment; it is through a continuous pattern, not a discrete pattern, of decision-making. The fuzzy set derived in this way is illustrated in Figure 12. It indicates a more resolute judgment, particularly in the representation of 'middle cotton grade'.

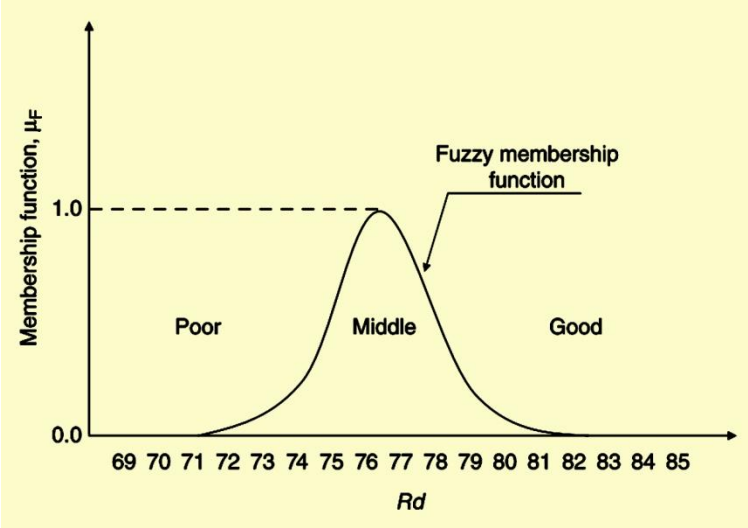

Figure 12. Fuzzy set–middle cotton grade (Reproduced from Ref. [3])

Fuzzy sets corresponding to poor or good grades might also be defined in the same way. This is illustrated in Figure 13 where the three sets developed overlap. This reflects the fact that a certain value of color reflectance may lead to a two-way judgment. The figure also indicates that there are no sharp changes in *Rd* groups. As *Rd* increases, membership of the 'good grade' gradually increases to 1.0; or as *Rd* decreases, membership of the 'poor grade' gradually declines to 0. Thus, each of the fuzzy sets described in Figure 13 can be regarded as the definition of a corresponding linguistic value, in this case 'poor grade', 'good grade' and 'middle grade'.

This point leads us to two different variables related to grade:

1. Color in *Rd*: a numerical variable with integer numerical values

2. Color group: a linguistic variable taking the linguistic values 'poor grade', 'good grade' and 'middle grade'.

In the context of determining cotton grade, color *Rd*, though numerical, represents the underlying measurement, which in this case drives everything else, but it is not easy to be interpreted. Color group, on the other hand, ranges over a more limited set of values. This makes it easier to comprehend and easier to use.

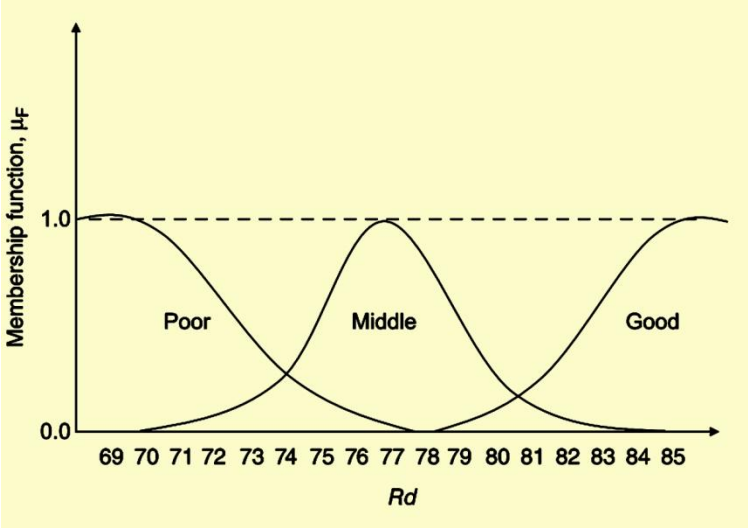

Figure 13. Fuzzy sets for cotton grade categories (Reproduced from Ref. [3])

This example illustrates the concept of membership function where, in practice, there are many parameters and many ways to characterize each parameter. In addition, parameters may indeed interact with one another leading to many decisions regarding the subjective measure. As we indicated earlier, cotton grade reflects many parameters that are interacting in a complex manner. Accordingly, the above approach should be expanded to accommodate all these parameters, individually and combined. This gives rise to a combination matrix of inputs, in response to which a fuzzy logic controller or a decision scheme can be developed.

It should be pointed out that the above example was only presented as a simple demonstration of some elements of fuzzy logic analysis. In recent years, fuzzy logic analysis has been used in numerous applications in which human judgment was accurately represented or simulated for control or modeling. In the area of developing fibrous products, many subjective phenomena such as appearance, hand and comfort can be characterized using fuzzy logic analysis.

References:

[1] G. F. Luger, *Artificial intelligence: structures and strategies for complex problem solving*. Pearson education, 2005.

[2] S. Russell and P. Norvig, *Artificial Intelligence: A Modern Approach, Third edition*. 2014.

[3] Y. Elmogahzy, *Engineering Textiles: Integrating the Design and Manufacture of Textile Products*. Elsevier Science, 2008.

PART II

Chapter 4

Chan-Vese Segmentation Model For Faster And Accurate Evaluation of Yarn Packing Density

Summary Sheet

- **Paper citation:**
  M. Eldessouki, S. Ibrahim, "Chan-Vese Segmentation Model For Faster And Accurate Evaluation of Yarn Packing Density," *(in press) Textile Research Journal*, 2014, DOI: 10.1177/0040517514557314.

- **Targeted problem:**
  The current methods of determining the yarn packing density have three main drawbacks; they are ***labor dependent***, they are ***time consuming***, and they ***approximate many parameters*** of the fibers and the yarn

- **Objective(s):**
  - Develop an algorithm for automating the segmentation of the yarn cross-sectional images
  - The algorithm should allocate yarn and fibers actual contours and the mass centers of fibers and the yarn
  - Calculation of the fibers radial distribution in the yarn cross-section
  - Calculation of the yarn's effective diameter
  - Calculation of the yarn's effective packing density
  - Simplify the calculation method in a user friendly graphical user interface (GUI)

- **Materials scope:**
  - Fibers of different cross-sectional shapes based on cellulosic materials (modal, viscose, and cotton)
  - Yarns produced using ring spinning technology

- **Computation method:**
  - Chan-Vese segmentation model
  - Level-set numerical methods

- **Paper significance:**
  - This work is the first in literature to implement an active contour method (such as Chan-Vese) for studying the yarn internal structure
  - The introduced method significantly reduces the time for measuring the yarn packing density compared to the traditional methods of measurement

- **Software**
  A software program with a user-friendly GUI was developed for this work and named "yarn packing density (YPD)". The YPD is available on the accompanied CD with a tutorial video demonstration. The program also has an image example on the CD so it can be tested. The program GUI is shown below:

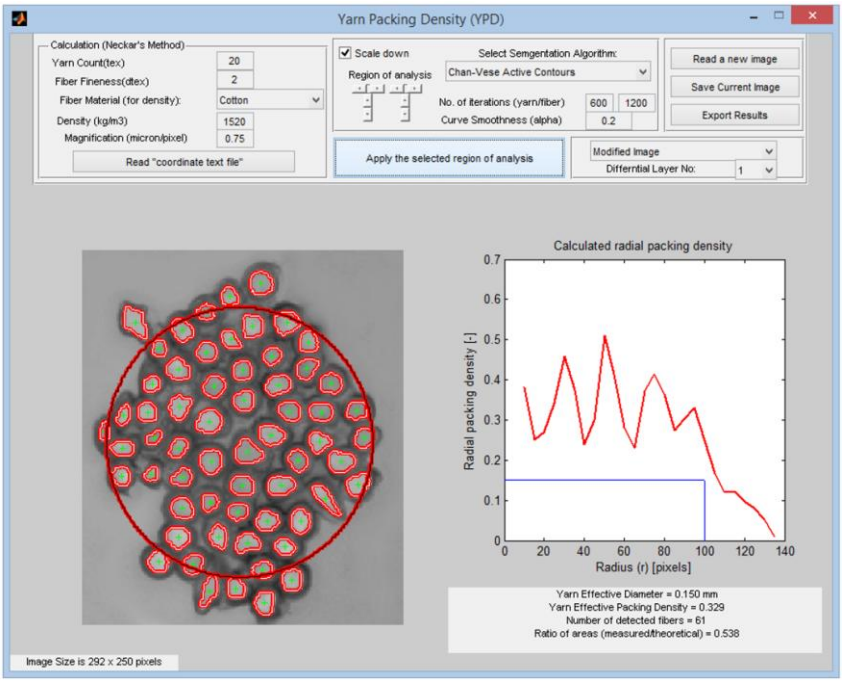

- **Comments:**

  The preparation of the yarn cross-section was described in the manuscript of this paper and the figure below shows graphically the sequence of these preparation steps (this figure is not part of the published manuscript and added here for clarity purposes).

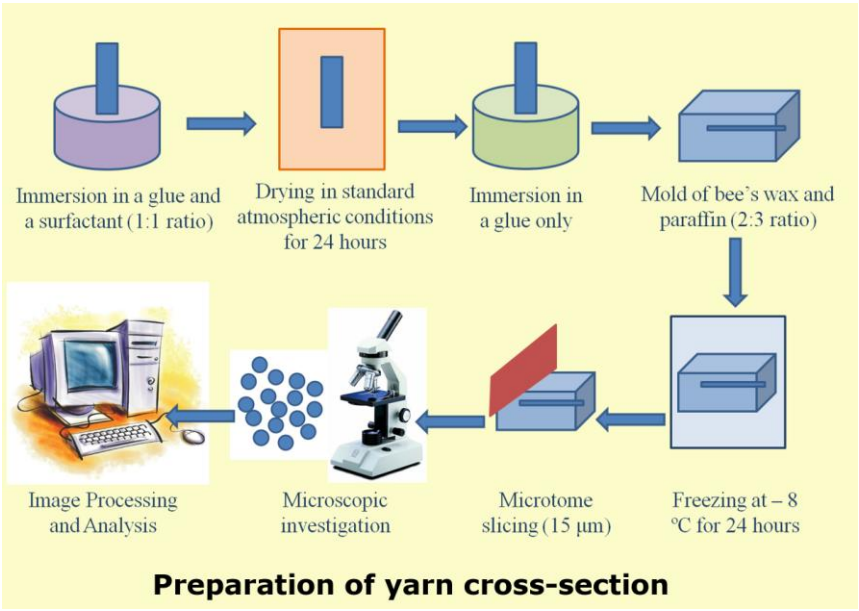

Chan-Vese Segmentation Model For Faster And Accurate Evaluation of Yarn Packing Density

Mohamed Eldessouki[1,2*], Sayed Ibrahim[3]

[1] *Technical University of Liberec, Faculty of Textile Engineering, Department Materials Engineering, Liberec, Czech Republic*

[2] *Mansoura University, Faculty of Engineering, Department of Textile Engineering, Mansoura, Egypt*

[3] *Technical University of Liberec, Faculty of Textile Engineering, Department Textile Technology, Liberec, Czech Republic*

* Corresponding author e-mail: eldesmo@auburn.edu

Abstract

Yarn packing density is an important parameter in correlating the internal structure of the yarn to its final properties and performance. The current methods of determining the yarn packing density have three main drawbacks; they are labor dependent, they are time consuming, and they approximate many parameters of the fibers and the yarn. The current work utilizes the Chan-Vese (CV) segmentation model to detect the actual contours of the yarn and the fibers inside its cross-section. This algorithm allows the automation of the process which reduces the time required for the analysis and makes it independent from the human element. The method also avoids the approximations involved in the traditional methods by calculating the actual areas of the fibers and the yarn which makes it more precise in determining the yarn packing density. A user friendly Graphical User Interface (GUI) was developed to utilize the CV algorithm and calculate different yarn parameters such as the yarn's radial packing density, the yarn's effective diameter, and the yarn's effective packing density. The area ratio factor (ARF) was used as a quick indicator of the accuracy of fiber segmentation. The CV algorithm was described in detail and tested with ring-spun yarns from different materials and the results were found to be in agreement with the reported values of such yarns. The introduced method can be extended to the evaluation of fibrous materials other than yarns.

1. Introduction:

Yarn packing density is a description of the internal yarn structure and the relative arrangement and distribution of fibers inside the yarn [1]–[3]. It is one of the major parameters that reflect the effect of yarn processing and technology on the yarn structure and its final properties [4]–[8]. Yarn packing density (μ) can be defined as the ratio between the fibers volume and the total volume of fibrous assembly, where $\mu \in <0,1>$. The fiber's *volume fraction* can be used alternatively in the literature to refer to the term *packing density*. Instead of its use in volumetric terms, it can also be interpreted as the ratio between the area of the fibers in a yarn cross-section (the substance area S_c) and the total cross-sectional area of yarn (S) that includes the substance area and the air-gaps between fibers. The cross-section can be divided into many annular rings

and the packing density of the individual sectors can be evaluated. The relationship expressing yarn packing density as a function of the radius (r) is called the radial packing density $\mu(r)$.

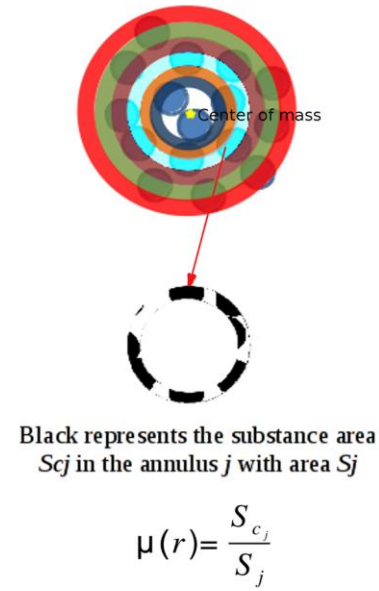

Figure 1. Calculation of the radial packing density

According to the Internal Standards IS 22-103-01/01 [9], the yarn packing density can be determined using two experimental methods which were found to be highly comparable; the direct method and the secant method. The direct method depends on tracing the borders of the fibers in the cross-sectional image using a special image processing software (*e.g.* LUCIA system) to create the real contours of the fibers. The center of gravity for each fiber is manually approximated in this method and the coordinates of these centers (x_i,y_i) are used to calculate the yarn center (x_0,y_0). The median of the centers' coordinates is used in determining the yarn center (rather than their arithmetic mean) because the median is not sensitive to the random positioning of the fibers. Rings of fixed thickness and centered at the calculated yarn center are constructed in the yarn image as shown in Figure 1 and the area of the fibers (S_{cj}) inside each ring (j) is calculated and divided by the area of the j^{th} ring to calculate the radial packing density (μ_r); that is:

$$\mu(r) = \frac{S_{c_j}}{S_j} \qquad (1)$$

The effective yarn diameter (d_{ef}) was found from the databases of measurements for different ring-spun and rotor-spun yarns that it corresponds to the yarn diameter at a radial packing density in the range between 0.15 and 0.17 [10], [11]. The effective yarn diameter can be estimated by interpolating the measured values of radial packing density $\mu(r)$ at the given packing density. The effective yarn packing density μ_{ef} can then be calculated as the ratio between the total fiber area (S_f) and the area of a circle with a diameter equals the calculated effective diameter (S_{ef}) as follows:

$$\mu_{ef} = \frac{S_f}{S_{ef}} \qquad (2)$$

The secant method, on the other hand, follows the same calculation procedures of the direct method but it does not use the actual shape of the fibers cross-section. The secant method substitutes the fibers with circles that are centered at the center of gravity of the individual fibers and having areas calculated from the fibers' fineness, density, position, and yarn twist. Secant method is suitable for cotton yarns or other highly twisted yarns, where it is difficult to recognize the individual contours of fiber. This procedure is not recommended, however, for yarns with a relatively high number of fibers in the cross-section (*e.g.* more than 200 fibers), unless all fiber contours can be focused during their imaging.

The above described methods of evaluation suffer from some corrections and approximations (such as the fibers' centers coordinates) that lead to less accurate values. Therefore, this work suggests a segmentation method that detects the actual geometries and cross sectional areas of the fibers and the yarn. The method detects the fibers and the yarn perimeters using automatic image processing and analysis techniques then allows the user to edit the detected edges for more precise adjustment. The suggested algorithm utilizes the detected images to calculate the yarn radial packing density, the effective yarn packing density, the effective yarn diameter, and the total number of fibers inside the yarn.

2. Methods:

Since the packing density is the ratio between the area of the fibers inside the yarn and the yarn's cross-sectional area, it is necessary to segment the image for calculating these two areas. Segmentation of images based on the *variational methods* [12] can be obtained by minimizing the appropriate cost functionals [13]. Therefore, for an image (I) with $I: \Omega \rightarrow \mathbb{R}$, where Ω is the image domain, the segmentation can be performed by evolving the regional contours of the image in the direction of negative energy gradient using appropriate partial differential equations (PDE). One of the first algorithms that utilizes variational methods was the *snakes algorithm*

[14] which introduces an explicit parametric curve $C: [0,1] \rightarrow \Omega$ to represent the region's contour. The parametric curve *C* evolves by locally minimizing the cost functional:

$$E(C) = -\int \mid \nabla I(C) \mid^2 ds + \nu_1 \int \mid C_s \mid^2 ds + \nu_2 \int \mid C_{ss} \mid^2 ds \qquad (3)$$

Where C_s and C_{ss} represent the first and second derivatives of the curve *C* with respect to the parameter *s*, respectively. The first term in equation (3) represents the *external energy* which accounts for the image information and called the *data term* while the last two terms can be interpreted as the *internal energy* and represents the *regularization terms* that account for the length of the contour and its stiffness.

In this study, the Chan-Vese (CV) model [15], [16] for active contours was used to detect the boundaries of the yarn in a given cross-sectional image. The CV model is based on techniques of *curve evolution*, *Mumford–Shah functional* for segmentation, and utilizes *level sets* [13], [17] to facilitate the solution [18]. In the level set formulation, the problem becomes a "*mean-curvature flow*" which results in evolving the active contour until a stop condition is met on the desired boundary. Because most classical snakes and active contour models rely on the edge-function (might be calculated from the image gradient $\mid \nabla I \mid$) to stop the curve evolution, these models can detect only objects with edges defined by a gradient. In the CV model, however, the stopping term is based on Mumford–Shah segmentation techniques and the model can, therefore, detect contours with or without gradient (for instance objects with very smooth boundaries or even with discontinuous boundaries). Also, the initial curve for the CV model can be anywhere in the image while interior contours are automatically detected [16].

2.1. Chan-Vese Segmentation Model

The objective of the Chan–Vese model is to partition the input image with a domain $\Omega \subset \mathbb{R}^n$ into two regions ($\Omega_1$and Ω_2), as shown in Figure 2, while maintaining two criteria; first, low intensity variance inside each region, second, a smooth boundary (Γ) between the regions. These regions can be defined as $\Omega_1 \subset \Omega$ and $\Omega_2 = \Omega \setminus \Omega_1$ while the boundary is defined as $\Gamma = \partial\Omega_1$.

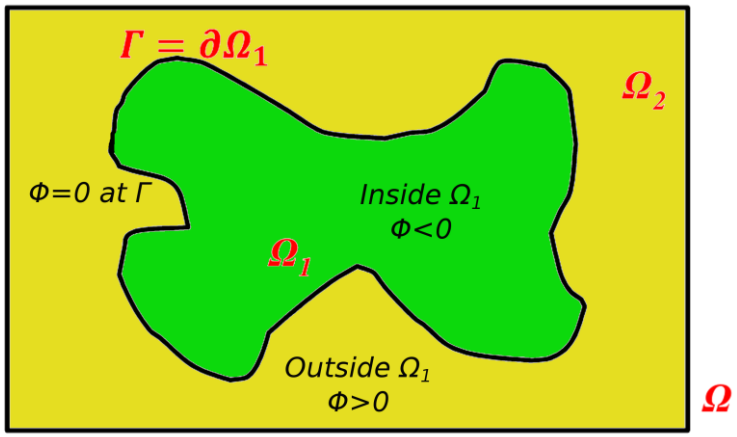

Figure 2. Chan-Vese Segmentation Model

To achieve this image partitioning, a cost (or objective) function is created and minimized. There are different models for the cost functions where the Mumford-Shah (MS) energy-based model was proven to be efficient. Based on the MS model, Chan and Vese suggested the following energy functional:

$$\xi(c_1, c_2, \Gamma) = \lambda_1 \int_{\Omega_1} | I_0(x,y) - c_1 |^2 \, dxdy + \lambda_2 \int_{\Omega_2} | I_0(x,y) - c_2 |^2 \, dxdy + \mu . length(\Gamma) + \nu . Area(inside(\Gamma)) \quad (4)$$

The energy (ξ) consists of two main terms; the *data* terms (the first two terms in equation (4)), and the *smoothness* or *curvature* terms (the last two terms in equation (4)). The "*data*" terms represent the energy inside and outside the curve Γ that evolutes during the calculation. This *data* part of the energy is the integration of the squared absolute difference between the intensity of the image at a pixel position x and y ($I_0(x,y)$) and the average intensity *inside* the region Ω_1 ($c_1 = [average(I_0)]_{\Omega_1}$) or the average intensity *outside* the region Ω_1 ($c_2 = [average(I_0)]_{\Omega \setminus \Omega_1}$). The *smoothness* terms represent penalty functions that force the curve towards the object inside the bounded region. $\lambda_1, \lambda_2, \mu, \nu$ are arbitrary positive constants that are

usually assigned the values $\lambda_1 = \lambda_2 = \lambda = 1$ and $\nu = 0$ while $\mu \geq 0$ is usually used according to the required smoothness level of the boundary curve. The constant ν was assigned to zero because the length and the area of Γ are comparable according to the isoperimetric inequality:

$$Area(inside(\Gamma)) \leq c.(length(\Gamma))^{\frac{N}{(N-1)}} \qquad (5)$$

Where: c is a constant that depends on the dimensionality N. The length of the curve can be expressed in the form:

$$length(\Gamma) = |\ \Gamma\ | = \int_{\Gamma}\ ds \qquad (6)$$

The energy functional ξ is called *curve evolution functional* because the regional contour Γ evolves in an active way during this functional minimization. Minimizing the functional ξ maintains the main criteria of the model; that is, the first criterion can be achieved by keeping the data terms at their minimum and the second criterion can be achieved by minimizing the smoothness terms. To solve this minimization problem for curve evolution, the *level set method* has been used extensively, because it allows for cusps, corners, and automatic topological changes [16].

2.2. Level set formulation:

The level set method [17] replaces the unknown curve $\Gamma \subset \Omega$ by the zero level-set of Lipschitz function $\phi: \Omega \rightarrow \mathbb{R}$ demonstrated in Figure 3 such that:

$$\phi(x,y) = \begin{cases} > 0 & (x,y) \in \Omega_1 \\ < 0 & (x,y) \in \Omega_2 \\ = 0 & (x,y) \in \Gamma \end{cases} \qquad (7)$$

Before substituting for the curve Γ in the energy functional, it can be noticed from equation (4) that the integration is performed over different regions. Therefore, the Heaviside function H is introduced and its derivative as the Dirac delta function δ_0 where:

$$H(z) = \begin{cases} 1, & if z \geq 0 \\ 0, & if z < 0 \end{cases}, \delta_0(z) = \frac{d}{dz} H(z) \qquad (8)$$

For the application of these functions during the computation, it is necessary to regularize them by their consideration over an infinitesimal interval $\epsilon \to 0$ that allows the continuity of the function over the domain. Therefore, the modified versions of the function H is denoted H_ϵ, which is continuous and has a derivative $\delta_\epsilon$as the.

Because the function ϕ has certain values at each region, taking it as an argument of the Heaviside function ($H(\phi(x,y))$) allows the integration over the whole image domain Ω instead of the integration over specific regions. Thus, each term of energy functional can be reformulated in terms of the level set function $\phi(x,y)$ as follows:

$$\int_{\Omega_1} | I_0(x,y) - c_1 |^2 \, dxdy = \int_{\Omega} | I_0(x,y) - c_1 |^2 \, H_\epsilon(\phi(x,y))dxdy \qquad (9)$$

$$\int_{\Omega_2} | I_0(x,y) - c_2 |^2 \, dxdy = \int_{\Omega} | I_0(x,y) - c_2 |^2 \, [1 - H_\epsilon(\phi(x,y))]dxdy \qquad (10)$$

$$length(\Gamma) = \int_{\Omega} | \nabla H_\epsilon(\phi(x,y)) | dxdy = \int_{\Omega} \delta_\epsilon(\phi(x,y)) | \nabla\phi(x,y) | dxdy \quad (11)$$

Therefore, by the application of the level set functions and unlike the expression of the energy functional $\xi(c_1, c_2, \Gamma)$ expressed in equation (4), the three integration terms of the energy functional turned to be integration on the same domain Ω as can be seen in the new equation for the energy which can be reformulated as:

$$\begin{aligned} \xi(c_1, c_2, \phi) = \lambda \int_{\Omega} & | I_0(x,y) - c_1 |^2 \, H_\epsilon(\phi(x,y))dxdy \\ + \lambda \int_{\Omega} & | I_0(x,y) - c_2 |^2 \, [1 - H_\epsilon(\phi(x,y))]dxdy \\ + \mu \int_{\Omega} & \delta_\epsilon(\phi(x,y)) | \nabla\phi(x,y) | dxdy \end{aligned} \qquad (12)$$

By minimizing the energy ($\xi \to 0$) and keeping the level set function ϕ fixed, it is possible from equation (12) to express the constants c_1 and c_2 as:

$$c_1 = \frac{\int_\Omega I_0(x,y)H_\epsilon(\phi(x,y))dxdy}{\int_\Omega H_\epsilon(\phi(x,y))dxdy},$$

$$\int_\Omega H_\epsilon(\phi(x,y))dxdy > 0 \text{ (i.e. non-empty } \Omega_1) \quad (13)$$

$$c_2 = \frac{\int_\Omega I_0(x,y)[1-H_\epsilon(\phi(x,y))]dxdy}{\int_\Omega [1-H_\epsilon(\phi(x,y))]dxdy},$$

$$\int_\Omega [1 - H_\epsilon(\phi(x,y))]dxdy > 0 \text{ (i.e. non-empty } \Omega_2) \quad (14)$$

To solve the minimization problem of ξ in equation (12), the constants c_1 and c_2 are kept constant and the associated Euler-Lagrange equation is deduced. Parameterizing the descent direction by an artificial time $t \geq 0$, the solution in terms of $\phi(t,x,y)$ can be determined as:

$$\frac{\partial \phi}{\partial t} = \delta_\epsilon(\phi)[\mu \text{div}(\frac{\nabla \phi}{|\nabla \phi|}) - \lambda(I_0 - c_1)^2 + \lambda(I_0 - c_2)^2] \quad (15)$$

2.3. Numerical Implementation of the Model

The regularized Heaviside function (H_ϵ) can be defined as:

$$H_\epsilon(\phi) = \frac{1}{2}(1 + \frac{2}{\pi}\tan^{-1}(\frac{\phi}{\epsilon})) \quad (16)$$

$$\delta_\epsilon(\phi) = H' = \frac{1}{\pi}\frac{\epsilon}{\epsilon^2 + \phi^2} \quad (17)$$

The solution for equation (15) can be accomplished numerically using the finite difference implicit scheme for discretization. Let the step in the space domain be the interval h and in the time domain be the interval Δt which allows the determination of the grid points $(x_i, y_j) = (ih, jh)$ for $1 \leq (i \text{ and } j) \leq M$ where M is the maximum number of grid points. Therefore, the function $\phi(t,x,y)$ can be approximated with ${}^n\phi_{i,j} = \phi(n\Delta t, x_i, y_j)$ with $n \geq 0$ being the total time and the initial condition ${}^0\phi = \phi_0$. Hence, equation (12) can be discretized in the form [16]:

$$\frac{{}^{n+1}\phi_{i,j} - {}^{n}\phi_{i,j}}{\Delta t} = \delta_h({}^{n}\phi_{i,j})\left[\frac{\mu}{h^2}({}^{x}\Delta_{-})\left(\frac{{}^{x}\Delta_{+}{}^{n+1}\phi_{i,j}}{\sqrt{\frac{({}^{x}\Delta_{+}{}^{n}\phi_{i,j})^2}{(h)^2} + \frac{({}^{n}\phi_{i,j+1} - {}^{n}\phi_{i,j-1})^2}{(2h)^2}}}\right)\right.$$
$$+\frac{\mu}{h^2}({}^{y}\Delta_{-})\left(\frac{{}^{y}\Delta_{+}{}^{n+1}\phi_{i,j}}{\sqrt{\frac{({}^{y}\Delta_{+}{}^{n}\phi_{i,j})^2}{(h)^2} + \frac{({}^{n}\phi_{i+1,j} - {}^{n}\phi_{i-1,j})^2}{(2h)^2}}}\right) \qquad (18)$$
$$\left.-\lambda(I_{0i,j} - c_1({}^{n}\phi))^2 + \lambda(I_{0i,j} - c_2({}^{n}\phi))^2\right]$$

Where:

$${}^{x}\Delta_{-}\phi_{i,j} = \phi_{i,j} - \phi_{i-1,j}, \quad {}^{x}\Delta_{+}\phi_{i,j} = \phi_{i+1,j} - \phi_{i,j}$$

$${}^{y}\Delta_{-}\phi_{i,j} = \phi_{i,j} - \phi_{i,j-1}, \; {}^{y}\Delta_{+}\phi_{i,j} = \phi_{i,j+1} - \phi_{i,j}$$

Equation (18) transformed equation (15) from a partial differential equation into a system of linear algebraic equations that can be solved using the iterative methods of linear algebra. For any input figure that needs to be segmented, the whole model can be applied and solved using the algorithm outlined in Figure 3.

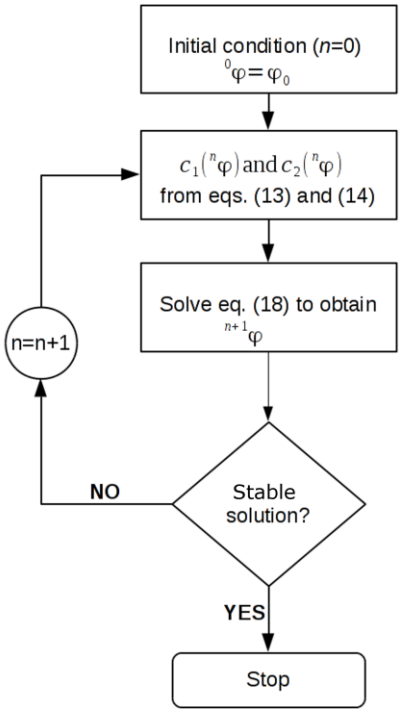

Figure 3. Numerical algorithm for implementing the CV model

3. Experimental setup:

Because some segmentation algorithms work better with synthetic fibers of circular cross-sections, three materials with different cross-sections, shown in Table 1, are used in this study to test the performance of the method. Ring-spun yarns were produced in different counts as listed in Table 1. The preparation of the yarn cross-section requires special care to preserve the twists and the shape of the yarn during its imaging. It is important to process the samples in a standard manner to maintain the repeatability of the results, hence the standard method "IS 46-108-01/01: Recommended procedure for preparation of samples, soft and hard sections (slices)" [19] was developed at the Technical University of Liberec for this purpose based on other standard methods (*e.g.* ČSN EN 12751 (80 0070)).

Table 1. Yarn and fiber specifications

Material	Yarn Count (tex)	Fiber Density (kg/m^3)	Fiber Fineness (dtex)	Fiber's cross-section
Lyocell	20	1500	1.5	
Viscose	16	1500	1.3	
Cotton	16	1520	1.7	

The standard preparation method can be briefly described as the yarn is soaked in a solution of a dispersion glue and a surfactant in a 1:1 concentration ratio. The 1,4-Bis(2-ethylhexyl) sulfosuccinate (also known as Spolion 8) surfactant was used as a dispersion and wetting agent in a concentration of 5 g/L. The applied glue was a universal Gama Fix Henkel which is available in office supply stores. After immersing the yarn in the mixed solution of the glue and the surfactant, the yarn sample is dried in standard atmospheric conditions for 24 hours. The yarn is then immersed only in the glue and dried at the same conditions. After getting dry, the yarn sample is embedded in a 2:3 mixture of bee's wax and paraffin, respectively, to form a mold block with dimensions of 3 x 1.5 cm. The sample mold is then left to solidify and placed in a freezer at – 8 ºC for 24 hours. After its hardening and solidification, the sample is ready for slicing into thin slices of 15 μm thickness using a microtome. The cross-sectional slice is then

placed on a transparent slide and the wax is dissolved by adding few drops of xylene. The image acquisition is performed using the CCD camera installed on a Nikon microscope and attached to a computer. The acquired images were enhanced by transforming the grayscale values using the "contrast-limited adaptive histogram equalization (CLAHE)" [20] algorithm. Three pictures of well focused samples were processed for each yarn to test the validity of the segmentation method.

4. Results and Discussion:

Samples of yarn cross-section are prepared as described in the experimental part and the yarn images are acquired using the camera on the microscope. The acquired yarn images are then introduced to the "Yarn Packing Density (YPD)" software, shown in Figure 4, that was developed to utilize the algorithms described above for calculation. The software reads the image and the user can select the whole image or assign a small region for analysis if the fibers are more concentrated at small part of the image.

4.1. Yarn contour:

Once the Chan-Vese (CV) model for segmentation is applied, the program starts with the outside borders of the image as initial conditions which allow the algorithm to stop at the outer contour lines of the yarn. The curve evolution of the algorithm at different iteration cycles is shown in Figure 5 which indicates that the algorithm was able to segment the picture in two regions that represent the image background and the yarn. The algorithm successfully segmented the image after about 300 iterations then no significant change in the yarn contour was detected. The time required for each iteration cycle and the total time required for segmenting the image depends on the image size and the hardware processing capabilities. It is, therefore, one of the drawbacks of this algorithm to take relatively long time during segmenting large size images and while researchers are trying to develop efficient algorithms to process massive amount of images [21], this algorithm depends on the image size and the available hardware resources to process the image. To accelerate the processing time of some large images, the program allows the user to choose scaling down the image. By scaling down the picture, the yarn image is resized and the segmentation algorithm is applied on the smaller version then the image is scaled-up again being ready for the next packing density calculations.

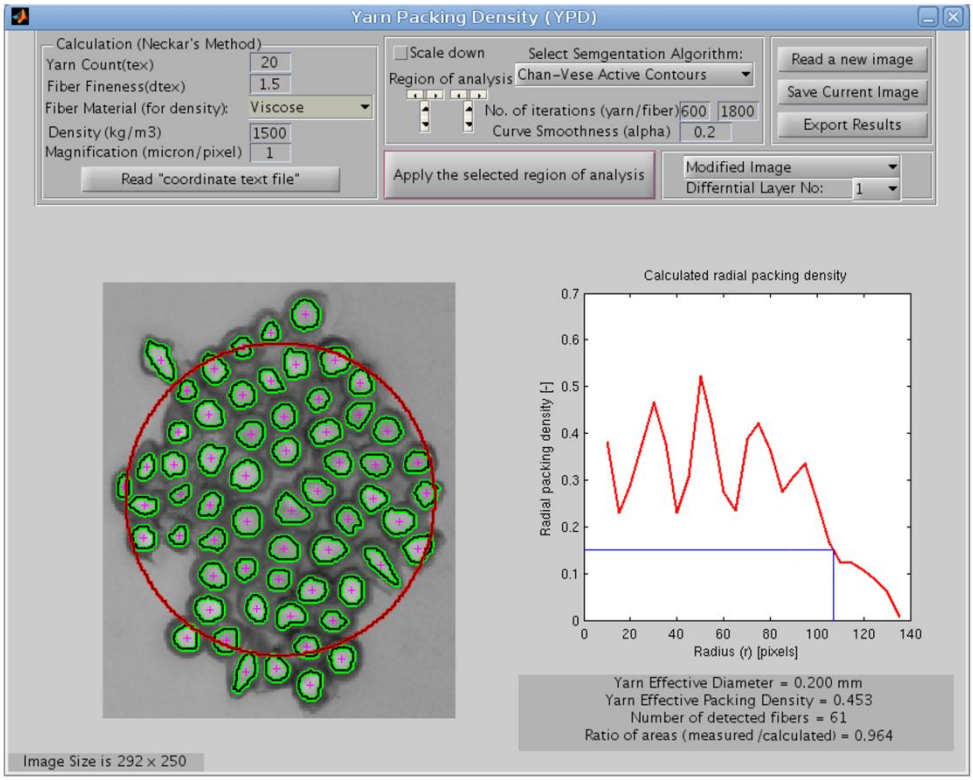

Figure 4. Developed GUI for implementing the CV-algorithm; Yarn Packing Density (YPD)

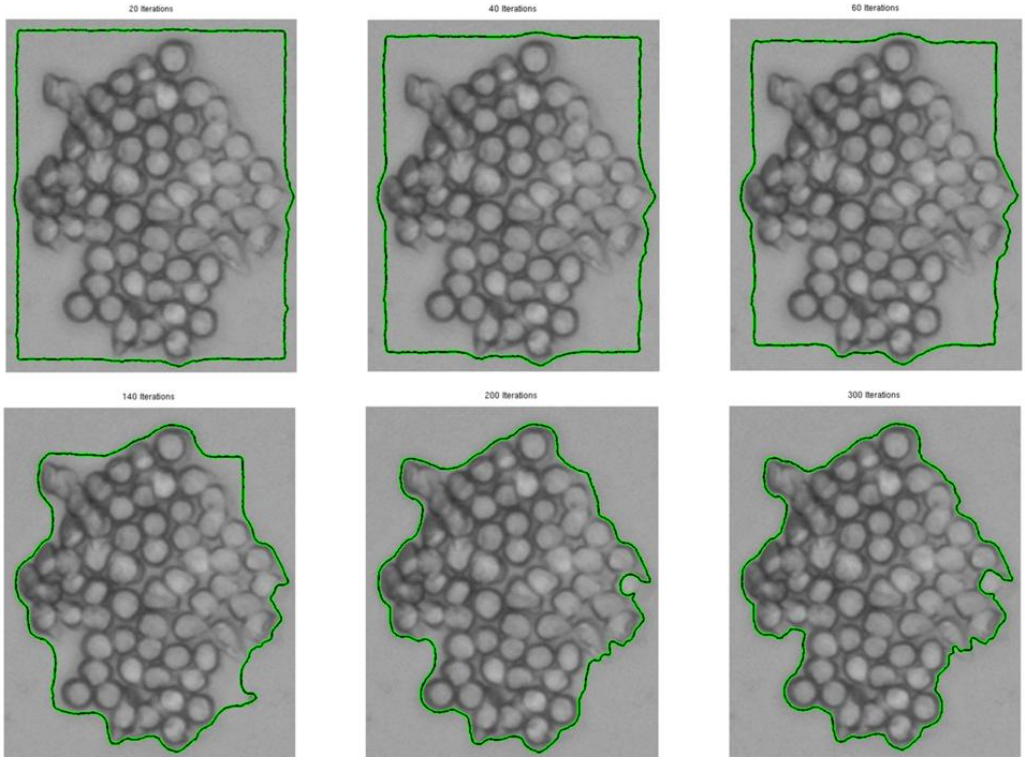

Figure 5. Curve evolution of the Chan-Vese (CV) algorithm at different iteration cycles

4.2. Fibers' contours:

After the determination of the yarn contour, the CV algorithm is applied again to determine the contours of the fibers inside the yarn cross-section. The initial condition for the fibers detection algorithm is a square approximated at the center of the image and propagates towards the edges of the yarn. The fiber detection takes more iteration cycles as the algorithm separates the image into many segments according to the number of fibers in the yarn cross-section. The detected fibers are shown in Figure 6 in binary format and highlighted with red color as superimposed to the yarn cross-sectional image. It can be noticed from this figure that the algorithm is successful in detecting the internal cross-section of the fibers while the walls of the fibers are considered as part of the space surrounding the fibers in the yarn. This can be considered as a source of error in determining the actual yarn packing density and it usually leads to lower values because the total fibers' area (the substance area) is decreased. On the other hand, the currently applied methods that approximate the yarn cross-section to a circle have a similar source of error by adding more area to the actual yarn cross-section. This source of error in the traditional method results in a similarity between the calculated values of our method and the traditional methods. It can also be noticed in Figure 6 that the utilized active contour method allows the detection of fibers with different cross-sectional areas which is not considered by the traditional methods (e.g. the secant method) that approximate the fibers cross-sections to circles with a constant diameter and area.

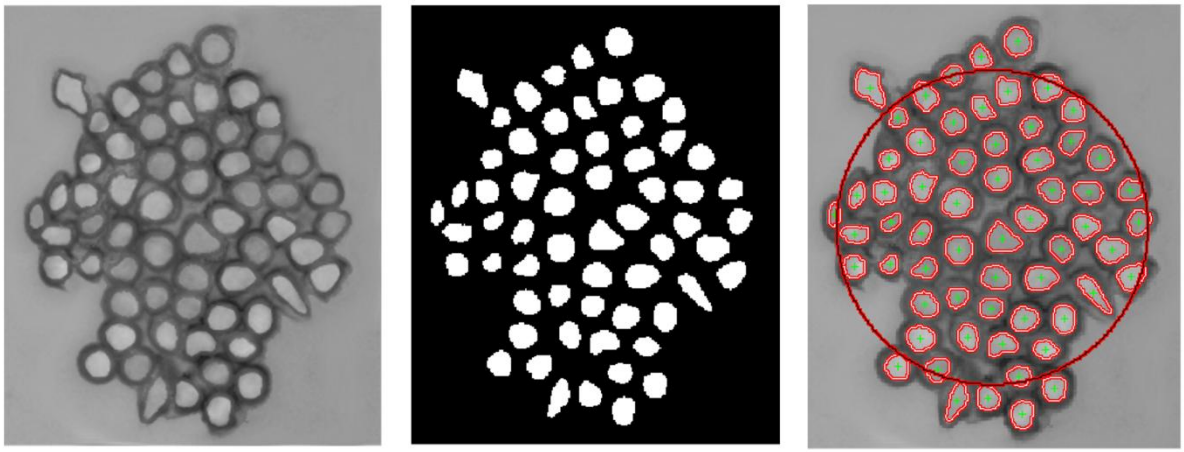

Figure 6. Lyocell yarn image (left); Detected fibers inside the yarn in binary format (middle); Highlight of the detected fibers (right) where the red circle shows the calculated effective yarn diameter, and the green points highlight the centres of the detected fibers

4.3. Packing density calculation:

Once the contours of the yarn and the fibers are detected, it is possible to calculate the radial packing density (μ_r). The process starts with calculating the yarn's center of gravity that is considered as the mass center of the object that represents the yarn and its coordinates (X_c, Y_c) is calculated from the constituent pixels of that object (X_i, Y_i). The mass center coordinates (X_c, Y_c) are calculated according to the following relation:

$$X_c = \frac{\sum_{i=1}^{n} A_i * X_i}{\sum_{i=1}^{n} A_i} \qquad Y_c = \frac{\sum_{i=1}^{n} A_i * Y_i}{\sum_{i=1}^{n} A_i} \qquad (19)$$

Where; n is the total number of pixels in the yarn object, A_i is the area of the i^{th} pixel that has coordinates (X_i, Y_i). Since all pixels having the same area, A_i is considered as one unit which makes the coordinate of the yarn's center as a mathematical mean of the coordinates of the pixels belonging to the yarn object.

The maximum diameter of the yarn object was then divided with equally displaced points which create concentric rings that are used in calculating the radial packing density. Examples of those rings are shown in Figure 7 where the areas of the fibers appear in the j^{th} ring are summed (S_{cj}) and divided by the area of that ring (S_j) to calculate the radial packing density (μ_r) as explained earlier in equation (1). The radial packing density can be plotted as a function of the radius as shown in the right bottom graph of Figure 4 which allows the determination of the yarn effective diameter (d_{ef}) by interpolating the radial packing density at 0.15. The estimated effective diameter for the studied yarn was determined to be about 0.20 mm. The effective yarn packing density μ_{ef} was calculated as the ratio between the total fiber area (S_f) and the area of the circle of effective diameter (S_{ef}) and was found to be 0.453.

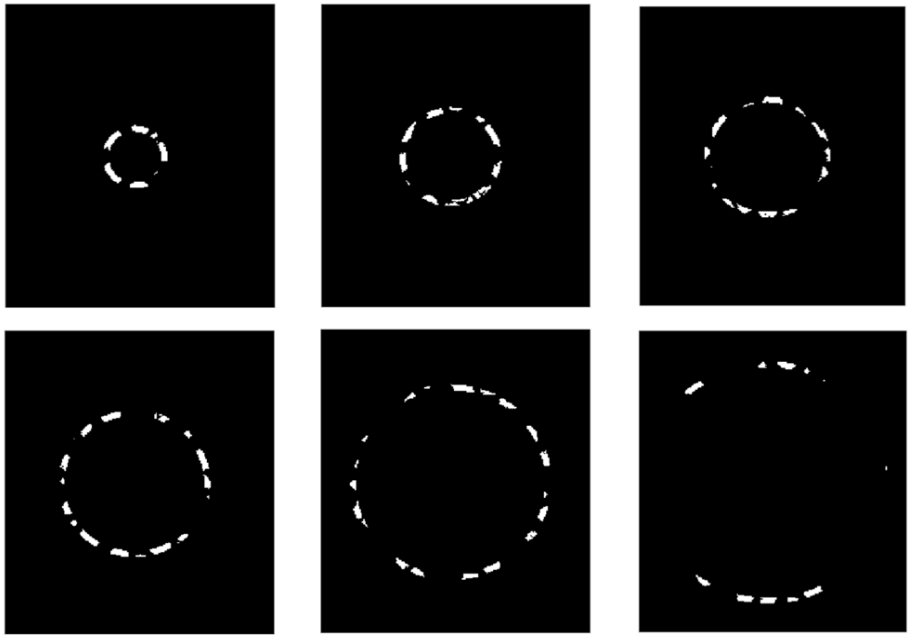

Figure 7. Examples of annular rings that are considered for calculating the yarn radial packing density

To check the accuracy of the measured area of the fibers, the area ratio factor (ARF) was used which can be defined as:

$$ARF = \frac{S_{meas.}}{S_{theor.}} \qquad (20)$$

Where $S_{meas.}$ is the area measured from the yarn picture and its segmentation. $S_{theor.}$ is the theoretical area of the substance (*i.e.* without voids or spaces between fibers) inside the yarn diameter. The $S_{theor.}$ can be calculated from the yarn and fiber parameters introduced in Table 1 as follow:

$$S_{theor.} = \frac{T_{yarn}}{\rho_{fiber}} . \kappa \qquad (21)$$

Where T_{yarn} is the yarn count, ρ_{fiber} is the fiber density, and κ is a conversion factor that depends on the image resolution and the units used. Since the theoretical area ($S_{theor.}$) is calculated from the yarn count and the fiber density, this area corresponds to the area of the material inside the yarn regardless of the distribution of this material (i.e. the area of the material regardless of the air gaps between the fibers or even the distribution of the fibers inside the yarn). The calculated ARF for the Lyocell yarn is 0.964 which means that the measured area is slightly lower than the theoretical area of the fibers inside the yarn. This result is expected as the segmentation algorithm does not consider the fiber's wall as part of the fiber, as mentioned earlier, which

affects the accuracy of the measured area. Considering this source of error, the measured area is still in a reasonable range.

4.4. Other yarn case studies:

A similar discussion can be extended to the other two yarn types (viscose and cotton), and their results are summarized in Table 2 while their images are demonstrated in Figure 8. It can be seen in Figure 8-b that some viscose fibers were considered as one big fiber during segmentation which is revealed to the shape of the yarn and the processing algorithm. It was shown earlier that the calculation algorithm segments the image in two stages; the first to detect the yarn contour and the second to detect the fibers inside the yarn. During the first stage and according to the yarn shape, more than one object can be detected in the image where, for example, the big blob fibers shown in Figure 8-b are relatively far from the main object where most of the fibers are concentrated. In the case of multiple objects produced during the first stage of yarn contour determination, the algorithm considers the object of the biggest area as the yarn body that will be processed during the second stage of fiber segmentation. Therefore, according to the yarn structure and the distribution of the fibers in the yarn cross-section, the fiber objects that may be relatively far from the main yarn body will not be processed during fiber segmentation which results in the less segmented fibers shown in Figure 8-b.

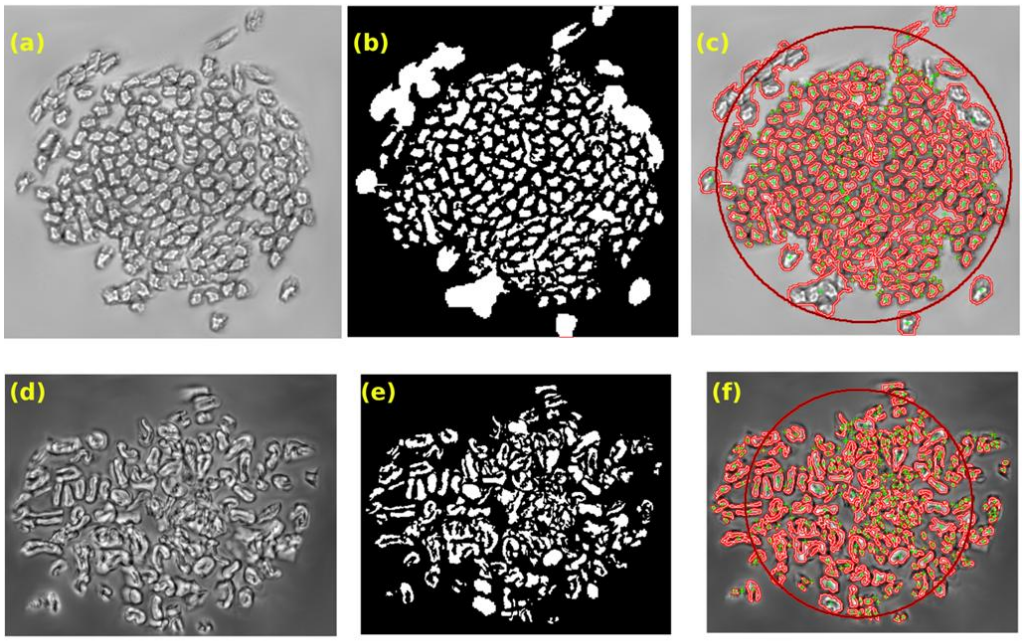

Figure 8. Cross-sectional image of viscose yarn (a) and cotton yarn (d); Segmented fibers in binary format for viscose (b) and cotton (e); Highlight of the detected fibers in the viscose yarn (c) and cotton yarn (f). The red circles in (c) and (f) have diameters of the calculated effective yarn diameter and the green points highlight the centres of the detected fibers.

Table 2. Average results of the measured samples

Yarn	Calculated Effective Diameter (mm)	Calculated Effective Packing Density	Area Ratio Factor (ARF)
Lyocell	0.200	0.453	0.964
Viscose	0.160	0.414	0.893
Cotton	0.155	0.387	0.785

The area ratio factor (ARF) for the measured samples is listed in Table 2 and can be used to quickly indicate if there is suspected sources of error during the segmentation. The lowest ARF value was found in cotton yarn samples which can be explained by the cross-sectional shape of the cotton fibers which is distinguished by the kidney shape with the lumen of the fiber at the middle as shown in Figure 8-d. By examining the binary image for the segmented cotton fibers in Figure 8-e, it can be seen that the segmentation algorithm subtracts the area of the internal fiber lumen from the total area of the fiber which results in less value of the measured area ($S_{meas.}$) and lower ARF value.

Due to the sample size limitations, it is important to notice that the resulting packing density values are not statistically significant and should not be considered as final values for these yarns. For the results to be significant, many cross-sectional samples at different positions along the yarn should be captured and analyzed. However, the quality of cross-sections during their slicing interferes with the imaging system and usually results in out-of-focus images that need extra processing and limits the number of high quality pictures that can be analyzed. Therefore, the small sample size used in the current analysis was applied to only verify the validity of the segmentation method and to get indicative numbers of the measured yarn parameters to have some insights about the system's constraints. It was observed that, the quality of the imaging system and the careful sample preparation are very important factors in deciding the reliability of the calculated results. The calculated packing densities of the given yarns (although need more samples for verification) are comparable to the results calculated using traditional methods for yarns of similar counts [11], [22], [23]. This agreement, however, contradicts our expectations of getting packing density values higher than the values obtained from traditional methods that add extra porosity to the yarn structure by considering a circular cross-sectional shape of the yarn. It

can be explained, on the other hand, by the decreased area of fibers detected by the automated CV segmentation method that does not consider the wall of the fiber (e.g. the Lyocell case) or the lumen (e.g. the cotton case) as parts of the total area of the fiber and, therefore, it is important to consider some correcting factors that compensate for this source of error after fiber segmentation. No correction factors were applied on the given results but it is pointed out here as a possibility for modifying the results.

5. Conclusion:

The Chan-Vese (CV) model was utilized to segment objects in the yarn cross-section to help detecting the actual contours of both the yarn and its constituent fibers. The detected yarn contour allows the use of the actual yarn cross-sectional shape which differs from the approximated circular contours that are considered in the conventional methods for calculating the yarn packing density. The area ratio factor (ARF) results have shown a deviation from the ideal ARF value (where ARF=1) due to the cross-section nature of each segmented fiber's type. One drawback of the introduced algorithm is its inability, with the given conditions, to consider the total area of the fiber (where the walls or the lumen of the fiber can be excluded) which results in lower calculated values of packing density. These low values, however, were found to be comparable to the results of the traditional methods as these methods approximate the yarn cross-section to a bigger circle. By considering the actual yarn contour (rather than its circular approximation), the measured packing density of the current samples is expected to be higher than the produced values. Generally, the segmentation method presented in this work was found to be faster and more reproducible than the traditional methods of calculating the packing density. Since this method is principally an image segmentation model that can be used to separate the fibers from the background, the method can be extended to segment different fibrous structures to calculate their porosity and packing density. Finally, the sample preparation and the quality of imaging system were found to be crucial factors in producing reliable results and the authors are currently working on alternative methods for image acquisition to be able to obtain enough sample size that produce statistically significant results.

References:

[1] R. H. Driscoll and R. Postle, "Modelling the Distribution of Fibres in a Yarn," *Journal of the Textile Institute*, vol. 79. pp. 140–143, 1988.

[2] D. Petrulis and S. Petrulyté, "Properties of close packing of filaments in yarn," *Fibres Text. East. Eur.*, vol. 11, no. 1, pp. 16–20, 2003.

[3] S. Zheng, Z. Zou, W. Shen, and L. Cheng, "A study of the fiber distribution in yarn cross section for vortex-spun yarn," *Text. Res. J.*, vol. 82, no. 15, pp. 1579–1586, 2012.

[4] P. S. Gracie, "Twist geometry and twist limits in yarns and cords," *J. Text. Inst. Trans.*, vol. 51, no. 7, pp. T271–T288, 1960.

[5] S. L. Phoenix, "Statistical theory for the strength of twisted fiber bundles with applications to yarns and cables," *Text. Res. J.*, vol. 49, no. 7, pp. 407–423, 1979.

[6] B. Neckář, "Compression and packing density of fibrous assemblies," *Text. Res. J.*, vol. 67, no. 2, pp. 123–130, 1997.

[7] A. Kumar, S. M. Ishtiaque, and K. R. Salhotra, "Study of effect of spinning process variables on the packing density of ring, rotor and air-jet yarns using the Taguchi method," *Autex Res. J.*, vol. 16, no. 3, p. T122, 2006.

[8] A. Kumar, S. M. Ishtiaque, and A. Das, "Impact of yarn extension on packing density of ring spun yarn," *Fibers Polym.*, vol. 13, no. 8, pp. 1071–1078, 2012.

[9] T. U. Liberec, "Yarn Packing Density, Direct method and Secant method," *Intern. Stand. Tech. Univ. Lib.*, pp. IS 22–103–01/01, 2004.

[10] B. Neckář, *Yarn forming, structure, properties.* Praha, Czech Republic: SNTL, 1990.

[11] D. Yilmaz, F. Goktepe, O. Goktepe, and D. Kremenakova, "Packing Density of Compact Yarns," *Textile Research Journal*, vol. 77. pp. 661–667, 2007.

[12] A. Mitiche and I. Ben Ayed, *Variational and level set methods in image segmentation*, vol. 5. Springer, 2010.

[13] D. Cremers, M. Rousson, and R. Deriche, "A Review of Statistical Approaches to Level Set Segmentation: Integrating Color, Texture, Motion and Shape," *International Journal of Computer Vision*, vol. 72. pp. 195–215, 2007.

[14] M. Kass, A. Witkin, and D. Terzopoulos, "Snakes: Active contour models," *Int. J. Comput. Vis.*, vol. 1, no. 4, pp. 321–331, 1988.

[15] T. Chan and L. Vese, "An active contour model without edges," in *Scale-Space Theories in Computer Vision*, Springer, 1999, pp. 141–151.

[16] T. F. Chan and L. A. Vese, "Active contours without edges," *Image Process. IEEE Trans.*, vol. 10, no. 2, pp. 266–277, 2001.

[17] S. Osher and R. P. Fedkiw, "Level Set Methods: An Overview and Some Recent Results," *J. Comput. Phys.*, vol. 169, pp. 463–502, 2001.

[18] X.-F. Wang, D.-S. Huang, and H. Xu, "An efficient local Chan–Vese model for image segmentation," *Pattern Recognit.*, vol. 43, no. 3, pp. 603–618, Mar. 2010.

[19] T. U. Liberec, "Recommended procedure for preparation of Samples, Soft and Hard sections (slices)," *Intern. Stand. Tech. Univ. Lib.*, pp. IS 46–108–01/01, 2004.

[20] E. D. Pisano, S. Zong, B. M. Hemminger, M. DeLuca, R. E. Johnston, K. Muller, M. P. Braeuning, and S. M. Pizer, "Contrast limited adaptive histogram equalization image processing to improve the detection of simulated spiculations in dense mammograms.," *J. Digit. imaging Off. J. Soc. Comput. Appl. Radiol.*, vol. 11, pp. 193–200, 1998.

[21] M. Eldessouki, S. Ibrahim, and J. Militky, "A Dynamic and Robust Image Processing Based Method for Measuring Yarn Diameter and Its Variation," *(In Press. Text. Res. Journal, DOI 10.1177/0040517514530032*.

[22] X. Y. Jiang, J. L. Hu, K. P. S. Cheng, and R. Postle, "Determining the cross-sectional packing density of rotor spun yarns," *Text. Res. J.*, vol. 75, no. 3, pp. 233–239, 2005.

[23] M. Salehi and M. S. Johari, "Study of fiber packing density of lyocell ring-spun yarns," *J. Text. Inst.*, vol. 102, no. 5, pp. 389–394, 2011.

Original article

Textile Research Journal

Textile Research Journal 0(00) 1–11

DOI: 10.1177/0040517514557314
trj.sagepub.com
SAGE

Chan-Vese segmentation model for faster and accurate evaluation of yarn packing density

Mohamed Eldessouki[1,2] and Sayed Ibrahim[3]

Abstract

Yarn packing density is an important parameter in correlating the internal structure of the yarn to its final properties and performance. The current methods of determining the yarn packing density have three main drawbacks: they are labor dependent, they are time consuming, and they approximate many parameters of the fibers and the yarn. The current work utilizes the Chan-Vese (CV) segmentation model to detect the actual contours of the yarn and the fibers inside its cross-section. This algorithm allows the automation of the process which reduces the time required for the analysis and makes it independent from the human element. The method also avoids the approximations involved in the traditional methods by calculating the actual areas of the fibers and the yarn which makes it more precise in determining the yarn packing density. A user-friendly graphical user interface (GUI) was developed to utilize the CV algorithm and calculate different yarn parameters such as the yarn's radial packing density, the yarn's effective diameter, and the yarn's effective packing density. The area ratio factor (*ARF*) was used as a quick indicator of the accuracy of fiber segmentation. The CV algorithm was described in detail and tested with ring-spun yarns from different materials and the results were found to be in agreement with the reported values of such yarns. The introduced method can be extended to the evaluation of fibrous materials other than yarns.

Keywords

chan-Vese model, radial packing density, segmentation, yarn effective packing density, yarn cross-sectional image analysis

Yarn packing density is a description of the internal yarn structure and the relative arrangement and distribution of fibers inside the yarn.[1–3] It is one of the major parameters that reflect the effect of yarn processing and technology on the yarn structure and its final properties.[4–8] Yarn packing density (μ) can be defined as the ratio between the fibers volume and the total volume of fibrous assembly, where $\mu < 0,1 >$. The fiber's *volume fraction* can be used alternatively in the literature to refer to the term *packing density*. Instead of its use in volumetric terms, it can also be interpreted as the ratio between the area of the fibers in a yarn cross-section (the substance area S_s) and the total cross-sectional area of yarn (S) that includes the substance area and the air-gaps between fibers. The cross-section can be divided into many annular rings and the packing density of the individual sectors can be evaluated. The relationship expressing yarn packing density as a function of the radius (r) is called the radial packing density $\mu(r)$.

According to the Internal Standards IS 22-103-01/01,[9] the yarn packing density can be determined using two experimental methods which were found to be highly comparable: the direct method and the secant method. The direct method depends on tracing the borders of the fibers in the cross-sectional image using a special image processing software (e.g. LUCIA system) to create the real contours of the fibers. The center of gravity for each fiber is manually approximated in this method and the coordinates of these centers (x_i, y_i) are used to calculate the yarn center (x_o, y_o). The median of the centers' coordinates is used in determining the yarn center (rather than their arithmetic mean) because the median is not sensitive to the random positioning of the fibers. Rings of fixed thickness and centered at the calculated yarn center are constructed in the yarn image as shown in Figure 1 and the area of the fibers (S_{ij}) inside each ring (j) is calculated and divided by the area of the jth ring to calculate the radial packing density (μ_r), that is

$$\mu(r) = \frac{S_{ij}}{S_j} \tag{1}$$

The effective yarn diameter (d_{ef}) was found from the databases of measurements for different ring-spun and rotor-spun yarns that it corresponds to the yarn diameter at a radial packing density in the range between 0.15 and 0.17.[10,11] The effective yarn diameter can be estimated by interpolating the measured values of radial packing density $\mu(r)$ at the given packing density. The effective yarn packing density μ_{ef} can then be calculated as the ratio between the total fiber area (S_f) and the area of a circle with a diameter equals the calculated effective diameter (S_{ef}) as follows:

$$\mu_{ef} = \frac{S_f}{S_{ef}} \tag{2}$$

The secant method, on the other hand, follows the same calculation procedures of the direct method but it does not use the actual shape of the fiber's cross-section. The secant method substitutes the fibers with circles that are centered at the center of gravity of the individual fibers and having areas calculated from the fibers' fineness, density, position, and yarn twist. Secant method is suitable for cotton yarns or other highly twisted yarns, where it is difficult to recognize the individual contours of fiber. This procedure is not recommended, however, for yarns with a relatively high number of fibers in the cross-section (e.g. more than 200 fibers), unless all fiber contours can be focused during their imaging.

The above-described methods of evaluation suffer from some corrections and approximations (such as the fibers' centers coordinates) that lead to less accurate values. Therefore, this work suggests a segmentation method that detects the actual geometries and cross sectional areas of the fibers and the yarn. The method detects the fibers and the yarn perimeters using automatic image processing and analysis techniques then allows the user to edit the detected edges for more precise adjustment. The suggested algorithm utilizes the detected images to calculate the yarn radial packing density, the effective yarn packing density, the effective yarn diameter, and the total number of fibers inside the yarn.

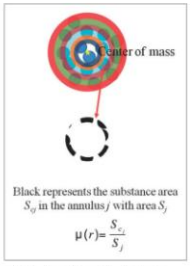

Figure 1. Calculation of the radial packing density.

Methods

Since the packing density is the ratio between the area of the fibers inside the yarn and the yarn's cross-sectional area, it is necessary to segment the image for calculating these two areas. Segmentation of images based on the *variational methods*[12] can be obtained by minimizing the appropriate cost functionals.[13] Therefore, for an image (I) with $I : \Omega \to \mathbb{R}$, where Ω is the image domain, the segmentation can be performed by evolving the regional contours of the image in the direction of negative energy gradient using appropriate partial differential equations (PDEs). One of the first algorithms that utilizes variational methods was the *snakes algorithm*,[14] which introduces an explicit parametric curve $C : [0, 1] \to \Omega$ to represent the region's contour. The parametric curve C evolves by locally minimizing the cost functional:

$$E(C) = -\int |\nabla I(C)|^2 \mathrm{d}s + \nu_1 \int |C_s|^2 \mathrm{d}s + \nu_2 \int |C_{ss}|^2 \mathrm{d}s. \tag{3}$$

where C_s and C_{ss} represent the first and second derivatives of the curve C with respect to the parameter s, respectively. The first term in equation (3) represents the *external energy* which accounts for the image information and called the *data term* while the last two terms can be interpreted as the *internal energy* and represents the *regularization terms* that account for the length of the contour and its stiffness.

In this study, the Chan-Vese (CV) model[13,16] for active contours was used to detect the boundaries of the yarn in a given cross-sectional image. The CV model is based on techniques of *curve evolution*, *Mumford–Shah functional* for segmentation, and utilizes *level sets*[15,17] to facilitate the solution.[18] In the level set formulation, the problem becomes a "*mean-curvature flow*" which results in evolving the active contour until a stop condition is met on the desired boundary. Because most classical snakes and active contour models rely on the edge function (might be calculated from the image gradient $|\nabla I|$) to stop the curve evolution, these models can detect only objects with edges defined by a gradient. In the CV model, however, the stopping term is based on Mumford–Shah segmentation techniques and the model can, therefore, detect contours with or without gradient (for instance, objects with very smooth boundaries or even with discontinuous boundaries). Also, the initial curve for the CV model can be anywhere in the image while interior contours are detected automatically.[16]

CV segmentation model

The objective of the CV model is to partition the input image with a domain $\Omega \subset \mathbb{R}^n$ into two regions (Ω_1 and Ω_2), as shown in Figure 2, while maintaining two criteria: first, low-intensity variance inside each region; second, a smooth boundary (Γ) between the regions. These regions can be defined as $\Omega_1 \subset \Omega$ and $\Omega_2 = \Omega \setminus \Omega_1$ while the boundary is defined as $\Gamma = \partial\Omega_1$.

To achieve this image partitioning, a cost (or objective) function is created and minimized. There are different models for the cost functions where the Mumford-Shah (MS) energy-based model was proven to be efficient. Based on the MS model, Chan and Vese suggested the following energy functional:

$$\xi(c_1, c_2, \Gamma) = \lambda_1 \int_{\Omega_1} |I_0(x,y) - c_1|^2 \mathrm{d}x\,\mathrm{d}y + \lambda_2 \int_{\Omega_2} |I_0(x,y) - c_2|^2 \mathrm{d}x\,\mathrm{d}y + \mu.length(\Gamma) + \nu.Area(inside(\Gamma)). \tag{4}$$

The energy (ξ) consists of two main terms: the *data* terms (the first two terms in equation (4)), and the *smoothness* or *curvature* terms (the last two terms in equation (4)). The "*data*" terms represent the energy inside and outside the curve Γ that evolutes during the calculation. This *data* part of the energy is the integration of the squared absolute difference between the intensity of the image at a pixel position x and y ($I_0(x, y)$) and the average intensity *inside* the region Ω_1 ($c_1 = [average(I_0)]_{\Omega_1}$) or the average intensity *outside* the region Ω_2 ($c_2 = [average(I_0)]_{\Omega\setminus\Omega_1}$). The *smoothness* terms represent penalty functions that force the curve towards the object inside the bounded region. Here $\lambda_1, \lambda_2, \mu, \nu$ are arbitrary positive constants that are usually assigned the values $\lambda_1 = \lambda_2 = \lambda = 1$ and $\nu = 0$ while $\mu \geq 0$ is usually used according to the required smoothness level of the boundary curve. The constant ν was assigned to zero because the length and the area of Γ are comparable according to the isoperimetric inequality:

$$Area(inside(\Gamma)) \leq c \cdot (length(\Gamma))^{\frac{N}{N-1}} \tag{5}$$

where c is a constant that depends on the dimensionality N. The length of the curve can be expressed in the form:

$$length(\Gamma) = |\Gamma| = \int_\Gamma ds \tag{6}$$

The energy functional ξ is called *curve evolution functional* because the regional contour Γ evolves in an active way during this functional minimization. Minimizing the functional ξ maintains the main criteria of the model; that is, the first criterion can be achieved by keeping the data terms at their minimum and the second criterion can be achieved by minimizing the smoothness terms. To solve this minimization problem for curve evolution, the *level set method* has been used extensively, because it allows for cusps, corners, and automatic topological changes.[16]

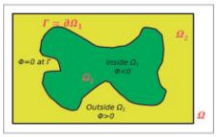

Figure 2. CV segmentation model.

Level set formulation

The level set method[17] replaces the unknown curve $\Gamma \subset \Omega$ by the zero level-set of Lipschitz function $\phi : \Omega \to \mathbb{R}$ demonstrated in Figure 3 such that

$$\phi(x,y) = \begin{cases} > 0 & (x,y) \in \Omega_2 \\ < 0 & (x,y) \in \Omega_1 \\ = 0 & (x,y) \in \Gamma \end{cases} \tag{7}$$

Before substituting for the curve Γ in the energy functional, it can be noticed from equation (4) that the integration is performed over different regions. Therefore, the Heaviside function H is introduced and its derivative as the Dirac delta function δ_0 where

$$H(z) = \begin{cases} 1, & \text{if } z \geq 0 \\ 0, & \text{if } z < 0 \end{cases} \cdot \delta_0(z) = \frac{d}{dz}H(z) \tag{8}$$

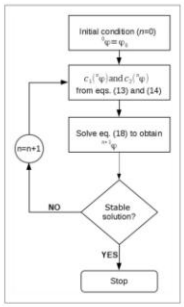

Figure 3. Numerical algorithm for implementing the CV model.

For the application of these functions during the computation, it is necessary to regularize them by their consideration over an infinitesimal interval $\epsilon \to 0$ that allows the continuity of the function over the domain. Therefore, the modified version of the function H is denoted H_ϵ, which is continuous and has a derivative δ_ϵ.

Because the function ϕ has certain values at each region, taking it as an argument of the Heaviside function ($H(\phi(x, y))$) allows the integration over the whole image domain Ω instead of the integration over specific regions. Thus, each term of energy functional can be reformulated in terms of the level set function $\phi(x, y)$ as follows:

$$\int_{\Omega_1} |I_0(x,y) - c_1|^2 \mathrm{d}x\,\mathrm{d}y = \int_\Omega |I_0(x,y) - c_1|^2 H_\epsilon(\phi(x,y))\mathrm{d}x\,\mathrm{d}y \tag{9}$$

$$\int_{\Omega_2} |I_0(x,y) - c_2|^2 \mathrm{d}x\,\mathrm{d}y = \int_\Omega |I_0(x,y) - c_2|^2 [1 - H_\epsilon(\phi(x,y))]\mathrm{d}x\,\mathrm{d}y \tag{10}$$

$$length(\Gamma) = \int_\Omega |\nabla H_\epsilon(\phi(x,y))|\mathrm{d}x\,\mathrm{d}y = \int_\Omega \delta_\epsilon(\phi(x,y))|\nabla\phi(x,y)|\mathrm{d}x\,\mathrm{d}y \tag{11}$$

Therefore, by the application of the level set function, and unlike the expression of the energy functional $\xi(c_1, c_2, \Gamma)$ expressed in equation (4), the three integration terms of the energy functional turned to be integration on the same domain Ω as can be seen in the new equation for the energy which can be reformulated as

$$\xi(c_1, c_2, \phi) = \lambda \int_\Omega |I_0(x,y) - c_1|^2 H_\epsilon(\phi(x,y))\mathrm{d}x\,\mathrm{d}y + \lambda \int_\Omega |I_0(x,y) - c_2|^2 [1 - H_\epsilon(\phi(x,y))]\mathrm{d}x\,\mathrm{d}y + \mu \int_\Omega \delta_\epsilon(\phi(x,y))|\nabla\phi(x,y)|\mathrm{d}x\,\mathrm{d}y \tag{12}$$

By minimizing the energy ($\xi \to 0$) and keeping the level set function ϕ fixed, it is possible from equation (12) to express the constants c_1 and c_2 as

$$c_1 = \frac{\int_\Omega I_0(x,y) H_\epsilon(\phi(x,y))\mathrm{d}x\,\mathrm{d}y}{\int_\Omega H_\epsilon(\phi(x,y))\mathrm{d}x\,\mathrm{d}y}, \quad \int_\Omega H_\epsilon(\phi(x,y))\mathrm{d}x\mathrm{d}y > 0 \text{ (i.e. non} - \text{empty } \Omega_1) \tag{13}$$

[1]Technical University of Liberec, Faculty of Textile Engineering, Department Materials Engineering, Liberec, Czech Republic.
[2]Mansoura University, Faculty of Engineering, Department of Textile Engineering, Mansoura, Egypt.
[3]Technical University of Liberec, Faculty of Textile Engineering, Department Textile Technology, Liberec, Czech Republic

Corresponding author:
Mohamed Eldessouki, Department Materials Engineering, Technical University of Liberec Studentská, 2 461 17 Liberec 1, Liberec, Czech Republic.
Email: eldesmo@auburn.edu

$$c_2 = \frac{\int_\Omega I_0(x,y)[1 - H_\varepsilon(\phi(x,y))]\mathrm{d}x\mathrm{d}y}{\int_\Omega [1 - H_\varepsilon(\phi(x,y))]\mathrm{d}x\mathrm{d}y} \quad (14)$$
$$\int_\Omega [1 - H_\varepsilon(\phi(x,y))]\mathrm{d}x\mathrm{d}y > 0 \text{ (i.e. non} - \text{empty } \Omega_1)$$

To solve the minimization problem of ξ in equation (12), the constants c_1 and c_2 are kept constant and the associated Euler–Lagrange equation is deduced. Parameterizing the descent direction by an artificial time $t \geq 0$, the solution in terms of $\phi(t, x, y)$ can be determined as

$$\frac{\partial \phi}{\partial t} = \delta_\varepsilon(\phi)\left[\mu \mathrm{div}\left(\frac{\nabla \phi}{|\nabla \phi|}\right) - \lambda(I_0 - c_1)^2 + \lambda(I_0 - c_2)^2\right] \quad (15)$$

Numerical implementation of the model

The regularized Heaviside function (H_ε) can be defined as

$$H_\varepsilon(\phi) = \frac{1}{2}\left(1 + \frac{2}{\pi}\tan^{-1}\left(\frac{\phi}{\varepsilon}\right)\right) \quad (16)$$

$$\delta_\varepsilon(\phi) = H' = \frac{\varepsilon}{\pi\varepsilon^2 + \phi^2} \quad (17)$$

The solution for equation (15) can be accomplished numerically using the finite difference implicit scheme for discretization. Let the step in the space domain be the interval h and in the time domain be the interval Δt which allows the determination of the grid points $(x_i, y_j) = (ih, jh)$ for $1 \leq (i \text{ and } j) \leq M$ where M is the maximum number of grid points. Therefore, the function $\phi(t, x, y)$ can be approximated with ${}^n\phi_{i,j} = \phi(n\Delta t, x_i, y_j)$ with $n \geq 0$ being the total time and the initial condition ${}^0\phi = \phi_0$. Hence, equation (15) can be discretized in the form:[16]

$$\frac{{}^{n+1}\phi_{i,j} - {}^n\phi_{i,j}}{\Delta t} = \delta_\varepsilon({}^n\phi_{i,j})\left[\frac{\mu}{h^2}({}^t\Delta_-)\right.$$
$$\times \left(\frac{{}^s\Delta_+{}^{n+1}\phi_{i,j}}{\sqrt{\frac{({}^t\Delta_+{}^n\phi_{i,j})^2}{\omega^2} + \frac{({}^s\Phi_{i+1,j} - {}^n\phi_{i,j})^2}{(2h)^2}}}\right)$$
$$+ \frac{\mu}{h^2}({}^t\Delta_-)\left(\frac{{}^s\Delta_+{}^{n+1}\phi_{i,j}}{\sqrt{\frac{({}^t\Delta_+{}^n\phi_{i,j})^2}{\omega^2} + \frac{({}^s\Phi_{i+1,j} - {}^n\phi_{i-1,j})^2}{(2h)^2}}}\right)$$
$$\left. - \lambda(I_{0i,j} - c_1({}^n\phi))^2 + \lambda(I_{0i,j} - c_2({}^n\phi))^2\right] \quad (18)$$

where

$${}^s\Delta_-\phi_{i,j} = \phi_{i,j} - \phi_{i-1,j}, \quad {}^s\Delta_+\phi_{i,j} = \phi_{i+1,j} - \phi_{i,j}$$
$${}^t\Delta_-\phi_{i,j} = \phi_{i,j} - \phi_{i,j-1}, \quad {}^t\Delta_+\phi_{i,j} = \phi_{i,j+1} - \phi_{i,j}$$

Equation (18) transformed equation (15) from a PDE into a system of linear algebraic equations that can be solved using the iterative methods of linear algebra. For any input figure that needs to be segmented, the whole model can be applied and solved using the algorithm outlined in Figure 3.

Experimental setup

Because some segmentation algorithms work better with synthetic fibers of circular cross-sections, three materials with different cross-sections, shown in Table 1, are used in this study to test the performance of the method. Ring-spun yarns were produced in different counts as listed in Table 1. The preparation of the yarn cross-section requires special care to preserve the twists and the shape of the yarn during its imaging. It is important to process the samples in a standard manner to maintain the repeatability of the results, hence the standard method "IS 46-108-01/01: Recommended procedure for preparation of samples, soft and hard sections (slices)"[19] was developed at the Technical University of Liberec for this purpose based on other standard methods (e.g. ČSN EN 12751 (80 0070)).

The standard preparation method can be briefly described as the yarn is soaked in a solution of a dispersion glue and a surfactant in a 1:1 concentration ratio. The 1,4-bis(2-ethylhexyl) sulfosuccinate (also known as Spolion 8) surfactant was used as a dispersion and wetting agent in a concentration of 5 g/l. The applied glue was a universal Gama Fix Henkel which is available in office supply stores. After immersing the yarn in the mixed solution of the glue and the surfactant, the yarn sample is dried in standard atmospheric conditions for 24 hours. The yarn is then immersed only in the glue and dried at the same conditions. After drying, the yarn sample is embedded in a 2:3 mixture of bee's wax and paraffin, respectively, to form a mold block with dimensions of 3 cm × 1.5 cm. The sample mold is then left to solidify and placed in a freezer at −8°C for 24 hours. After its hardening and solidification, the sample is ready for slicing into thin slices of 15 μm thickness using a microtome. The cross-sectional slice is then placed on a transparent slide and the wax is dissolved by adding few drops of xylene. The image acquisition is performed using the CCD camera installed on a Nikon microscope and attached to a computer. The acquired images were enhanced by transforming the grayscale values using the "contrast-limited adaptive histogram equalization (CLAHE)" algorithm.[20] Three pictures of well-focused samples were processed for each yarn to test the validity of the segmentation method.

Table 1. Yarn and fiber specifications

Material	Yarn count (tex)	Fiber density (kg/m³)	Fiber fineness (dtex)	Fiber's cross-section
Lyocell	20	1500	1.5	
Viscose	16	1500	1.3	
Cotton	16	1520	1.7	

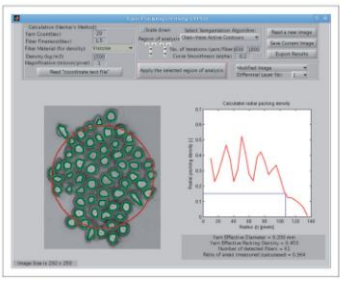

Figure 4. Developed GUI for implementing the CV algorithm, YPD.

Results and discussion

Samples of yarn cross-section are prepared as described in the experimental part and the yarn images are acquired using the camera on the microscope. The acquired yarn images are then introduced to the "Yarn Packing Density (YPD)" software, shown in Figure 4, that was developed to utilize the algorithms described above for calculation. The software reads the image and the user can select the whole image or assign a small region for analysis if the fibers are more concentrated at small part of the image.

Yarn contour

Once the CV model for segmentation is applied, the program starts with the outside borders of the image as initial conditions which allow the algorithm to stop at the outer contour lines of the yarn. The curve evolution of the algorithm at different iteration cycles is shown in Figure 5 which indicates that the algorithm was able to segment the picture in two regions that represent the image background and the yarn. The algorithm successfully segmented the image after about 300 iterations then no significant change in the yarn contour was detected. The time required for each iteration cycle and the total time required for segmenting the image depends on the image size and the hardware processing capabilities. It is, therefore, one of the drawbacks of this algorithm to take relatively long time during segmenting large size images and while researchers are trying to develop efficient algorithms to process massive amounts of images,[21] this algorithm depends

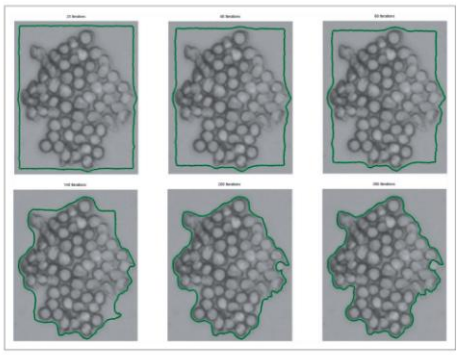

Figure 5. Curve evolution of the CV algorithm at different iteration cycles.

on the image size and the available hardware resources to process the image. To accelerate the processing time of some large images, the program allows the user to choose scaling down the image. By scaling down the picture, the yarn image is resized and the segmentation algorithm is applied on the smaller version then the image is scaled-up again being ready for the next packing density calculations.

Fibers' contours

After the determination of the yarn contour, the CV algorithm is applied again to determine the contours of the fibers inside the yarn cross-section. The initial condition for the fibers detection algorithm is a square approximated at the center of the image and propagates towards the edges of the yarn. The fiber detection takes more iteration cycles as the algorithm separates the image into many segments according to the number of fibers in the yarn cross-section. The detected fibers are shown in Figure 6 in binary format and highlighted with red color as superimposed to the yarn cross-sectional image. It can be noticed from this figure that the algorithm is successful in detecting the internal cross-section of the fibers while the walls of the fibers are considered as part of the space surrounding the fibers in the yarn. This can be considered as a source of error in determining the actual yarn packing density and it usually leads to lower values because the total fibers' area (the substance area) is decreased. On the other hand, the currently applied methods that approximate the yarn cross-section to a circle have a similar source of error by adding more area to the actual yarn cross-section. This source of error in the traditional method results in a similarity between the calculated values of our method and the traditional methods. It can also be noticed in Figure 6 that the utilized active contour method allows the detection of fibers with different cross-sectional areas which is not considered by the traditional methods (e.g. the secant method) that approximate the fibers cross-sections to circles with a constant diameter and area.

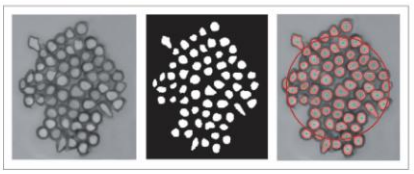

Figure 6. Lyocell yarn image (left); detected fibers inside the yarn in binary format (middle); highlight of the detected fibers (right) where the red circle shows the calculated effective yarn diameter, and the green points highlight the centers of the detected fibers.

Packing density calculation

Once the contours of the yarn and the fibers are detected, it is possible to calculate the radial packing density (μ_r). The process starts with calculating the yarn's center of gravity that is considered as the mass center of the object that represents the yarn and its coordinates (X_c, Y_c) is calculated from the constituent pixels of that object (X_i, Y_i). The mass center coordinates (X_c, Y_c) are calculated according to the following relation:

$$X_c = \frac{\sum_{i=1}^{n} A_i * X_i}{\sum_{i=1}^{n} A_i}, \quad Y_c = \frac{\sum_{i=1}^{n} A_i * Y_i}{\sum_{i=1}^{n} A_i} \quad (19)$$

where n is the total number of pixels in the yarn object, A_i is the area of the ith pixel that has coordinates (X_i, Y_i). Since all pixels having the same area, A_i is considered as one unit which makes the coordinate of the yarn's center as a mathematical mean of the coordinates of the pixels belonging to the yarn object.

The maximum diameter of the yarn object was then divided with equally displaced points which create concentric rings that are used in calculating the radial packing density. Examples of those rings are shown in Figure 7 where the areas of the fibers appear in the jth ring are summed (S_{rj}) and divided by the area of that ring (S_j) to calculate the radial packing density (μ_r) as explained earlier in equation (1). The radial packing density can be plotted as a function of the radius as shown in the right bottom graph of Figure 4 which allows the determination of the yarn effective diameter (d_{ef}) by interpolating the radial packing density at 0.15. The estimated effective diameter for the studied yarn was determined to be about 0.20 mm. The effective yarn packing density μ_{ef} was calculated as the ratio between the total fiber area (S_f) and the area of the circle of effective diameter (S_{ef}) and was found to be 0.453.

To check the accuracy of the measured area of the fibers, the ARF was used which can be defined as

$$ARF = \frac{S_{meas.}}{S_{theor.}} \quad (20)$$

where $S_{meas.}$ is the area measured from the yarn picture and its segmentation, $S_{theor.}$ is the theoretical area of the substance (i.e. without voids or spaces between fibers) inside the yarn diameter. The $S_{theor.}$ can be calculated from the yarn and fiber parameters introduced in Table 1 as follows:

$$S_{theor.} = \frac{T_{yarn}}{\rho_{fiber}} \cdot \kappa \quad (21)$$

where T_{yarn} is the yarn count, ρ_{fiber} is the fiber density, and κ is a conversion factor that depends on the image resolution and the units used. Since the theoretical area ($S_{theor.}$) is calculated from the yarn count and the fiber density, this area corresponds to the area of the material inside the yarn regardless of the distribution of this material (i.e. the area of the material regardless of the air gaps between the fibers or even the distribution of the fibers inside the yarn). The calculated ARF for the Lyocell yarn is 0.964 which means that the measured area is slightly lower than the theoretical area of the fibers inside the yarn. This result is expected as the segmentation algorithm does not consider the fiber's wall as part of the fiber, as mentioned earlier, which affects the accuracy of the measured area. Considering this source of error, the measured area is still in a reasonable range.

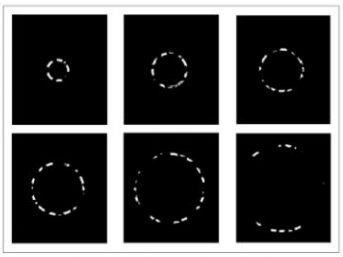

Figure 7. Examples of annular rings that are considered for calculating the yarn radial packing density.

Table 2. Average results of the measured samples

Yarn	Calculated effective diameter (mm)	Calculated effective packing density	Area ratio factor (ARF)
Lyocell	0.200	0.453	0.964
Viscose	0.160	0.414	0.893
Cotton	0.155	0.387	0.785

Other yarn case studies

A similar discussion can be extended to the other two yarn types (viscose and cotton), and their results are summarized in Table 2 while their images are demonstrated in Figure 8. It can be seen in Figure 8(b) that some viscose fibers were considered as one big fiber during segmentation which is revealed to the shape of the yarn and the processing algorithm. It was shown earlier that the calculation algorithm segments the image in two stages; the first to detect the yarn contour and the second to detect the fibers inside the yarn. During the first stage and according to the yarn shape, more than one object can be detected in the image where, for example, the big blob fibers shown in Figure 8(b) are relatively far from the main object where most of the fibers are concentrated. In the case of multiple objects produced during the first stage of yarn contour determination, the algorithm considers the object of the biggest area as the yarn body that will be processed during the second stage of fiber segmentation. Therefore, according to the yarn structure and the distribution of the fibers in the yarn cross-section, the fiber objects that may be relatively far from the main yarn body will not be processed during fiber segmentation which results in the less segmented fibers shown in Figure 8(b).

The ARF for the measured samples is listed in Table 2 and can be used to quickly indicate if there is suspected sources of error during the segmentation. The lowest ARF value was found in cotton yarn samples which can be explained by the cross-sectional shape of the cotton fibers which is distinguished by the kidney shape with the lumen of the fiber at the middle as shown in Figure 8(d). By examining the binary image for the segmented cotton fibers in Figure 8(e), it can be seen that the segmentation algorithm subtracts the area of the internal fiber lumen from the total area of the fiber which results in less value of the measured area (S_{fiber}) and lower ARF value.

Due to the sample size limitations, it is important to notice that the resulting packing density values are not statistically significant and should not be considered as final values for these yarns. For the results to be significant, many cross-sectional samples at different positions along the yarn should be captured and analyzed. However, the quality of cross-sections during their slicing interferes with the imaging system and usually results in out-of-focus images that need extra processing and limits the number of high-quality pictures that can be analyzed. Therefore, the small sample size used in the current analysis was applied to only verify the validity of the segmentation method and to get indicative numbers of the measured yarn parameters to have some insights about the system's constraints. It was observed that the quality of the imaging system and the careful sample preparation are very important factors in deciding the reliability of the calculated results. The calculated packing densities of the given yarns (although need more samples for verification) are comparable to the results calculated using traditional methods for yarns of similar counts.[11,22,23] This agreement, however, contradicts our expectations of getting packing density values higher than the values obtained from traditional methods that add extra porosity to the yarn structure by considering a circular cross-sectional shape of the yarn. It can be explained, on the other hand, by the decreased area of fibers detected by the automated CV segmentation method that does not consider the wall of the fiber (e.g. the Lyocell case) or the lumen (e.g. the cotton case) as parts of the total area of the fiber and, therefore, it is important to consider some correcting factors that compensate for this source of error after fiber segmentation. No correction factors were applied on the given results but it is pointed out here as a possibility for modifying the results.

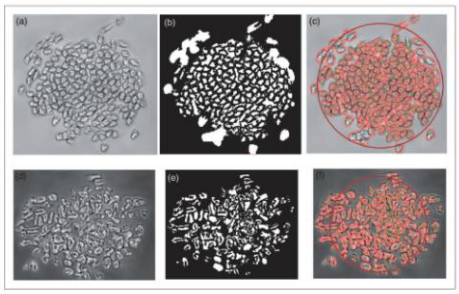

Figure 8. Cross-sectional image of viscose yarn (a) and cotton yarn (d); Segmented fibers in binary format for viscose (b) and cotton (e); Highlight of the detected fibers in the viscose yarn (c) and cotton yarn (f). The red circles in (c) and (f) have diameters of the calculated effective yarn diameter and the green points highlight the centers of the detected fibers.

Conclusion

The CV model was utilized to segment objects in the yarn cross-section to help in detecting the actual contours of both the yarn and its constituent fibers. The detected yarn contour allows the use of the actual yarn cross-sectional shape which differs from the approximated circular contours that are considered in the conventional methods for calculating the yarn packing density. The ARF results have shown a deviation from the ideal ARF value (where ARF=1) due to the cross-section nature of each segmented fiber's type. One drawback of the introduced algorithm is its inability, with the given conditions, to consider the total area of the fiber (where the walls or the lumen of the fiber can be excluded) which results in lower calculated values of packing density. These low values, however, were found to be comparable to the results of the traditional methods as these methods approximate the yarn cross-section to a bigger circle. By considering the actual

yarn contour (rather than its circular approximation), the measured packing density of the current samples is expected to be higher than the produced values. In general, the segmentation method presented in this work was found to be faster and more reproducible than the traditional methods of calculating the packing density. Since this method is principally an image segmentation model that can be used to separate the fibers from the background, the method can be extended to segment different fibrous structures to calculate their porosity and packing density. Finally, the sample preparation and the quality of imaging system were found to be crucial factors in producing reliable results and the authors are currently working on alternative methods for image acquisition to be able to obtain enough sample size that produce statistically significant results.

Funding

This work was supported by ESF operational program "Education for Competitiveness" in the Czech Republic in the framework of project "Support of engineering of excellent research and development teams at the Technical University of Liberec" (grant number CZ.1.07/2.3.00/30.0065).

Acknowledgements

The authors also gratitude the time and effort of Professor Bohuslav Neckář for his fruitful and constructive discussions. We would like also to thank Professor Michal Vik for his help in capturing some of the microscopic images.

References

1. Driscoll RH and Postle R. Modelling the distribution of fibres in a yarn. *J Text Inst* 1988; 79: 140–143.
2. Petrulis D and Petrulytė S. Properties of close packing of filaments in yarn. *Fibres Text East Eur* 2003; 11: 16–20.
3. Zheng S, Zou Z, Shen W and Cheng L. A study of the fiber distribution in yarn cross section for vortex-spun yarn. *Text Res J* 2012; 82: 1579–1586.
4. Gracie PS. Twist geometry and twist limits in yarns and cords. *J Text Inst Trans* 1960; 51(7): T271–T288.
5. Phoenix SL. Statistical theory for the strength of twisted fiber bundles with applications to yarns and cables. *Text Res J* 1979; 49: 407–423.
6. Neckář B. Compression and packing density of fibrous assemblies. *Text Res J* 1997; 67: 123–130.
7. Kumar A, Ishtiaque SM and Salhotra KR. Study of effect of spinning process variables on the packing density of ring, rotor and air-jet yarns using the Taguchi method. *Autex Res J* 2006; 16(3): T122.
8. Kumar A, Ishtiaque SM and Das A. Impact of yarn extension on packing density of ring spun yarn. *Fibers Polym* 2012; 13: 1071–1078.
9. Liberec TU. Yarn packing density, direct method and secant method. *Intern Stand Tech Univ Lib*. 2004IS 22-103-01.01.
10. Neckář B. *Yarn forming, structure, properties*. Praha, Czech Republic: SNTL, 1990.
11. Yilmaz D, Goktepe F, Goktepe O and Kremenakova D. Packing density of compact yarns. *Text Res J* 2007; 77: 661–667.
12. Mitiche A and Ben Ayed I. *Variational and level set methods in image segmentation*. Vol. 5, New York: Springer, 2010.
13. Cremers D, Rousson M and Deriche R. A review of statistical approaches to level set segmentation: integrating color, texture, motion and shape. *Int J Comput Vis* 2007; 72: 195–215.
14. Kass M, Witkin A and Terzopoulos D. Snakes: active contour models. *Int J Comput Vis* 1988; 1: 321–331.
15. Chan T and Vese L. An active contour model without edges. In: *Scale-Space Theories in Computer Vision*. New York: Springer, 1999, pp.141–151.
16. Chan TF and Vese LA. Active contours without edges. *IEEE Trans Image Process* 2001; 10: 266–277.
17. Osher S and Fedkiw RP. Level set methods: an overview and some recent results. *J Comput Phys* 2001; 169: 463–502.
18. Wang X-F, Huang D-S and Xu H. An efficient local Chan–Vese model for image segmentation. *Pattern Recognition* 2010; 43: 603–618.
19. Liberec TU. Recommended procedure for preparation of samples, soft and hard sections (slices). *Intern Stand Tech Univ Lib*. 2004IS 46-108-01.01.
20. Pisano ED, Zong S, Hemminger BM, DeLuca M, Johnston RE, Muller K, et al. Contrast limited adaptive histogram equalization image processing to improve the detection of simulated spiculations in dense mammograms. *J Digit Imaging Off J Soc Comput Appl Radiol* 1998; 11: 193–200.
21. Eldessouki M, Ibrahim S and Militky J. A dynamic and robust image processing based method for measuring yarn diameter and its variation. *Text Res J*, in press. DOI: 10.1177/0040517514530032.
22. Jiang XY, Hu JL, Cheng KPS and Postle R. Determining the cross-sectional packing density of rotor spun yarns. *Text Res J* 2005; 75: 233–239.
23. Salehi M and Johari MS. Study of fiber packing density of Lyocell ring-spun yarns. *J Text Inst* 2011; 102: 389–394.

PART II

Chapter 5

A Dynamic and Robust Image Processing Based Method for Measuring The Yarn Diameter and Its Variation

Summary Sheet

- **Paper citation:**
  M. Eldessouki, S. Ibrahim, and J. Militky, "A Dynamic and Robust Image Processing Based Method for Measuring Yarn Diameter and Its Variation," *Textile Research Journal*, vol. 84, no. 18, pp.1948-1960, 2014, DOI: 10.1177/0040517514530032.

- **Targeted problem:**
  Microscopic method for measuring the yarn diameter is a ***static*** in nature as it collects data on ***short distances*** along the yarn length, on the other hand, the data collected by commercial methods are treated in a ***black box system*** without clear understanding of the results

- **Objective(s):**
  - Develop a system of high speed camera for capturing the yarn running in speeds comparable to those of commercial instruments
  - Develop a robust algorithm with little computation requirements for analyzing the acquired images
  - Treat the collected data in a "transparent box system" based on time-series analysis with a clear interpretation of the results
  - Compare the methods performance with commercial devices

- **Materials scope:**
  - Two cotton yarns of different counts were produced using the ring spinning technology
  - One of the yarns was has slubs along its length and selected to provide more information about the system performance with variable diameters

- **Computation method:**
  - Yarn images were analyzed using a newly and simple developed algorithm
  - Measured diameters were analyzed using different statistical and time series methods to detect the short-term, the long-term, and the periodic variations in the yarn diameter

- **Paper significance:**
  - The image analysis method developed in this work is a new simple method that is computationally inexpensive and can handle massive amount of images within a reasonable time.
  - The developed data-treatment algorithm is powerful enough to handle data collected from the image analysis method or to handle the raw data that might be obtained from the commercial measuring instruments and standardize the results with a transparent explanation

- **Software**
  A software program with a user-friendly GUI was developed for this work and named DiaLib®. The DiaLib® consists of two modules for image analysis and for data treatment. The software is available on the accompanied CD with a tutorial video demonstration. The program also has some examples on the CD so it can be tested. The program GUI is shown below:

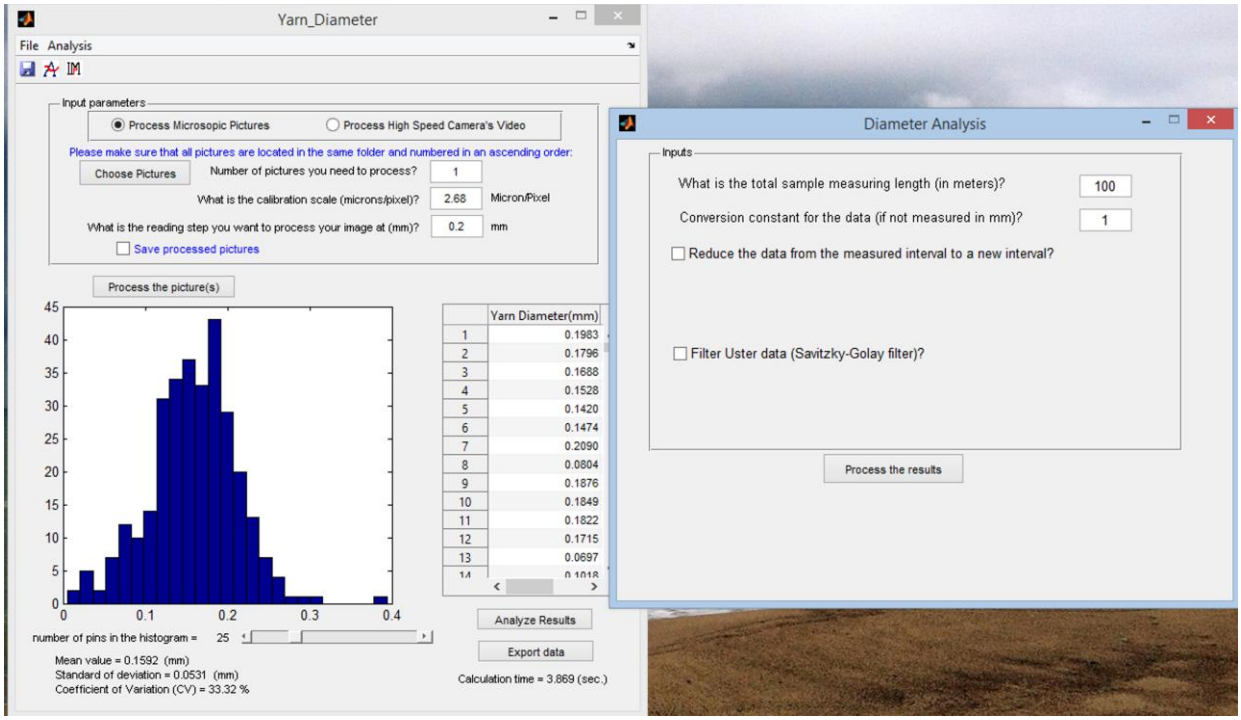
Yarn_Diameter
File Analysis
Input parameters
Process Microsopic Pictures
Process High Speed Camera's Video
Please make sure that all pictures are located in the same folder and numbered in an ascending order:
Choose Pictures
Number of pictures you need to process? 1
What is the calibration scale (microns/pixel)? 2.68 Micron/Pixel
What is the reading step you want to process your image at (mm)? 0.2 mm
Save processed pictures
Process the picture(s)
Yarn Diameter(mm)
1 0.1983
2 0.1796
3 0.1688
4 0.1528
5 0.1420
6 0.1474
7 0.2090
8 0.0804
9 0.1876
10 0.1849
11 0.1822
12 0.1715
13 0.0697
number of pins in the histogram = 25
Analyze Results
Export data
Mean value = 0.1592 (mm)
Standard of deviation = 0.0531 (mm)
Coefficient of Variation (CV) = 33.32 %
Calculation time = 3.869 (sec.)
Diameter Analysis
Inputs
What is the total sample measuring length (in meters)? 100
Conversion constant for the data (if not measured in mm)? 1
Reduce the data from the measured interval to a new interval?
Filter Uster data (Savitzky-Golay filter)?
Process the results

A Dynamic and Robust Image Processing Based Method for Measuring The Yarn Diameter and Its Variation

Mohamed Eldessouki[1,2], Sayed Ibrahim[3], Jiři Militky[1]

[1]*Technical University of Liberec, Faculty of Textile Engineering, Materials Engineering Department, Liberec, Czech Republic*

[2]*Department of Textile Engineering, Faculty of Engineering, Mansoura University, Mansoura, Egypt*

[3]*Technical University of Liberec, Faculty of Textile Engineering, Textile Technology Department, Liberec, Czech Republic*

Abstract

The yarn diameter is an effective property in determining fabric structure and processing settings. There are different systems of measuring the yarn diameter; among them is the image analysis of the yarn's microscopic images. This method is considered to be more precise than other methods, but it is "static" in nature as it measures the property at scattered intervals and does not reflect the continuous variation of the yarn diameter. The goal of the current work is to measure the yarn diameter and its variation over a long length of yarn at fixed intervals to consider the "dynamic" change in the property. To achieve this goal, a high-speed camera (HSC) with a proper magnification was used to capture the images of the yarn and a new robust algorithm was developed to analyze the massive amount of yarn pictures in a reasonable time. The collected data for the yarn diameter were analyzed and compared to the results of the commercial Uster Evenness Tester IV. The results of the HSC were very comparable to the results of Uster and they were able to detect the short-term, the long-term, and the periodic variation of the yarn diameter.

1. Introduction

Yarn diameter is an important parameter that is used in all the calculations and modeling of fabric parameters [1] such as weave angle, yarn densities in warp and weft directions, yarn crimp ratio, cover ratio, fabric weight, and fabric volumetric density. The yarn diameter has also a direct impact on some of the measured fabric properties that affect the fabric dimensional and mechanical parameters [2]. Fabric performance and comfort depend on the yarn diameter as it correlates to the fabric air and water permeability. The settings of winding machines (e.g. cleaning knife) and most of the machines in the subsequent processes depend on the yarn diameter. On the other hand, the "exact" measurement of the yarn diameter is very difficult because of the inherent yarn unevenness and irregularity. That leads the textile specialists to talk about the yarn "size" or "count" instead of its "diameter". However, yarn count may not precisely indicating the yarn diameter as two yarns with the same count may have two different diameters due to the changes in other parameters such as the fiber density and the yarn twist factor. Therefore, a good method of measuring the yarn diameter should maintain two basic features; it should measure the diameter with high precision and accuracy. It also should be able to determine the irregularities that occur in diameter at different bases (short and long term variations as well as the periodic variations).

The principles of measuring the yarn diameter can be classified [3] into four main categories that are summarized with their pros and cons in Table 1. These methods are:

- ***The capacitive measurement***: this is an indirect method of measuring the variation in yarn linear density (yarn count) which correlates to the yarn diameter through empirical relations from which the variation in yarn diameter can be calculated. The major drawback of this method is the indirect measurement of the yarn diameter (in fact, the mass variation is measured not the diameter but due to the high correlation between both parameters, it is possible to measure one parameter and infer the other [4, 5]). This method also depends on the testing environmental conditions because the capacitors are usually affected by the temperature and humidity. The resolution of this method is relatively low where the capacitors sample the data every 8mm (e.g. old versions of Uster tester).

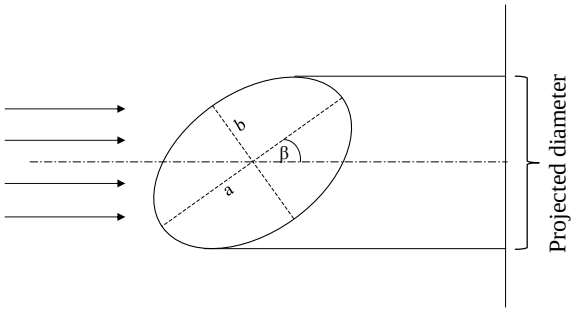

Figure 1. Schematic representation of the optical yarn diameter measurement system

- ***The optical measurement***: this method is widely common [6] in commercial devices where high resolutions (e.g. 0.25 mm) can be obtained. This method determines the diameter after shedding a beam of laser light on the yarn and analyzing its projected image on a light sensor, Figure 1. The results of this method are highly dependent on the direction (the angle β) of the yarn as the projected image of the elliptical shape of the yarn may be larger or lower than the actual diameter. This method does not affect with the testing humidity or the fiber blend variation [7] although it might be affected with the presence of lint and yarn hairiness. During these measuring methods, the yarn exists under a slight tension in the longitudinal direction which causes a compression in the transverse direction and may lead to changes in the measured diameter.

- ***The mechanical (electro-mechanical) measurement***: in this method, the yarn runs between two sensors (fixed and freely moved) where the movement of the freely moved sensor is magnified for measuring the diameter. These sensors are implemented in different ways (cylinders, flat surface…etc) among them a device similar to the tongue and groove mechanism used on drawing frames [3]. The yarn passes through the grove and the tongue is attached to an arm that works as displacement amplifier to record the yarn diameter and its variations.

- ***The small scale microscopic measurement***: This laboratory method is, principally, an optical method but it can be distinguished from the other optical methods by its small scale of measurements where the yarn diameter is measured in two directions; the cross section or the longitudinal view of the yarn [8]. The cross section of the yarn should be carefully cut at different positions and the diameter can be captured under the microscope with an appropriate magnification. Similarly, the yarn diameter is measured from the longitudinal projections of the yarn under the microscope at randomly different positions to account

for the elliptical shape of the yarn [9]. Measurements can be done on the computer by a visual inspection or automatically using some image analysis techniques.

Table 1. Advantages and disadvantages of the methods for measuring yarn diameter

	Advantages	Disadvantages
Capacitive	- Works with the common yarn irregularity measurement systems - Primitive method	- Low resolution - Depends on the testing environment - Affected by other fiber properties (e.g. material type, fineness, specific density) and yarn parameters (e.g. twist, production technology)
Optical	- High resolution - Does not depend on testing environment - Simple and fast	- Measures the projected diameter not the real diameter - Yarn under tension reduces the measured diameter - Affected with the lint and hairiness
Mechanical	- Direct contact with the yarn	- Depends on the applied load during measurement
Small scale measurement	- Precise method - Measures the actual diameter	- Time consuming and tedious method - Not suitable for practical application in production scales

The microscopic evaluation of yarn diameter is preferred for academicians in laboratories for its accuracy and it is used to calibrate the other methods. This method, however, is time consuming and needs many repeating samples which makes it unsuitable for practical testing in production environments. It is also important to notice that the measurements of this method are "static" as they give information about the yarn at "*scattered*" points across the length of the yarn. This means; it does not capture the continuity of the variation in the measured property along the yarn and cannot usually detect the short-term, the long-term, or the periodic variation of the yarn diameter.

This work aims at tackling the problems of the microscopic evaluation method and presents a new computer vision based system to measure the yarn diameter and its variation utilizing video processing and analysis algorithms. A high speed camera (HSC) is used to capture the yarn images and it was used to allow testing speeds comparable to speeds of the known commercial devices. A new image analysis algorithm is developed to enhance the captured images by eliminating the yarn hairiness and hence to obtain the yarn diameter. The continuity of the obtained results at fixed interval allows their treatment as time series which unveils some of the yarn characteristics that produced from the commercial instruments. Two case studies are used in order to validate the presented system results; one of them is a

regular ring-spun yarn and the other is a slub-yarn. Both yarns are tested simultaneously on the presented system and on the Uster Evenness Tester IV.

2. Experimental Setup

2.1. Computer vision setup

Pre-investigation of the system and the analysis algorithm was initially performed using yarn samples evaluated under the optical microscope. Olympus microscope was used with an automated stage to capture the yarn images along a certain distance with a magnification scale of 2.68 µm/pixel. The setup of the microscope is shown in Figure 2 with the motorized stage and the digital camera that is connected to the computer. The microscope system captures a longitudinal view of the yarn then the stage moves automatically with a predefined distance to capture another image. The obtained images were stitched and superimposed together to form a single picture of the whole yarn.

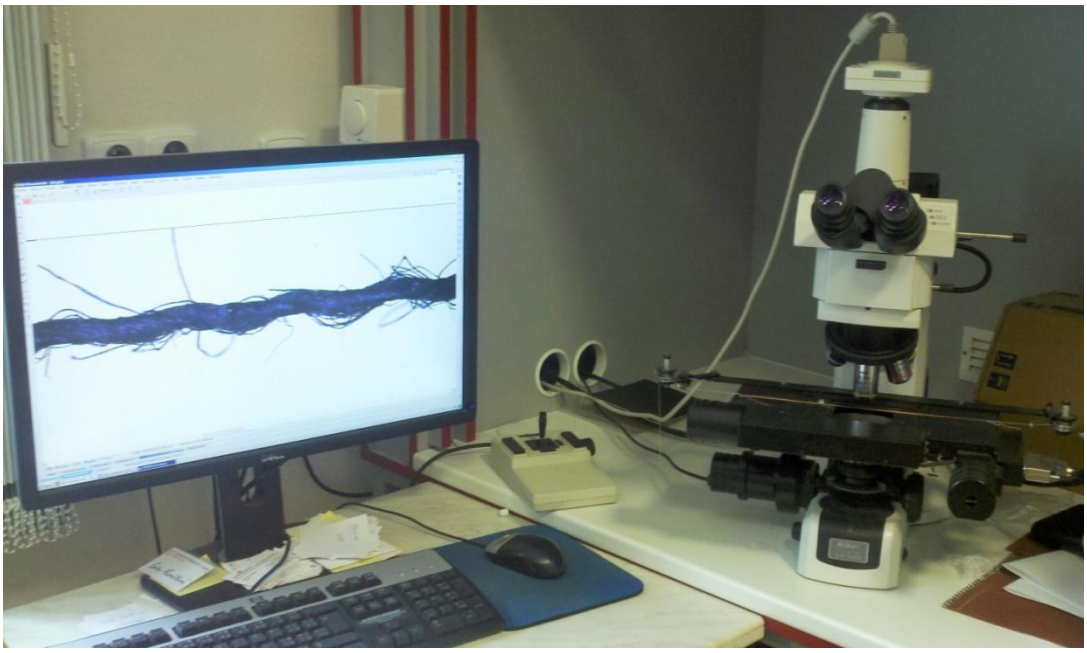

Figure 2. Microscopic setup with a motorized stage and CCD camera connected to the computer

Because of the slow image acquisition with the automated microscope, alternative systems of acquisition were considered. A video camera with appropriate magnification lenses was applied; however, the yarn speed for this camera setup was about 15 m/min which is less than the practical testing speeds of the commercial instruments. To run the yarns at 100 m/min (which is the testing speeds of other instruments such as Uster evenness tester IV), a high speed camera (HSC) was used. Olympus i-speed 3 high speed camera was installed with appropriate macro-lenses. The HSC captured yarn images with a speed of 150 frames per second (fps), the used shutter speed was 200X, and the resolution of individual frames in the recorded video was 1280x1024 pixels with a magnification scale of 10.2 µm/pixel. The yarn was lighted

with a special Xenon lamp directed with an optical fiber to the HSC shooting zone. To avoid the effect of tension changes during the experiments, the yarn was running in front of the camera under constant tension using the tension compensation mechanism of Lawson Hemphill Constant Tension Transport (CTT) tester. The introduced computer vision system for measuring the yarn diameter (that includes the video camera setup with the analysis software) was assigned a name DiaLib®.

2.2. Tested samples:

Two yarn samples were examined and analyzed using the suggested method and the results were verified against the measurements on the commercial Uster evenness tester IV. The first yarn sample is a normal ring-spun 100% cotton yarn with a count of 20 tex. The second yarn sample is a cotton slub-yarn produced by deliberately changing the draft on the spinning frame. The yarn count was 23 tex and the slub thickness was designed to be as twice as the yarn original diameter. The slubs were distributed across the yarn in two populations with slub-lengths of 50 mm and 100 mm. The inter-slub separation distance was designed to be 150 mm. The yarn was tested on Uster evenness tester IV for its diameter and irregularity and the images of the yarn were captured using the high speed camera. The yarn speed during testing on the Uster and the HSC was 100 m/min.

3. Methods

3.1. Image processing and analysis:

The longitudinal view of the yarn sample was acquired with a proper magnification using a digital camera connected to the computer. The acquired images were converted to binary with a suitable threshold to allow faster processing. The yarn diameter is calculated by counting the pixels belonging to the yarn body at specified intervals. The existence of yarn hairiness with protruding fibers does not allow the direct and automatic finding of the yarn limits (where the diameter can be measured) because those protruding fibers will be outside the actual diameter. Therefore, the automatic measurement of the yarn diameter is faced with three obstacles; firstly, the exclusion of the yarn hairiness from the yarn body. Secondly, the filling of the voids inside the yarn body that occur during the conversion to binary images (due to the shading differences in the microscope images). Thirdly, the standard algorithms for edge detection (to remove the hairiness) and object filling (to remove the voids) are relatively slow (as they convert the image back and forth between its spatial and spectral domains) and there is a need to increase the speed of the processing algorithm. These obstacles will be folded many times in accordance with the interval distance between the measurements and the number of the images to be processed. For example, there is about 350 slices in an image of a yarn with length ≈ 7 cm and interval between readings of 0.2 mm, and this number reaches many thousands for longer yarn samples.

To face these challenges, a new algorithm was developed to be robust with the increase in number of pictures and sampling points. To find the yarn body in an image (let us call it I1), two other images of the yarn were created by translating the yarn image in the vertical direction with distances ±δ (let us call the created shifted images; I2 and I3). Then, the three images are added together and the summation matrix is

logically compared to a certain threshold to produce a binary image with filled yarn body and trimmed off the majority of yarn hairiness.

To demonstrate the algorithm, an example is shown in Figure 3 with a small scale matrix with a height of 20 pixels (while actual yarn images have a height of 1024 pixels). The example in Figure 3 shows one vector (a column that can be called C1) that represents what is extracted from the binary matrix of the yarn image at a certain cutting interval, and the same calculations can be extended for all intervals in the yarn image. The example shown in Figure 3 represents the black background with zeroes and the white elements of the yarn with ones. The representation vector C1 corresponds to a slice of the image where the yarn body is represented with a series of ones (including some voids of zeroes) and a part of the protruding fiber at the top of the vector. This vector was shifted upward with a distance (δ) of 2 pixels (which resulted in another vector that can be called C2) and shifted downward with the same δ (to result in a third vector C3). The vector C4 is the summation of C1, C2, and C3 then it is logically compared to consider the positions with numbers less than or equal to one as background (substituting a value of zero at these positions) and the positions of values greater than one to be foreground (substituting a value of one). The resulted vector C5 shows the solid yarn body without voids or yarn hairiness from the protruding fibers.

To compare the suggested algorithm with the "traditional" edge detection techniques, it is important to understand how these techniques work. The traditional edge detection techniques generally depend on converting the image from its spatial domain into frequency domain to apply some filters on the image then the image is converted back to its spatial domain. After this process, the detection algorithm applies some programming loops to determine the yarn boundaries and remove the hairiness. These traditional methods are computationally expensive and depend on the available hardware resources in completing these tasks. Our suggested method, however, analyzes pictures in their spatial domain only and avoids the loops that consume the computer resources. As the time for any image processing method depends on the used algorithm and the available hardware resources, the suggested system used a personal computer with an Intel core i3 processor to analyze ≈ 10000 pictures in ≈ eight minutes.

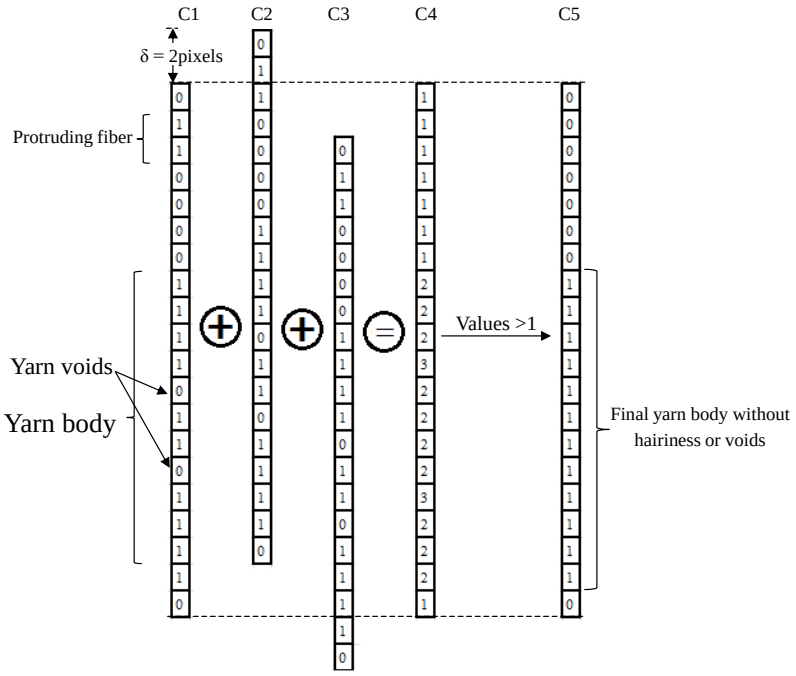

Figure 3. Example of the suggested algorithm to remove hairiness and fill-in yarn voids to find yarn body and diameter

Although this algorithm is relatively fast and robust compared to the standard edge detection and image filling algorithms, it has some drawbacks and errors that may occur during the processing. These errors result from the dependency of the algorithm on the deliberate choice of the image shifting (δ) and on the position of the protruding fibers and voids (which are random). After considering different values for the image shifting (δ) and its effect on the calculation accuracy, it was found that a δ value is approximately equal to the thickness of the protruding fiber is a good choice in most cases. Therefore, the value of δ is calculated during the analysis based on the magnification scale and the fiber's average diameter that are given by the user. To illustrate the errors that may occur, Figure 4 shows a vector from the yarn image similar to the one shown in Figure 3 with a minor change in the position of the protruding fiber which resulted in an error as indicated in C5 by considering one extra pixel as part of the yarn body. A similar error can occur for consecutive voids with a close proximity. Considering the image scale (where one pixel is about 2.6 µm for the microscopic images to 10 µm for the camera images) and the averaging of the thousands of readings to calculate the yarn diameter, the calculation error of this algorithm can be found in the order of 10^{-6} mm per pixel. This error order is relatively small and does not significantly affect the final results of yarn diameter.

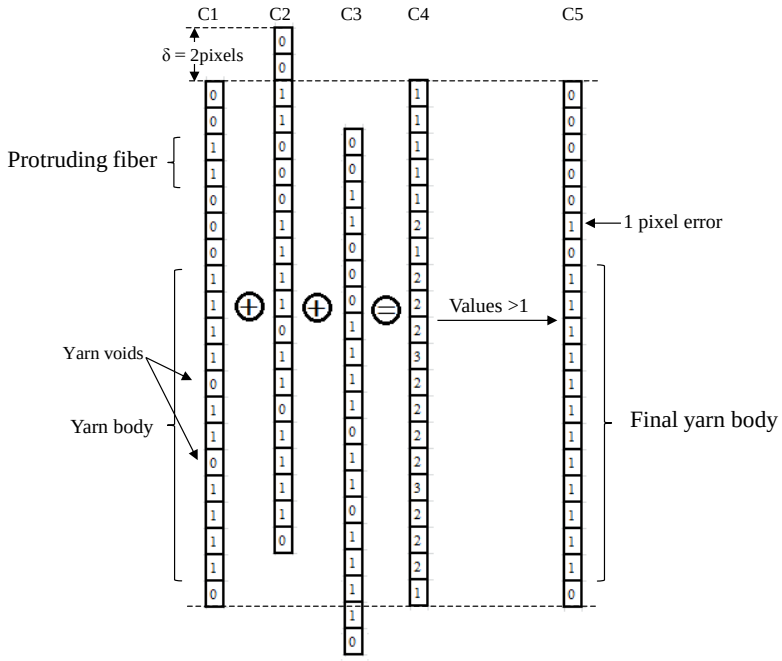

Figure 4. Example of the suggested algorithm with an error in the hairiness removal

3.2. Data analysis and parameterization:

The data obtained from the analysis of the high speed camera (HSC) images are taken at regular intervals (space and time intervals) which allow the data to be treated as time series. Beside the normal statistics that can be derived for any set of data, the discussion here will focus on the parameters that depend on the data continuity to demonstrate the advantages of the introduced procedure (with the dynamic measurement of the yarn) over the static procedures.

The length-variance curve:

The length-variance curve (LVC) determines the relationship between the variability of the yarn diameter and the measurement intervals. The variability (*CB*) is expressed as the coefficient of variation and can be measured at a certain yarn cut length (λ) according to [10]:

$$CB(\lambda) = \frac{s(\lambda)}{\bar{x}(\lambda)} \qquad (1)$$

Where, $s(\lambda)$ denotes the standard deviation of yarn diameter and $\bar{x}(\lambda)$is the average value at a given cut length λ. The "cut length" represents the distance between two consecutive diameter readings on the measurement system and these calculations are repeated at different cut lengths to construct the LVC.

Deviation rate:

The deviation rate (*DR*) measures the frequency (the rate of occurrence) for a diameter value to deviate from the yarn mean diameter plus or minus a certain sensitivity limit (α). For the deviation rate

calculation, the function $p(n,\alpha)$ should be calculated to allow the frequency calculation. This function can be defined as [11, 12]:

$$p(n,\alpha)=\begin{cases}1 & f(x_n)\geq(1+\alpha)\bar{\mu}\\ 0 & (1-\alpha)\bar{\mu}< f(x_n)<(1+\alpha)\bar{\mu}\\ 1 & (1-\alpha)\bar{\mu}\geq f(x_n)\end{cases} \quad (2)$$

The deviation rate can be calculated from the function $p(n,\alpha)$ according to the relation:

$$DR_{\alpha}[\%]=\frac{\sum_{n=1}^{N}p(n,\alpha)}{N}*100 \quad (3)$$

Where n is an index, α is the sensitivity limit, $f(x_n)$ is the diameter value, $\bar{\mu}$ is the mean diameter of the yarn sample, and N is the total number of readings.

Absolute mean deviation

The absolute mean deviation (U%) is a commonly used term to define the mass irregularity of yarns and can be used to define the irregularity in diameter as well. It can be calculated for a series of diameter readings (x_n) using the relation:

$$U[\%]=\frac{\sum_{n=1}^{N}|x_n-\bar{\mu}|}{N*\bar{\mu}}*100 \quad (4)$$

Integral deviation rate

The integral deviation rate (*IDR*) accounts for the diameter's absolute mean deviation at certain sensitivity limit (α) and it can be considered as a generalization formula for the U% (where U% = *IDR* at α=0). The starting function for the *IDR* calculation is the function $y(n)$, similar to the frequency function $p(n,\alpha)$, where:

$$y(n,\alpha)=\begin{cases}|f(x_n)-(1+\alpha)\bar{\mu}| & f(x_n)\geq(1+\alpha)\bar{\mu}\\ 0 & (1-\alpha)\bar{\mu}< f(x_n)<(1+\alpha)\bar{\mu}\\ |f(x_n)-(1-\alpha)\bar{\mu}| & (1-\alpha)\bar{\mu}\geq f(x_n)\end{cases} \quad (5)$$

Then, the IDR can be calculated according to:

$$IDR_{\alpha}[\%]=\frac{\sum_{n=1}^{N}y(n,\alpha)}{N*\bar{\mu}}*100 \quad (6)$$

Autocorrelation function

Autocorrelation is an expression for the correlation of a time series with its own past and future values. The autocorrelation function (ACF) that measures the correlation of a data series $x(n)$ with itself shifted by some delay (lag) m can be calculated from the auto-covariance function[13]:

$$C(m)=\frac{1}{N-m}\sum_{n=1}^{N-m}(x(n)-\bar{\mu}).(x(n+m)-\bar{\mu}) \quad (7)$$

And the sample auto-correlation function at the lag m can be calculated as:

$$\rho(m)=\frac{C(m)}{C(0)},\qquad m=1,2,3,\ldots.M<N \quad (8)$$

4. Results and discussion

It is worthy at the beginning of the discussion to clarify four points regarding the suggested algorithm and the selected yarn samples. First, the proposed method as well as all methods that measure the diameter with a single yarn projection (i.e. using only one camera or sensor) work under the basic assumption that: during the measurement of longer lengths of yarn, the yarn rotates around its axis and the huge amount of collected readings will eventually account for the elliptical shape of the yarn. Second, the choice of the slub-yarn as a second case study versus the normal ring-spun yarn is based on the continuous and periodic variation of yarn diameter in these yarns which should clarify the performance of the proposed system in measuring the yarn diameter and detecting the different types of its variation.

Third, the results of the HSC tested yarns were compared to Uster Evenness Tester IV although the most recent version of Uster Tester V has a special configuration for measuring the slub-yarns and gives more detailed and relatively precise information about the special structure of these fancy yarns. This study, however, meant to verify the validity of the applied algorithm even if it does not compete with the advanced hardware and software implemented by Uster. Four, Uster Tester is the most used instrument in industry and is able to deal with the measurement as a function of time and results in useful information such as LVC, spectrogram…etc. On the other hand, the suggested algorithm is relatively cheap and "transparent box" system that enables us to verify the results obtained from Uster and other instruments that work on the optical principle. Also, the suggested algorithm allows functions and parameters that are not produced by commercial instruments to be calculated (e.g. autocorrelation function, fractal dimensions,...etc) and these parameters are out the scope of the current study.

4.1. Microscopic images

The yarn samples were tested on the microscope setup where the individual captured frames represent a length of about 2.9 mm of the yarn length. The microscope software applies a picture stitching algorithm (for a collection of about 25 pictures) that considers the overlapping of the pictures to create a single image (of about 7 cm) as shown in Figure 5-a. The operation was repeated for a total sample length of 3 m. The individual pictures (for the 7 cm) were processed and an example for a magnified part of the yarn is shown in Figure 5-b. The yarn diameter can be calculated at any required reading interval where the minimum interval is about 2.68 µm (that is equivalent to 1 pixel). A yarn image that was processed at an interval of 0.2 mm is shown as a superimposed image of the actual yarn and the detected boundaries in Figure 5-c where the white parts of the vertical lines represent the detected yarn boundaries at each interval. It can be seen in the processed image that the automated algorithm was capable of detecting the yarn boundaries and considering the yarn body despite of the differences in the gray levels inside the yarn. The method, however, failed to remove the whole protruding fiber as circled in Figure 5-c (the first reading to the right). The reason for the system to consider this hairiness inside the yarn diameter is, partially, because of its close proximity to the yarn body and its positioning in a vertical way (which resulted in more pixels in the cross-section compared to the positioning of horizontal fibers). After all, the method was able to remove about half of the circled protruding fiber and the remaining part is much less

than 10% of the yarn diameter which makes this error almost negligible after averaging the thousands of reading.

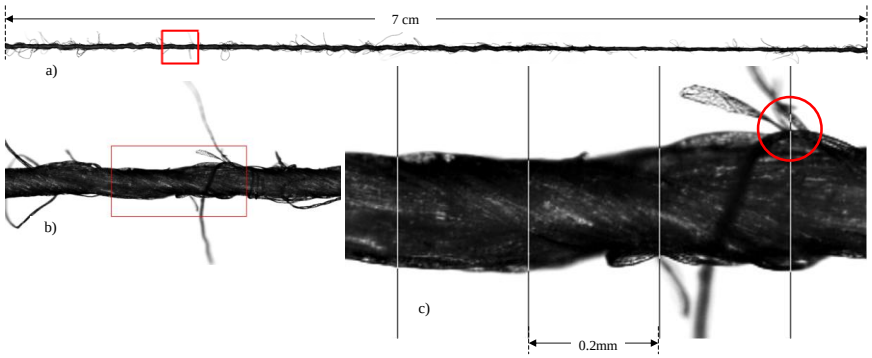

Figure 5. a) Longitudinal view of the yarn as captured under the microscope; b) the magnification of the window drawn in a; c) a magnification of the window drawn in b with illustration of the diameter measuring intervals

4.2. The high speed camera

A 100 m of the each yarn sample (a one minute run) was recorded and the sampling of the yarn diameter from the video was flexible to be adjusted at any interval (with a minimum distance of about 0.01 mm between diameter readings). To compare the HSC with the USTER tester results the measurement interval was adjusted to 0.3 mm to match the interval used in Uster measurements. Two sets of data produced from the HSC with a set of measurement at 0.3 mm and another set of readings that averages every 8 mm to match the results produced by Uster tester. Once videos were processed and the results from HSC were collected, the analysis was performed to produce the statistical and spectral features of the yarn diameter. We should point out that: Uster tester uses two perpendicular cameras to measure the yarn diameter and reports two results; the one obtained from the two cameras and the other from values measured using one camera.

4.2.1. Basic statistics and short-term variation

Table 2. Uster and HSC diameter results for the tested yarn samples

		Uster		HSC	
		0.3mm	**8mm**	**0.3mm**	**8mm**
Normal yarn	**Average diameter (mm)**	0.22	0.218 (2D*)	0.235	0.235
	CV (%)	18.68 (2D)	13.40 (2D)	23.34	13.53
		19.82 (1D**)			
Slub-yarn	**Average diameter (mm)**	0.26	0.259 (2D*)	0.239	0.24
	CV (%)	33.47 (2D)	31.58 (2D)	36.86	30.33
		34.01 (1D**)			

* Values measured using two perpendicular cameras

** Values measured using one camera

The results of both the Uster tester and the HSC are summarized in Table 2 at the two measurement intervals 0.3 and 8 mm for both yarn samples. The average yarn diameter for both yarn samples is comparable when measured using Uster and obtained from the suggested method. The variability of values, on the other hand, as expressed in terms of the coefficient of variation (CV) is slightly different especially as measured at short intervals of 0.3 mm. It is also observed that the CV values are generally higher at short measurement intervals; that is expected as more variability is encountered at these lengths. This increase is also in agreement with the behavior of the length variation curve where higher variation is usually found at shorter measuring lengths. Although the slub-yarn has two different diameters as can be clearly seen in the bimodal histograms of Figure 6, the results of Uster report a single value for the diameter (with a high variation) which is the mean of all values if considered as a normal distribution. The diameters calculated from the high speed camera are also shown in Figure 6 with a bimodal histogram for the slub-yarn sample. The theoretical normal distribution curves calculated from the HSC analysis are shown in the figure with mean values relatively close to the data obtained from Uster. The availability of the raw data from the HSC allows the analysis of the two averages of the bimodal distribution for the slub-yarn. The Hartigan's DIP method [14, 15] was used for testing the unimodality and the finite mixture distributions method [16-18] was applied to separate the bimodal curve. Analysis of the bimodal distribution indicates that the first mode is 0.301 mm (standard deviation 0.066 mm) and the second mode is 0.192 mm (standard deviation 0.024 mm).

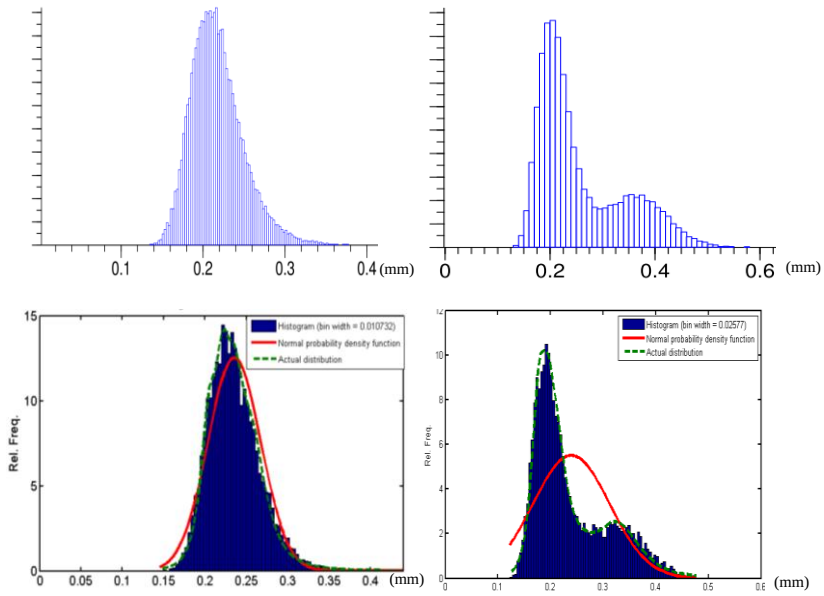

Figure 6. Histogram for the yarn diameter measured by Uster (top) and produced from the analysis of HSC (bottom) for the normal yarn (left) and the slub-yarn (right)

4.2.2. Long term variation

The long term variation in the yarn diameter can be detected using the length-variance curve (LVC). The application of the image processing allows the determination of the yarn diameter at different intervals which permitted the construction of the LVC. The LVC for the tested yarns are shown in Figure 7 as produced from the applied algorithm and compared to the curve obtained from Uster evenness tester. The theoretical LVC for an ideal yarn can be represented by an inclined straight line (on a diagram with double logarithmic scale) and any deviation from the ideal line corresponds to a long term variation. It can be seen from the figure that the results of the HSC are very comparable to the results of the Uster tester and the LVC curve for the normal yarn is almost straight while being curved for the slub-yarn. The LVC is very useful in comparing the regularity of different yarns and the similarity between the curves produced from Uster and from the HSC is an evident for the validity of using this method in the yarn diameter measurement for long lengths.

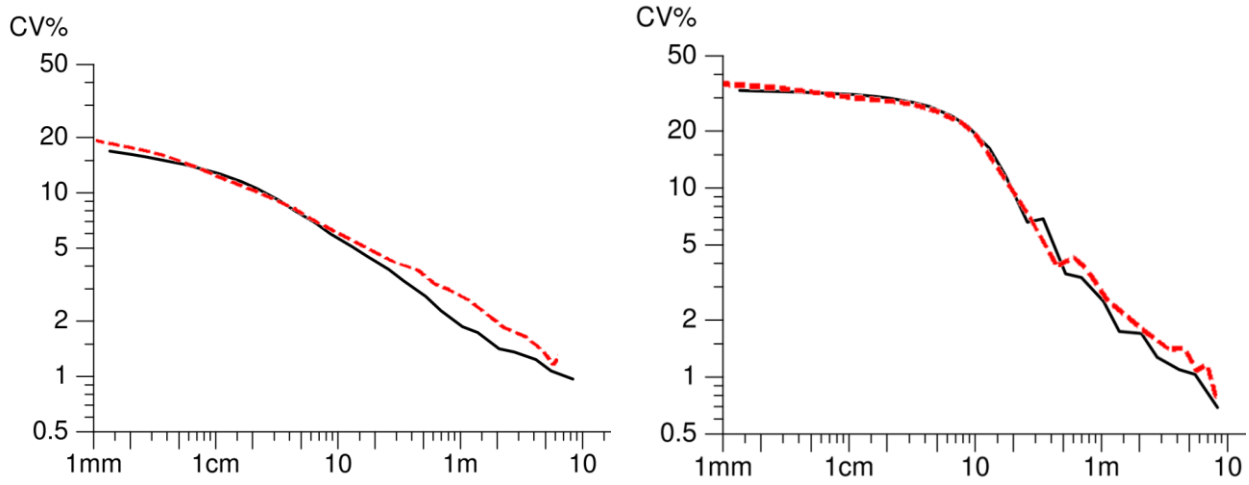

Figure 7. Length variation curve (LVC) for the yarn diameter measured by Uster (solid black) and produced from the developed HSC analysis (dashed red) for the normal yarn (left) and the slub-yarn (right)

The deviation rate percentage refers to the cumulative yarn length with diameters above or below a certain limit defined as a percentage of total sample length [19]. For example, if 30% is the calculated *DR* at α=10% for a yarn with average diameter *d*, it means that 30% of the total tested length has a diameter bigger than 1.1*d* or smaller than 0.9*d*. The deviation rate measured by Uster is illustrated in Figure 8 as well as the values calculated from the HSC. The curves were calculated at different measurement lengths where the *DR*% was calculated at the original interval of 0.3mm and was smoothed for lengths λ = 1.5, 3, and 10 m of the yarn samples. By smoothing we mean the averaging of the data and consider one reading for each length λ. For example, at λ=1.5 m an average for 5000 readings from the readings with λ=0.3 mm were considered as one reading in the subsequent calculations. The curves shown in Figure 8 for the HSC were calculated as α changes in the interval [-40:100] and demonstrated for the slub-yarn in the interval [-30:50] for illustration purposes. The general trend of the calculated curves is similar to those produced by

Uster although the slight differences in numbers are found and can be attributed to the differences of the individual readings. The IDR is also shown in Figure 8 with a similar trend albeit the calculated *IDR*% at α=0 for the different curves are more separated than the same values of *DR* at the same level of α.

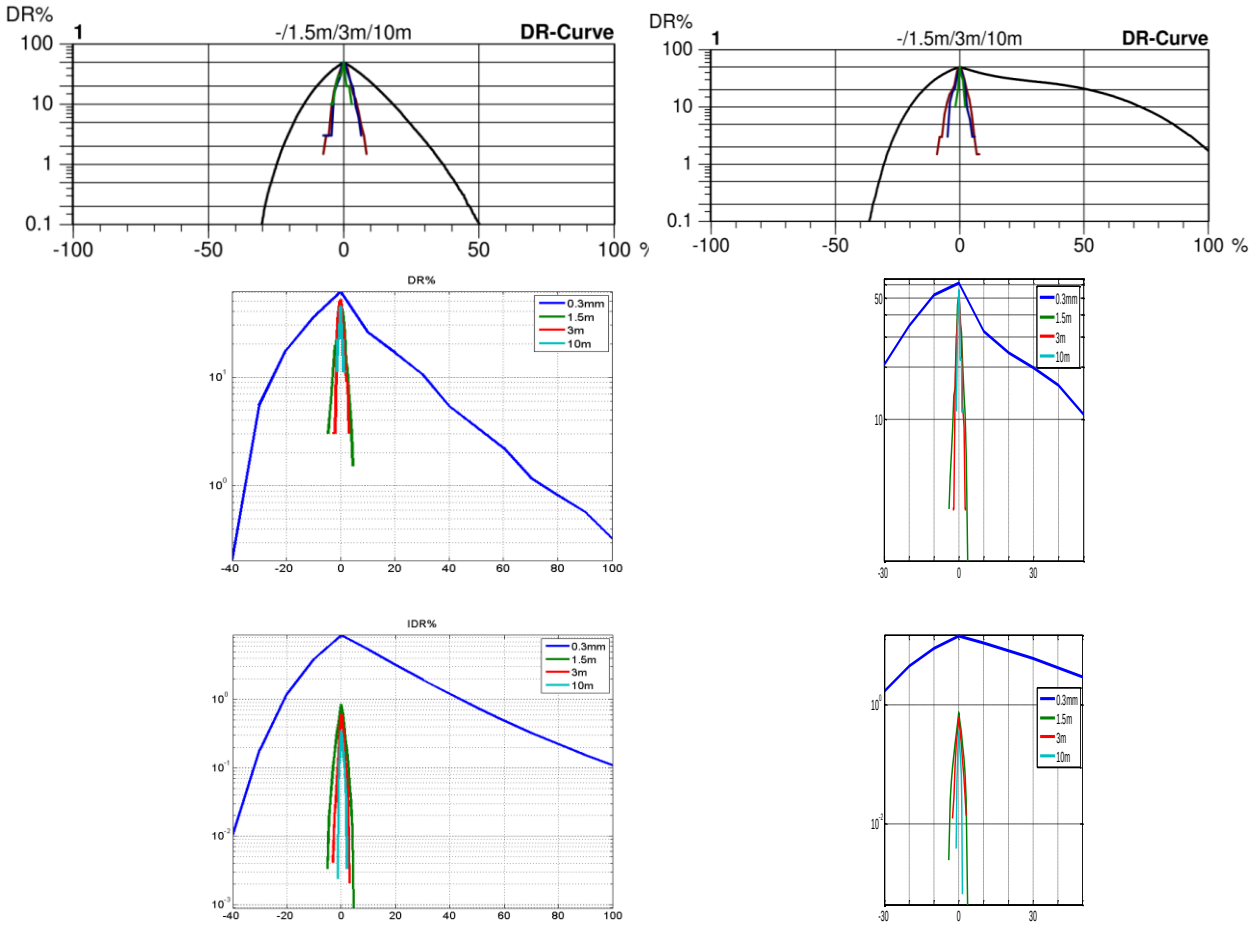

Figure 8. The DR% (middle) and the IDR% (bottom) of yarn diameter as calculated from the HSC algorithm and compared to the DR% obtained from Uster (top) for the normal yarn (left) and the slub-yarn (right)

4.2.3. Periodic variations

The periodic variations can be detected using the spectrogram. Although spectrograms are "commonly" used to demonstrate the mass periodic variability, Uster Tester also "optionally" produces a similar spectrogram for the diameter variability. The rules applied in explaining the mass spectrogram are similarly used in explaining the diameter spectrogram. The yarn diameter spectrograms which are illustrated in Figure 9as obtained from Uster tester for both yarn samples. The spectrograms produced from the data obtained from the HSC image analysis are shown also in Figure 9which indicates a relatively high similarity with the fault peaks detected by Uster for the slub-yarn sample while no similarity can be detected for the normal yarn. The contrast between the HSC calculated spectrograms for both samples is very indicative for the existence of periodicity along the yarn samples. For the slub-yarn,

where periodic variation exists, the HSC's spectrogram has dominant peaks that match the ones obtained from Uster, while in the normal yarn, with little periodic variation, the calculated spectrogram does not have such dominant peaks. The peaks shown on the HSC's spectrogram for the normal yarn are illusive as the vertical scale of the curve is very small compared to the slub-yarn's calculated curve. The four dominant peaks on the spectrogram produced from the HSC for the slub-yarn sample are located at about 0.07, 0.13, 0.25, and 0.42 m which can be found on the Uster spectrogram at the same wavelengths. The peak at the wavelength around 7.5 cm can be attributed to mechanical faults and drafting waves and the peak that is located around 13 cm can be attributed to the inter-slub distance and the peak around 25 cm can be attributed to the pattern of the long slub (10 cm) plus its inter-slub distance (15 cm). The peak at 45 cm can be attributed to the whole repeat for the pattern of the two slub populations (that is 5+15+10+15 cm).

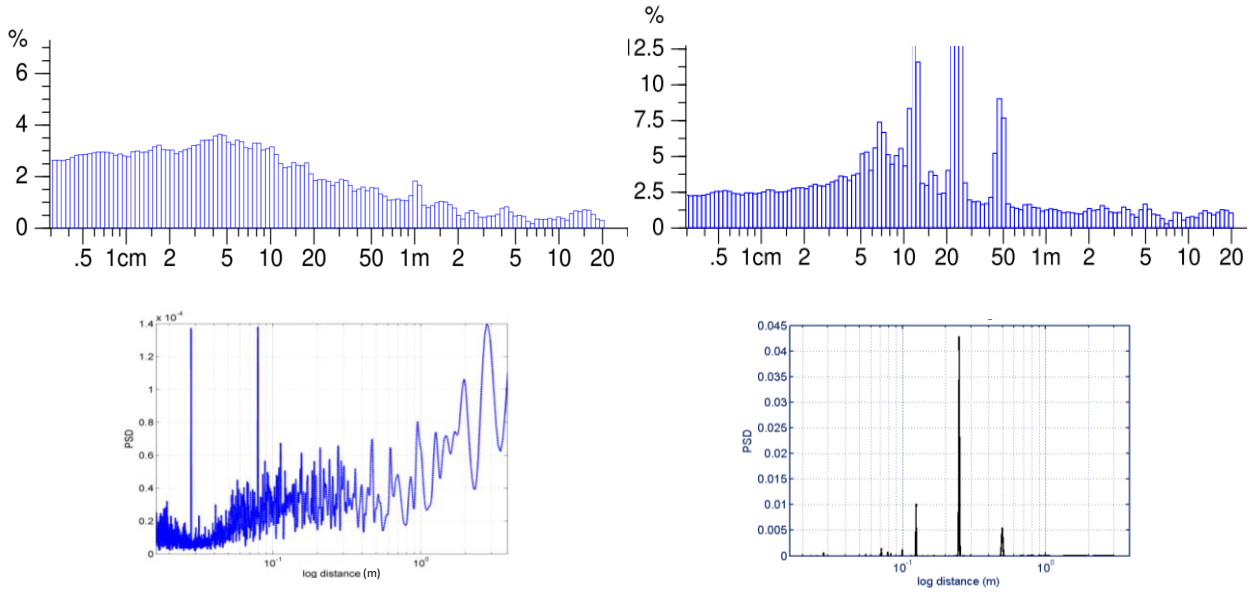

Figure 9. Spectrogram for the yarn diameter measured by Uster (top) and produced from the developed analysis (bottom) for the normal yarn (left) and the slub-yarn (right)

The autocorrelation function is another means for detecting the periodic variation but not produced by Uster evenness tester. The autocorrelation functions for the data collected on the HSC for both yarn samples are shown in Figure 10. The lack of periodicity in the normal yarn samples is demonstrated by the low correlation value and without repeating pattern. The slub-yarn sample, on the other hand, has positive correlation peaks at lags of about 30 and 60 (with a relatively lower correlation value at the former) and those peaks appear repeatedly. There is also a negative correlation peak at a lag of ≈ 15 that repeats in intervals of about 30 lags. Since the yarn diameter readings considered in the calculations were collected at intervals of 8mm, it can be seen that the positive correlation peaks represent a repeated pattern in the yarn diameter at intervals of about 24 cm (for the peak at ≈ 30) and 48 cm (for the peak at ≈

60). Those intervals are in a close agreement to the values obtained from the spectrogram for the patterns of both; the long slub, and the whole slub repeat, respectively. Similarly, the negative correlation values correspond to distances of ≈ 14 cm can be attributed to the inter-slub distance where the repeat occurs at this interval between the high and the low diameters.

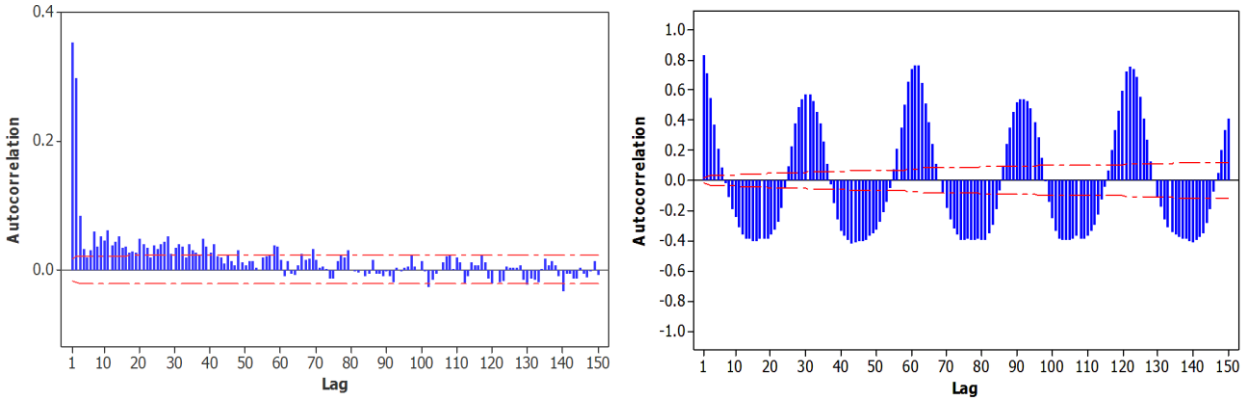

Figure 10. Autocorrelation function for yarn diameter measured at 8mm for the normal yarn (left) and the slub-yarn (right); with 5% significance limits indicated by the dotted line

4. Conclusion

The yarn diameter was analyzed using a computer vision system that utilizes a high speed camera. The images were processed using our developed robust technique that is relatively fast in removing the yarn hairiness and in filling the voids inside the yarn body. The data obtained from the applied algorithm were found to be significantly comparable to the commercial available instruments such as Uster evenness tester. The developed analysis was capable of detecting the short term, the long term, and the periodic variations of yarn diameter. To the best of the authors' knowledge, this work is the first to process the images of continuous long length of yarns to allow its time-series treatment. The newly developed processing algorithm demonstrated a fast and robust ability in treating the massive amount of yarn images compared to traditional edge detecting and processing methods. The robustness and flexibility of the suggested DiaLib® system opens the door for a relatively precise, cheap, and "transparent box" method for measuring the yarn diameter with a wealth of information that can be drawn during the analysis and may not be obtained from the commercial instruments.

References:

[1] R. Kovar, "Length of the yarn in plain-weave crimp wave," *Journal of The Textile Institute*, vol. 102, pp. 582-597, 2011/07/01 2011.

[2] G. A. V. Leaf, "The mechanics of plain woven fabrics," *International Journal of Clothing Science and Technology*, vol. 16, pp. 97-107, 2004/02/01/ 2004.

[3] M. R. Mahmoudi and W. Oxenham, "A new electro-mechanical method for measuring yarn thickness," *AUTEX Research Journal*, vol. 2, pp. 28-37, 2002.

[4] V. Carvalho, M. Belsley, R. Vasconcelos, and F. Soares, "A comparison of mass parameters determination using capacitive and optical sensors," *Procedia Chemistry*, vol. 1, pp. 766-769, 9// 2009.

[5] V. Carvalho, R. Vasconcelos, F. Soares, and M. Belsley, "Yarn Diameter and Linear Mass Correlation," *Journal of Nondestructive Evaluation*, vol. 28, pp. 49-54, 2009/06/01 2009.

[6] V. H. Carvalho, P. J. Cardoso, M. S. Belsley, R. M. Vasconcelos, and F. O. Soares, "Yarn Diameter Measurements Using Coherent Optical Signal Processing," *Sensors Journal, IEEE*, vol. 8, pp. 1785-1793, 2008.

[7] V. Carvalho, F. O. Soares, and M. Belsley, "A comparative study between yarn diameter and yarn mass variation measurement systems using capacitive and optical sensors," *Indian Journal of Fibre & Textile Research*, vol. 33, pp. 119-125, June, 2008 2008.

[8] J. Voborova, A. Garg, B. Neckar, and S. Ibrahim, "Yarn properties measurement: an optical approach," in *2nd International Textile, Clothing & Design Conference*, Dubrovnik, Croatia, 2004.

[9] S. Ibrahim, J. Militky, D. Kremenakova, and R. Mishra, "Characterization of Yarn Diameter Measured on Different Systems," presented at the International Conference: Textiles & Fashion, Bangkok, Thailand, 2012.

[10] J. Ma and N. A. Korobov, "The Calculational Method for Spectrogram and Variance-Length Curve of Yarn Based on Multiresolution Analysis," in *Parallel and Distributed Computing, Applications and Technologies, 2005. PDCAT 2005. Sixth International Conference on*, 2005, pp. 993-996.

[11] V. Carvalho, J. L. Monteiro, F. O. Soares, and R. M. Vasconcelos, "Yarn Evenness Parameters Evaluation: A New Approach," *Textile Research Journal*, vol. 78, pp. 119-127, February 1, 2008 2008.

[12] V. Carvalho, P. Cardoso, M. Belsley, R. Vasconcelos, and F. Oliveira, "Yarn irregularity parameterisation using optical sensors," 2009/01// 2009.

[13] D. C. Montgomery, C. L. Jennings, and M. Kulahci, *Introduction to time series analysis and forecasting*. Hoboken, N.J.: Wiley-Interscience, 2008.

[14] J. A. Hartigan and P. M. Hartigan, "The dip test of unimodality," *The Annals of Statistics*, pp. 70-84, 1985.

[15] P. M. Hartigan, "Computation of the dip statistic to test for unimodality," *Journal of the Royal Statistical Society. Series C (Applied Statistics)*, vol. 34, pp. 320-325, 1985.

[16] B. S. Everitt and D. J. Hand, "Finite mixture distributions," *Monographs on Applied Probability and Statistics, London: Chapman and Hall, 1981*, vol. 1, 1981.

[17] D. M. Titterington, A. F. M. Smith, and U. E. Makov, *Statistical analysis of finite mixture distributions* vol. 7: Wiley New York, 1985.

[18] M. Krifa, "Fiber Length Distribution in Cotton Processing: A Finite Mixture Distribution Model," *Textile Research Journal*, vol. 78, pp. 688-698, 2008.

[19] G. H. Rong and K. Slater, "Analysis of Yarn Unevenness by Using a Digital-signal-processing Technique," *Journal of The Textile Institute*, vol. 86, pp. 590-599, 1995/01/01 1995.

Original article

Textile Research Journal

Textile Research Journal
2014, Vol. 84(18) 1948–1960

DOI: 10.1177/0040517514530032
trj.sagepub.com
SAGE

A dynamic and robust image processing based method for measuring the yarn diameter and its variation

Mohamed Eldessouki[1,2], Sayed Ibrahim[3] and Jiří Militký[1]

Abstract

The yarn diameter is an effective property in determining fabric structure and processing settings. There are different systems of measuring the yarn diameter; among them is the image analysis of the yarn's microscopic images. This method is considered to be more precise than other methods, but it is "static" in nature as it measures the property at scattered intervals and does not reflect the continuous variation of the yarn diameter. The goal of the current work is to measure the yarn diameter and its variation over a long length of yarn at fixed intervals to consider the "dynamic" change in the property. To achieve this goal, a high-speed camera (HSC) with a proper magnification was used to capture the images of the yarn and a new robust algorithm was developed to analyze the massive amount of yarn pictures in a reasonable time. The collected data for the yarn diameter were analyzed and compared to the results of the commercial Uster Evenness Tester IV. The results of the HSC were very comparable to the results of Uster and they were able to detect the short-term, the long-term, and the periodic variation of the yarn diameter.

Keywords

yarn diameter, robust image analysis, long-term variation, periodic variation

Yarn diameter is an important parameter that is used in all the calculations and modeling of fabric parameters[1] such as weave angle, yarn densities in warp and weft directions, yarn crimp ratio, cover ratio, fabric weight, and fabric volumetric density. The yarn diameter has also a direct impact on some of the measured fabric properties that affect the fabric dimensional and mechanical parameters.[2] Fabric performance and comfort depend on the yarn diameter as it correlates to the fabric air and water permeability. The settings of winding machines (e.g. cleaning knife) and most of the machines in the subsequent processes depend on the yarn diameter. On the other hand, the "exact" measurement of the yarn diameter is very difficult because of the inherent yarn unevenness and irregularity. That leads the textile specialists to talk about the yarn "size" or "count" instead of its "diameter". However, yarn count may not precisely indicate the yarn diameter, as two yarns with the same count may have two different diameters due to the changes in other parameters such as the fiber density and the yarn twist factor.

Therefore, a good method of measuring the yarn diameter should maintain two basic features; it should measure the diameter with high precision and accuracy. It also should be able to determine the irregularities that occur in diameter at different bases (short- and long-term variations as well as the periodic variations).

The principles of measuring the yarn diameter can be classified[3] into four main categories that are

[1]Technical University of Liberec, Faculty of Textile Engineering, Materials Engineering Department, Liberec, Czech Republic
[2]Department of Textile Engineering, Faculty of Engineering, Mansoura University, Mansoura, Egypt
[3]Technical University of Liberec, Faculty of Textile Engineering, Textile Technology Department, Liberec, Czech Republic

Corresponding author:
Mohamed Eldessouki, Materials Engineering Department, Technical University of Liberec, Studentská 2, 461 17 Liberec 1, Liberec, Czech Republic.
Email: mohamed.eldessouki@tul.cz

summarized with their pros and cons in Table 1. These methods are:

- The capacitive measurement: This is an indirect method of measuring the variation in yarn linear density (yarn count) which correlates to the yarn diameter through empirical relations from which the variation in yarn diameter can be calculated. The major drawback of this method is the indirect measurement of the yarn diameter (in fact, the mass variation is measured, not the diameter, but due to the high correlation between both parameters it is possible to measure one parameter and infer the other[4,5]). This method also depends on the testing environmental conditions because the capacitors are usually affected by the temperature and humidity. The resolution of this method is relatively low where the capacitors sample the data every 8 mm (e.g. old versions of the Uster tester).
- The optical measurement: This method is widely used[6] in commercial devices where high resolutions (e.g. 0.25 mm) can be obtained. This method determines the diameter after shedding a beam of laser light on the yarn and analyzing its projected image on a light sensor (Figure 1). The results of this method are highly dependent on the direction (the angle β) of the yarn as the projected image of the elliptical shape of the yarn may be larger or lower than the actual diameter. This method does not affect with the testing humidity or the fiber blend variation,[7] although it might be affected with the presence of lint and yarn hairiness. During these measuring methods, the yarn exists under a slight tension in the longitudinal direction which causes a compression in the transverse direction and may lead to changes in the measured diameter.
- The mechanical (electro-mechanical) measurement: In this method, the yarn runs between two sensors (fixed and freely moved) where the movement of the freely moved sensor is magnified for measuring the diameter. These sensors are implemented in different ways (cylinders, flat surface, etc.), among them a device similar to the tongue and groove mechanism used on drawing frames.[2] The yarn passes through the grove, and the tongue is attached to an arm that works as displacement amplifier to record the yarn diameter and its variations.
- The small scale microscopic measurement: This laboratory method is, principally, an optical method but it can be distinguished from the other optical methods by its small scale of measurements where the yarn diameter is measured in two directions; the cross section or the longitudinal view of the yarn.[8] The cross section of the yarn should be carefully cut at different positions and the diameter can be captured under the microscope with an appropriate magnification. Similarly, the yarn diameter is measured from the longitudinal projections of the yarn under the microscope at randomly different positions to account for the elliptical shape of the

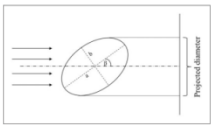

Figure 1. Schematic representation of the optical yarn diameter measurement system.

Table 1. Advantages and disadvantages of the methods for measuring yarn diameter

	Advantages	Disadvantages
Capacitive	– Works with the common yarn irregularity measurement systems – Primitive method	– Low resolution – Depends on the testing environment – Affected by other fiber properties (e.g. material type, fineness, specific density) and yarn parameters (e.g. twist, production technology)
Optical	– High resolution – Does not depend on testing environment – Simple and fast	– Measures the projected diameter not the real diameter – Yarn under tension reduces the measured diameter – Affected with the lint and hairiness
Mechanical	– Direct contact with the yarn	– Depends on the applied load during measurement
Small scale measurement	– Precise method - Measures the actual diameter	– Time consuming and tedious method – Not suitable for practical application in production scales

yarn.[9] Measurements can be done on the computer by a visual inspection or automatically using some image analysis techniques.

The microscopic evaluation of yarn diameter is preferred for academicians in laboratories for its accuracy and it is used to calibrate the other methods. This method, however, is time consuming and needs many repeated samples, which makes it unsuitable for practical testing in production environments. It is also important to notice that the measurements of this method are "static" as they give information about the yarn at "scattered" points across the length of the yarn. This means; it does not capture the continuity of the variation in the measured property along the yarn and cannot usually detect the short-term, the long-term or the periodic variation of the yarn diameter.

This work aims at tackling the problems of the microscopic evaluation method and presents a new computer vision based system to measure the yarn diameter and its variation utilizing video processing and analysis algorithms. A high-speed camera (HSC) is used to capture the yarn images, and it was used to allow testing speeds comparable to speeds of the known commercial devices. A new image analysis algorithm is developed to enhance the captured images by eliminating the yarn hairiness and hence to obtain the yarn diameter. The continuity of the obtained results at fixed interval allows their treatment as a time series, which unveils some of the yarn characteristics that are produced from the commercial instruments. Two case studies are used in order to validate the presented system results; one of them is a regular ring-spun yarn and the other is a slub-yarn. Both yarns are tested simultaneously on the presented system and on the Uster Evenness Tester IV.

Experimental setup

Computer vision setup

Pre-investigation of the system and the analysis algorithm was initially performed using yarn samples evaluated under the optical microscope. An Olympus microscope was used with an automated stage to capture the yarn images along a certain distance with a magnification scale of 2.68 μm/pixel. The setup of the microscope is shown in Figure 2 with the motorized stage and the digital camera that is connected to the computer. The microscope system captures a longitudinal view of the yarn then the stage moves automatically with a predefined distance to capture another image. The obtained images were stitched and superimposed together to form a single picture of the whole yarn.

Because of the slow image acquisition with the automated microscope, alternative systems of acquisition were considered. A video camera with appropriate magnification lenses was applied; however, the yarn speed for this camera setup was about 15 m/min, which is less than the practical testing speeds of the commercial instruments. To run the yarns at 100 m/min (which is the testing speeds of other instruments such as Uster Evenness Tester IV), an HSC was used. The Olympus i-speed 3 HSC was installed with appropriate macro-lenses. The HSC captured yarn images with a speed of 150 frames per second (fps), the used shutter speed was 200×, and the resolution of individual frames in the recorded video was 1280 × 1024 pixels with a magnification scale of 10.2 μm/pixel. The yarn was lighted with a special Xenon lamp directed with an optical fiber to the HSC shooting zone. To avoid the effect of tension changes during the experiments, the yarn was running in front of the camera under constant tension using the tension compensation mechanism of Lawson Hemphill Constant Tension Transport (CTT) tester. The introduced computer vision system for measuring the yarn diameter (that includes the video camera setup with the analysis software) was assigned the name DiaLib®.

Tested samples

Two yarn samples were examined and analyzed using the suggested method and the results were verified against the measurements on the commercial Uster Evenness Tester IV. The first yarn sample is a normal ring-spun 100% cotton yarn with a count of 20 tex. The second yarn sample is a cotton slub-yarn produced by deliberately changing the draft on the spinning frame. The yarn count was 23 tex and the slub thickness was designed to be twice the yarn original diameter. The slubs were distributed across the yarn in two

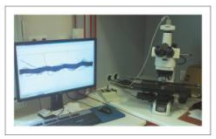

Figure 2. Microscopic setup with a motorized stage and CCD camera connected to the computer.

populations with slub-lengths of 50 mm and 100 mm. The inter-slub separation distance was designed to be 150 mm. The yarn was tested on Uster Evenness Tester IV for its diameter and irregularity and the images of the yarn were captured using the high speed camera. The yarn speed during testing on the Uster and the HSC was 100 m/min.

Methods

Image processing and analysis

The longitudinal view of the yarn sample was acquired with a proper magnification using a digital camera connected to the computer. The acquired images were converted to binary with a suitable threshold to allow faster processing. The yarn diameter is calculated by counting the pixels belonging to the yarn body at specified intervals. The existence of yarn hairiness with protruding fibers does not allow the direct and automatic finding of the yarn limits (where the diameter can be measured) because those protruding fibers will be outside the actual diameter. Therefore, the automatic measurement of the yarn diameter is faced with three obstacles; firstly, the exclusion of the yarn hairiness from the yarn body. Secondly, the filling of the voids inside the yarn body that occur during the conversion to binary images (due to the shading differences in the microscope images). Thirdly, the standard algorithms for edge detection (to remove the hairiness) and object filling (to remove the voids) are relatively slow and there is a need to increase the speed of the processing algorithm. These obstacles will be folded many times in accordance with the interval distance between the measurements and the number of the images to be processed. For example, there is about 350 slices in an image of a yarn with length ≈ 7 cm and interval between readings of 0.2 mm, and this number reaches many thousands for longer yarn samples.

To face these challenges, a new algorithm was developed to be robust with the increase in number of pictures and sampling points. To find the yarn body in an image (let us call it I1), two other images of the yarn were created by translating the yarn image in the vertical direction with distances ±δ (let us call the created shifted images I2 and I3). Then, the three images are added together and the summation matrix is logically compared to a certain threshold to produce a binary image with filled yarn body and trimmed of the majority of yarn hairiness.

To demonstrate the algorithm, an example is shown in Figure 3 with a small scale matrix with a height of 20 pixels (while actual yarn images have a height of 1024 pixels). The example in Figure 3 shows one vector (a column that can be called C1) that represents what is extracted from the binary matrix of the yarn

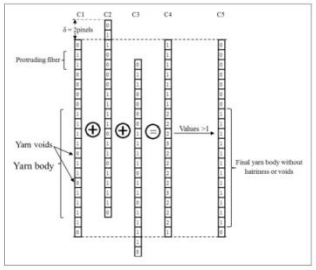

Figure 3. Example of the suggested algorithm to remove hairiness and fill-in yarn voids to find yarn body and diameter.

image at a certain cutting interval, and the same calculations can be extended for all intervals in the yarn image. The example shown in Figure 3 represents the black background with zeroes and the white elements of the yarn with ones. The representation vector C1 corresponds to a slice of the image where the yarn body is represented with a series of ones (including some voids of zeroes) and a part of the protruding fiber at the top of the vector. This vector was shifted upward with a distance (δ) of 2 pixels (which resulted in another vector that can be called C2) and shifted downward with the same δ (to result in a third vector C3). The vector C4 is the summation of C1, C2 and C3; then it is logically compared to consider the positions with numbers less than or equal to one as background (substituting a value of zero at these positions) and the positions of values greater than one to be foreground (substituting a value of one). The resulted vector C5 shows the solid yarn body without voids or yarn hairiness from the protruding fibers.

To compare the suggested algorithm with "traditional" edge detection techniques, it is important to understand how these techniques work. Traditional edge detection techniques generally depend on converting the image from its spatial domain into a frequency domain to apply some filters on the image and then the image is converted back to its spatial domain. After this process, the detection algorithm applies some programming loops to determine the yarn boundaries and remove the hairiness. These traditional methods are computationally expensive and depend on the available hardware resources in completing these tasks. Our suggested method, however, analyzes pictures in their spatial domain only and avoids the loops that consume the computer resources. As the time for any image processing method depends on the used algorithm and the available hardware resources, the suggested system used a personal computer with an Intel Core i3 processor to analyze ≈ 10,000 pictures in ≈ 8 min.

Although this algorithm is relatively fast and robust compared to the standard edge detection and image filling algorithms, it has some drawbacks and errors that may occur during the processing. These errors result from the dependency of the algorithm on the deliberate choice of the image shifting (δ) and on the position of the protruding fibers and voids (which are random). After considering different values for the image shifting (δ) and its effect on the calculation accuracy, it was found that a δ value is approximately equal to the thickness of the protruding fiber is a good choice in most cases. Therefore, the value of δ is calculated during the analysis based on the magnification scale and the fiber's average diameter that are given by the user. To illustrate the errors that may occur, Figure 4

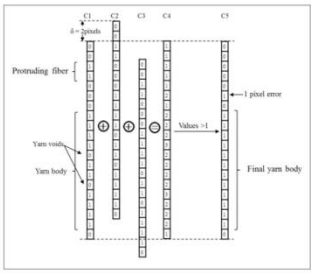

Figure 4. Example of the suggested algorithm with an error in the hairiness removal.

shows a vector from the yarn image similar to the one shown in Figure 3 with a minor change in the position of the protruding fiber which resulted in an error as indicated in C5 by considering one extra pixel as part of the yarn body. A similar error can occur for consecutive voids with a close proximity. Considering the image scale (where one pixel is about 2.6 μm for the microscopic images to 10 μm for the camera images) and the averaging of the thousands of readings to calculate the yarn diameter, the calculation error of this algorithm can be found in the order of 10^{-6} mm per pixel. This error order is relatively small and does not significantly affect the final results of yarn diameter.

Data analysis and parameterization

The data obtained from the analysis of the HSC images are taken at regular intervals (space and time intervals), which allow the data to be treated as time series. Beside the normal statistics that can be derived for any set of data, the discussion here will focus on the parameters that depend on the data continuity to demonstrate the advantages of the introduced procedure (with the dynamic measurement of the yarn) over the static procedures.

The length-variance curve. The length-variance curve (LVC) determines the relationship between the variability of the yarn diameter and the measurement intervals. The variability (CB) is expressed as the coefficient of variation and can be measured at a certain yarn cut length (λ) according to Ma and Korobov:[10]

$$CB(\lambda) = \frac{s(\lambda)}{\bar{x}(\lambda)} \quad (1)$$

where, $s(\lambda)$ denotes the standard deviation of yarn diameter and $\bar{x}(\lambda)$ is the average value at a given cut length λ. The "cut length" represents the distance between two consecutive diameter readings on the measurement system and these calculations are repeated at different cut lengths to construct the LVC.

Deviation rate. The deviation rate (DR) measures the frequency (the rate of occurrence) for a diameter value to deviate from the yarn mean diameter plus or minus a certain sensitivity limit (α). For the deviation rate calculation, the function $p(n, \alpha)$ should be calculated to allow the frequency calculation. This function can be defined as:[11,12]

$$p(n,\alpha) = \begin{cases} 1 & f(x_n) \geq (1+\alpha)\bar{\mu} \\ 0 & (1-\alpha)\bar{\mu} < f(x_n) < (1+\alpha)\bar{\mu} \\ 1 & (1-\alpha)\bar{\mu} \geq f(x_n) \end{cases} \quad (2)$$

The deviation rate can be calculated from the function $p(n, \alpha)$ according to the relation:

$$DR_\alpha[\%] = \frac{\sum_{n=1}^{N} p(n,\alpha)}{N} * 100 \quad (3)$$

where n is an index, α is the sensitivity limit, $f(x_n)$ is the diameter value, $\bar{\mu}$ is the mean diameter of the yarn sample and N is the total number of readings.

Absolute mean deviation. The absolute mean deviation ($U\%$) is a commonly used term to define the mass irregularity of yarns and can be used to define the irregularity in diameter as well. It can be calculated for a series of diameter readings (x_n) using the relation:

$$U_\alpha[\%] = \frac{\sum_{n=1}^{N} |x_n - \bar{\mu}|}{N * \bar{\mu}} * 100 \quad (4)$$

Integral deviation rate. The integral deviation rate (IDR) accounts for the diameter's absolute mean deviation at certain sensitivity limit (α) and it can be considered as a generalization formula for the $U\%$ (where $U\% = \text{IDR}$ at $\alpha = 0$). The starting function for the IDR calculation is the function $y(n)$, similar to the frequency function $p(n, \alpha)$, where:

$$y(n,\alpha) = \begin{cases} |f(x_n) - (1+\alpha)\bar{\mu}| & f(x_n) \geq (1+\alpha)\bar{\mu} \\ 0 & (1-\alpha)\bar{\mu} < f(x_n) < (1+\alpha)\bar{\mu} \\ |f(x_n) - (1-\alpha)\bar{\mu}| & (1-\alpha)\bar{\mu} \geq f(x_n) \end{cases} \quad (5)$$

Then, the IDR can be calculated according to:

$$IDR_\alpha[\%] = \frac{\sum_{n=1}^{N} y(n,\alpha)}{N * \bar{\mu}} * 100 \quad (6)$$

Autocorrelation function. Autocorrelation is an expression for the correlation of a time series with its own past and future values. The autocorrelation function (ACF) that measures the correlation of a data series $x(n)$ with itself shifted by some delay (lag) m can be calculated from the auto-covariance function:[13]

$$C(m) = \frac{1}{N-m} \sum_{n=1}^{N-m} (x(n) - \bar{\mu}) \cdot (x(n+m) - \bar{\mu}) \quad (7)$$

And the sample auto-correlation function at the lag m can be calculated as:

$$\rho(m) = \frac{C(m)}{C(0)}, \quad m = 1, 2, 3, \ldots, M < N \quad (8)$$

Results and discussion

It is worthy at the beginning of the discussion to clarify four points regarding the suggested algorithm and the selected yarn samples. First, the proposed method as well as all methods that measure the diameter with a single yarn projection (i.e. using only one camera or sensor) work under the basic assumption that: during the measurement of longer lengths of yarn, the yarn rotates around its axis and the huge amount of collected readings will eventually account for the elliptical shape of the yarn. Second, the choice of the slub-yarn as a second case study versus the normal ring-spun yarn is based on the continuous and periodic variation of yarn diameter in these yarns which should clarify the performance of the proposed system in measuring the yarn diameter and detecting the different types of its variation.

Third, the results of the HSC tested yarns were compared to the Uster Evenness Tester IV although the most recent version of the Uster Tester V has a special configuration for measuring the slub-yarns and gives more detailed and relatively precise information about the special structure of these fancy yarns. This study, however, was intended to verify the validity of the applied algorithm even if it does not compete with the advanced hardware and software implemented by Uster. Fourth, the Uster Tester is the most used instrument in industry and is able to deal with the measurement as a function of time and results in useful information such as LVC, spectrographic data, and so on. On the other hand, the suggested algorithm is a relatively cheap and "transparent box" system that enables us to verify the results obtained from Uster and other instruments that work on the optical principle. Also, the suggested algorithm allows functions and parameters that are not produced by commercial instruments to be calculated (e.g. autocorrelation function, fractal dimensions, etc.) and these parameters are out the scope of the current study.

Microscopic images

The yarn samples were tested on the microscope setup where the individual captured frames represent a length of about 2.9 mm of the yarn length. The microscope software applies a picture stitching algorithm (for a collection of about 25 pictures) that considers the overlapping of the pictures to create a single image (of about 7 cm) as shown in Figure 5(a). The operation was repeated for a total sample length of 3 m. The individual pictures (for the 7 cm) were processed and an example for a magnified part of the yarn is shown in Figure 5(b). The yarn diameter can be calculated at any required reading interval where the minimum interval is about 2.68 μm (that is equivalent to 1 pixel). A yarn image that was processed at an interval of 0.2 mm is shown as a superimposed image of the actual yarn and the detected boundaries in Figure 5(c) where the white parts of the vertical lines represent the detected yarn boundaries at each interval. It can be seen in the processed image that the automated algorithm was capable of detecting the yarn boundaries and considering the yarn body despite of the differences in the gray levels inside the yarn. The method, however, failed to remove the whole protruding fiber as circled in Figure 5(c) (the first reading to the right). The reason for the system to consider this hairiness inside the yarn diameter is, partially, because of its close proximity to the yarn body and its positioning in a vertical way (which resulted in more pixels in the cross-section compared to the positioning of horizontal fibers). After all, the method was able to remove about half of the circled protruding fiber

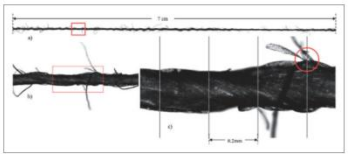

Figure 5. (a) Longitudinal view of the yarn as captured under the microscope; (b) the magnification of the window drawn in (a); (c) a magnification of the window drawn in (b) with illustration of the diameter measuring intervals.

and the remaining part is much less than 10% of the yarn diameter which makes this error almost negligible after averaging the thousands of reading.

The high speed camera

A 100 m of the each yarn sample (a one minute run) was recorded and the sampling of the yarn diameter from the video was flexible to be adjusted at any interval (with a minimum distance of about 0.01 mm between diameter readings). To compare the HSC with the Uster Tester results, the measurement interval was adjusted to 0.3 mm to match the interval used in Uster measurements. Two sets of data produced from the HSC with a set of measurement at 0.3 mm and another set of readings that were averaged every 8 mm to match the results produced by Uster Tester. Once the videos were processed and the results from HSC were collected, the analysis was performed to produce the statistical and spectral features of the yarn diameter. We should point out that the Uster Tester uses two perpendicular cameras to measure the yarn diameter and reports two results; the one obtained from the two cameras and the other from values measured using one camera.

Basic statistics and short-term variation. The results of both the Uster Tester and the HSC are summarized in Table 2 at the two measurement intervals 0.3 mm and 8 mm for both yarn samples. The average yarn diameter for both yarn samples is comparable when measured using Uster and obtained from the suggested method. The variability of values, on the other hand, as expressed in terms of the coefficient of variation (CV) is slightly different especially as measured at short intervals of 0.3 mm. It is also observed that the CV values are generally higher at short measurement intervals; that is expected as more variability is encountered at these lengths. This increase is also in agreement with the behavior of the length variation curve where higher variation is usually found at shorter measuring lengths. Although the slub-yarn has two different diameters as can be clearly seen in the bimodal histograms of Figure 6, the results of Uster report a single value for the diameter (with a high variation) which is the mean of all values if considered as a normal distribution. The diameters calculated from the high speed camera are also shown in Figure 6 with a bimodal histogram for the slub-yarn sample. The theoretical normal distribution curves calculated from the HSC analysis are shown in the figure with mean values relatively close to the data obtained from Uster. The availability of the raw data from the HSC allows the analysis of the two averages of the bimodal distribution for the slub-yarn. The Hartigan's DIP method[14,15]was used for testing the unimodality and the finite mixture distributions method[16–18] was applied to separate the bimodal curve. Analysis of the bimodal distribution indicates that the first mode is 0.301 mm (standard deviation 0.066 mm) and the second mode is 0.192 mm (standard deviation 0.024 mm).

Long-term variation. The long-term variation in the yarn diameter can be detected using the LVC. The application of the image processing allows the determination of the yarn diameter at different intervals, which permitted the construction of the LVC. The LVC for the tested yarns are shown in Figure 7 as produced from the applied algorithm and compared to the curve obtained from Uster Evenness Tester. The theoretical LVC for an ideal yarn can be represented by an inclined straight line (on a diagram with double logarithmic scale) and any deviation from the ideal line corresponds to a long-term variation. It can be seen from the figure that the results of the HSC are very comparable to the results of the Uster Tester and the LVC curve for the normal yarn is almost straight while being curved for the slub-yarn. The LVC is very useful in comparing the

Table 2. Uster and HSC diameter results for the tested yarn samples

		Uster		HSC	
		0.3 mm	8 mm	0.3 mm	8 mm
Normal yarn	Average diameter (mm)	0.22	0.218 (2D[a])	0.235	0.235
	CV (%)	18.68 (2D) 19.82 (1D[b])	13.40 (2D)	23.34	13.53
Slub-yarn	Average diameter (mm)	0.26	0.259 (2D[b])	0.239	0.24
	CV (%)	33.47 (2D) 34.01 (1D[b])	31.58 (2D)	36.86	30.33

[a]Values measured using two perpendicular cameras.
[b]Values measured using one camera.

regularity of different yarns and the similarity between the curves produced from Uster and from the HSC is an evident for the validity of using this method in the yarn diameter measurement for long lengths.

The deviation rate percentage refers to the cumulative yarn length with diameters above or below a certain limit defined as a percentage of total sample length.[19] For example, if 30% is the calculated *DR* at

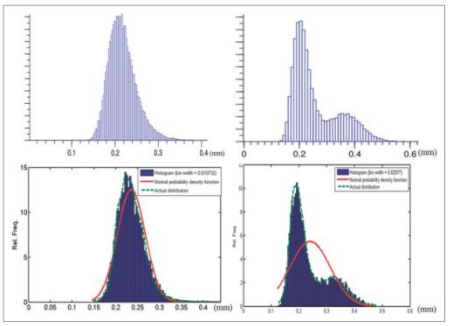

Figure 6. Histogram for the yarn diameter measured by Uster (top) and produced from the analysis of HSC (bottom) for the normal yarn (*left*) and the slub-yarn (*right*).

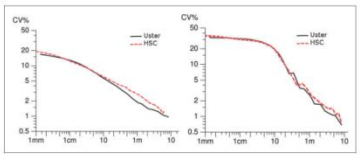

Figure 7. LVC for the yarn diameter measured by Uster and produced from the developed HSC analysis for the normal yarn (*left*) and the slub-yarn (*right*).

$\alpha = 10\%$ for a yarn with average diameter d, it means that 30% of the total tested length has a diameter bigger than $1.1d$ or smaller than $0.9d$. The deviation rate measured by Uster is illustrated in Figure 8 as well as the values calculated from the HSC. The curves were calculated at different measurement lengths where the *DR*% was calculated at the original interval of 0.3 mm and was smoothed for lengths $\lambda = 1.5$, 3, and 10 m of the yarn samples. By smoothing we mean the averaging of the data and consider one reading for each length λ. For example, at $\lambda = 1.5$ m an average for 5000 readings from the readings with $\lambda = 0.3$ mm were considered as one reading in the subsequent calculations. The curves shown in Figure 8 for the HSC were calculated as α changes in the interval [−40:100] and demonstrated for the slub-yarn in the interval [−30:50] for illustration purposes. The general trend of the calculated curves is similar to those produced by Uster, although slight differences in numbers are found and can be attributed to the differences of the individual readings. The IDR is also shown in Figure 8 with a similar trend, albeit the calculated IDR% at $\alpha = 0$ for the different curves are more separated than the same values of DR at the same level of α.

Periodic variations. The periodic variations can be detected using the spectrogram. Although spectrograms are "commonly" used to demonstrate the mass periodic variability, the Uster Tester also "optionally" produces a similar spectrogram for the diameter variability. The rules applied in explaining the mass spectrogram are similarly used in explaining the diameter spectrogram. The yarn diameter spectrograms which are illustrated in Figure 9 as obtained from the Uster Tester for both yarn samples. The spectrograms produced from the data obtained from the HSC image analysis are shown also in Figure 9, which indicates a relatively high similarity with the fault peaks detected by Uster for the slub-yarn sample, while no similarity can be detected for the normal yarn. The contrast between the HSC calculated spectrograms for both samples is very indicative of the existence of periodicity along the

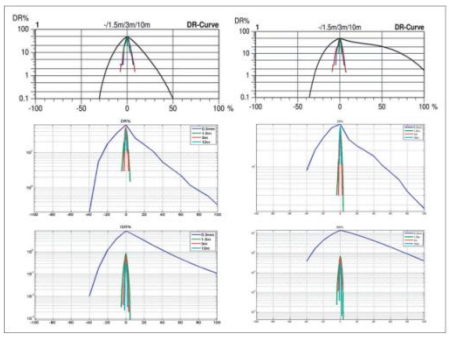

Figure 8. The DR% (*middle*) and the IDR% (bottom) of yarn diameter as calculated from the HSC algorithm and compared to the DR% obtained from Uster (top) for the normal yarn (*left*) and the slub-yarn (*right*).

yarn samples. For the slub-yarn, where periodic variation exists, the HSC's spectrogram has dominant peaks that match the ones obtained from Uster, while in the normal yarn, with little periodic variation, the calculated spectrogram does not have such dominant peaks. The peaks shown on the HSC's spectrogram for the normal yarn are illusive, as the vertical scale of the curve is very small compared to the slub-yarn's calculated curve. The four dominant peaks on the spectrogram produced from the HSC for the slub-yarn sample are located at about 0.07, 0.13, 0.25 and 0.42 m, which can be found on the Uster spectrogram at the same wavelengths. The peak at the wavelength around 7.5 cm can be attributed to mechanical faults and drafting waves and the peak that is located around 13 cm can be attributed to the inter-slub distance and the peak around 25 cm can be attributed to the pattern of the long slub (10 cm) plus its inter-slub distance (15 cm). The peak at 45 cm can be attributed to the whole repeat for the pattern of the two slub populations (that is 5 + 15 + 10 + 15 cm).

The autocorrelation function is another means for detecting the periodic variation but not produced by the Uster Evenness Tester. The autocorrelation functions for the data collected on the HSC for both yarn samples are shown in Figure 10. The lack of periodicity

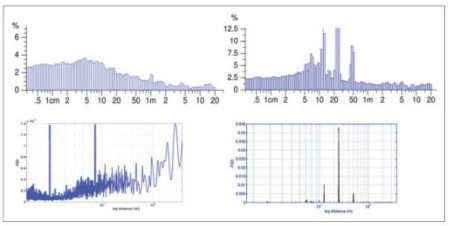

Figure 9. Spectrogram for the yarn diameter measured by Uster (top) and produced from the developed analysis (bottom) for the normal yarn (*left*) and the slub-yarn (*right*).

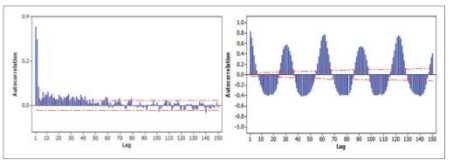

Figure 10. Autocorrelation function for yarn diameter measured at 8 mm for the normal yarn (*left*) and the slub-yarn (*right*); with 5% significance limits indicated by the dotted line.

in the normal yarn samples is demonstrated by the low correlation value and without repeating pattern. The slub-yarn sample, on the other hand, has positive correlation peaks at lags of about 30 and 60 (with a relatively lower correlation value at the former) and those peaks appear repeatedly. There is also a negative correlation peak at a lag of ≈ 15 that repeats in intervals of about 30 lags. Since the yarn diameter readings considered in the calculations were collected at intervals of 8 mm, it can be seen that the positive correlation peaks represent a repeated pattern in the yarn diameter at intervals of about 24 cm (for the peak at ≈ 30) and 48 cm (for the peak at ≈ 60). Those intervals are in a close agreement with the values obtained from the spectrogram for the patterns of both; the long slub, and the whole slub repeat, respectively. Similarly, the negative correlation values corresponding to distances of ≈ 14 cm can be attributed to the inter-slub distance where the repeat occurs at this interval between the high and the low diameters.

Conclusion

The yarn diameter was analyzed using a computer vision system that utilizes an HSC. The images were processed using our developed robust technique that is relatively fast in removing the yarn hairiness and in filling the voids inside the yarn body. The data obtained from the applied algorithm were found to be significantly comparable to the commercial available instruments such as the Uster Evenness Tester. The developed analysis was capable of detecting the short-term, the long-term, and the periodic variations of yarn diameter. To the best of the authors' knowledge, this work is the first to process the images of continuous long-length of yarns to allow its time-series treatment. The newly developed processing algorithm demonstrated a fast and robust ability in treating the massive amount of yarn images compared to traditional edge detecting and processing methods. The robustness and flexibility of the suggested DiaLib® system opens the door for a relatively precise, cheap, and "transparent box" method for measuring the yarn diameter with a wealth of information that can be drawn during the analysis and may not be obtained from the commercial instruments.

Acknowledgment

We would like to thank Dr Martin Bílek for providing the high speed camera and Dr Eva Moučková for samples testing.

Funding

This work was supported by ESF operational program "Education for Competitiveness" in the Czech Republic in the framework of the project "Support of engineering of excellent research and development teams at the Technical University of Liberec" (grant number CZ.1.07/2.3.00/30.0065).

References

1. Kovar R. Length of the yarn in plain-weave crimp wave. *J Text Inst* 2011; 102: 582–597.
2. Leaf GAV. The mechanics of plain woven fabrics. *Int J Cloth Sci Tech* 2004; 16: 97–107.
3. Mahmoudi MR and Oxenham W. A new electro-mechanical method for measuring yarn thickness. *AUTEX Res J* 2002; 2: 28–37.
4. Carvalho V, Belsley M, Vasconcelos R, et al. A comparison of mass parameters determination using capacitive and optical sensors. *Procedia Chem* 2009; 1: 766–769.
5. Carvalho V, Vasconcelos R, Soares F, et al. Yarn diameter and linear mass correlation. *J Nondestruct Eval* 2009; 28: 49–54.
6. Carvalho V, Cardoso PJ, Belsley MS, et al. Yarn diameter measurements using coherent optical signal processing. *IEEE Sens J* 2008; 8: 1785–1793.
7. Carvalho V, Soares FO and Belsley M. A comparative study between yarn diameter and yarn mass variation measurement systems using capacitive and optical sensors. *Ind J Fib Text Res* 2008; 33: 119–125.
8. Voborova J, Garg A, Neckar B, and Ibrahim S. *Yarn properties measurement: an optical approach*. 2nd International Textile, Clothing & Design Conference – Magic World of Textiles, Dubrovnik, Croatia, 3–6 October 2004, pp.1–6 (ISBN 953-7105-05-9).
9. Ibrahim S, Militky J, Kremenakova D and Mishra R. *Characterization of Yarn Diameter Measured on Different Systems*. The 4th RMUTP International Conference: Textiles & Fashion, 3–4 July 2012, Bangkok, Thailand, Section I, pp.1–15 (ISBN 978-974-625-563-9).
10. Ma J and Korobov NA. The calculational method for spectrogram and variance-length curve of yarn based on multiresolution analysis, sixth international conference on parallel and distributed computing. *Applications and Technologies*. 5–8 December 2005, pp.993–996.
11. Carvalho V, Monteiro JL, Soares FO, et al. Yarn evenness parameters evaluation: A new approach. *Text Res J* 2008; 78: 119–127.
12. Carvalho V, Cardoso P, Belsley M, Vasconcelos RM, Soares FO. Yarn irregularity parameterisation using optical sensors. *Fibres & textiles in Eastern Europe* 2009; 17(1): 26–32.
13. Montgomery DC, Jennings CL and Kulahci M. *Introduction to Time Series Analysis and Forecasting*. Hoboken, NJ: Wiley-Interscience, 2008.
14. Hartigan JA and Hartigan PM. The dip test of unimodality. *Ann Stat* 1985; 70–84.
15. Hartigan JA and Hartigan PM. The dip test of unimodality. *The Annals of Statistics* 1985; 13(1): 70–84.

16. Everitt BS and Hand DJ. *Finite Mixture Distributions (Monographs on Applied Probability and Statistics)*. Vol. 1, London: Chapman and Hall, 1981.
17. Titterington DM, Smith AFM and Makov UE. *Statistical Analysis of Finite Mixture Distributions*. Vol. 7, New York: Wiley, 1985.
18. Krifa M. Fiber length distribution in cotton processing: A finite mixture distribution model. *Text Res J* 2008; 78: 688–698.
19. Rong GH and Slater K. Analysis of yarn unevenness by using a digital-signal-processing technique. *J Text Inst* 1995; 86: 590–599.

PART II

Chapter 6

An Automated Fabric Fault Detection and Classification System Based on Computer Vision and Soft Computing

Summary Sheet

- **Paper citation:**
  H. Eldeeb, M. Mohy, T. Elbagoury, K. Aboseda, E. Shady, and M. Eldessouki, "An Automated Fabric Fault Detection and Classification System Based on Computer Vision and Soft Computing," *ACC JOURNAL*, vol. XIX, issue A, pp. 16-24, 2013.

- **Targeted problem:**
  Fabric fault detection is performed ***manually*** through visual inspection by ***human operators*** with ***fluctuating performance*** due to the ***work fatigue***, ***subjective evaluation***, and ***variable labor experiences***

- **Objective(s):**
  - Develop a prototype for automated fabric fault detection
  - Develop computer vision algorithms to handle the acquired images
  - Develop soft-computing algorithms for classifying the detected images
  - Create an integrated system with a database that reports the statistics of the most frequent faults and their probable reasons

- **Materials scope:**
  - Fabrics produced with weaving technology with "plain" fabric structure
  - Nine fabric fault categories were produced and tested

- **Computation method:**
  - Spatial and spectral features were extracted from the acquired fabric images
  - Artificial neural networks with different structures and order were implemented

- **Paper significance:**
  - The introduced machine prototype is capable to run at speeds of 10 m/min which is relatively suitable at the applied states of hardware and software
  - The system was trained and is capable of identifying a relatively high number of fabric faults categories

- **Software**
  A software program with a user-friendly GUI was developed for this paper. The software is available on the accompanied CD with a tutorial video demonstration. The program also has some examples on the CD so it can be tested. The program GUI is shown below:

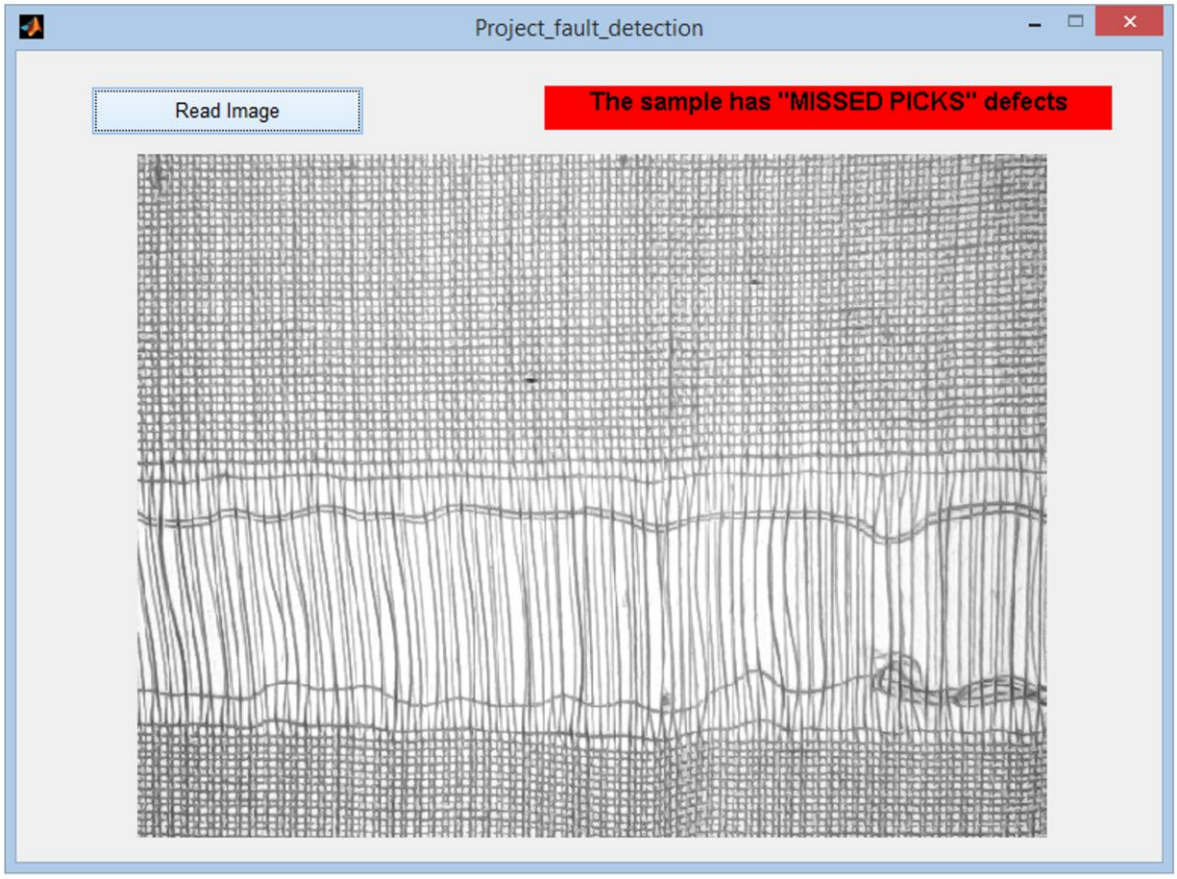
Project_fault_detection
Read Image
The sample has "MISSED PICKS" defects

An Automated Fabric Fault Detection and Classification System Based on Computer Vision and Soft Computing

Hadir Eldeeb[1], Mahmoud Mohy[1], Tamer Elbagoury[1], Khaled Aboseda[1], Ebraheem Shady[1], Mohamed Eldessouki[1,2*]

[1] *Department of Textile Engineering, Faculty of Engineering, Mansoura University, Mansoura, Egypt*

[2] *Department of Materials Engineering, Faculty of Textiles, Technical University of Liberec, Liberec, Czech Republic*

* Corresponding author, E-mail: mohamed.eldessouki@tul.cz

Abstract

Fabric inspection is one of the essential quality control processes in weaving mills. The automation of this process using computer vision systems is expected to increase the efficiency of the process and increase the total profit revenues on the long run. This work introduces a computer vision system that has the capability to detect and classify a relatively large number of fabric defects. Image enhancement techniques were used in processing the fabric acquired images. Spatial and spectral features were extracted from the processed images and used as inputs to soft-computing classifiers. Two approaches were used in the classification with the aim of reducing the calculation time required during the image analysis. The successful classification rate was 97.3% using the direct approach that has a slightly longer processing time. The performance of the classifiers in the hierarchical approach ranges between 91 to 100% depending on the classification level and the used image features. Results of this work with high classification rate and short processing time are promising to apply the introduced technique in real time fabric inspection systems.

1. Introduction

The conventional inspection process in the weaving mills usually depends on human visual inspection which only detects 60 to 70% out of the total fabric defects. The other defects pass without detection and cause several problems in the following processes of manufacturing. In addition, fixing defects is a complicated process and the defective parts are usually discarded as wastes that might be recycled or sold at low prices (usually 45 to 65% from the free defect price). Several researchers tried to solve this problem using image processing techniques and implemented different spatial and spectral methods for image analysis and feature extraction. Kuo and Su [1] applied the co-occurrence matrix and gray relational analysis. The gray relational analysis was also used to investigate correlations of the analyzed factors among the selected features in a randomized factor sequence through image processing. The system classified different defects such as broken warps, broken wefts, holes, and oil stains with 94% recognition accuracy of the system.

Shady et al. [2] used image analysis and neural networks for six different knitted fabric defects detection and classification. Statistical approaches and Fourier Transforms were used for feature extraction and artificial neural networks were used to classify the defects. The results of using the Fourier transform features were slightly more successful than the statistical approach in detecting the defect-free samples and classifying most of the defects. Mallik and Datta [3] presented a theoretical based technique for real-time fabric defect detection using a joint transform correlator that is extension of Fourier transform analysis. The joint power spectrum showed better classification results compared to the Fourier and experimental results. The technique introduced reasonable results for identifying and classifying some defects such as the existence of thick yarns, knots, and missing yarns.

Hu and Tsai [4] used wavelet packet transform and an artificial neural network (ANN) to inspect four kinds of fabric defects. The approach was reliable and effective in classifying fabric defects with a total classification rate of 100% for a wavelet function with a maximum vanishing moment of four and three resolution levels. Wen et al. [5] also used wavelet transform and co-occurrence matrix to extract features of textured images. The system was able to detect whether the fabric is defective or not at 92% rate of success. Also, the system was able to locate the defect position at 84% rate of success.

It can be seen from the survived literature that most of the applied detection systems were able to classify a few number of defects which may not be efficient in practical production environments. Therefore, this work introduces an automated fabric fault detection and classification (FFDC) system to detect and classify a larger number of woven fabric defects.

2. Methods

The overview of the FFDC computer vision system is shown in Figure 1. The system utilizes a digital camera to acquire and transmit fabric images to a computer which enhances and extracts some features for each image. The features are then processed using an Artificial Intelligence (AI) technique to detect and classify the fabric defects. Also, the FFDC system predicts the sources of the defects to be fixed. These defects are recorded in a database providing a report of the frequent defects for fixing their sources and consequently increasing the quality of the manufactured fabrics. Therefore, applying such automatic system in weaving mills is expected to increase the profit and the product quality.

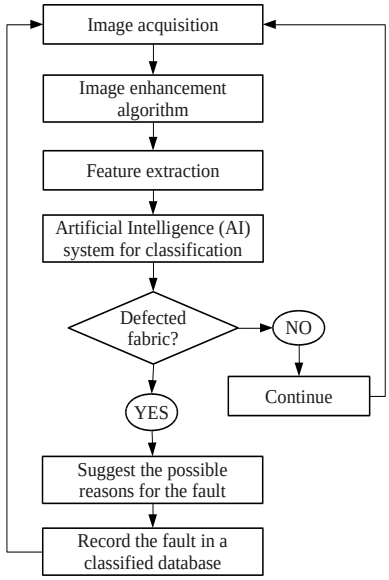

Figure 1. Flow chart of the FFDC algorithm

2.1. Image enhancement

The size of the acquired images is 3088 x 2056 pixels which represents a fabric sample with dimension of 30 x 20 mm. To make defects more detectable in the acquired images, each image was divided into nine sub-images. Image enhancement was applied to remove the noise and hairiness from the woven fabric images and adjust their gray levels, shown in Figure 2. The enhanced images should facilitate the allocation of the fabric defects.

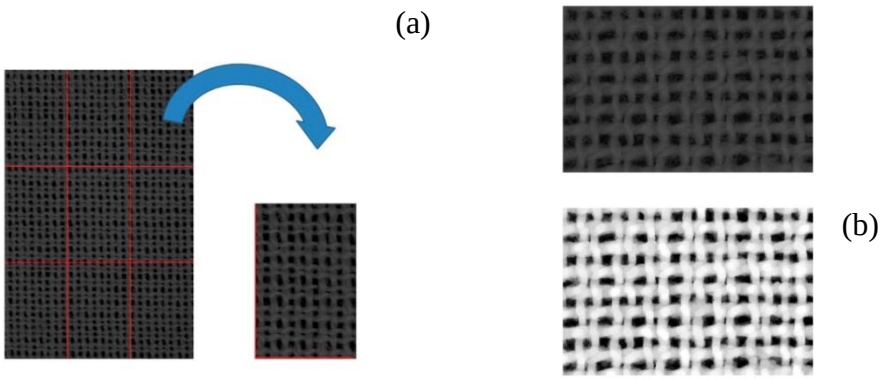

Figure 2. (a) A fabric image that was divided into nine sub-images; (b) A true-color image (top) and enhanced image (bottom) after noise removal and gray level adjustment

2.2. Feature extraction

The feature pool consists of three statistical and six spectral features. The statistical features (the mean, the summation, and the standard of deviation) were chosen for their simplicity and faster calculation. The determination of the statistical features was performed according to the following relations:

The mean :

$$\bar{x} = \frac{1}{n}\sum_{i=1}^{n} x_i \qquad (1)$$

The summation of columns or rows:

$$R = \sum_{i=1}^{n} x_i \qquad (2)$$

The standard deviation:

$$s = \sqrt{\frac{1}{n-1}\sum_{i=1}^{n}(x_i - \overline{x})^2} \qquad (3)$$

The spectral features were based on the Fourier transform technique that transforms pictures from their spatial domain to the spectral domain. If the image is considered as a function *f(m,n)* with two discrete spatial variables *m* and *n*, then the two-dimensional Fourier transform *F(m,n)* is defined by the relationship:

$$F(w_1, w_2) = \sum_{m=-\infty}^{\infty}\sum_{n=-\infty}^{\infty} f(m,n)\ e^{-j\omega_1 m}\ e^{-j\omega_2 n} \qquad (4)$$

After transforming the image to the spectral domain, the power spectrum of the image can be calculated and some dominant peaks can be used as image features. An example of some of these features is illustrated in Figure 3.

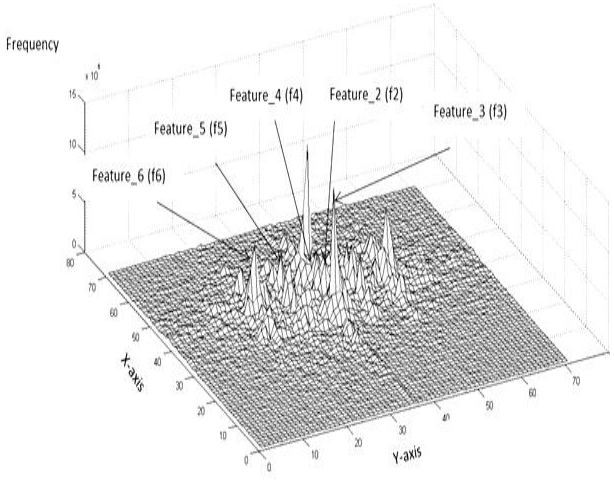

Figure 3. Some spectral features of the Fourier transformed image

2.3. Artificial neural network

Artificial neural networks (ANN) were used as soft computing techniques for classifying defected and non-defected samples. Different network architectures were used and the optimized network structure was found to include a multi-layer network with two hidden layers (25 neurons per layer). The input and output layers were adjusted according to the used features and the required fault categories. Three groups of features were used: statistical features only, spectral features only, and combination of statistical and spectral features. The classification went through two approaches by either identifying the defect type directly from the input features (the direct approach) or by identifying the defect at different levels (hierarchical or stepwise approach). In the hierarchical approach the classification was done on three steps; the first step classifies if the fabric sample is defected or defect-free. The second step classifies the defect category (warp, weft, or areal) and the third step identifies the defect type.

3. Experimental setup

The fabric samples used in this study were manufactured at "Samanoud Company for Woven & Pile Fabrics" on a Sulzer-Ruti weaving machine. The fabric structure is plain weave 1/1 with a yarn count of 20/1 Ne for warp and 14/1 Ne for weft. The densities of warp and weft yarns are 20 and 18 per cm, respectively. The chosen defects were intentionally introduced on the machine based on the knowledge of defects sources. The used defects, shown in Figure 4, were categorized into three main categories; defects in warp direction (Wrong draw and warp float), defects in weft direction (double pick, Stop mark with high density, Stop mark with low density, and missing picks), and areal defects (hole, slubs, and fabric blotchs).

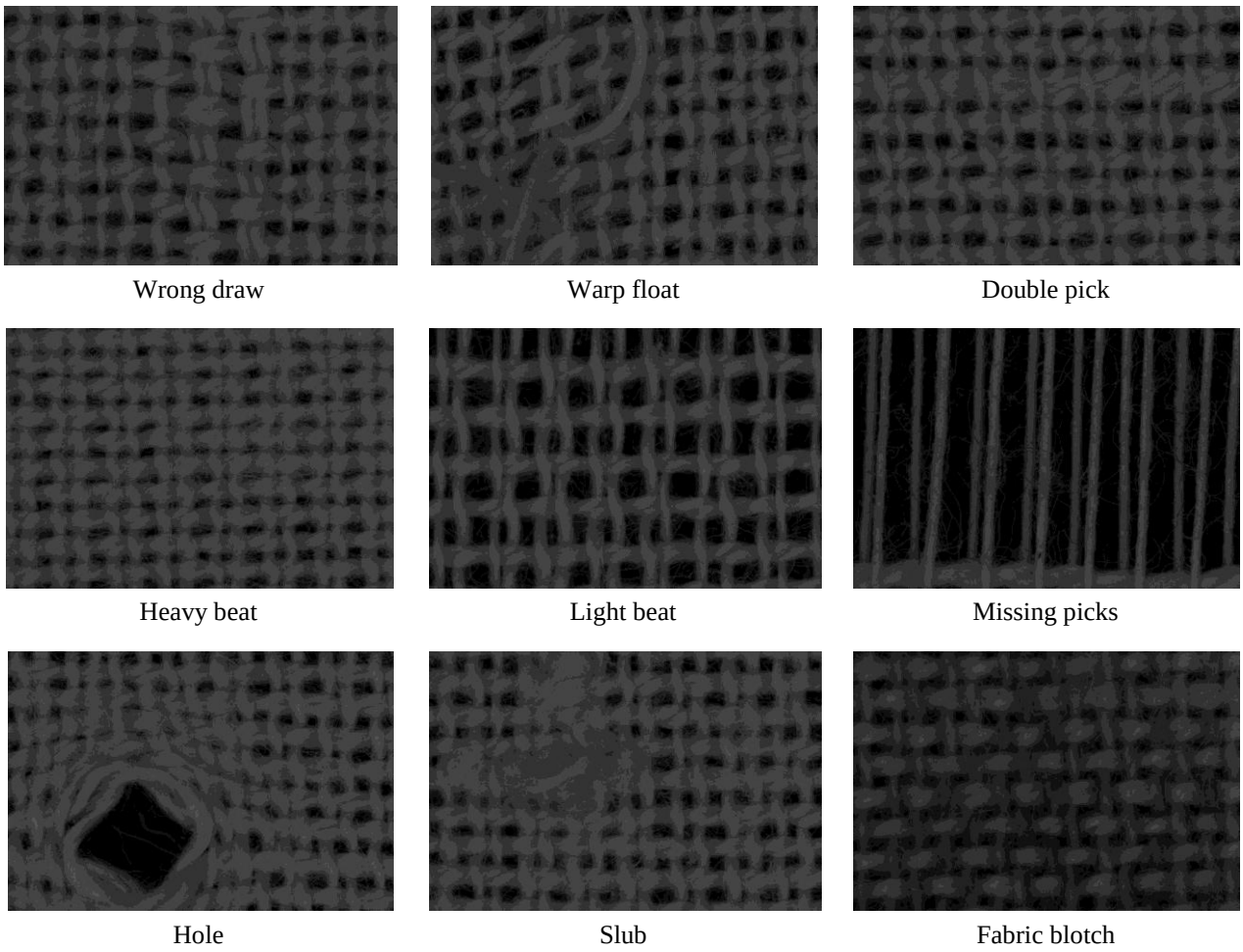

Figure 4. Images for some fabric faults

4. Results and Discussions

The set of image features was divided into three groups for the artificial neural network (ANN) training, validating, and testing. The results of the testing sets are summarized in Table 1 for the direct and the hierarchical approaches. The results of the direct approach show that the classification using Fourier features only get better results than using statistical features only and the application of both features (statistical and spectral) gets the best results among the three inputs.

Table 1. The overall performance of the ANN classification system

		Statistical features	Spectral features	Statistical and spectral features
	Direct approach	84.5	92.7	97.3
hierarchical approach	Defect or defect-free	91	89	87
	Warp, weft, or areal	89.3	95.3	94.7
	Warp defects	100	95	100
	Weft defects	100	100	100
	Areal defects	90	93.3	100

The hierarchical approach was suggested in this study to minimize the calculation time allowing a real time processing of the fabric samples. According to this approach, no further processing for the defect-free samples is required in the case of their classification at the first stage. Defected samples go for further classification in the next classifiers by categorizing the defect (warp, weft, or areal) in the second ANN. The category is considered as an input of the next classifier to determine the exact fault type.

The results of the hierarchical approach differ according to the level of classification as shown in Table 1 and the testing of the classifiers using different features show that:

- *First classifier*: The purpose of this classifier is to determine if the fabric is defected or not. The classification using only the spectral features gets better results than using both types of features (statistical and spectral) while using only the statistical features gets the best results. This result may be counter intuitive; however, the consideration of many features as inputs for the classifier may "confuse" the system and decrease its classification performance. Therefore, optimizing the input features should be considered to reduce the number of inputs for the system. The principle component analysis (PCA) technique might be useful for input reduction and optimization.

- *Second classifier*: The purpose of this classifier is to categorize the fabric faults (warp, weft or areal). The best classification results were obtained using the Fourier spectral features while the combination of the spectral and spatial features performs better than the application of statistical features only.

- *Third classifier*: The purpose of this classifier is to identify the fault and produce its exact type. The performance of this classifier depends on the fault category as shown in Table 1 where the combination of statistical and spectral features gives the best classification results with 100% rate of successful classification. It is noticeable that the classifier has the ability to differentiate the weft defects using any set of features (statistical only, spectral only, or their combination) although having the highest number of faults in this category. The 100% successful classification for the warp and weft categories using statistical features only may be useful in the real-time classification because of the short time calculation of the spatial features.

5. Conclusion

This work utilizes a digital camera to acquire and transmit fabric images to a computer which enhances and extracts the features for individual images. The features are then processed using an artificial intelligence technique to classify the fabric faults. Two approaches were implemented in this study with direct classification approach and hierarchical classification approach. The results of the direct approach show that the use of a combination of statistical and spectral features gives a 97.3% successful classification. The hierarchical approach aimed to reduce the processing time and its testing shows the dependence of the classifiers performance on the given set of features. The application of a whole set of statistical and spectral features performs the best in most classification categories while statistical features only were enough (with their short calculation time) in determining if the fabric is defected or not and in determining the faults within the warp and weft categories. Results of this study are promising and may allow the application of the introduced technique in real time fabric inspection systems because of the high successful classification rate and the relatively short processing time.

References

[1] C.-F. J. Kuo and T.-L. Su, "Gray Relational Analysis for Recognizing Fabric Defects," *Textile Research Journal,* vol. 73, pp. 461-465, 2003.

[2] E. Shady, Y. Gowayed, M. Abouiiana, S. Youssef, and C. Pastore, "Detection and Classification of Defects in Knitted Fabric Structures," *Textile Research Journal,* vol. 76, pp. 295-300, 2006.

[3] B. Mallik and A. K. Datta, "Defect Detection in Fabrics with a Joint Transform Correlation Technique: Theoretical Basis and Simulation," *Textile Research Journal,* vol. 69, pp. 829-835, 1999.

[4] M. C. Hu and I. S. Tsai, "Fabric Inspection Based on Best Wavelet Packet Bases," *Textile Research Journal,* vol. 70, pp. 662-670, 2000.

[5] C.-Y. Wen, S.-H. Chiu, W.-S. Hsu, and G.-H. Hsu, "Defect Segmentation of Texture Images with Wavelet Transform and a Co-occurrence Matrix," *Textile Research Journal,* vol. 71, pp. 743-749, 2001.

An Automated Fabric Fault Detection and Classification System Based on Computer Vision and Soft Computing

Hadir Eldeeb
Mahmoud Mohy
Tamer Elbagoury
Khaled Aboseda
Ebraheem Shady
*** Mohamed Eldessouki**

Mansoura University
Faculty of Engineering
Department of Textile Engineering
Mansoura, Egypt
* mohamed.eldessouki@gmail.com

Abstract

Fabric inspection is one of the essential quality control processes in weaving mills. The automation of this process using computer vision systems is expected to increase the efficiency of the process and increase the total profit revenues on the long run. This work introduces a computer vision system that has the capability to detect and classify a relatively large number of fabric defects. Image enhancement techniques were used in processing the fabric acquired images. Spatial and spectral features were extracted from the processed images and used as inputs to soft-computing classifiers. Two approaches were used in the classification with the aim of reducing the calculation time required during the image analysis. The successful classification rate was 97.3% using the direct approach that has a slightly longer processing time. The performance of the classifiers in the series approach ranges between 91 to 100% depending on the classification level and the used image features. Results of this work with high classification rate and short processing time are promising to apply the introduced technique in real time fabric inspection systems.

Introduction

The conventional inspection process in the weaving mills usually depends on human visual inspection which only detects 60 to 70% out of the total fabric defects. The other defects pass without detection and cause several problems in the following processes of manufacturing. In addition, fixing defects is a complicated process and the defective parts are usually discarded as wastes that might be recycled or sold at low prices (usually 45 to 65% from the free defect price). Several researchers have tried to solve this problem using image processing techniques and implemented different spatial and spectral methods for image analysis and feature extraction. Kuo and Su [1] applied the co-occurrence matrix and gray relational analysis. The gray relational analysis was also used to investigate correlations of the analyzed factors among the selected features in a randomized factor sequence through image processing. The system classified different defects such as broken warps, broken wefts, holes, and oil stains with 94% recognition accuracy of the system.

Shady et al. [2] used image analysis and neural networks for six different knitted fabric defects detection and classification. Statistical approaches and Fourier Transforms were used for feature extraction and artificial neural networks were used to classify the defects. The results of using the Fourier transform features were slightly more successful than the statistical approach in detecting the defect-free samples and classifying most of the defects.

Mallik and Datta [3] presented a theoretical based technique for real-time fabric defect detection using a joint transform correlator that is extension of Fourier transform analysis. The joint power spectrum showed better classification results compared to the Fourier and experimental results. The technique introduced reasonable results for identifying and classifying some defects such as the existence of thick yarns, knots, and missing yarns.

Hu and Tsai [4] used wavelet packet transform and an artificial neural network (ANN) to inspect four kinds of fabric defects. The approach was reliable and effective in classifying fabric defects with a total classification rate of 100% for a wavelet function with a maximum vanishing moment of four and three resolution levels. Wen et al. [5] also used wavelet transform and co-occurrence matrix to extract features of textured images. The system was able to detect whether the fabric is defective or not at 92% rate of success. Also, the system was able to locate the defect position at 84% rate of success.

It can be seen from the survived literature that most of the applied detection systems were able to classify a few number of defects which may not efficient in practical production environments. Therefore, this work introduces an automated fabric fault detection and classification (FFDC) system to detect and classify a larger number of woven fabric defects.

1 Methods

The overview of the FFDC computer vision system is shown in Figure 1. The system utilizes a digital camera to acquire and transmit fabric images to a computer which enhances and extracts some features for each image. The features are then processed using an Artificial Intelligence (AI) technique to detect and classify the fabric defects. Also, the FFDC system predicts the sources of the defects to be fixed. These defects are recorded in a database providing a report of the frequent defects for fixing their sources and consequently increasing the quality of the manufactured fabrics. Therefore, applying such automatic system in weaving mills is expected to increase the profit and the product quality.

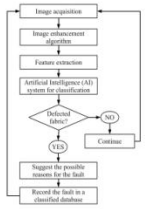

Source: Own

Fig. 1: *Flow chart of the FFDC algorithm*

1.1 Image enhancement

The size of the acquired images is 3088 x 2056 pixels which represents a fabric sample with dimension of 30 x 20 mm. To make defects more detectable in the acquired images, each

image was divided into nine sub-images. Image enhancement was applied to remove the noise and hairiness from the woven fabric images and adjust their gray levels, shown in Figure 2. The enhanced images should facilitate the allocation of the fabric defects.

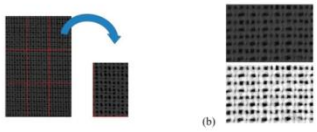

Source: Own

Fig. 2: *(a) A fabric image that was divided into nine sub-images; (b) A true-color image (top) and enhanced image (bottom) after noise removal and gray level adjustment*

1.2 Feature extraction

The feature pool consists of three statistical and six spectral features. The statistical features (the mean, the summation, and the standard of deviation) were chosen for their simplicity and faster calculation. The determination of the statistical features was performed according to the following relations:

The mean

$$\bar{x} = \frac{1}{n}\sum_{i=1}^{n} x_i \tag{1}$$

The summation of columns or rows:

$$R = \sum_{i=1}^{n} x_i \tag{2}$$

The standard deviation:

$$s = \sqrt{\frac{1}{n-1}\sum_{i=1}^{n}(x_i - \bar{x})^2} \tag{3}$$

The spectral features were based on the Fourier transform technique that transforms pictures from their spatial domain to the spectral domain. If the image is considered as a function *f(m,n)* with two discrete spatial variables *m* and *n*, then the two-dimensional Fourier transform *F(m,n)* is defined by the relationship:

$$F(w_1, w_2) = \sum_{m=-\infty}^{\infty}\sum_{n=-\infty}^{\infty} f(m,n)\; e^{-j\omega_1 m}\, e^{-j\omega_2 n} \tag{4}$$

After transforming the image to the spectral domain, the power spectrum of the image can be calculated and some dominant peaks can be used as image features. An example of some of these features is illustrated in Figure 3.

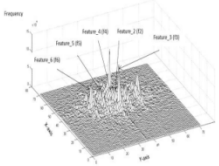

Source: Own

Fig. 3: *Some spectral features of the Fourier transformed image*

1.3 Artificial neural network

Artificial neural networks (ANN) were used as soft computing techniques for classifying defected and non-defected samples. Different network architectures were used and the optimized network structure includes a multi-layer network with two hidden layers (25 neurons per layer). The input and output layers were adjusted according to the used features and the required fault categories. Three groups of features were used: solely statistical features, solely spectral features, and combination of statistical and spectral features. The classification went through two approaches by either identifying the defect type directly from the input features (the direct approach) or by identifying the defect at different levels (series approach). In the series approach the classification three steps have been taken; the first step classifies if the fabric sample is defected or defect-free. The second step classifies the defect category (warp, weft, or areal) and the third step identifies the defect type.

2 Experimental setup

The fabric samples used in this study were manufactured at "Samanoud Company for Woven & Pile Fabrics" on a Sulzer-Ruti weaving machine. The fabric structure is plain weave 1/1 with a yarn count of 20/1 Ne for warp and 14/1 Ne for weft. The densities of warp and weft yarns are 20 and 18 per cm, respectively. The chosen defects were intentionally introduced on the machine based on the knowledge of defects sources. The used defects, shown in Figure 4, were categorized into three main categories; defects in warp direction (double end and float warp), defects in weft direction (double pick, heavy peat, light peat, and missing picks), and areal defects (hole, knots, and stains).

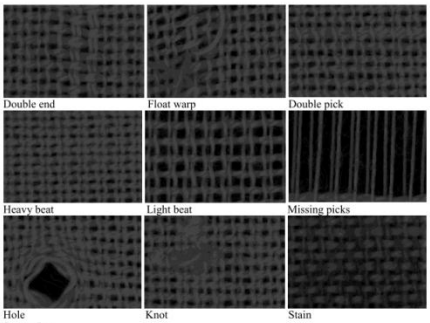

Source: Own

Fig. 4: *Images for some fabric faults*

3 Results and Discussions

The set of image features was divided into three groups for the artificial neural network (ANN) training, validating, and testing. The results of the testing sets are summarized in Table 1 for the direct and the series approaches. The results of the direct approach show that the classification using only Fourier features gets better results than using solely statistical features and the application of both features (statistical and spectral) gets the best results among the three inputs.

Tab. 1: *The overall performance of the ANN classification system*

		Statistical features	Spectral features	Statistical and spectral features
	Direct approach	84.5	92.7	97.3
Series approach	Defect or defect-free	91	89	87
	Warp, weft, or areal	89.3	95.3	94.7
	Warp defects	100	95	100
	Weft defects	100	100	100
	Areal defects	90	93.3	100

Source: Own

The series approach was suggested in this study to minimize the calculation time allowing a real time processing of the fabric samples. According to this approach, no further processing for the defect-free samples is required in the case of their classification at the first stage. Defected samples go for further classification in the next classifiers by categorizing the defect (warp, weft, or areal) in the second ANN. The category is considered as an input of the next classifier to determine the exact fault type.

The results of the series approach differ according to the level of classification as shown in Table 1 and the testing of the classifiers using different features show that:

- *First classifier*: The purpose of this classifier is to determine if the fabric is defected or not. The classification using only Fourier features gets better results than using both types of features (statistical and spectral) while using the statistical features only gets the best results. This result may be counter intuitive; however, the consideration of many features as inputs for the classifier may "confuse" the system and decrease its classification performance. Therefore, optimizing the input features should be considered to reduce the number of inputs for the system. The principle component analysis technique might be useful for input reduction and optimization.
- *Second classifier*: The purpose of this classifier is to categorize the fabric fault (warp, weft or areal). The best classification results were obtained using the Fourier spectral features while the combination of the spectral and spatial features performs better than the application of statistical features only.
- *Third classifier*: The purpose of this classifier is to identify the fault and produce its exact type. The performance of this classifier depends on the fault category as shown in Table 1 where the combination of statistical and spectral features gives the best classification results with 100% rate of successful classification. It is noticeable that the classifier has the ability to differentiate the weft defects using any set of features (statistical only, spectral only, or their combination) although having the highest number of faults in this category. The 100% successful classification for the warp and weft categories using solely statistical features may be useful in the real-time classification because of the short time calculation of these spatial features.

Conclusion

This work utilizes a digital camera to acquire and transmit fabric images to a computer which enhances and extracts the features for individual images. The features are then processed using an artificial intelligence technique to classify the fabric faults. Two approaches were implemented in this study with direct classification approach and series approach. The results of the direct approach show that the use of a combination of statistical and spectral features gives a 97.3% successful classification. The series approach aimed to reduce the processing time and its testing shows the dependence of the classifiers performance on the given set of features. The application of a whole set of statistical and spectral features performs best in most classification categories while solely statistical features only were sufficient (with their short calculation time) in determining whether the fabric was defected or not and in determining the faults within the warp and weft categories. The results of this study are promising and may allow the application of the introduced technique in real time fabric inspection systems because of the high successful classification rate and the relatively short processing time.

Literature

[1] KUO, C.-F. J.; SU, T.-L.: Gray Relational Analysis for Recognizing Fabric Defects. *Textile Research Journal*, vol. 73, pp. 461-465, 2003.

[2] SHADY, E.; GOWAYED, Y.; ABOUHANA, M.; YOUSSEF, S.; PASTORE, C.: Detection and Classification of Defects in Knitted Fabric Structures. *Textile Research Journal*, vol. 76, pp. 295-300, 2006.

[3] MALLIK, B.; DATTA, A. K.: Defect Detection in Fabrics with a Joint Transform Correlation Technique: Theoretical Basis and Simulation. *Textile Research Journal*, vol. 69, pp. 829-835, 1999.

[4] HU, M. C.; TSAI, I. S.: Fabric Inspection Based on Best Wavelet Packet Bases. *Textile Research Journal*, vol. 70, pp. 662-670, 2000.

[5] WEN, C.-Y.; CHIU, S.-H.; HSU, W.-S.; HSU, G.-H.: Defect Segmentation of Texture Images with Wavelet Transform and a Co-occurrence Matrix. *Textile Research Journal*, vol. 71, pp. 743-749, 2001.

Hadir Eldeeb; Mahmoud Mohy; Tamer Elbagoury; Khaled Aboseda; Ebraheem Shady; Mohamed Eldessouki

Automatizace kontroly tkanin pomocí počítačových kamerových systémů

Kontrola tkanin je jedním ze základních procesů řízení kvality v tkalcovnách. Od automatizace tohoto procesu pomocí počítačových kamerových systémů se očekává zvýšení efektivnosti procesu a z dlouhodobého hlediska celkové zvýšení zisků. Tato práce představuje počítačový kamerový systém, který má schopnost rozpoznat a klasifikovat relativně velké množství textilních vad. Při zpracovávání obrazu tkaniny byly použity techniky na jeho vylepšení. Ze zpracovaných obrazů byly extrahovány prostorové a spektrální vlastnosti a použity jako vstupy do výpočtových klasifikátorů. V klasifikaci byly použity dva přístupy s cílem snížit dobu výpočtu potřebnou při analýze obrazu. Úspěšná klasifikace činila 97,3 % pomocí přímého přístupu, který má o něco delší dobu zpracování. Výkonnost klasifikátorů série se pohybuje v rozmezí 91 až 100 % v závislosti na klasifikačním stupni a použitých obrazových funkcích. Výsledky této práce s vysokou mírou úspěšnosti klasifikace a krátkou dobou zpracování slibují možnost zavést tuto techniku do kontrolních systémů tkanin v reálném čase.

Eine automatisierte Textilfehleraufdeckung und eine auf Computervision und elastische Berechnungen basierte Klassifizierung

Die Kontrolle von Geweben ist eine der wichtigsten Vorgänge bei der Gestaltung von Qualität in Webereibetrieben. Von einer Automatisierung dieses Prozesses mit Hilfe von computergesteuerten Kamerasystemen werden eine Steigerung der Effektivität des Prozesses und insgesamt eine langfristige Gewinnsteigerung erwartet. Die vorliegende Arbeit stellt ein computergesteuertes Kamerasystem vor, welches die Fähigkeit besitzt, eine relativ große Menge an Textilfehlern zu erkennen und zu klassifizieren. Bei der Verarbeitung des Gewebebildes wurden Techniken zu dessen Verbesserung verwendet. Aus den verarbeiteten Bildern wurden räumliche und spektrale Eigenschaften extrahiert und als Eingang in Berechnungsklassifikatoren genutzt. Bei der Klassifizierung wurden von zwei Ansätzen ausgegangen mit dem Ziel, die Zeitdauer der zur Bildanalyse notwendigen Zeitdauer zu senken. Die erfolgreiche Klassifizierung betrug mit Hilfe des direkten Ansatzes 97,3%. Dieser Ansatz benötigt eine etwas längere Bearbeitungszeit. Die Leistungsfähigkeit der Klassifikatoren bewegt sich zwischen 91 und 100%, in Abhängigkeit vom Klassifikationsgrad und den verwendeten Bildfunktionen. Die Ergebnisse der vorliegenden Arbeit, die auf einem hohen Klassifikationsmaß und einer geringen Bearbeitungszeitberuhen, versprechen die Möglichkeit, diese Technik in einer realen Zeit in die Kontrollsysteme der Gewebe einzuführen.

Automatyzacja kontroli tkanin przy pomocy komputerowych systemów wizyjnych

Kontrola tkanin należy do podstawowych procesów zarządzania jakością w tkalniach. Od automatyzacji tego procesu przy pomocy komputerowych systemów wizyjnych oczekuje się zwiększenia efektywności procesu a długofalowo ogólnego zwiększenia zysków. Niniejsze opracowanie przedstawia komputerowy system kamer, który potrafi rozpoznać i klasyfikować stosunkowo dużą ilość wad tekstyliów. Przy przetwarzaniu obrazu tkaniny wykorzystano techniki mające na celu jego ulepszenie. Z przetworzonych obrazów ekstrahowano właściwości przestrzenne i spektralne, które wykorzystano jako dane wejściowe do klasyfikatorów obliczeniowych. W klasyfikacji zastosowano dwa podejścia w celu skrócenia

czasu wyliczeń niezbędnego do analizy obrazu. Udana klasyfikacja wynosiła 97,3% przy podejściu bezpośrednim, które ma o nieco dłuższy czas wykonania. Wydajność klasyfikatorów serii mieści się w granicach 91 do 100% w zależności od stopnia klasyfikacyjnego i zastosowanych funkcji obrazu. Wyniki tej pracy z wysokim stopniem klasyfikacji i krótkim czasem opracowania są obiecującą możliwością wprowadzenia tej techniki do systemów kontroli tkanin w czasie rzeczywistym.

PART II

Chapter 7

The Application of Principal Component Analysis to Boost The Performance of The Automated Fabric Fault Detector And Classifier

Summary Sheet

- **Paper citation:**
  M. Eldessouki, M. Hassan, K. Qashqary, and E. Shady, "The Application of Principal Component Analysis to Boost The Performance of The Automated Fabric Fault Detector And Classifier," *FIBERS & TEXTILES in Eastern Europe*, vol. 22, no. 4(106), pp. 51–57, 2014.

- **Targeted problem:**
  Fabric fault detection is performed ***manually*** through visual inspection by ***human operators*** with ***fluctuating performance***, on the other hand, the feature datasets obtained from image analysis have ***redundant data*** that are ***inter-correlated***

- **Objective(s):**
  - Develop computer vision algorithms to analyze the fabrics' acquired images and extract different types of features
  - Reduce the dimensionality of the obtained features dataset to remove the redundant data
  - Create a smart system that is capable of detecting and classifying fabric's faults once appear in a fabric's image

- **Materials scope:**
  - Fabrics produced with weaving technology with "plain" fabric structure
  - Nine fabric fault categories were produced and tested

- **Computation method:**
  - Spatial and spectral features were extracted from the acquired fabric images
  - Principle component analysis was implemented to reduce the features dimensionality
  - Artificial neural networks were implemented for the detecting and classification tasks

- **Paper significance:**
  - The implemented principal component analysis (PCA) reduced the dimensionality of the input feature dataset without sacrificing the amount of information in the original dataset which enhanced the processing time and increased the classifier's performance

- **Software**
  The software program developed with this paper utilizes the same GUI for the paper presented in the last chapter. Therefore, no need to present it here again.

The Application of Principal Component Analysis to Boost The Performance of The Automated Fabric Fault Detector And Classifier

Mohamed Eldessouki[2*], Mounir Hassan[1,2], Khadijah Qashqari[3] and Ebraheem Shady[2]

[1] *Department of Computer Science, Faculty of Computing and Information Technology, King Abdulaziz University, Saudi Arabia*

[2] *Department of Textile Engineering, Faculty of Engineering, Mansoura University, Egypt*

[3] *Department of Fashion Design, Faculty of Art & Design, King Abdulaziz University, Saudi Arabia*

* Corresponding author: eldesmo@auburn.edu

Abstract

There is a growing need to replace the visual fabric inspection with automated systems that detect and classify fabric defects. The digital processing of the fabric images utilizes different methods that offer a large set of image features. The correlation between those features lead to problems during the fabric fault classification and reduces the performance of the classifiers. This work extracted a combination of statistical (spatial) and Fourier transform (spectral) features from the fabric images of the most frequent faults. The principal component analysis (PCA) was implemented to reduce the dimensionality of the input feature dataset which achieved a reduction to 36% of the original data size with preserving 99% of the information in the original dataset. The features processed using the PCA were fed to an artificial neural network (ANN) to classify the fault categories and compared to another ANN that worked with the whole feature dataset. The performance of the network that was implemented after the application of the PCA increased to 90% of correct classification rate as compared to 73.3% for the other network.

1. Introduction

The early intervention to fix, or remove, fabric faults is one of the mandatory tasks required by all fabric manufacturers. The undetected defects cause many problems downstream in the production line and result in end products with lower quality that result in cost burden and non-profitable products. Automatic fault detection systems offer good alternatives to replace the traditional human fabric inspection with computer vision systems that analyze fabrics in a systematic manner and aiming for consistent performance. The efficiency of these automated systems, however, depends on many parameters and varies according to the quality of the hardware and the analysis algorithm.

There are many research articles in the field of automatic fabric fault detection and classification that can be found in published reviews [1, 2]. Among those stand some common methods for feature extraction and fault classification as shown in Figure 1. The methods of feature extraction vary to include spatial (statistical) features [3], spectral features (fast Fourier

Transform) [4], combination of spatial and spectral features [5-10], as well as other methods that may utilize wavelet transformers [11, 12]. The extracted features are fed to a classification system that was implemented by researchers in different ways. Among these classifiers are the artificial neural networks (ANN) with its different types [13, 14], fuzzy inference systems [15], neuro-fuzzy systems[16, 17], as well as other classification systems [18].

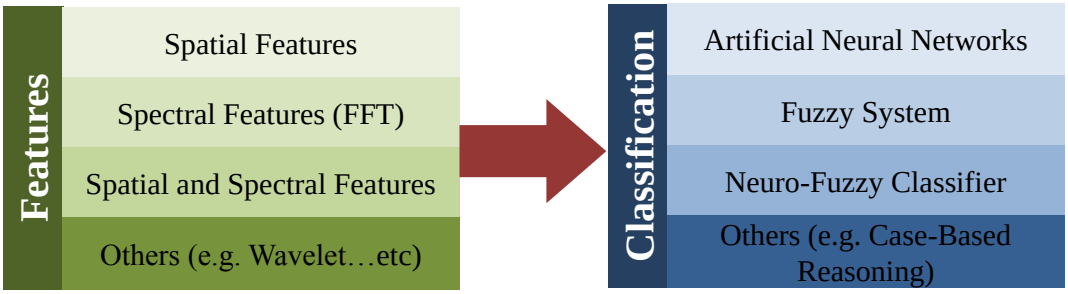

Figure 1. Different methods available in the literature for feature extraction and classification

In this work, some of the high frequently occurring defects that represent the main categories of faults (warp, weft, and areal directions) were studied. A system of image acquisition and enhancement was developed and a number of spatial and spectral features was extracted. The classification was done using pattern recognition artificial neural networks (ANNs) that were fed with the whole features and with the reduced dataset after the application of the principal component analysis (PCA) technique. The performance of the two ANN classifiers was evaluated.

2. Fabric faults

There is a large amount of fabric defects that may be caused by different sources and production technologies. Spinning faults, for example, should be mended before fabric production (either by weaving or knitting) otherwise it will lead to fabric faults that may not be fixed at all. Therefore, the scope of this study will be only the faults that occur during the weaving process and focus on plain woven fabrics only. The studied fabric faults might be considered as sever faults and had to be fixed or removed. The defect-free sample is shown in Figure 2-a and the defected samples can be categorized into three main categories; defects in warp direction, defects in weft direction, and areal defects. There are different names that can be found in the literature for the same defect; however the ASTM definition and description for these faults [19] will be considered in this work.

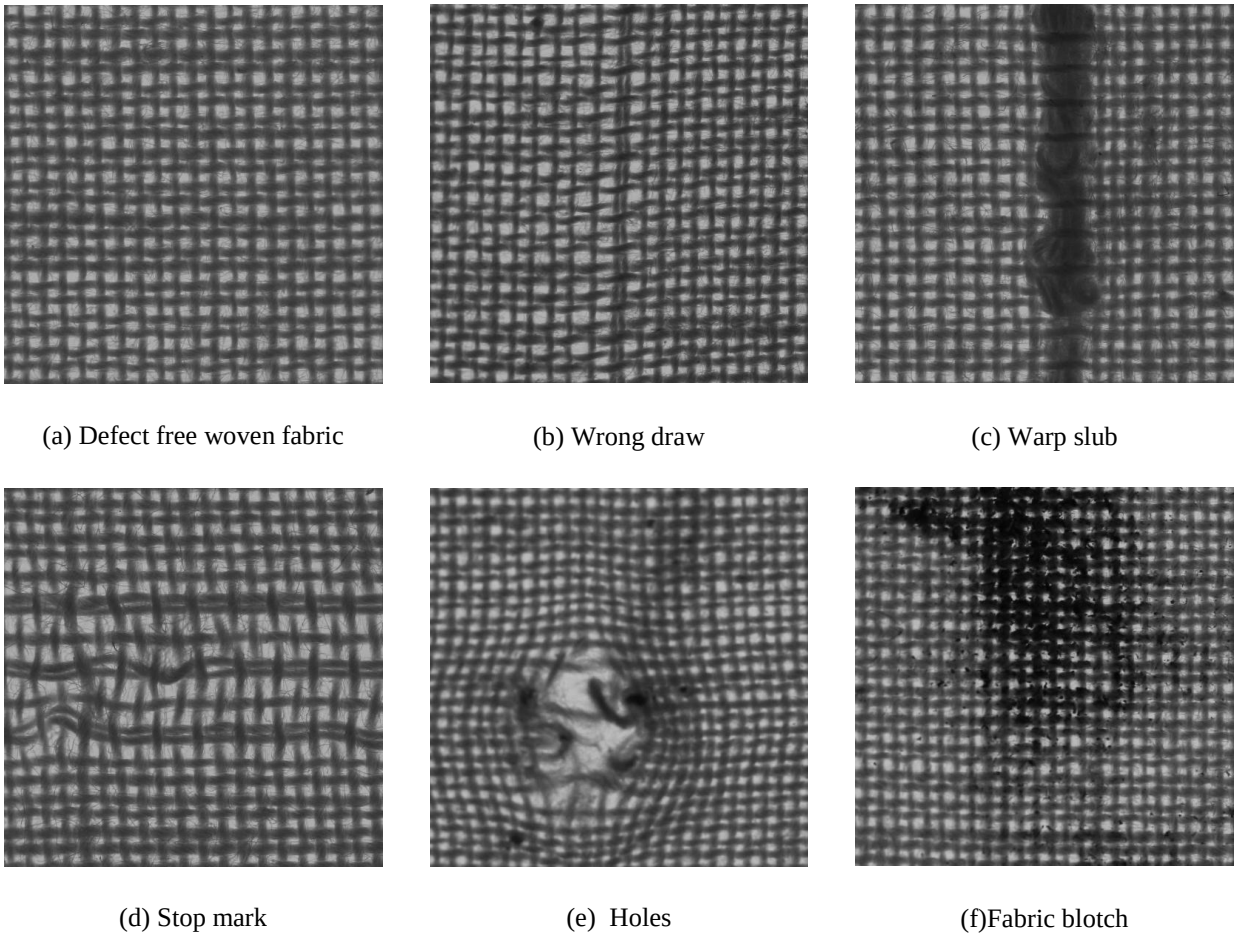

(a) Defect free woven fabric (b) Wrong draw (c) Warp slub

(d) Stop mark (e) Holes (f)Fabric blotch

Figure 2. Images of defect-free (a) and some defected (b-f) fabrics

Warp direction

Wrong draw: This fault results when one or more warp ends incorrectly drawn in the harness or the reed. The fault is shown in Figure 2-b and can also be called "wrong draft", "misdraw", or "double end". This fault may be considered as a sever defect because it appears through the whole length of the fabric if not fixed.

Slub: This fault shows in the fabric as an abruptly thickened place in a yarn. This fault can occur in warp or weft directions, but it was considered only in warp direction in this study. The other names of the same fault are lump, piecing, slough-off, and slug. All these names can are considered in ASTM standards. This fault may occur due to malfunctioning in warp sensors and it is shown in Figure 2-c.

Weft direction

Stop mark: This appears as a visible change in the density of the weave across the width of the fabric caused by the tension on the warp not being adjusted properly after the loom has been stopped. This fault may be called as "set mark", or "light beat-up" and is shown in Figure 2-d

Area faults

Hole: It is an imperfection in the fabric where one or more yarns are sufficiently damaged to create an aperture. In case of a relatively large hole, it might be called "smash" that is characterized by broken warp ends and floating picks. The smash may be equivalently called a "break-out" and is shown in Figure 2-e.

Stain: It is an area of discoloration that penetrates the fabric surface. If this discoloration is caused by grease or oil and the off-colored area appears at any shape, it is called a "blotch" or "oil spot" and an example of this fault is shown in Figure 2-f.

3. Methodology

3.1. Samples

The fabric samples were manufactured on a Sulzer-Ruti weaving machine. The fabric structure is plain weave 1/1 with a yarn count of 20/1 Ne for warp and 14/1 Ne for weft. The densities of warp and weft yarns are 20 and 18 per cm, respectively. The chosen defects were intentionally introduced on the weaving machine based on the knowledge of defects sources.

3.2. Image acquisition

The image acquisition setup is shown in Figure 3and utilizes a Canon digital camera (model: EOS 450D) with CMOS sensor. The system is installed with a "Remote Live View Shooting" where online monitoring of the pictures and their adjustment can be done on the computer using the EOS Utility software. The camera uses 35mm EF-S lenses and captures images at resolution of 72 dot per inch (dpi). The fabric sample is placed on an inspection table that is equipped with a concentrated LED lights in a box that is placed directly under the shooting area. To remove the noise and interference of the surrounding lights, a suitable shield was installed between the camera and the shooting area.

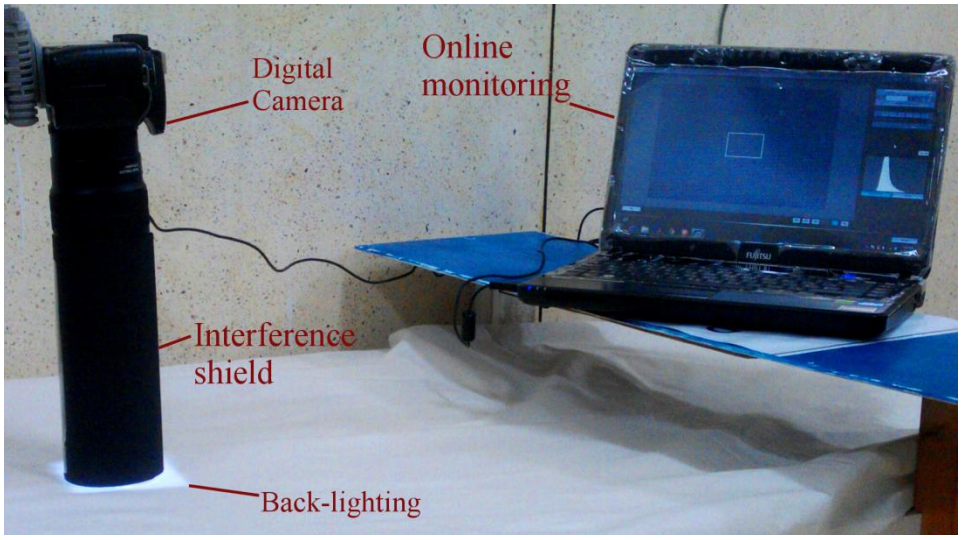

Figure 3. Fabric image acquisition setup

3.3. Image enhancement

The developed system applies initial enhancements on the original images to reduce the noise (e.g. hairiness) and improve their contrast. The system uses the contrast-limited adaptive histogram equalization (CLAHE) [20] algorithm to enhance the contrast of the grayscale image by transforming the values. The algorithm can be described briefly as it operates on small regions (windows) in the image. Each window's contrast is enhanced, so that the histogram of the output region approximately matches the specified histogram. The neighboring windows are then combined using bilinear interpolation to eliminate artificially induced boundaries. The contrast, especially in homogeneous areas, can be limited to avoid amplifying any noise that might be present in the image.

3.4. Image analysis and feature extraction

If the fabric image can be defined in the spatial domain by the matrix *P(x,y)* where:*x* is the row number in the image ($1 \leq x \leq N$),*y* is the column number ($1 \leq y \leq M$),and N and M are the number of rows and columns, respectively. Therefore, the features that can be extracted from this image are summarized below.

3.4.1. Statistical features

A total set of twenty spatial (statistical) features can be extracted from the fabric images. To obtain these features, the sum of individual gray-scale level values in the weft direction (rows) is calculated in the vector$R(m_j)$ where:

$$R(m_j) = \sum_{i=1}^{N} P(x_i, y_j)$$

Similarly, the sum of individual gray-scale values in the warp direction (columns) is calculated as:

$$C(n_i) = \sum_{j=1}^{M} P(x_i, y_j)$$

The first selected feature is the sum of all the gray-scale values in the image which can be calculated as:

$$f_1 = \sum_{i=1}^{N} C(n_i)$$

The next two features f_2 and f_3 represent the mean of sum of rows (f_2) and the mean of sum of columns (f_3). The relation for the first feature in the weft direction is:

$$f_2 = \frac{1}{M} \sum_{j=1}^{M} R(m_j)$$

Similarly for the feature in the warp direction is:

$$f_3 = \frac{1}{N} \sum_{i=1}^{N} C(n_i)$$

For space constraints, the equations will be listed for the features in weft (rows) direction only and similar relations can be written for the warp (columns) direction by replacing $R(m_i)$with $C(n_i)$.

The standard deviation of the sum of rows (f_4) and for the sum of columns (f_5) can be calculated as:

$$f_4 = \sqrt{\frac{1}{M} \sum_{j=1}^{M} (R(m_j) - \bar{R})^2}\ , \bar{R} = f_2$$

The features f_6 *and* f_7 represent the median value of the sum of rows and columns:

$$f_6 = median(R(m_j))$$

The features f_8 and f_{10} represent the minimum and maximum values, respectively, for the sum of rows and f_9 and f_{11} represent the same values for the columns. These features can be written as:

$$f_8 = min\left(R(m_j)\right), \qquad f_{10} = max(R(m_j))$$

The range of the sum of rows and columns was chosen to be, respectively, the features f_{12} and f_{13}:

$$f_{12} = range(R(m_j))$$

The entropy of the image represents the feature f_{14}:

$$f_{14} = -\sum_{i=1}^{N}\sum_{j=1}^{M} P(x_i, y_j) * log\ (P(x_i, y_j))$$

The k^{th} order moment for the sum of rows can be calculated from the function

$$f_a = \frac{1}{M}\sum_{j=1}^{M}(R(m_j) - \bar{R})^k$$

The second, third, and fourth order moments can be calculated as features f_{15}, f_{17}, and f_{19} (a= 15, 17 and 19) for the rows as well as the featuresf_{16}, f_{18}, and f_{20} (i.e. a= 16, 18 and 20) for the columns.

3.4.2. Spectral features

A fabric image of size *M* x *N* can be transformed from its spatial domain *P(x,y)* to the spectral domain $\hat{P}(u,v)$ using the discrete Fourier transform (DFT) which can be expressed in mathematical form as:

$$\hat{P}(u,v) = \frac{1}{MN}\sum_{x=0}^{M-1}\sum_{y=0}^{N-1} P(x,y)e^{-2\pi i(\frac{ux}{M}+\frac{vy}{N})}$$

Where *x* and *y* are the image spatial variables that correspond to the coordinates inside the image, while *u* and *v* represent the transformed frequency variables. Once the image is transformed, the power spectrum of the transformed image can be calculated as:

$$PW(u,v) = \left|\hat{P}(u,v)\right|^2 = R^2(u,v) + I^2(u,v)$$

Where $\left|\hat{P}(u,v)\right|$is known as the Fourier spectrum, $R^2(u,v)$ and $I^2(u,v)$are the real and imaginary parts of the transformed image $\hat{P}(u,v)$. Shifting the power spectrum is done by implementing the exponential properties of the transformer:

$$\Im[P(x,y)(-1)^{x+y}] = \hat{P}\left(u - \frac{M}{2}, v - \frac{N}{2}\right)$$

Where $\mathfrak{F}[\,.\,]$is the Fourier transform of an argument and this equation tells that the origin of the Fourier transform $\hat{P}$ *(0,0)* of the image $P(x,y)(-1)^{x+y}$is located at *u=M/2* and *v=N/2* which causes the shifting of the spectrum to these coordinates. The first selected spectral feature is taken as the DC peak which represents the zero frequency in the image (hence originated the name DC referring to the direct current with zero frequency in electrical circuits). This peak is dominating because it represents the average gray level of the image as can be seen from the equation:

$$f_{21} = \hat{P}(0,0) = \frac{1}{MN}\sum_{x=0}^{M-1}\sum_{y=0}^{N-1} P(x,y)$$

The peaks at frequencies other than zero are important in summarizing information of the image and revealing its features. To visualize the other peaks and for the illustration purposes, the DC peak is suppressed to zero as illustrated in Figure 4. The peaks at the two basic orthogonal directions can be extracted as shown in Figure 5 and Figure 6which represent the zero˚ and 90˚ directions, respectively. For each direction the first four peaks were considered for being features and for each peak both the magnitude (amplitude) and the frequency were extracted as individual features. Therefore, the features f_{22}, f_{23}, f_{24}, and f_{25} were extracted from the zero direction as the amplitudes of the peaks and features f_{26}, f_{27}, f_{28}, and f_{29} were extracted as the frequencies (locations) of the peaks. Similarly, the features f_{30}up to f_{37} were extracted from the 90˚ direction as the amplitudes and frequencies of the peaks in this direction.

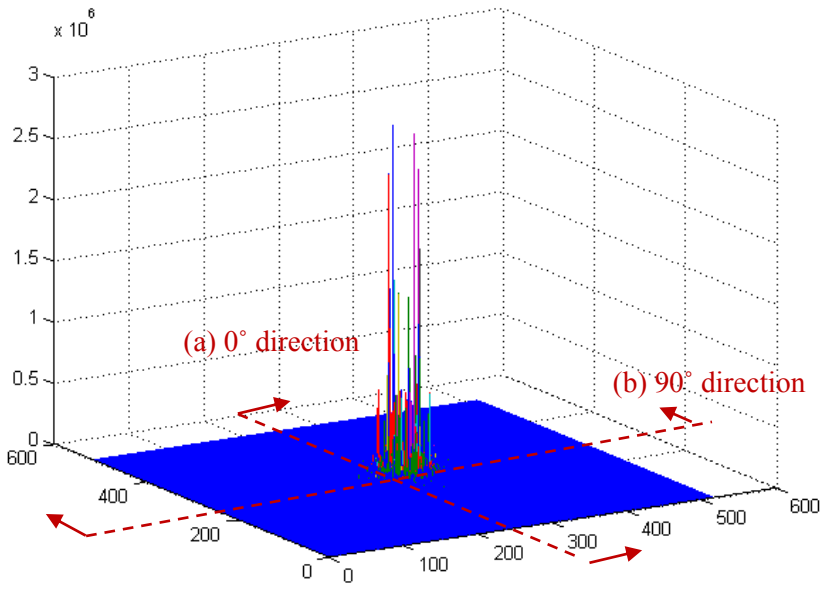

Figure 4. Fourier spectrum of the fabric image after suppressing the DC peak

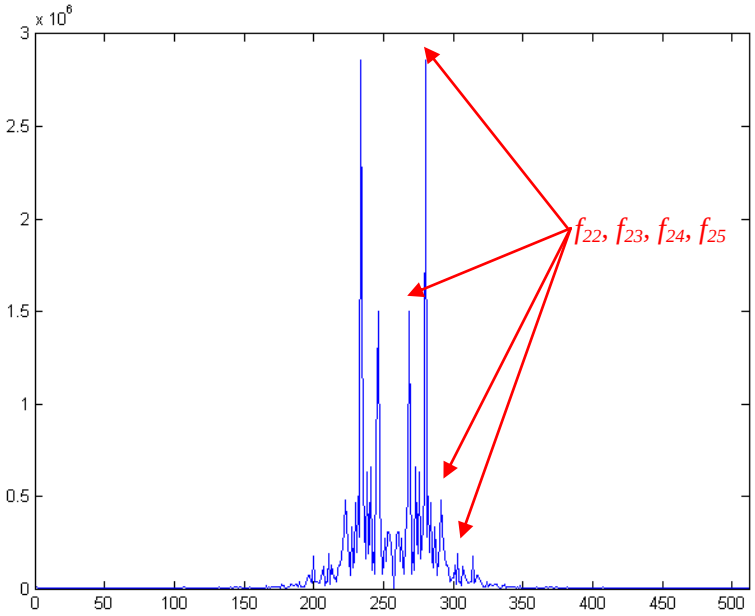

Figure 5. Peaks in the 0˚ direction (plan (a) in Figure 4)

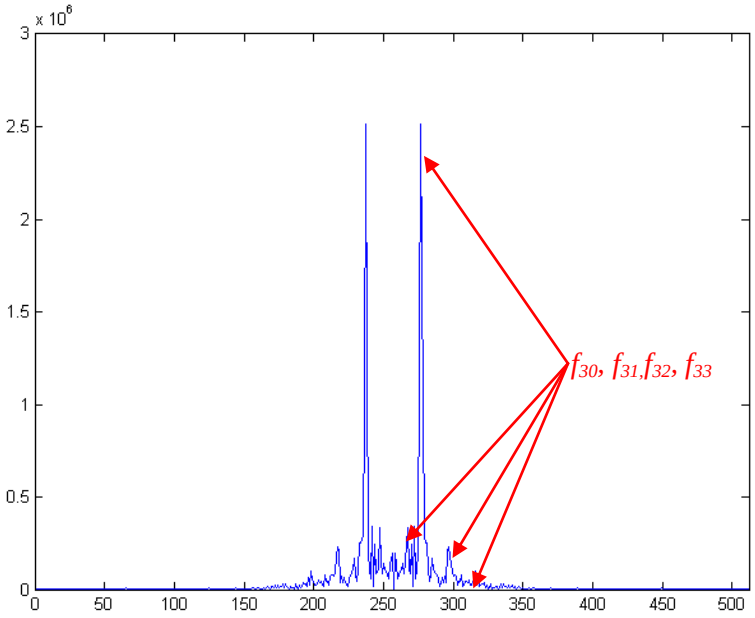

Figure 6. Peaks in the 90˚ direction (plan (b) in Figure 4)

3.5. Principal component analysis (PCA)

Although many features can be extracted from the images as shown before, some of them are highly correlated and some may not be affecting the model's predictability than others. The analysis for the most influential parameters can be performed using the principal component analysis (PCA) which is a method for linear transformation of a set of *n* dimensional data by projecting on an orthonormal set of *r* axes, where $r \leq n$. The new *r* axes are uncorrelated and called principal components because they are rotated in such a way that the axes are oriented along the direction of the highest variability of data. This in turn implies the highest amount of information represented by this data. In the situations where $1 \leq r << n$, a great reduction in the dimensionality can be achieved with the preservation of a high percentage of information in the original data. This high preservation is achieved because the first few principal components are usually chosen to represent the highest variability in the system. The dimensional reduction of the correlated data to uncorrelated components is very useful as it increases the robustness of the predictive models such as the artificial neural networks.

For a dataset ***A*** with *n* number of factors and *m* repeats or points for that factor and represented in the form:

$$A = \begin{bmatrix} a_{i,j} & \cdots & a_{i,m} \\ \vdots & \ddots & \vdots \\ a_{n,j} & \cdots & a_{n,m} \end{bmatrix}, i = 1, 2, .. n \ \& \ j = 1,2, \dots m$$

The PCA procedure starts with normalizing the input dataset ***A*** to another set ***B*** that is translated to have a mean of zero and scaled to have a standard deviation of 1 for all the i^{th} factors. This normalization is important to neutralize the predictive models from any bias towards any of the input factors. The normalization can be achieved by constructing $\boldsymbol{B}=b_{i,j}$ where:

$$b_{i,j} = \frac{a_{i,j} - \bar{a_i}}{\sigma_i \sqrt{n}} \ ,$$

$$\bar{a_i} = \frac{1}{m} \sum_{j=1}^{m} a_{i,j} \ ,$$

$$\sigma_i{}^2 = \frac{1}{m} \sum_{j=1}^{m} (a_{i,j} - \bar{a_i})^2$$

In these relations, $\bar{a}_i$ is the mean of events for the i^{th} factor, and σ_i is its standard deviation. After the data normalization, the correlation matrix $\boldsymbol{C}$ can be calculated from the normalized data $\boldsymbol{B}$ according to the relation [21]:

$$C_{ik} = \sum_{j=1}^{m} b_{j,i} b_{j,k} = \frac{1}{m} \sum_{j=1}^{m} \frac{(a_{i,j} - \bar{a}_i)(a_{i,k} - \overline{a_k})}{\sigma_i \sigma_k}$$

The principle components are oriented toward the eigenvectors of the correlation matrix and have a variance equals to the associated eigenvalues. This can be represented mathematically in the form:

$$C\,\Psi = \Lambda\,\Psi$$

Where $\Lambda\ and\ \Psi$ represent the eigenvalues and the eigenvectors, respectively. The first principal component PC_1 is usually chosen to have the highest variance allocated with the highest eigenvalue λ_1 and directed towards ψ_1. The second principal component PC_2 is orthonormal to PC_1 and is chosen to have the next highest variance associated with λ_2. In general, all principal components PC_k ($k=1,2\ldots\ r \leq n$) can be calculated in the same way. Each principal component contributes to the total variance by a percentage (v_k) that can be calculated from the relation:

$$v_k = \frac{\lambda_k}{\sum_{i=1}^{n} \lambda_i} = \frac{\lambda_k}{n}$$

Since the first principal components are associated with the highest λ values, the dimensionality of the original data can be reduced to a limited number of components without losing the information (variability) embedded in the original data. Therefore, the PCA results in removing the redundancy in the original data (caused by the collinear variables) and reveals the effective dimensionality of the dataset [22].

4. Results and discussion:

The set of the combined spatial and spectral features was calculated for all fabric images. The extracted features were found to have different behaviors as some features were found to cluster and converge for a certain fabric category while diverge for other categories. To illustrate the features' behavior, the feature f_1 is used as an example that is shown in Figure 7 where the feature values are represented on the y-axis and the fabric fault category numbers are represented on the x-axis. The category No. 1 represents the "defect free" fabrics, category No. 2 represents fabrics "wrong draw", category No. 3 represents fabrics with "slubs", category No. 4 represents

fabrics with “stop marks”, category No. 5 represents fabrics with “holes”, and category No. 6 represents “stained” fabrics.

It can be seen from the figure that f_1 is concentrated with low dispersion for certain groups such as the defect free (category No. 1) where 65 readings are plotted on the graph with a relatively low variance. On the other hand, the same feature is scattered in representing other categories such as the case of stained fabric (category No. 7) where 20 values are plotted and having a high dispersion. It can be detected from the behavior of the features that some of them are able to distinguish a category or more from the other categories. The combination of the features allows the detection of the fault classes in the situations where no single feature can be used to distinguish the sample. The behavior of features also indicates the differences and similarities between the groups. For example, it can be seen that category No. 1 and category No. 4 are very close in their features values which may lead to a difficulty in differentiating these categories during the classification step.

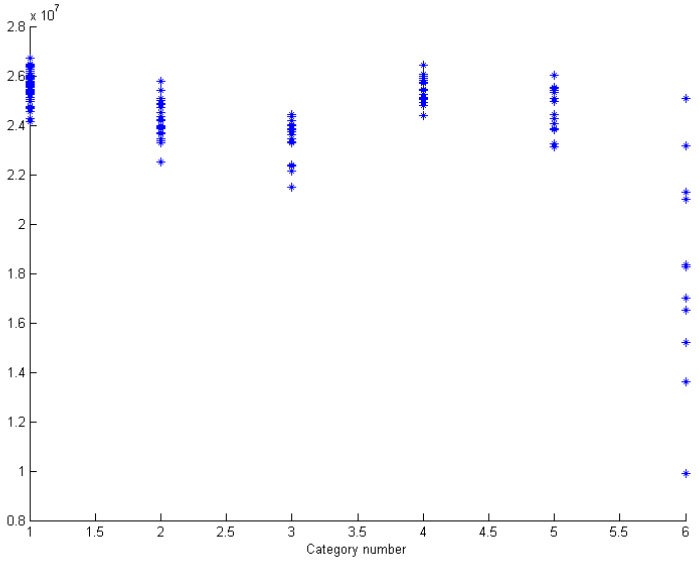

Figure 7. Feature f_1 for different fabric fault categories

The original dataset of features has high correlations between the features and decreasing the dimensionality of the data will be useful during the classification. Applying the PCA to the feature dataset results in 36 principal components, which is the same number of the inputs. However, not all of these principal components are useful according to the information they preserve from the original dataset. It was found that the principal components that represent 99%

of the total variance are the first thirteen components, as shown in Table 1, which means a reduction of the data dimensionality by about 64%. The use of the remaining principal components will increase the dimensionality of the data without offering a lot of information regarding the original data. Since the principal components are uncorrelated, the presentation of the projected data on the new principal component axes demonstrates their usefulness. Figure 8 shows the scores plot obtained from the PCA with a representation of the PC2 versus PC1for different fabric fault categories. Two main conclusions can be withdrawn from this figure; firstly, there is no distribution pattern for the plotted data which is scattered on the graph. This emphasizes the importance of the PCA procedure where no correlations between the principal components exist. Secondly, although the data are being scattered, they form clusters that might be useful in the classification of faults during the application of the ANN. Those clusters are not crisp for all groups but they have relatively distinguishable centers that are separated apart and even the category that is not shown in the figure (for stained fabrics) was excluded because it was far from the plotted categories which will shrink the scale of the figure if included.

Table 1. The the principal components' variance and their percentages

Component	Eigenvalue	Percentage (%)	Cumulative (%)
PC1	9.57	30.56	30.56
PC2	5.40	17.22	47.78
PC3	4.10	13.08	60.85
PC4	3.22	10.29	71.14
PC5	2.70	8.61	79.75
PC6	1.69	5.39	85.14
PC7	1.22	3.88	89.02
PC8	0.79	2.51	91.53
PC9	0.69	2.21	93.74
PC10	0.52	1.67	95.41
PC11	0.41	1.32	96.73
PC12	0.40	1.26	98.00
PC13	0.33	1.06	99.06

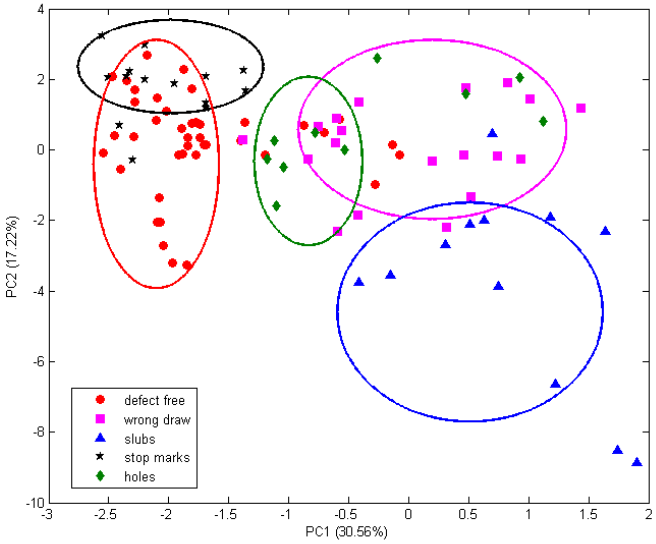

Figure 8. Scores plot for PC1 and PC2 for different fabric fault categories

The classification of the fabric faults was performed using pattern recognition artificial neural networks (ANN) which are special cases of the feed-forward neural networks that utilize certain transfer functions (tansig) and training algorithms. Two ANN were constructed during the study with the same architecture and only differ in the number of neurons in the input layer. The first network (called ANN1) was constructed using all features as inputs as demonstrated in Figure 9. ANN1 has two hidden layers that include 25 neuron in the hidden layer and 6 neurons in the output layer. The network was trained on a part of the dataset that represents all fabric fault categories and was selected randomly. The network also was tested on the remaining part of the dataset that was not used during the training. The second network (ANN2) was constructed with 13 neurons in the input layer as the PCA was applied on the inputs of this network. The network (ANN2) was trained and tested on the same training and testing datasets used with the first network (ANN1).

Table 2. Comparison of the performance of ANN1 and ANN2

	ANN1 (Full feature set)	ANN2 (Reduced feature set after PCA)
Correct Classification Rate (CCR) [%]	73.33	90
False Alarm Rate (FAR) [%]	15	5
False Negative Rate (FNR) [%]	20	7.5

Miss-Classification Rate (MCR) [%]	7.5	5

The performance of the ANNs can be quantitatively assessed from the results of the testing fabric images as summarized in Table 2 and shown in Figure 10 and Figure 11. Four measures were used to compare the performance of both ANNs. The first measure is the percentage of correct classification rate (CCR) which represents the percentage of all faults that were successfully classified on the networks. The CCR for the ANN1 was found to be 73.33% while it was increased to 90% for the ANN2. The false alarm rate (FAR) is the second comparison measure and refers to the number of defect free samples that were classified as faulty samples expressed as a percentage from the total number of the defect free samples. The FAR was found to be 15% for ANN1 and decreased to 5% for ANN2 which is considered as an improvement in the performance. On the other hand, the third measure is the false negative rate (FNR) which refers to the faulty samples that are classified as defect-free samples was found to be 20% for ANN1 while it was decreased to 7.5% with ANN2. The relatively high FNR of faulty fabrics that pass through the system (ANN1) without being detected should be taken serious because this will lead to a faulty end product if the system was industrially applied. The percentage of the faults that were detected but classified in the wrong category is considered as the fourth comparing measure and called the miss-classification rate (MCR). The MCR was found to be 7.5% for the ANN1 and improved to 5% by the application of the ANN2.

It is worthy to point out that, the similarity in the features of category No. 1 and category No. 4 (as noted earlier during the discussion of feature f_1Figure 7) might be the reason for a major part on the FNR in both networks that failed to detect the stop-mark defects. This result holds true because the first order statistical features applied in this study are usually not able to handle this type of fabric faults as long as the fabric picture has a similar number of threads even if they are irregularly distributed.

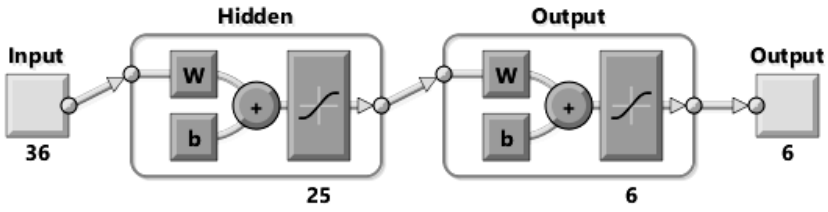

Figure 9.ANN with all features considered as inputs

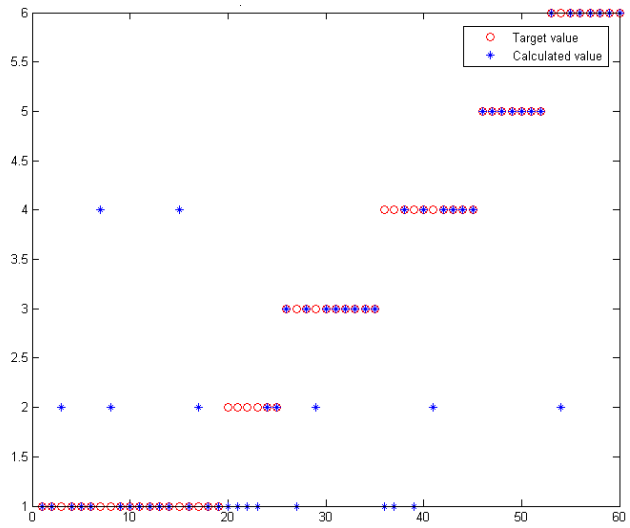

Figure 10. Performance of ANN1 (without PCA) in predicting different fabric fault categories

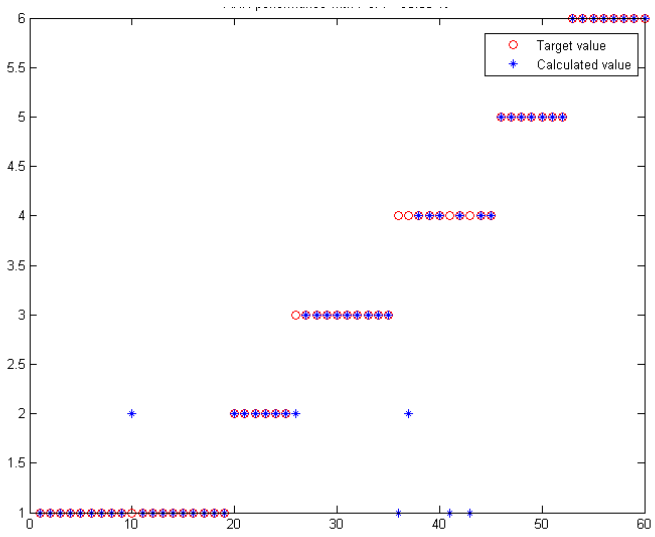

Figure 11. Performance of ANN2 (with PCA) in predicting different fabric fault categories

5. Conclusion

This work utilizes a digital camera to acquire and transmit fabric images to a computer which enhances and extracts the features of images. A large set of features composed of statistical and spectral features (using FFT) was used. The observation of the features shows different behaviors in the way they converge or diverge for a certain fabric fault. The PCA was used to reduce the number of features without losing the high variation in the data. A reduction to 36% of the original data size was achieved with preserving about 99% of the information in the original data. Two artificial neural networks were constructed with the same architecture and one of them was fed with the full feature dataset and the other was fed with the reduced dataset. The performance of the network that was implemented after the application of the PCA surpasses the performance of the other network in all aspect of characterization.

References

[1] H. Y. T. Ngan, G. K. H. Pang, and N. H. C. Yung, "Automated fabric defect detection—A review," *Image and Vision Computing*, vol. 29, pp. 442-458, 2011.

[2] P. M. Mahajan, S. R. Kolhe, and P. M. Patil, "A review of automatic fabric defect detection techniques," *Advances in Computational Research*, vol. 1, pp. 18-29, 2009.

[3] C.-F. J. Kuo and T.-L. Su, "Gray Relational Analysis for Recognizing Fabric Defects," *Textile Research Journal*, vol. 73, pp. 461-465, 2003.

[4] B. Mallik and A. K. Datta, "Defect Detection in Fabrics with a Joint Transform Correlation Technique: Theoretical Basis and Simulation," *Textile Research Journal*, vol. 69, pp. 829-835, 1999.

[5] B. Mallik-Goswami and A. K. Datta, "Detecting Defects in Fabric with Laser-Based Morphological Image Processing," *Textile Research Journal*, vol. 70, pp. 758-762, 2000.

[6] A. Sakaguchi, G. H. Wen, Y.-i. Matsumoto, K. Toriumi, and H. Kim, "Image Analysis of Woven Fabric Surface Irregularity," *Textile Research Journal*, vol. 71, pp. 666-671, 2001.

[7] E. Shady, Y. Gowayed, M. Abouiiana, S. Youssef, and C. Pastore, "Detection and Classification of Defects in Knitted Fabric Structures," *Textile Research Journal*, vol. 76, pp. 295-300, 2006.

[8] L. Xiuping, W. Zhijie, S. Zhixun, and K.-F. Choi, "Slub Extraction in Woven Fabric Images Using Gabor Filters," *Textile Research Journal*, vol. 78, pp. 320-325, 2008.

[9] A. S. Malek, "Online fabric inspection by image processing technology," Université de Haute Alsace-Mulhouse, 2012.

[10] H. G. Bu, X. B. Huang, J. Wang, and X. Chen, "Detection of Fabric Defects by Auto-Regressive Spectral Analysis and Support Vector Data Description," *Textile Research Journal*, vol. 80, pp. 579-589, 2010.

[11] M. C. Hu and I. S. Tsai, "Fabric Inspection Based on Best Wavelet Packet Bases," *Textile Research Journal*, vol. 70, pp. 662-670, 2000.

[12] C.-Y. Wen, S.-H. Chiu, W.-S. Hsu, and G.-H. Hsu, "Defect Segmentation of Texture Images with Wavelet Transform and a Co-occurrence Matrix," *Textile Research Journal*, vol. 71, pp. 743-749, 2001.

[13] A. Tilocca, P. Borzone, S. Carosio, and A. Durante, "Detecting Fabric Defects with a Neural Network Using Two Kinds of Optical Patterns," *Textile Research Journal*, vol. 72, pp. 545-550, 2002.

[14] C. W. M. Yuen, W. K. Wong, S. Q. Qian, D. D. Fan, L. K. Chan, and E. H. K. Fung, "Fabric Stitching Inspection Using Segmented Window Technique and BP Neural Network," *Textile Research Journal*, vol. 79, pp. 24-35, 2009.

[15] H. T. Choi, S. H. Jeong, S. R. Kim, J. Y. Jaung, and S. H. Kim, "Detecting Fabric Defects with Computer Vision and Fuzzy Rule Generation. Part II: Defect Identification by a Fuzzy Expert System," *Textile Research Journal*, vol. 71, pp. 563-573, 2001.

[16] C.-C. Huang and W.-H. Yu, "Fuzzy Neural Network Approach to Classifying Dyeing Defects," *Textile Research Journal*, vol. 71, pp. 100-104, 2001.

[17] C.-C. Huang and I. C. Chen, "Neural-Fuzzy Classification for Fabric Defects," *Textile Research Journal*, vol. 71, pp. 220-224, 2001.

[18] J.-J. Lin, "Pattern Recognition of Fabric Defects Using Case-Based Reasoning," *Textile Research Journal*, vol. 80, pp. 794-802, 2010.

[19] D. Committee, "Terminology Relating to Fabric Defects," ASTM International 2012.

[20] E. Pisano, S. Zong, B. Hemminger, M. DeLuca, R. E. Johnston, K. Muller, *et al.*, "Contrast Limited Adaptive Histogram Equalization image processing to improve the detection of simulated spiculations in dense mammograms," *Journal of Digital Imaging*, vol. 11, pp. 193-200, 1998.

[21] H. P. Singh, R. K. Gulati, and R. Gupta, "Stellar Spectral Classification using Principal Component Analysis and Artificial Neural Networks," *Monthly Notices of the Royal Astronomical Society*, vol. 295, pp. 312-318, 1998.

[22] W. B. Faulkner, E. F. Hequet, J. Wanjura, and R. Boman, "Relationships of cotton fiber properties to ring-spun yarn quality on selected High Plains cottons," *Textile Research Journal*, vol. 82, pp. 400-414, 2012.

Mohamed Eldessouki[2], Mounir Hassan[1,2], Khadijah Qashqari[3] Ebraheem Shady[2]

[1] Computer Science Department, Faculty of Computing and Information Technology, King Abdulaziz University, Jeddah, Saudi Arabia

[2] Textile Engineering Department, Faculty of Engineering, Mansoura University, Mansoura, Egypt

[3] Fashion Design Department, Faculty of Art & Design, King Abdulaziz University, Jeddah, Saudi Arabia

E-mail: mmhassan@kau.edu.sa

Application of Principal Component Analysis to Boost the Performance of an Automated Fabric Fault Detector and Classifier

Abstract

There is a growing need to replace visual fabric inspection with automated systems that detect and classify fabric defects. The digital processing of fabric images utilises different methods that offer a large set of image features. The correlation between those features lead to problems during fabric fault classification and reduces the performance of the classifiers. This work extracted a combination of statistical (spatial) and Fourier transform (spectral) features from fabric images of the most frequent faults. Principal component analysis (PCA) was implemented to reduce the dimensionality of the input feature dataset, which achieved a reduction to 36% of the original data size while preserving 99% of information in the original dataset. The features processed using the PCA were fed to an artificial neural network (ANN) to classify the fault categories and then compared to another ANN that worked with the whole feature dataset. The performance of the network that was implemented after application of the PCA increased to 90% of the correct classification rate as compared to 73.3% for the other network.

Key words: *fabric fault detector, image processing, artificial neural networks ,principal component analysis.*

Introduction

Early intervention to fix, or remove, fabric faults is one of the mandatory tasks required by all fabric manufacturers. Undetected defects cause many problems downstream in the production line and result in end products with lower quality, creating a cost burden and non-profitable products. Automatic fault detection systems offer good alternatives to replace traditional human fabric inspection with computer vision systems that analyse fabrics in a systematic manner and aim at consistent performance. The efficiency of these automated systems, however, depends on many parameters and varies according to the quality of the hardware and the analysis algorithm.

There are many research articles in the field of automatic fabric fault detection and classification that can be found in published reviews [1, 2]. Among those some common methods for feature extraction and fault classification can be found as shown in ***Figure 1***. The methods of feature extraction vary, including spatial (statistical) features [3], spectral features (fast Fourier Transform) [4], a combination of spatial and spectral features [5 - 10], as well as other methods that may utilise wavelet transformers [11, 12]. The features extracted are fed to a classification system that has been implemented by researchers in different ways. Among these classifiers are artificial neural networks (ANN) of different types [13, 14], fuzzy inference systems [15], neuro-fuzzy systems [16, 17], as well as other classification systems [18].

In this work, some highly frequently occurring defects that represent the main categories of faults (warp, weft, and areal directions) were studied. A system of image acquisition and enhancement was developed and a number of spatial and spectral features extracted. The classification was done using pattern recognition artificial neural networks (ANNs) that were fed with the whole features and with the reduced dataset after application of the principal component analysis (PCA) technique. The performance of the two ANN classifiers was evaluated.

Figure 1. *Different methods available in the literature for feature extraction and classification.*

Fabric faults

There is a large amount of fabric defects that may be caused by different sources and production technologies. Spinning faults, for example, should be mended before fabric production (either by weaving or knitting) otherwise it will lead to fabric faults that may not be fixed at all. Therefore the scope of this study was only faults that occur during the weaving process and focusing on plain woven fabrics only. The fabric faults studied might be considered as severe faults and had to be fixed or removed. A defect-free sample is shown in ***Figure 2.a*** and the defected samples can be categorised into three main categories: defects in the warp and weft directions, and areal defects. There are different names that can be found in literature for the same defect; however the ASTM definition and description for these faults [19] will be considered in this work.

Warp direction

Wrong draw: This fault results when one or more warp ends are incorrectly drawn in the harness or reed. The fault is shown in ***Figure 2.b*** and can also be called "wrong draft", "misdraw", or "double end". This fault may be considered as a severe defect because it appears throughout the whole length of the fabric if not fixed.

Slub: This fault shows in the fabric as an abruptly thickened place in a yarn. It can occur in the warp or weft direction, but it was considered only in the warp direction in this study. Other names of the same fault are lump, piecing, slough-off, and slug. All these names are considered in ASTM standards. This fault may occur due to malfunctioning in warp sensors, shown in ***Figure 2.c***.

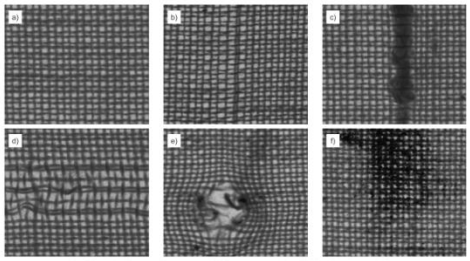

Figure 2. *Images of: a) defect-free, b) wrong draw, c) warp slub, d) stop mark, e) holes, f) fabric blotch woven fabrics.*

Weft direction

Stop mark: This appears as a visible change in the density of the weave across the width of the fabric caused by the tension on the warp not being adjusted properly after the loom has been stopped. This fault may be called a "set mark", or "light beat-up", shown in ***Figure 2.d***.

Area faults

Hole: It is an imperfection in the fabric where one or more yarns are sufficiently damaged to create an aperture. In case of a relatively large hole, it might be called a "smash", which is characterised by broken warp ends and floating picks. The smash may be equivalently called a "break-out", shown in ***Figure 2.e***.

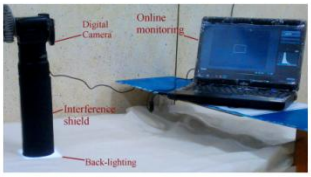

Figure 3. *Fabric image acquisition setup.*

Stain: It is an area of discoloration that penetrates the fabric surface. If this discoloration is caused by grease or oil and the off-colored area appears in any shape, it is called a "blotch" or "oil spot", an example of which is shown in ***Figure 2.f***.

Methodology

Samples

Fabric samples were manufactured on a Sulzer-Ruti weaving machine. The fabric structure was plain weave 1/1 with a yarn count of 29.5 tex for the warp and 42 tex for the weft. The densities of warp and weft yarns are 20 and 18 per cm, respectively. The defects chosen were intentionally introduced on the weaving machine based on knowledge of the defects' sources.

Image acquisition

The image acquisition setup is shown in ***Figure 3***, utilising a Canon digital camera (model: EOS 450D) with CMOS sensor. The system is installed with "Remote Live View Shooting", where online monitoring of the pictures and their adjustment can be done on a computer using EOS Utility software. The camera uses 35 mm EF-S lenses and captures images at a resolution of 72 dots per inch (dpi). The fabric sample is placed on an inspection table that is equipped with concentrated LED lights in a box placed

directly under the shooting area. To remove the noise and interference of the surrounding lights, a suitable shield was installed between the camera and shooting area.

Image enhancement

The system developed applies initial enhancements to the original images to reduce noise (e.g. hairiness) and improve their contrast. The system uses the contrast-limited adaptive histogram equalisation (CLAHE) [20] algorithm to enhance the contrast of the grayscale image by transforming the values. The algorithm can be described briefly as it operates in small regions (windows) in the image. Each window's contrast is enhanced so that the histogram of the output region approximately matches the histogram specified. The neighboring windows are then combined using bilinear interpolation to eliminate artificially induced boundaries. The contrast, especially in homogeneous areas, can be limited to avoid amplifying any noise that might be present in the image.

Image analysis and feature extraction

If the fabric image can be defined in the spatial domain by the matrix $P(x,y)$, where: x is the row number in the image ($1 \le x \le N$), y the column number ($1 \le y \le M$), and N & M are the number of rows and columns, respectively, the features that can be extracted from this image are summarised as below.

Statistical features

A total set of twenty spatial (statistical) features can be extracted from the fabric images. To obtain these features, the sum of individual gray-scale level values in the weft direction (rows) is calculated in the vector $R(m_j)$, where:

$$R(m_j) = \sum_{i=1}^{N} P(x_i, y_j) \qquad (1)$$

Similarly the sum of individual gray-scale values in the warp direction (columns) is calculated as:

$$C(n_j) = \sum_{j=1}^{M} P(x_i, y_j) \qquad (2)$$

The first feature selected is the sum of all the gray-scale values in the image, which can be calculated as:

$$f_1 = \sum_{j=1}^{N} C(n_j) \qquad (3)$$

The next two features, f_2 and f_3, represent the mean of the sum of rows (f_2) and that of the sum of columns (f_3). The relation for the first feature in the weft direction is:

$$f_2 = \frac{1}{M} \sum_{j=1}^{M} R(m_j) \qquad (4)$$

Similarly for the feature in the warp direction:

$$f_3 = \frac{1}{N} \sum_{i=1}^{N} C(n_i) \qquad (5)$$

For space constraints, the equations will be listed for the features in the weft (rows) direction only and similar relations can be written for the warp (columns) direction by replacing $R(m_j)$ with $C(n_i)$.

The standard deviation of the sum of rows (f_4) and for the sum of columns (f_5) can be calculated as:

$$f_4 = \sqrt{\frac{1}{M} \sum_{j=1}^{M} (R(m_j) - \bar{R})^2} \qquad (6)$$

$$R = f_2$$

Features f_6 *and* f_7 represent the median value of the sum of rows and columns:

$$f_6 = mediana\ (R(m_j))$$

Features f_8 and f_{10} represent the minimum and maximum values, respectively, for the sum of rows and f_9 and f_{11} represent the same values for the columns. These features can be written as:

$$f_8 = min(R(m_j)),\ f_{10} = max(R(m_j))$$

The range of the sum of rows and columns was chosen to be, respectively, features f_{12} and f_{13}:

$$f_{12} = ranget(R(m_j))$$

The entropy of the image represents feature f_{14}:

$$f_{14} = -\sum_{i=1}^{N} \sum_{j=1}^{M} P(x_i, y_j) \times \log\left(P(x_i, y_j)\right) (7)$$

The k^{th} order moment for the sum of rows can be calculated from the function

$$f_n = \frac{1}{M} \sum_{j=1}^{M} (R(m_j) - \bar{R})^k \qquad (8)$$

The second, third and fourth order moments can be calculated as features f_{15}, f_{17}, and f_{19} (α = 15, 17 and 19) for the rows as well as features f_{16}, f_{18}, and f_{20} (i.e. α = 16, 18 and 20) for the columns.

Spectral features

A fabric image of size $M \times N$ can be transformed from its spatial domain $P(x,y)$ to the spectral domain $\bar{P}(u,v)$ using the discrete Fourier transform (DFT), which can be expressed in a mathematical form as:

$$\bar{P}(u,v) = \frac{1}{MN} \sum_{x=0}^{M-1} \sum_{y=0}^{N-1} P(x,y) e^{-2\pi i \left(\frac{ux}{M} + \frac{vy}{N}\right)} \qquad (9)$$

Where x and y are the image spatial variables that correspond to the coordinates inside the image, while u and v represent the frequency variables transformed. Once the image is transformed, its power spectrum can be calculated as:

$$PW(u,v) = |\bar{P}(u,v)|^2 = R^2(u,v) \qquad (10)$$

Where $|\bar{P}(u,v)|$ is known as the Fourier spectrum, and $R^2(u,v)$ and $\bar{I}^2(u,v)$ are the real and imaginary parts of the image transformed $\bar{P}(u,v)$. Shifting the power spectrum is done by implementing the exponential properties of the transformer:

$$\Im[P(x,y)(-1)^{x+y}] = \bar{P}(u-M/2,\ v-N/2) \qquad (11)$$

Where $\Im$ [.] is the Fourier transform of an argument, stating the origin of the Fourier transform. $\bar{P}(0,0)$ of image $P(x,y)(-1)^{x+y}$ is located at $u = M/2$ and $v = N/2$, which causes the shifting of the spectrum to these coordinates. The first spectral feature selected is taken as the DC peak, which represents zero frequency in the image (thus originated the name DC, referring to direct current with zero frequency in electrical circuits). This peak dominates because it represents the average grey level of the image, as can be seen from the equation:

$$f_{21} = \bar{P}(0,0) = \frac{1}{MN} \sum_{x=0}^{M-1} \sum_{y=0}^{N-1} P(x,y) \qquad (12)$$

The peaks at frequencies other than zero are important in summarising information of the image and revealing its features. To visualise the other peaks and for illustration purposes, the DC peak is suppressed to zero, as illustrated in ***Figure 4***. The peaks in the two basic orthogonal directions can be extracted as shown in ***Figures 5*** and ***6***, which represent the 0° and 90° directions, respectively. For each direction the first four peaks were considered as features and for each peak both the magnitude (amplitude) and frequency

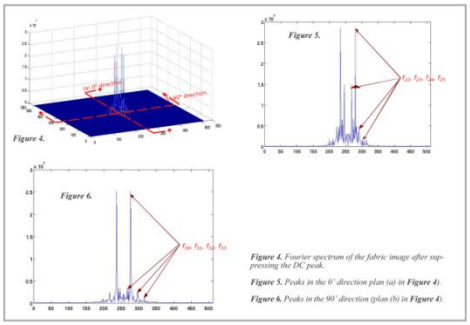

Figure 4. *Fourier spectrum of the fabric image after suppressing the DC peak.*

Figure 5. *Peaks in the 0° direction plan (a) in* ***Figure 4***).

Figure 6. *Peaks in the 90° direction (plan (b) in* ***Figure 4***).

were extracted as individual features. Therefore features f_{22}, f_{23}, f_{24}, and f_{25} were extracted from the zero direction as the amplitudes of the peaks, and features f_{26}, f_{27}, f_{28}, and f_{29} were extracted as the frequencies (locations) of the peaks. Similarly features f_{30} up to f_{37} were extracted from the 90° direction as the amplitudes and frequencies of the peaks in this direction.

Principal component analysis (PCA)

Although many features can be extracted from the images as shown before, some of them are highly correlated and some may not affect the model's predictability as others. Analysis to establish the most influential parameters can be performed using principal component analysis (PCA), which is a method for the linear transformation of a set of n dimensional data by projecting on an orthonormal set of r axes, where $r \le n$. The new r axes are uncorrelated and called principal components because they are rotated in such a way that the axes are oriented along the direction of the highest variability of data. This, in turn, implies the highest amount of information represented by this data. In situations where $1 \le r << n$, a great reduction in dimensionality can be achieved with the preservation of a high percentage of information in the original data. This high preservation is achieved because the first few principal components are usually chosen to represent the highest variability in the system. The dimensional reduction of the correlated data to uncorrelated components is very useful as it increases the robustness of predictive models such as artificial neural networks.

Dataset $\boldsymbol{A}$ with n number of factors and m repeats or points for that factor can be represented in the form:

$$\boldsymbol{A} = \begin{bmatrix} a_{1,1} & \cdots & a_{1,m} \\ \vdots & \ddots & \vdots \\ a_{n,1} & \cdots & a_{n,m} \end{bmatrix},$$

$$, i = 1, 2, \ldots n \ \&\ j = 1, 2, \ldots m$$

The PCA procedure starts with normalising the input dataset $\boldsymbol{A}$ to another set $\boldsymbol{B}$ that is translated to have a mean of zero and scaled to have a standard deviation of 1 for all the i^{th} factors. This normalisation is important to neutralise the predictive models from any bias towards any of the input factors. The normalisation can be achieved by constructing $\boldsymbol{B} = b_{i,j}$ where:

$$b_{i,j} = \frac{a_{i,j} - \bar{a}_i}{\sigma_i \sqrt{n}} \qquad (13)$$

$$\bar{a}_i = \frac{1}{m} \sum_{j=1}^{m} a_{i,j} \qquad (14)$$

$$\sigma_i^2 = \frac{1}{m} \sum_{j=1}^{m} (a_{i,j} - \bar{a}_i)^2 \qquad (15)$$

In these relations, $\bar{a}_i$ is the mean of events for the i^{th} factor, and σ_i is its standard deviation. After the data normalisation, the correlation matrix $\boldsymbol{C}$ can be calculated from the normalized data $\boldsymbol{B}$ according to the relation [21]:

$$C_{i,k} = \frac{1}{m} \sum_{j=1}^{m} b_{i,j}\ b_{j,k} = \frac{1}{m} \sum_{j=1}^{m} \frac{(a_{i,j} - \bar{a}_i)(a_{i,k} - \bar{a}_k)}{\sigma_i\ \sigma_k} \qquad (16)$$

The principle components are oriented toward the eigenvectors of the correlation matrix and have a variance equal to the associated eigenvalues. This can be represented mathematically in the form:

$$C\ \Psi = \Lambda\ \Psi$$

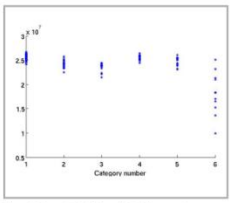

Figure 7. Feature f_1 for different fabric fault categories.

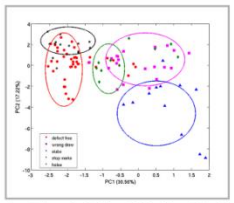

Figure 8. Scores plot for PC1 and PC2 for different fabric fault categories.

Where Λ and V represent the eigenvalues and eigenvectors, respectively. The first principal component PC_1 is usually chosen to have the highest variance allocated with the highest eigenvalue λ_1 and directed towards φ_1. The second principal component PC_2 is orthonormal to PC_1 and is chosen to have the next highest variance associated with λ_2. In general, all principal components PC_k ($k = 1, 2..., r \leq n$) can be calculated in the same way. Each principal component contributes to the total variance by a percentage (v_k) that can be calculated from the relation:

$$v_k = \frac{\lambda_k}{\sum_{i=1}^{n} \lambda_i} = \frac{\lambda_k}{n} \quad (17)$$

Since the first principal components are associated with the highest λ values, the dimensionality of the original data can be reduced to a limited number of components without losing the information (variability) embedded in the original data. Therefore the PCA results in removing the redundancy in the original data (caused by the collinear variables) and reveals the effective dimensionality of the dataset [22].

Results and discussion

The set of combined spatial and spectral features was calculated for all fabric images. The features extracted were found to have different behaviours as some were found to cluster and converge for a certain fabric category while diverge for other categories. To illustrate the features' behaviour, feature f_1 is used as an example, shown in ***Figure 7***, where the feature values are represented on the y-axis and fabric fault category numbers on the x-axis. Category No. 1 represents "defect free" fabrics, category No. 2 "wrong draw" fabrics, category No. 3 fabrics with "slubs", category No. 4 fabrics with "stop marks", category No. 5 fabrics with "holes", and category No. 6 represents "stained" fabrics.

It can be seen from the figure that f_1 is concentrated with low dispersion for certain groups such as the defect free (category No. 1), where 65 readings are plotted on the graph with relatively low variance. On the other hand, the same feature is scattered in representing other categories such as the case of stained fabric (category No. 6), where 20 values are plotted and have a high dispersion. It can be detected from the behaviour of the features that from some of them we are able to distinguish a category or more from the other categories. The combination of features allows the detection of fault classes in situations where no single feature can be used to distinguish the sample. The behaviour of features also indicates the differences and similarities between the groups. For example, it can be seen that categories No. 1 and No. 4 are very close in their feature values, which may lead to difficulty in differentiating these categories during the classification step.

The original dataset of features has high correlations between the features and decreasing the dimensionality of the data will be useful during the classification. Applying PCA to the feature dataset results in 36 principal components, which is the same number of the inputs. However, not all of these principal components are useful according to the information they preserve from the original dataset. It was found that the principal components, which represent 99% of the total variance, are the first thirteen components, as shown in ***Table 1***, which means a reduction in data dimensionality of about 64%. The use of the remaining principal components will increase the dimensionality of the data without offering a lot of information regarding the original data. Since the principal components are uncorrelated, presentation of the data projected on the new principal component axes demonstrates their usefulness. ***Figure 8*** shows the scores plot obtained from the PCA with a representation of PC2 versus PC1 for different fabric fault categories. Two main conclusions can be drawn from this figure: Firstly there is no distribution pattern for the data plotted, which is scattered on the graph. This emphasises the importance of the PCA procedure, where no correlations between the principal components exist. Secondly, although the data are scattered, they form clusters that might be useful in the classification of faults during application of the ANN. Those clusters are not crisp for all groups but they have relatively distinguishable centres that are separated apart, and even the category that is not shown in the figure (for stained fabrics) was excluded because it was far from the categories plotted, which will shrink the scale of the figure if included.

Classification of the fabric faults was performed using pattern recognition artificial neural networks (ANN), which are special cases of feedforward neural networks that utilise certain transfer functions (tansig) and training algorithms. There is a weight for each connection link (W) and a bias term (b) which are adjusted during the training process. Two ANN's were constructed during the study with the same architecture, only differing in the number of neurons in the input layer. The first network (called ANN1) was constructed using all features as inputs, as demonstrated in ***Figure 9***. ANN1 has two hidden layers that include 25 neurons in the hidden layer and 6 neurons in the output layer. The network was trained for a part of the dataset that represents all fabric fault categories and was selected randomly. The network also was tested for the remaining part of the dataset that was not used during the training. A second network (ANN2) was constructed with 13 neurons in the input layer as the PCA was applied to the inputs of this network. The network (ANN2) was trained and tested for the same training and testing datasets used with the first network (ANN1).

The performance of the ANNs can be quantitatively assessed from the results of the fabric images tested, as summarised in ***Table 2*** and shown in ***Figures 10 & 11***. Four measures were used to compare the performance of both ANNs. The first measure is the percentage of the correct classification rate (CCR), which represents the percentage of all faults that were successfully classified in the networks. The CCR for ANN1 was found to be 73.33%, while it increased to 90% for ANN2. The false alarm rate (FAR) is the second comparison measure and refers to the number of defect free samples that were classified as faulty samples, expressed as a percentage of the total number of defect free samples. The FAR was found to be 15% for ANN1, while it decreased to 5% for ANN2, which is considered as an improvement in performance. On the other hand, the third measure i.e. the false negative rate (FNR), which refers to the faulty samples that are classified as defect-free, was found to be 20% for ANN1, while it decreased to 7.5% with ANN2. The relatively high FNR of faulty fabrics that pass through the system (ANN1) without being detected should be taken seriously because this will lead to a faulty end product if the system is industrially applied. The percentage of faults that were detected but classified in the wrong category is con-

Table 1. Variance of principal components and their percentages.

Component	Eigenvalue	Percentage, %	Cumulative, %
PC1	9.57	30.56	30.56
PC2	5.40	17.22	47.78
PC3	4.10	13.08	60.85
PC4	3.22	10.29	71.14
PC5	2.70	8.61	79.75
PC6	1.69	5.39	85.14
PC7	1.22	3.88	89.02
PC8	0.79	2.51	91.53
PC9	0.69	2.21	93.74
PC10	0.52	1.67	95.41
PC11	0.41	1.32	96.73
PC12	0.40	1.26	98.00
PC13	0.33	1.06	99.06

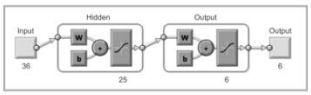

Figure 9. ANN with all features considered as inputs: 36, 25, 6, and 6 number of neurons.

Table 2. Comparison of the performance of ANN1 and ANN2.

	ANN1 (Full feature set)	ANN2 (Reduced feature set after PCA)
Correct classification rate (CCR), %	73.33	90
False alarm rate (FAR), %	15	5
False negative rate (FNR), %	20	7.5
Miss-classification rate (MCR), %	7.5	5

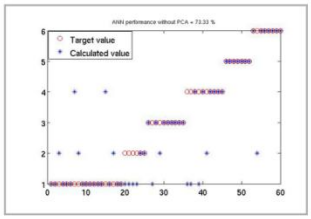

Figure 10. Performance of ANN1 (without PCA) in predicting different fabric fault categories.

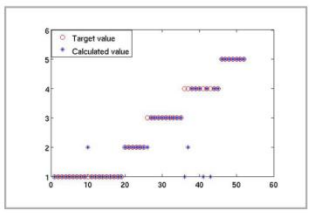

Figure 11. Performance of ANN2 (with PCA) in predicting different fabric fault categories.

sidered as the fourth comparing measure, called the miss-classification rate (MCR). The MCR was found to be 7.5% for ANN1, which improved to 5% with the application of ANN2.

It is worthy to note that the similarity in the features of categories No. 1 and No. 4 (as noted earlier during the discussion of feature f_1 (***Figure 7***) might be the reason for a major part of the FNR in both networks failing to detect stop-mark defects. This result holds true because the first order statistical features applied in this study are usually not able to handle these types of fabric faults as long as the fabric picture has a similar number of threads, even if they are irregularly distributed.

Conclusion

This work utilised a digital camera to acquire and transmit fabric images to a computer which enhances and extracts the features thereof. A large set of features composed of statistical and spectral features (using FFT) was used. Observation of the features shows different behaviours in the way they converge or diverge for a certain fabric fault. PCA was used to reduce the number of features without losing the high variation in data. A reduction to 36% of the original data size was achieved while preserving about 99% of the information in the original data. Two artificial neural networks were constructed with the same architecture and one of them was fed with the full feature dataset and the other with the reduced dataset. The performance of the network implemented after application of the PCA surpasses that of the other network in all aspects of characterisation.

Acknowledgment

This project was funded by the Deanship of Scientific Research (DSR), King Abdulaziz University, Jeddah, Saudi Arabia, under grant No. (108/364/1432). The authors, therefore, acknowledge with thanks DSR technical and financial support.

References

1. Ngan HYT, Pang GKH, Yung NHC. Automated fabric defect detection - A review. *Image and Vision Computing* 2011; 29: 442-458.
2. Mahajan PM, Kolhe SR, Patil PM. A review of automatic fabric defect detection techniques. *Advances in Computational Research* 2009; 1: 18-29.
3. Kuo C-FJ, Su T-L. Gray Relational Analysis for Recognizing Fabric Defects. *Textile Research Journal* 2003; 73: 461-465.
4. Mallik B, Datta AK. Defect Detection in Fabrics with a Joint Transform Correlation Technique: Theoretical Basis and Simulation. *Textile Research Journal* 1999; 69: 829-835.
5. Malik-Goswami B, Datta AK. Detecting Defects in Fabric with Laser-Based Morphological Image Processing. *Textile Research Journal* 2000; 70: 758-762.
6. Sakaguchi A, Wen GH, Matsumoto Y-i, Toriumi K, Kim H. Image Analysis of Woven Fabric Surface Irregularity. *Textile Research Journal* 2001; 71: 666-671.
7. Shady E, Gowayed Y, Abouiana M, Youssef S, Pastore C. Detection and Classification of Defects in Knitted Fabric Structures. *Textile Research Journal* 2006; 76: 295-300.
8. Xiuping L, Zhijie W, Zhixun S, Choi K-F. Slub Extraction in Woven Fabric Images Using Gabor Filters. *Textile Research Journal* 2008; 78: 320-325.
9. Malek AS. *Online fabric inspection by image processing technology.* Université de Haute Alsace-Mulhouse, 2012.
10. Bu HG, Huang XB, Wang J, Chen X. Detection of Fabric Defects by Auto-Regressive Spectral Analysis and Support Vector Data Description. *Textile Research Journal* 2010; 80: 579-589.
11. Hu MC, Tsai IS. Fabric Inspection Based on Best Wavelet Packet Bases. *Textile Research Journal* 2000; 70: 662-670.
12. Wen C-Y, Chiu S-H, Hsu W-S, Hsu G-H. Defect Segmentation of Texture Images with Wavelet Transform and a Co-occurrence Matrix. *Textile Research Journal* 2001; 71: 743-749.
13. Tilocca A, Borzone P, Carosio S, Durante A. Detecting Fabric Defects with a Neural Network Using Two Kinds of Optical Patterns. *Textile Research Journal* 2002; 72: 545-550.
14. Yuen CWM, Wong WK, S. Q. Qian, D. D. Fan, L. K. Chan, and E. H. K. Fung, „Fabric Stitching Inspection Using Segmented Window Technique and BP Neural Network," *Textile Research Journal* 2009; 79: 24-35.
15. Choi HT, Jeong SH, Kim SR, Jaung JY, Kim SH. Detecting Fabric Defects with Computer Vision and Fuzzy Rule Generation. Part II: Defect Identification by a Fuzzy Expert System. *Textile Research Journal* 2001; 71: 563-573.
16. Huang C-C, Yu W-H. Fuzzy Neural Network Approach to Classifying Dyeing Defects. *Textile Research Journal* 2001; 71: 100-104.
17. Huang C-C, Chen IC. Neural-Fuzzy Classification for Fabric Defects. *Textile Research Journal* 2001; 71: 220-224.
18. Lin J-J. Pattern Recognition of Fabric Defects Using Case-Based Reasoning. *Textile Research Journal* 2010; 80: 794-802.
19. Terminology Relating to Fabric Defects. ASTM International 2012. http://www.astm.org/Standards/D3990.htm
20. Pisano E, Zong S, Hemminger B, DeLuca M, Johnston RE, Muller K, et al. Contrast Limited Adaptive Histogram Equalization image processing to improve the detection of simulated spiculations in dense mammograms. *Journal of Digital Imaging* 1998; 11: 193-200.
21. Singh HP, Gulati RK, Gupta R. Stellar Spectral Classification using Principal Component Analysis and Artificial Neural Networks. *Monthly Notices of the Royal Astronomical Society* 1998; 295: 312-318.
22. Faulkner WB, Hequet EF, Wanjura J, Boman R. Relationships of cotton fiber properties to ring-spun yarn quality on selected High Plains cottons. *Textile Research Journal* 2012; 82: 400-414.

Received 04.11.2013 Reviewed 09.01.2014

PART II

Chapter 8

Integrated Computer Vision and Soft Computing System For Classifying The Pilling Resistance of Knitted Fabrics

Summary Sheet

- **Paper citation:**

  M. Eldessouki, M. Hassan, H. A. Bukhari, and K. Qashqari, "Integrated Computer Vision and Soft Computing System For Classifying The Pilling Resistance of Knitted Fabrics," *FIBERS & TEXTILES in Eastern Europe*, vol. 22, no. 6(108), pp. 106-112, 2014.

- **Targeted problem:**

  Although of being an important performance parameter, the fabric pilling is measured according to ***many standard systems*** and all of them depend on the ***subjective evaluation*** of ***human operators***, on the other hand, research trials in the literature focus ***only*** on ***separate*** evaluation ***stages*** and ***very few integrated systems*** for evaluation can be found

- **Objective(s):**
  - Collect all the methods available in the literature on the different stages of pilling evaluation
  - Develop analysis algorithms that implement fast and efficient techniques for pills segmentation and quantization
  - Develop a simple and user friendly integrated system for the pilling evaluation of knitted fabrics
  - Test the performance of the system with knitted samples of different structures and colors

- **Materials scope:**
  - EMPA Standards (SN 198525) photographs were used as evaluation reference for training the artificial intelligence system
  - Fabrics produced with knitting technology of different structures and colors

- **Computation method:**
  - First order statistical features and simple pilling descriptors were extracted from the acquired fabric images
  - Artificial neural networks with different structures was implemented for classification

- **Paper significance:**
  - A comprehensive review of the available literature on pilling evaluation with a categorization of the published work were presented in this paper
  - The suggested system implements fast and efficient techniques for pills segmentation and quantization
  - The system also introduces a new method for creating sampling dataset that is large enough to suite the training and testing processes required in building the applied artificial intelligent classifiers

- **Software**

  A software program with a user-friendly GUI was developed for this paper. The software is similar to the one developed with the paper in the next chapter but with different set of features and classification system. The program for the next paper is included on the accompanied CD with a tutorial video demonstration. The program's GUI is shown below:

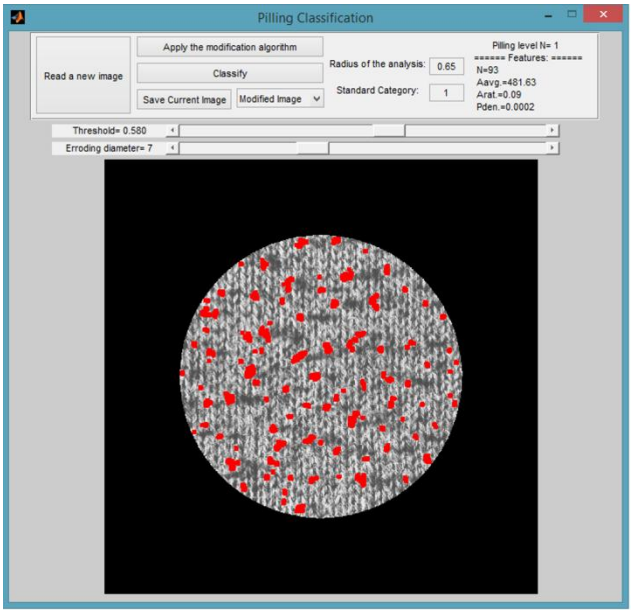
Pilling Classification
Read a new image
Apply the modification algorithm
Classify
Save Current Image
Modified Image
Radius of the analysis:
0.65
Standard Category:
1
Pilling level N= 1
====== Features: ======
N=93
Aavg.=481.63
Arat.=0.09
Pden.=0.0002
Threshold= 0.580
Erroding diameter= 7

Integrated Computer Vision and Soft Computing System For Classifying The Pilling Resistance of Knitted Fabrics

Mohamed Eldessouki[2,4*], Mounir Hassan[1,2], Hanan A. Bukhari[3] and Khadijah Qashqari[3]

[1] *Department of Computer Science, Faculty of Computing and Information Technology, King Abdulaziz University, Saudi Arabia*

[2] *Department of Textile Engineering, Faculty of Engineering, Mansoura University, Egypt*

[3] *Department of Fashion Design, Faculty of Art & Design, King Abdulaziz University, Saudi Arabia*

[4] *Department of Materials Engineering, Technical University of Liberec, Czech Republic*

* Corresponding author: eldesmo@auburn.edu

Abstract

Fabric pilling is one of the important properties that affect fabric appearance. The testing of fabrics pilling in the available standard methods, however, depends on the subjective samples evaluation. Objective fabric pilling evaluation using image processing techniques goes through four main stages that include binarization, segmentation, quantization, and classification. The literature about the topic focuses only on one or more of these stages while there is a growing need for an integrated system that combines the most effective techniques of each stage and introduces them in a way that does not depend on the subjective evaluation of human operators. This work tries to tackle this problem and creates an integrated system for classifying the knitted fabrics pilling resistance. The system introduced a new method for generating image library based on the photographs of the EMPA Standards to allow the training and testing of the soft-computing classifier. The suggested method was tested using knitted samples of different structures and colors and the results show high robustness performance in dealing with these samples. The quantitative pilling classification produced from the suggested system shows high agreement with the subjective operators' evaluation with a Spearman's correlation coefficient of +0.85.

1. Introduction

Fabric wear performance is equally a critical phenomenon for the manufacturers and the consumers. Changes in the surface of a fabric during processing, use, and care may be as obvious (e.g. the loss of structural integrity due to abrasion or the changes in fabric's color and texture), or it may be as subtle as fuzzing and pilling. According to the ASTM standard terminology related to textiles [1], pills can be defined as "bunches or balls of tangled fibers which are held to the surface of a fabric by one or more fibers". Although fabric pilling is less likely to affect the functional performance of textiles, it frequently results in consumer dissatisfaction and subsequent disposal of textile products before they reach the end of their useful wear life [2].

There is a wide range of parameters that affect the fabric pilling that are related to:yarn parameters (e.g. twist, hairiness…etc), spinning technology (e.g. ring spinning, rotor, compact spinning…etc), fabric producing technology (e.g. weaving, knitting…etc), as well as other processing parameters[3]. Knitted fabrics are commonly used because of their flexibility and cheap production costs. However, knitted fabrics are less stable than woven fabrics since they are produced from low twisted yarns and have slack constructions which lead to a low abrasion resistance and pilling performance.

Although most of the theoretical and empirical research on the surface wear dates back before the 1950s when durability of military uniforms was a priority [2], the majority of standard testing methods depend on accelerated fabric wear using laboratory devices that simulate the frictional mechanisms lead to surface wear and pilling formation. The available standards recommend comparing samples that gone under this accelerated wear process with standard photographs of different pilling grades where expert operators can make their judgment on the samples which makes their evaluation human dependent and very subjective process. Although the majority of pilling standard evaluation methods assign a ranking system that ranges between 1 and 5 (where 1 is assigned to a sever pilling and 5 is assigned to no pilling), the existence of different standards (e.g. ASTM, SN, EN ISO,…etc) creates a lot of confusion as samples that are ranked using different standards may result in different pilling grade. This calls researchers for finding alternative objective evaluation methods that may help to standardize those standard methods [4].

The introduction of image analysis as a method for evaluating the fabric pilling started in the late 80's with a try to replace the applied subjective evaluation methods [5]. The application of the image processing and analysis in the evaluation of fabric pilling goes through four stages and the majority of the research work on this topic tried to focus on one or more of these stages to modify the total outcome their systems. The main four objective pilling evaluation stages can be summarized as:

- Fabric's surface digitization
- Pills detection and segmentation
- Pills quantization (numerical description)
- Pills rating and classification

The fabric surface digitization is the process of converting the fabric surface to a digital form that can be dealt with on computer systems. This process can be done using a digital scanner [6-10], a camera [4, 11-13],a light projected on camera [14], a camera attached to a microscope [15], optical triangulation topographic reconstruction of the fabric surface[16-18], a laser line

projected on the surface of the fabric specimen[19], or a stereovision surface reconstruction using two CCD cameras[19].

Pills detection and segmentation is the process of separating the surface fuzz and pills from the complicated fabric structure background. This process was obtained using simple techniques such as the application of a binarization threshold on the fabric images [5, 19], or after processing the raw fabric images using spatial and spectral techniques. The raw image processing may include some filters for noise reduction or edge detection [9, 14], a background dilation and erosion[11, 16], a fabric pattern detection and isolation using Fast Fourier Transform (FFT)[4, 10, 11, 13, 20]or the different techniques of wavelet transforms [6-8, 20-23]. The pill detection was also performed using a template matching algorithm [13] and edge flow detection [24, 25]. For the colored images, pills were detected manually by blending the color channels of the fabric image [15].

The pills quantization is the next stage after segmenting pills from the fabric image. The process focuses on extracting some features that numerically represent the pills population to allow a quantitative discrimination between the different images. The feature descriptors can be divided in two categories; one that depends on the final image of the segmented pills, and the second that utilizes the spectral decomposition and analysis that was performed during the pills segmentation. The first category of features includes simple features such as the number of pills, the total pixel area of pilling, mean area of pills, the relative area of the pills to the total surface area, the sum of the gray values of pill images, the total volume of pills, as well as the distributions of pills, their shape, orientation angle, contrast, and density or uniformity of pills spatial distribution on the fabric surface [4, 5, 8, 10-13, 15, 16, 19]. The descriptor features can also be calculated from the gray-scale image of the processed surface or from the simulated fabric surface and includes roughness, skewness, as well as pills number, volume (total and average volumes), height (maximum and average), area (total and average), and fractal dimension [9, 14].

The second category of features includes the wavelet detail coefficients from the decomposition levels at the horizontal, the vertical and the diagonal orientations [21]. It can be defined also as the horizontal detailed coefficient (especially at scale close to the inter-yarn distances in the fabric) [6], as well as the energies of the reconstructed sub-images indifferent spatial orientations [22, 23]. Other statistical features can also be extracted from the wavelet decompositions such as the range, the inter-quartile range, the variance, the standard deviation, the mean absolute deviation, the median absolute deviation, the standard error and the coefficient of variation [7].

The classification stage can be considered as the ultimate goal of the whole process where a “successful” rating of images allows the trust of the method to replace the available subjective

analysis. Classification models use the extracted set of features as inputs that can be used to generate the final rating of the image. The classification models may implement empirical and statistical methods such as the multi-variable linear regression [8, 13, 19] and discriminant analysis [7, 21, 22], or may implement artificial intelligent methods such as the application of different types of the artificial neural networks [14, 23].

It is worthy to notice from this literature survey that the majority of the available published papers are more oriented toward one or more evaluation stages by altering and detailing their techniques while some papers may focus on one stage only [24, 25]. Therefore, there is a lack of integrated systems that manipulate the efficient practices and techniques of each evaluation stage to create a robust and effective evaluation process. This paper tries to bridge this gap by creating a simple and user friendly integrated system for the pilling evaluation of knitted fabrics. The suggested system implements fast and efficient techniques for pills segmentation and quantization. The system also introduces a new method for creating sampling dataset that is large enough to suite the training and testing processes required in building the applied artificial intelligent classifier.

2. Methods of Analysis

2.1. Standard Image Preparation:

The standard evaluation photographs that are used for comparison were obtained from the EMPA Standards (SN 198525). The EMPA standards characterize the size of pill as large, medium, and small and assign a grading scale for each category [4]. The three categories of the standard pictures are shown in Figure 1 and each category depends on the pill size, the yarn count, and the fabric structural density. In each of these categories the pilling is evaluated by giving a number between 1 and 5 where the former refers to sever pilling and the later refers to no pilling. To allow better space for the operators' evaluation, the EMPA standard merges every two pilling ranks in one picture which gives four standard pictures (that represent 1-2, 2-3, 3-4, 4-5 ranking). Figure 1 shows the rank 1-2 in each knitted fabrics' pilling category.

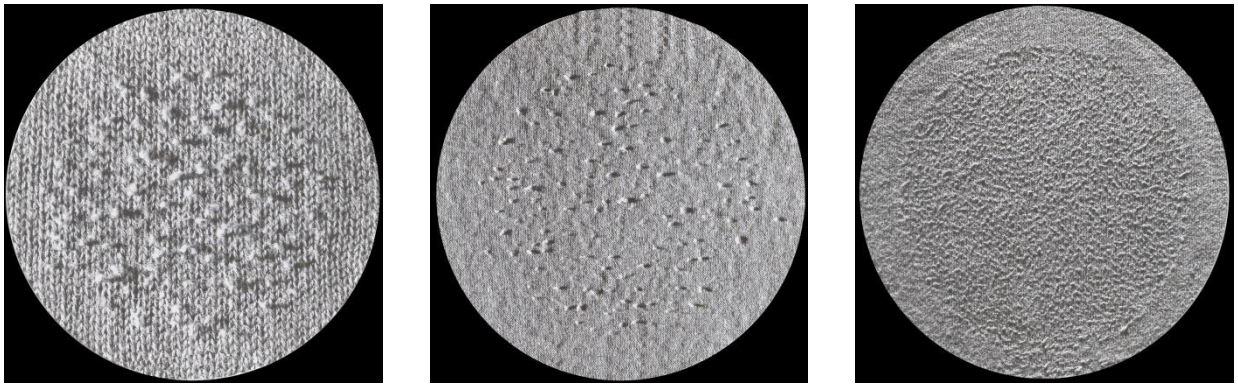

(a) Standard category K1 (b) Standard category K2 (c) Standard category K3

Figure 1. Pilling pictures of the three EMPA standard categories (all pictures represent the level 1-2 pilling of each category)

The standard knitted photographs were digitized by scanning to the computer with a resolution of 600 x 600 dpi. As these standard pictures are unique for each level, only twelve pictures (3 categories x 4 rating images/category) can be scanned. On the other hand, the intelligent classification systems need many samples for training and testing. Some researchers dealt with this problem by scanning the same standard image four times to enlarge the size of their dataset [23]. However, this technique may not be efficient in comparison with actual samples of wide varieties of structures and colors. Our method suggested a simulation of the real situation where actual fabric sample (after their rendering to remove the structure and the color effects) are distorted and noised images of the standard sample (after similar processing). Therefore, the current method suggests adding random noise to the standard images which allows the system robustness in detecting pills of actual samples. It also allows generating dataset that is sufficient for the artificial intelligent classifier training and testing.

To add the random noise to the standard pictures, different filter kernels were created with random parameters and each filter was convoluted with the standard image to create a "noised" or "blurred" image. Five different modifications were applied with the use of the "averaging", "disk", "Gaussian", and "motion" filters, as well as the "partial spatial rearrangement". Each filter and modification was applied with random parameters three times on the standard picture which creates 15 different duplicates from the same standard photograph. The "partial spatial rearrangement" modification was applied by randomly selecting sub-image from the original picture and placing it randomly at a different position of the image which creates a partial rearrangement of the picture's elements. A representation of the original image and samples from the resulted image after the application of the noised filters are shown in Figure 2.

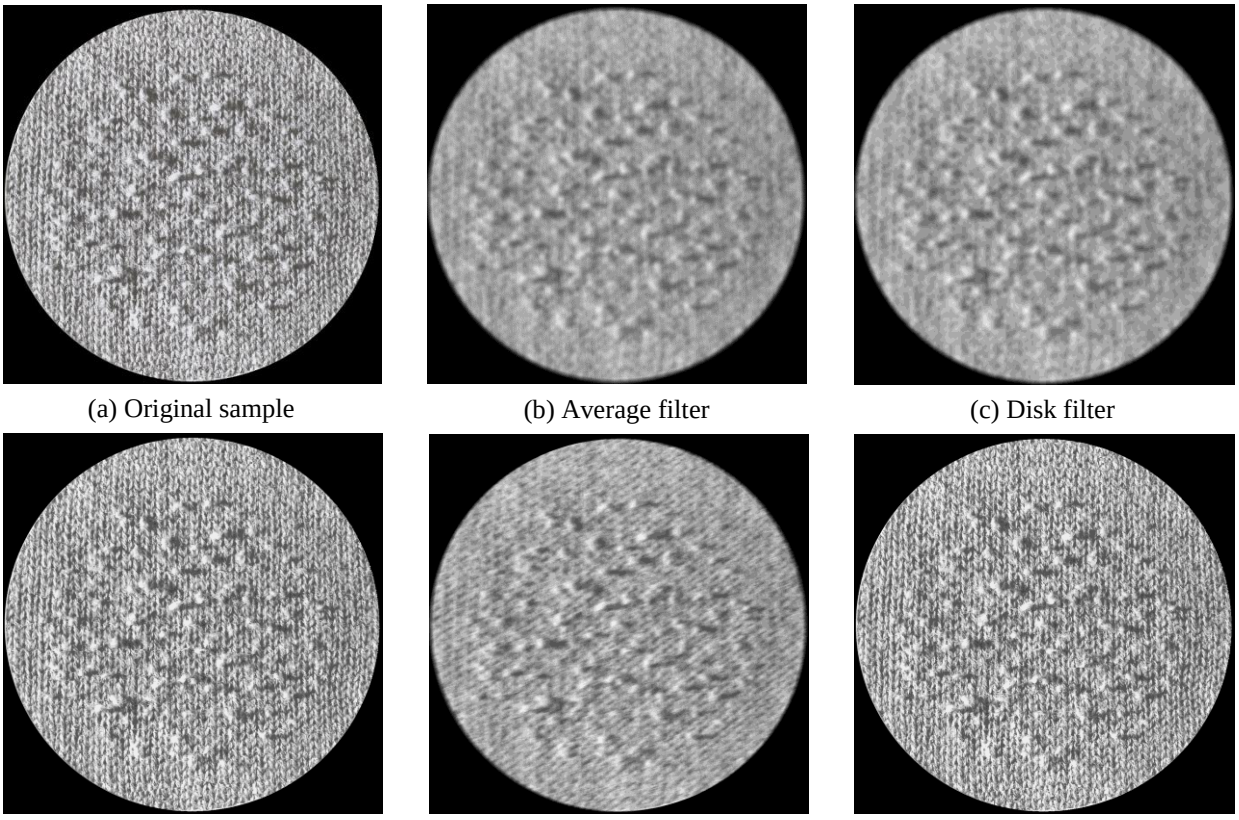

(a) Original sample (b) Average filter (c) Disk filter

(d) Gaussian filter (e) Motion filter (f) Partial rearrangement

Figure 2. Examples for different shapes of the same fabric sample after applying random filters

2.2. Pills Segmentation:

There are different pills detection and segmentation techniques as summarized in the introduction of this paper. The simple, fast, and efficient algorithms were selected from these techniques to be applied in the suggested system. Digital images are enhanced by applying a morphological opening that includes erosion and dilation algorithms on the grayscale image. The morphological opening algorithm enhances the image and reduces the background noise by removing elements below a certain size. The algorithm uses a structuring element in a disk shape with a diameter proportionate to the fabric standard category. As the standard samples have three categories with different ranges of pill sizes, yarn counts, and fabric density, the disk element with a small diameter was used with the category of fine yarn count and dense fabric. The image produced from the previous algorithm with low background noise is then subjected to

binarization with a specific threshold that results in a number of objects that represent the pills fabric. Figure 3 demonstrates the segmentation algorithm where Figure 3-a shows a fabric image with a certain *region of analysis* that is circled in the figure. The region of analysis can be changed by the user and it was introduced for two reasons; first, to focus the analysis on the region of the sample that goes under abrasion during Martindale testing. Second, to allow the system independency from the sample picture's size and resolution. Figure 3-b shows the binary image of the fabric with the segmented pills. To demonstrate the efficacy of the applied algorithm Figure 3-c shows the superimposed images of the original fabric highlighted with the segmented pills.

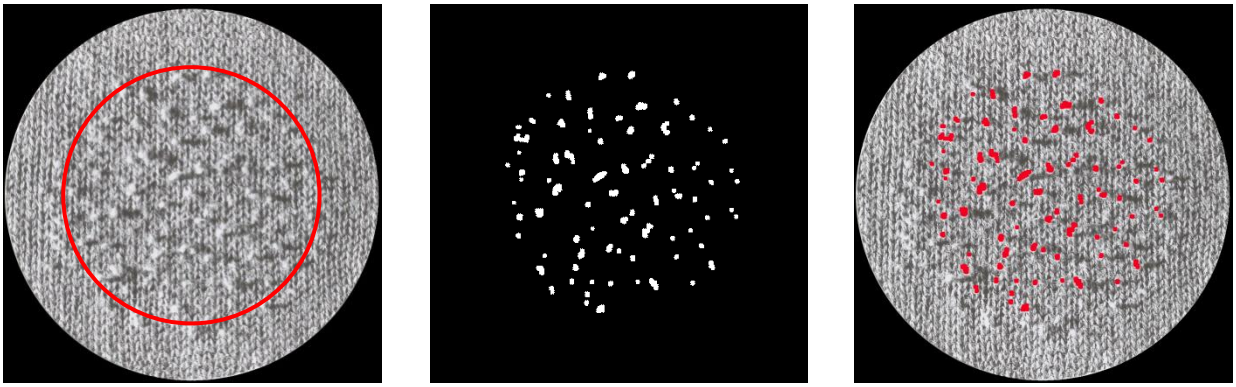

(a) Original fabric image with the "region of analysis" circled in red

(b) Binary image

(c) Combined image

Figure 3. Knitted fabric image with its preparation steps to detect its pilling

2.3. Pills Quantization:

It is necessary in any objective evaluation to quantize the property under investigation. This quantization process applies many techniques as demonstrated earlier. Among the most common characteristic features, the following features were extracted from the segmented images:

Number of pills:

The number of pills is used as a characteristic feature because it shows the severity of deterioration in the fabric surface due to abrasion. To calculate the number of pills, the labeled pixels of the binary image were used to test the connectivity of pixels and therefore finding the objects in the image. Pixels may be neighbors but not connected, as long as their values are different, and the connectivity of neighboring pixels can be determined in 4 or 8 directions which therefore affects the number of the obtained objects. In the current fabric images, pixel connectivity of 8 was used and the number of the detected objects (N) was considered as a representation to the number of pills on the fabric surface.

Pills average area:

The area of each obtained pill (object) A_i is calculated by summing up the number of pixels in each object. The average pill size ($A_{avg.}$) is calculated according to the relation:

$$A_{avg.} = \frac{\sum_{i=1}^{N} A_i}{N} \qquad (1)$$

Pills area ratio:

Unlike the ASTM pilling definition mentioned in the introduction, the "Textile Institute Textile Terms and Definitions" includes the density of the pills that should be great enough for light not to pass through them to the fabric surface and cause a shadow to be casted on the surface [12]. Therefore, the extent of pills on the fabric surface is considered using two characteristic features that are the area ratio ($A_{rat.}$) and the density (ρ_{pills}). The area ratio is defined as the ratio of the area of all pills that covers the surface to the area of the region of analysis ($A_{analysis}$) within the fabric image. The area ratio ($A_{rat.}$) is calculated as:

$$A_{rat.} = \frac{\sum_{i=1}^{N} A_i}{A_{analysis}} \qquad (2)$$

Pills density:

The pills' areal density (ρ_{pills}) can be expressed as the number of pills per unit area of region of analysis in the fabric image. It can be expressed mathematically as:

$$\rho_{pills} = \frac{N}{A_{analysis}} \qquad (3)$$

2.4. Pilling Classification:

After generating the library of the standard images and their derivatives, the pictures were processed and analyzed to generate the features dataset according to the procedures described in the previous sections. The features dataset consists of the features extracted from the noised images as well as the features obtained from the original picture. However; to avoid the system bias, the noised samples represented 30% of the size of the dataset and the remaining percentage represented the original standard picture (that is 15 pictures for the noised samples and 35 repeated pictures of the original standard). The final features dataset consisted of 600 readings where each one of the three standard categories (K1, K2, and K3) form a third of the readings. The feature dataset was then split randomly into a training dataset that represents 80% and a testing dataset that represents the remaining 20% of the data. The training dataset (of the four

pilling features and the standard category number) was fed to a pattern recognition artificial neural network (ANN). The ANN is shown in Figure 4and consists of a one hidden layer with 15 neurons and an output layer where all neurons are having sigmoid transfer functions. The output of the ANN is a single number that represents the rating of the fabric sample with the introduced features.

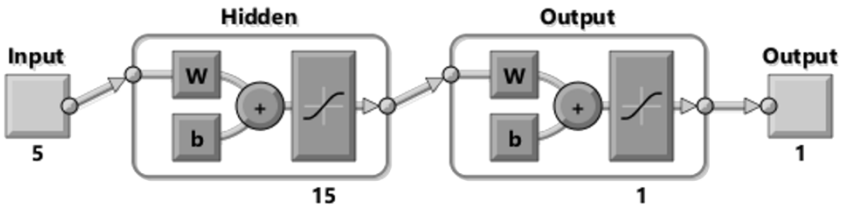

Figure 4. The architecture of the ANN used for pilling classification

2.5. Statistical analysis:

Spearman's coefficient of rank correlation (r_s) was used to measure the association between the two sets of observations by human operators and the computer pilling evaluation that are expressed in an ordinal scale. The Spearman's coefficient can be formulated as:

$$r_s = 1 - \frac{6\sum d^2}{n(n^2-1)} \qquad (4)$$

Where; d is the difference between the observations in the two groups and n is the number of samples in comparison.

3. Experimental Setup

Five knitted fabrics with different structures and color are specified as listed in Table 1. To test the system ability in detecting the fabric pilling regardless of the color shade, the tested samples were selected to have different colors. Samples were tested on Martindale instrument for their fabric pilling resistance where two circular specimens of 140 mm diameters from each sample were placed on the machine head. The lower specimen face is up and the specimen is placed on the top of a standard felt of 140 mm diameter. The upper specimen is mounted on a holder of 90 mm diameter with a standard felt of the same size and fixed to the holder with an elastic ring. The upper holder is installed on the machine where the faces of the upper and lower specimens are in contact to each other. The samples were tested under 2.5 cN/cm^2 pressure for 10,000 cycles of Lissajous figure with 24 mm stroke.

Table 1. Tested knitted sample specifications

	Color	Structure	Weight/Area (g/m^2)	Course/dm*	Wales/dm*	Yarn Count (tex)

K1	White	Interlock	235	147	106	21
K2	Blue	Interlock	228	180	94	22
K3	Gray	Jersey	143	181	139	20
K4	White	Interlock	222	150	112	19
K5	Red	Jersey	180	157	102	22

*dm = decimeter = 0.1 m

The measured samples were evaluated visually by five different operators against the photographs of the EMPA Standards (SN 198525). The measured samples were then digitized using the setup, schematically shown in Figure 5, and processed using the developed software algorithm to obtain the pilling classes. The image acquisition system consists of a digital CCD camera that is equipped with a macro lenses to capture the sample surface details. The captured image resolution of 300 dpi and the image dimensions was 2048x1536 pixels. Lighting is critical for the imaging system and two light sources that equally distribute the light on the surface of the fabric were applied. The sample was tilted with a slight angel to the horizontal plane to allow contrasting the pills with their shadow.

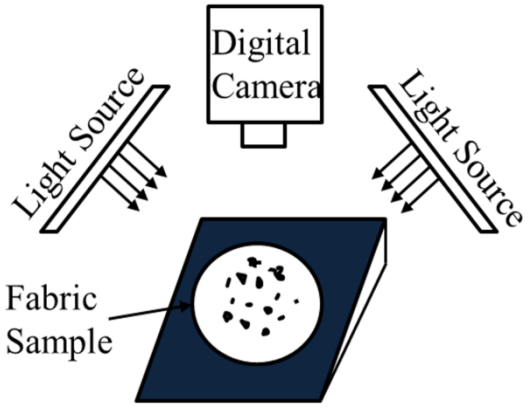

Figure 5. Schematic representation for the image acquisition setup

4. Results and discussion:

The photographs of the EMPA Standards (SN 198525) were acquired and the library of the training images was constructed after the application of the filters with the random parameters. The images were then processed for pilling segmentation and the quantization process was performed to create the features dataset. After training the ANN classifier, the performance was tested using the remaining 120 readings (that form the testing dataset) and their results are presented in Figure 6. The performance of the developed ANN is 87.5% as expressed in terms of

the correct classification rate (CCR) where the predicted sample pilling class matches with the targeted pilling level.

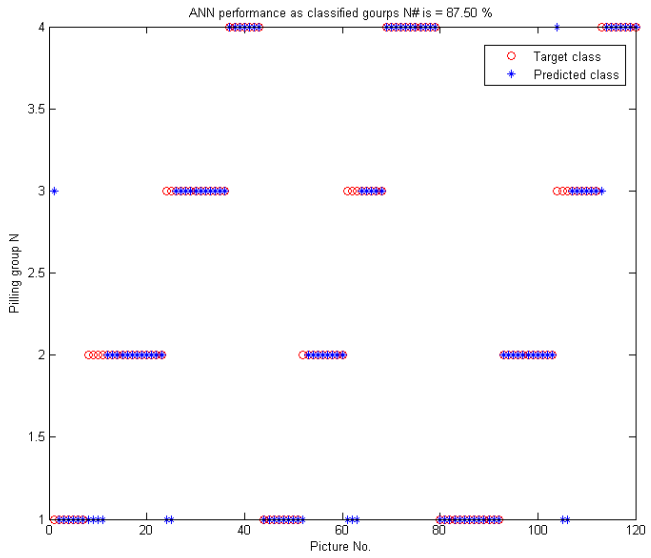

Figure 6. The performance of the ANN in pilling classification (the CCR is 87.5%)

Pilling Classification (PC) software developed to handle the digital images of the tested fabrics. The graphical user interface (GUI) of the program is shown in Figure 7 where the user can read the image, specify the standard comparison category, and determine the region of analysis for the fabric image. Once the user hits the "Apply the modification algorithm" the modified fabric image will appear on the program's window with two controllers for the threshold and the eroding diameter. Adjusting the eroding allows the removal of the background noise in the fabric main structure and tuning the threshold level determines the detected pilling size and density. The results of changing any value will interactively appear in the fabric's image. After reaching a suitable detection levels for the pills on the fabric surface, the user can classify the pills by pressing the "Classify" button and the program will recall the trained ANN classifier for predicting the sample pilling. The program produces the pilling level as well as the characteristic pilling features in the program's window. The user can save the pills segmented image or the superimposed image as well as the numerical results. All fabric sample images can be treated in a similar manner.

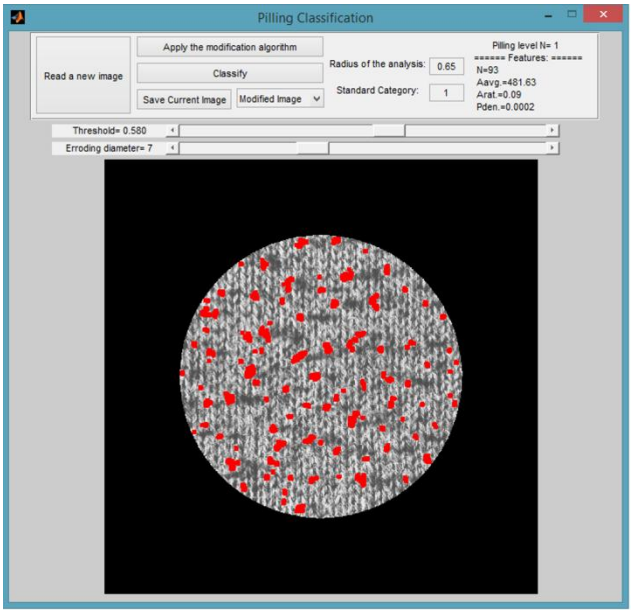

Figure 7. The interface of the developed Pilling Classification software

The actual knitted fabric samples were tested for their pilling resistance performance on Martindale tester as described earlier. The samples were then introduced to five operators to rank the pilling level in comparison to the standard images. The samples were also digitized using the setup shown in Figure 5 and processed on the PC software developed for the current method. The results of the human subjective evaluation as well as the ANN classifier's objective evaluation are listed in Table 2. The human operator's evaluation was calculated as the mode of ranking for individual operators. The evaluation of the knitted samples showed that they are distributed mainly between three ranks of pilling. The Spearman's coefficient of rank correlation between the two categories (*i.e.* the last two columns in Table 2) is +0.85 which implies a good agreement between the two sets of results.

Table 2. Pilling level in the actual samples as obtained subjectively from 5 operators and as obtained objectively using the ANN classifier

	Operator 1	Operator 2	Operator 3	Operator 4	Operator 5	Operators' evaluation	ANN evaluation
K1	2	2	2	3	2	2	1
K2	3	3	2	3	5	3	4
K3	2	2	1	2	2	2	1
K4	2	1	2	2	2	2	2
K5	1	1	1	2	1	1	1

The actual samples treated for their pilling classification using the suggested system are shown in Figure 8. It should be noticed from the processed images that the region of analysis might differ between the samples because this part will be decided by the operator according to the introduced sample. This difference of the areas of analysis is the reason behind normalizing the features according to the used area. This significantly improves the performance of the system as it allows its flexibility to deal with images of different sizes (i.e. regardless of the digitization method) and different areas of analysis.

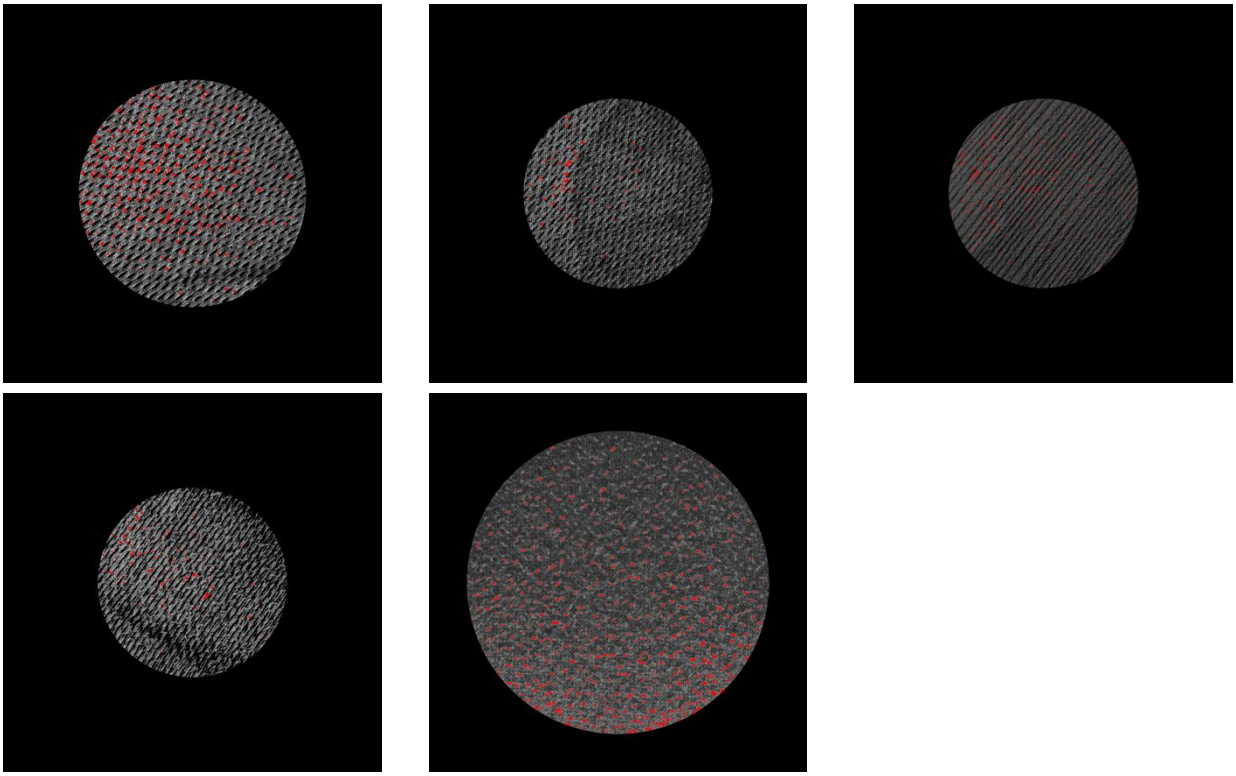

Figure 8. Images of actual samples as processed for their pilling level

Conclusion

An integrated system for the objective evaluation of knitted fabric pilling was introduced. The system utilizes simple and effective techniques from the commonly available in the literature to integrate the four main stages of the evaluation process. This work introduced a new method that simulates the real evaluation situations to generate an image library based on the EMPA standard photographs. The generated images were processed and produced features dataset with a sufficient number of data for training and testing the artificial neural network classifier. The ANN classifier shows robustness in handling actual fabric samples with different structures and

colors. The introduced system is user friendly and does not depend on the human experience of the process which enables standardized evaluation for pilling resistance of knitted fabrics.

References

[1] D. Committee, "Terminology Relating to Textiles," ASTM International 2003.

[2] P. A. Annis. (2005) Surface Wear Analysis of Fabrics. *ASTM Standardization News*.

[3] S. L. Paek, "Pilling, Abrasion, and Tensile Properties of Fabrics from Open-End and Ring Spun Yarns 1," *Textile Research Journal*, vol. 59, pp. 577-583, 1989.

[4] B. K. Behera and T. E. M. Mohan, "Objective measurement of pilling by image processing technique," *International Journal of Clothing Science and Technology*, vol. 17, pp. 279-291, 2005.

[5] A. Konda, L. C. Xin, Y. Okoshi, and K. Toriumi, "Evaluation of Pilling by Means of Computer Image Analysis Part 2 : Evaluation of Pilling Classes," *Sen'i Kikai Gakkaishi (Journal of the Textile Machinery Society of Japan)*, vol. 41, pp. T152-T161, 1988.

[6] S. Palmer and X. Wang, "Objective classification of fabric pilling based on the two-dimensional discrete wavelet transform," *Textile research journal*, vol. 73, pp. 713-720, 2003.

[7] S. R. Palmer, I. Joud, and X. Wang, "Characterization and application of objective pilling classification to patterned fabrics," *Journal of the textile institute*, vol. 96, pp. 423-430, 2005.

[8] S. C. Kim and T. J. Kang, "Image analysis of standard pilling photographs using wavelet reconstruction," *Textile research journal*, vol. 75, pp. 801-811, 2005.

[9] D. Semnani and H. Ghayoor, "Detecting and measuring fabric pills using digital image analysis," *World Academy of Science, Engineering and Technology*, vol. 49, pp. 897-900, 2009.

[10] S. Y. Yun, S. Kim, and C. K. Park, "Development of an objective fabric pilling evaluation method. I. Characterization of pilling using image analysis," *Fibers and Polymers*, vol. 14, pp. 832-837, 2013.

[11] Y. Torres and R. Navarro, "Automatic method based on image analysis for pilling evaluation in fabrics," *Optical Engineering*, vol. 37, pp. 2937-2947, 1998.

[12] C. H. Hsi, R. R. Bresee, and P. A. Annis, "Characterizing fabric pilling by using image-analysis techniques. Part I: Pill detection and description," *Journal of the Textile Institute*, vol. 89, pp. 80-95, 1998.

[13] B. Xin, J. Hu, and H. Yan, "Objective evaluation of fabric pilling using image analysis techniques," *Textile Research Journal*, vol. 72, pp. 1057-1064, 2002.

[14] X. Chen and X. B. Huang, "Evaluating fabric pilling with light-projected image analysis," *Textile research journal*, vol. 74, pp. 977-981, 2004.

[15] J. Izabela, "Assessment of a Fabric Surface after the Pilling Process Based on Image Analysis," *Fibres & Textiles in Eastern Europe*, vol. 17, p. 73, 2009.

[16] A. de Oliveira Mendes, P. T. Fiadeiro, R. A. L. Miguel, and J. M. Lucas, "Optical estimation of a set of pilling coefficients for textile fabrics," *Textile Research Journal*, vol. 79, pp. 410-417, 2009.

[17] A. de Oliveira Mendes, P. T. Fiadeiro, and R. A. L. Miguel, "Subjective and objective pilling evaluations of textile fabrics: a comparison," *Textile Research Journal*, vol. 80, pp. 1887-1897, 2010.

[18] A. de Oliveira Mendes, P. T. Fiadeiro, and R. A. L. Miguel, "Virtual subjective pilling evaluation: an alternative," *Textile Research Journal*, vol. 81, pp. 892-901, 2011.

[19] T. J. Kang, D. H. Cho, and S. M. Kim, "Objective evaluation of fabric pilling using stereovision," *Textile research journal*, vol. 74, pp. 1013-1017, 2004.

[20] S. Palmer, J. Zhang, and X. Wang, "New methods for objective evaluation of fabric pilling by frequency domain image processing," *Research journal of textile and apparel*, vol. 13, pp. 11-23, 2009.

[21] J. Zhang, X. Wang, and S. Palmer, "Objective grading of fabric pilling with wavelet texture analysis," *Textile research journal*, vol. 77, pp. 871-879, 2007.

[22] J. Zhang, X. Wang, and S. Palmer, "Objective pilling evaluation of wool fabrics," *Textile research journal*, vol. 77, pp. 929-936, 2007.

[23] J. Zhang, X. Wang, and S. Palmer, "Objective pilling evaluation of nonwoven fabrics," *Fibers and polymers*, vol. 11, pp. 115-120, 2010.

[24] Z.-T. Xiao and H.-W. Yang, "Fabric Pilling Segmentation Based on Edgeflow Algorithm," pp. 1744-1748.

[25] L. Xiaojun, "Segmentation for Fabric Pilling Images Based on Edge Flow," pp. 369-372.

Mohamed Eldessouki[2,4], Hanan A. Bukhari[3], Mounir Hassan[1,2], Khadijah Qashqari[3]

[1]Faculty of Computing and Information Technology, King Abdulaziz University, Jeddah, Saudi Arabia
[2]Department of Textile Engineering, Faculty of Engineering, Mansoura University, Egypt
[3]Department of Fashion Design, Faculty of Art & Design, King Abdulaziz University, Jeddah, Saudi Arabia
[4]Department of Materials Engineering, Technical University of Liberec, Liberec, Czech Republic

Integrated Computer Vision and Soft Computing System for Classifying the Pilling Resistance of Knitted Fabrics

Abstract

Fabric pilling is one of the important properties that affect fabric appearance. The testing of fabric pilling using the standard methods available, however, depends on subjective sample evaluation. Objective fabric pilling evaluation using image processing techniques comprises four main stages that include binarisation, segmentation, quantisation, and classification. Literature on the topic focuses only on one or more of these stages while there is a growing need for an integrated system that combines the most effective techniques of each stage and introduces them in a way that does not depend on the subjective evaluation of human operators. This work tries to tackle this problem and creates an integrated system for classifying the pilling resistance of knitted fabrics. The system introduced a new method for generating an image library based on photographs of the EMPA Standards to allow the training and testing of a soft-computing classifier. The method suggested was tested using knitted samples of different structures and colours and the results show their high robustness performance. The quantitative pilling classification produced from the system suggested shows high agreement with the subjective operators' evaluation with a Spearman's correlation coefficient of +0.85.

Key words: *pilling of knitted fabric, pill segmentation, pill quantisation, soft-computing classifier, artificial neural networks.*

Introduction

Fabric wear performance is a critical phenomenon equally for both manufacturers and consumers. Changes in the surface of a fabric during processing, use, and care may be obvious (e.g. the loss of structural integrity due to abrasion or the changes in fabric's colour and texture), or it may be as subtle as fuzzing and pilling. According to ASTM standard terminology related to textiles [1], pills can be defined as "bunches or balls of tangled fibres which are held to the surface of a fabric by one or more fibres". Although fabric pilling is less likely to affect the functional performance of textiles, it frequently results in consumer dissatisfaction and subsequent disposal of textile products before they reach the end of their useful wear life [2].

There is a wide range of parameters that affect fabric pilling that are related to yarn parameters (e.g. twist, hairiness… etc), spinning technology (e.g. ring spinning, rotor, compact spinning…etc), fabric producing technology (e.g. weaving, knitting … etc), as well as other processing parameters [3]. Knitted fabrics are commonly used because of their flexibility and cheap production costs. However, knitted fabrics are less stable than woven ones since they are produced from low twisted yarns and have slack constructions which lead to low abrasion resistance and pilling performance.

Although most theoretical and empirical research on surface wear dates back before the 1950s, when the durability of military uniforms was a priority[2], the majority of standard testing methods depend on accelerated fabric wear using laboratory devices that simulate the frictional mechanisms leading to surface wear and pilling formation. The standards available recommend comparing samples that have undergone this accelerated wear process, with standard photographs of different pilling grades, where expert operators can make their judgment on the samples, which makes their evaluation human dependent and a very subjective process. Although the majority of pilling standard evaluation methods assign a ranking system that ranges between 1 and 5 (where 1 is assigned to sever pilling and 5 to no pilling), the existence of different standards (e.g. ASTM, SN, EN ISO, … etc) creates a lot of confusion as samples that are ranked using different standards may result in different pilling grades. This calls for researchers to find alternative objective evaluation methods that may help to standardise the standard ones [4].

The introduction of image analysis as a method for evaluating fabric pilling started in the late 80's with an attempt to replace the subjective evaluation methods applied [5]. The application of image processing and analysis in the evaluation of fabric pilling consists in four stages and the majority of the research work on this topic tried to focus on one or more of these stages to modify the total outcome of their systems. The main four objective pilling evaluation stages can be summarised as:

- Fabric's surface digitisation,
- Pill detection and segmentation,
- Pill quantisation (numerical description),
- Pill rating and classification,

Fabric surface digitisation is the process of converting the fabric surface to a digital form that can be dealt with on computer systems. This process can be done using a digital scanner [6 - 10], camera [4, 11 - 13], light projected on a camera [14], a camera attached to a microscope [15], optical triangulation topographic reconstruction of the fabric surface [16 - 18], a laser line projected on the surface of the fabric specimen [19], or a stereovision surface reconstruction using two CCD cameras [19].

Pill detection and segmentation is the process of separating the surface fuzz and pills from the complicated fabric structure background. This process was obtained using simple techniques such as

Eldessouki M, Hassan M, Bukhari HA, Qashqari K. Integrated Computer Vision and Soft Computing System for Classifying the Pilling Resistance of Knitted Fabrics. *FIBRES & TEXTILES in Eastern Europe* 2014; 22, 6(108): 106-112.

the application of a binarisation threshold on fabric images [5, 19], or after processing raw fabric images using spatial and spectral techniques. The raw image processing may include some filters for noise reduction or edge detection [9, 14], background dilation and erosion [11, 16], fabric pattern detection and isolation using Fast Fourier Transform (FFT) [4, 10, 11, 13, 20] or different techniques of wavelet transforms [6-8, 20-23]. Pill detection was also performed using a template matching algorithm[13]and edge flow detection [24, 25]. For the coloured images, pills were detected manually by blending the colour channels of the fabric image [15].

Pill quantisation is the next stage after segmenting pills from the fabric image. The process focuses on extracting some features that numerically represent the pill population to allow quantitative discrimination between the different images. The feature descriptors can be divided into two categories: one that depends on the final image of the segmented pills, and the other that utilises the spectral decomposition and analysis performed during the pill segmentation. The first category of features includes simple features such as the number of pills, the total pixel area of pilling, the mean area of pills, the relative area of pills to the total surface area, the sum of the gray values of pill images, the total volume of pills, as well as the distributions of pills, their shape, orientation angle, contrast, and density or uniformity of the pills' spatial distribution on the fabric surface[4, 5, 8, 10-13, 15, 16, 19]. The descriptor features can also be calculated from the gray-scale image of the processed surface or from the simulated fabric surface and includes roughness, skewness as well as the pill number, volume (total and average volumes), height (maximum and average), area (total and average), and fractal dimension [9, 14].

The second category of features includes the wavelet detail coefficients from the decomposition levels at horizontal, vertical and diagonal orientations [21].It can also be defined as the horizontal detailed coefficient (especially at a scale close to the inter-yarn distances in the fabric) [6], as well as the energies of the reconstructed sub-image's indifferent spatial orientations [22, 23]. Other statistical features can also be extracted from the wavelet decompositions, such as the range, interquartile range, variance, standard deviation, the mean absolute deviation, median absolute deviation, the standard error and the coefficient of variation [7].

The classification stage can be considered as the ultimate goal of the whole process, where a "successful" rating of images allows the trust of the method to replace the available subjective analysis. Classification models use the extracted set of features as inputs that can be used to generate the final rating of the image. For the classification models empirical and statistical methods may be implemented such as multi-variable linear regression [8, 13, 19]and discriminant analysis [7, 21, 22],or artificial intelligent methods such as the application of different types of artificial neural networks [14, 23].

It is worth noticing from the literature survey that the majority of published papers available are more oriented toward one or more evaluation stages by altering and detailing their techniques, while some papers may focus on one stage only [24, 25]. Therefore there is a lack of integrated systems that manipulate the efficient practices and techniques of each evaluation stage to create a robust and effective evaluation process. This paper tries to bridge this gap by creating a simple and user friendly integrated system for the pilling evaluation of knitted fabrics. The system suggested implements fast and efficient techniques for pill segmentation and quantisation. The system also introduces a new method for creating a sampling dataset that is large enough to suit training and testing processes required in building the artificial intelligent classifier applied.

Methods of analysis

Standard image preparation

The standard evaluation photographs used for comparison were obtained from the EMPA Standards (SN 198525). The EMPA standards characterise the size of the pill as large, medium, and small and assign a grading scale for each category [4]. The three categories of the standard pictures are shown in ***Figure 1***, with each category depending on the pill size, yarn count, and fabric structural density. In each of these categories the pilling is evaluated by giving a number between 1 and 5, where the former refers to severe pilling and the later to no pilling. To allow better space for the operator's evaluation, the EMPA standard merges every two pilling ranks in one picture which gives four standard pictures (that represent 1-2, 2-3, 3-4 & 4-5 ranking). ***Figure 1*** shows rank 1-2 in each knitted fabric's pilling category.

The standard photographs of knitted were digitised by scanning to a computer with the resolution of 600 × 600 dpi. As these standard pictures are unique for each level, only twelve pictures (3 categories × 4

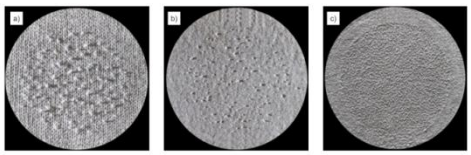

Figure 1. *Pilling pictures of the three EMPA standard categories (all pictures represent the level 1-2 pilling of each category): a) Standard category K1, b) Standard category K2, c) Standard category K3.*

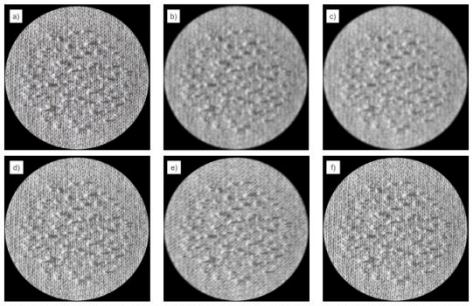

Figure 2. *Examples for different shapes of the same fabric sample after applying random filters: a) Original sample, b) Average filter, c) Disk filter, d) Gaussian filter, e) Motion filter, f) Partial rearrangement.*

rating images/category) can be scanned. On the other hand, the intelligent classification systems need many samples for training and testing. Some researchers have dealt with this problem by scanning the same standard images four times to enlarge the size of their dataset [23]. However, this technique may not be efficient in comparison with actual samples of wide varieties of structures and colours. Our method suggests simulation of the real situation where the actual fabric samples (after their rendering to remove the structure and colour effects) are distorted and there are noised images of the standard sample (after similar processing). Therefore the current method suggests adding random noise to the standard images to allow system robustness in detecting pills of the actual samples. It also enables to generate a dataset that is sufficient for the artificial intelligent classifier training and testing.

To add random noise to the standard pictures, different filter kernels were created with random parameters and each filter was convoluted with the standard image to create a "noised" or "blurred" image. Five different modifications were applied with the use of "averaging", "disk", "Gaussian", and "motion" filters, as well as "partial spatial rearrangement". Each filter and modification was applied with random parameters three times on the standard picture, which creates 15 different duplicates from the same standard photograph. "Partial spatial rearrangement" modification was applied by randomly selecting a sub-image from the original picture and placing it randomly in a different position of the image to create a partial rearrangement of the picture's elements. A representation of the original image and samples from the resulting image after the application of noised filters is shown in ***Figure 2***.

Pills segmentation

There are different pill detection and segmentation techniques, as summarised in the introduction of this paper. Simple, fast, and efficient algorithms were selected from these techniques to be applied in the system suggested. Digital images are enhanced by applying a morphological opening that includes erosion and dilation algorithms on the grayscale image. The morphological opening algorithm enhances the image and reduces the background noise by removing elements below a certain size. The algorithm uses a structuring element in a disk shape with a diameter proportionate to the fabric standard category. As the standard samples have three categories with different ranges of pill sizes, yarn counts and fabric density, a disk element with a small diameter was used for the category of fine yarn count and dense fabric. The image produced from the previous algorithm with low background noise is then subjected to binarisation with a specific threshold that results in a number of objects that represent the pills' fabric. ***Figure 3*** demonstrates the segmentation algorithm and ***Figure 3.a*** shows a fabric image with a certain *region of analysis*, circled in the figure. The region of analysis can be changed by the user, introduced for two reasons: first to focus the analysis on the region of the sample that goes under abrasion during Martindale testing. Second to allow system independency from the sample picture's size and resolution. ***Figure 3.b*** shows a binary image of the fabric with segmented pills. To demonstrate the efficacy of the algorithm applied, ***Figure 3.c*** shows superimposed images of the original fabric highlighted with the segmented pills.

Pill quantisation

It is necessary in any objective evaluation to quantise the property under investigation. This quantisation process applies

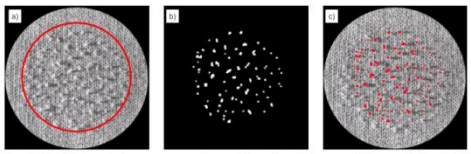

Figure 3. *Knitted fabric image with its preparation steps to detect its pilling: a) Original fabric image with the "region of analysis" circled in red, b) Binary image, c) Combined image.*

many techniques, as demonstrated earlier. Among the most common characteristic features, the following were extracted from the segmented images:

Number of pills

The number of pills is used as a characteristic feature because it shows the severity of deterioration on the fabric surface due to abrasion. To calculate the number of pills, the labelled pixels of the binary image were used to test the connectivity of pixels and therefore find the objects in the image. Pixels may be neighbours but are not connected as long as their values are different and the connectivity of neighboring pixels can be determined in 4 or 8 directions, which thus affects the number of objects obtained. In the current fabric images, a pixel connectivity of 8 was used and the number of objects detected (N) was considered as a representation of the number of pills on the fabric surface.

Pills' average area

The area of each pill (object) A_i obtained is calculated by summing up the number of pixels in each object. The average pill size (A_{avg}) is then calculated according to the relation:

$$A_{avg} = \frac{\sum_{i=1}^{N} A_i}{N} \quad (1)$$

Pills' area ratio

Unlike the ASTM pilling definition mentioned in the introduction, the "Textile Institute Textile Terms and Definitions" includes the density of pills that should be great enough for light not to pass through them to the fabric surface and cause a shadow to be cast on the surface [12]. Therefore the extent of pills on the fabric surface is considered using two characteristic features, which are the area ratio (A_{rat}) and density (ρ_{pills}). The area ratio is defined as the ratio of the area of all pills that cover the surface to the area of the region of analysis ($A_{analysis}$) within the fabric image. The area ratio (A_{rat}) is calculated as:

$$A_{rat} = \frac{\sum_{i=1}^{N} A_i}{A_{analysis}} \quad (2)$$

Pill density

The pills' areal density (ρ_{pill}) can be expressed as the number of pills per unit area of the region of analysis in the fabric image. It can be expressed mathematically as:

$$\rho_{pills} = \frac{N}{A_{analysis}} \quad (3)$$

Pilling Classification

After generating a library of standard images and their derivatives, the pictures were processed and analysed to generate a featur dataset according to the procedures described in the previous sections. The features dataset consists of the features extracted from the noised images as well as those obtained from the original picture. However; to avoid system bias, the noised samples represented 30% of the size of the dataset and the remaining percentage represented the original standard picture (that is 15 pictures for noised samples and 35 repeated pictures of the original standard). The final feature dataset consisted of 600 readings where each one of the three standard categories (K1, K2, and K3) form a third of the readings. The feature dataset was then split randomly into a training dataset that represents 80% and one that represents the remaining 20% of the data. The training dataset (of the four pilling features and standard category number) was fed to a pattern recognition artificial neural network (ANN). The ANN is shown in ***Figure 4*** and consists of a one hidden layer with 15 neurons and an output layer where all neurons have sigmoid transfer functions. The output of the ANN is a single number that represents the rating of the fabric sample with the features introduced.

Statistical analysis

Spearman's coefficient of rank correlation (r_s) was used to measure the association between the two sets of observations by human operators and the computer pilling evaluation, expressed on an ordinal scale. Spearman's coefficient can be formulated as:

$$r_s = 1 - \frac{6\sum d^2}{n(n^2-1)} \quad (4)$$

Where d is the difference between the observations in the two groups and n the number of samples in comparison.

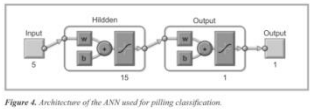

Figure 4. *Architecture of the ANN used for pilling classification.*

Table 2. Pilling level in the actual samples obtained subjectively from 5 operators and objectively obtained using the ANN classifier.

Symbol	Operator					Operators' evaluation	ANN evaluation
	1	2	3	4	5		
K1	2	2	2	3	2	2	1
K2	3	3	2	3	5	3	4
K3	2	2	1	2	2	2	1
K4	2	1	2	2	2	2	2
K5	1	1	1	2	1	1	1

Experimental setup

Five knitted fabrics with different structures and colours are specified as listed in ***Table 1***. To test the system's ability to detect fabric pilling regardless of the colour shade, test samples were selected to have different colours. The samples were tested on a Martindale instrument for their fabric pilling resistance, where two circular specimens of 140 mm diameter from each sample were placed on the machine head. The lower specimen's face is up and a specimen is placed on the top of a standard felt of 140 mm diameter. The upper specimen is mounted on a holder of 90 mm diameter with a standard felt of the same size and fixed to the holder with an elastic ring. The upper holder is installed on the machine where the faces of the upper and lower specimens are in contact with each other. The samples were tested under 2.5 cN/cm^2 pressure for 10,000 cycles of Lissajous figure with a 24 mm stroke.

The samples measured were evaluated visually by five different operators against the photographs of the EMPA Standards (SN 198525). The samples measured were then digitised using the setup schematically shown in ***Figure 5*** and processed using the software algorithm developed to obtain the pilling classes. The image acquisition system consists of a digital CCD camera equipped with a macro lenses to capture sample surface details. An image resolution of 300 dpi was captured and the image dimensions were 2048 × 1536 pixels. Lighting is critical for the imaging system, therefore two light sources that equally distribute light on the surface of the fabric were applied. The sample was tilted at a slight angle to the horizontal plane to allow to contrast the pills with their shadow.

Results and discussion

Photographs of the EMPA Standards (SN 198525) were acquired and a library of training images constructed after application of the filters with random parameters. Images were then processed for pilling segmentation and the quantisation process was performed to create a feature dataset. After training the ANN classifier, the performance was tested using the remaining 120 readings (that form the testing dataset), the results of which are presented in ***Figure 6***. The performance of the ANN developed is 87.5%, as expressed in terms of the correct classification rate (CCR), where the sample pilling class predicted matches with the pilling level targeted.

Pilling Classification (PC) software was developed to handle digital images of the fabrics tested. The graphical user interface (GUI) of the program is shown in ***Figure 7***, where the user can read the image, specify the standard comparison category, and determine the region of analysis for the fabric image. Once the user hits "Apply the modification algorithm" the modified fabric image will appear on the program's window with two controllers for the threshold and eroding diameter. Adjusting the eroding allows the removal of background noise in the main fabric structure and tuning the threshold level determines the pilling size and density detected. The results of changing any value will interactively appear in the fabric's image. After reaching a suitable detection level for the pills on the fabric surface, the user can classify them by pressing the "Classify" button and the program will recall the ANN classifier trained for predicting the sample pilling. The program produces the pilling level as well as characteristic pilling features in the program's window. The user can save the pill's segmented image or the superimposed image, as well as numerical results. All fabric sample images can be treated in a similar manner.

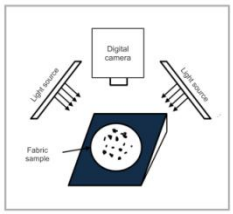

Figure 5. Schematic representation for the image acquisition setup.

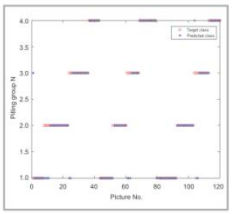

Figure 6. Performance of the ANN in pilling classification (the CCR is 87.5%).

The actual knitted fabric samples were tested for their pilling resistance performance on a Martindale tester as described earlier. The samples were then introduced to five operators to rank the pilling level in comparison to the standard images. The samples were also digitised using the setup shown in ***Figure 5*** and then processed on PC software developed for the current method. Results of the human subjective evaluation as well as the ANN classifier's objective evaluation are listed in ***Table 2***. The human operator's evaluation was calculated as the mode of ranking for individual operators. The evaluation of the knitted samples showed that they are distributed mainly between the three ranks of pilling. Spearman's coefficient of rank correlation between the two categories (*i.e.* the last two columns in ***Table 2***) is +0.85, which implies a good agreement between the two sets of results.

The actual samples treated for their pilling classification using the system suggested are shown in ***Figure 8***. It should be noted from the processed images that the region of analysis might differ between the samples because this part will be decided by the operator according to the sample introduced . This difference in the areas of analysis is the reason behind normalising the features according to the area used, which significantly improves the performance of the system as it allows its flexibility to deal with images of different sizes (i.e. regardless of the digitisation method) and different areas of analysis.

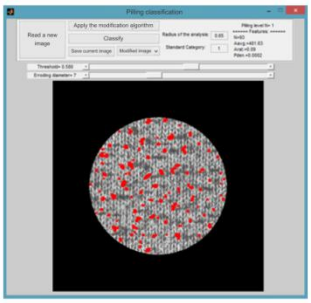

Figure 7. Interface of pilling classification software developed.

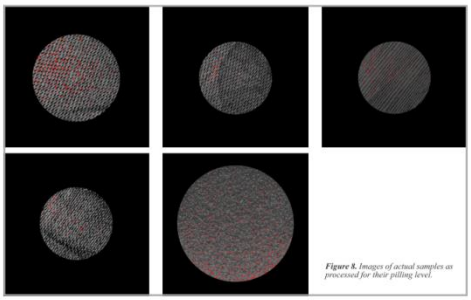

Figure 8. Images of actual samples as processed for their pilling level.

Conclusion

An integrated system for objective evaluation of the pilling of knitted fabric was introduced. The system utilises simple and effective techniques from those commonly available in the literature to integrate the four main stages of the evaluation process. This work introduced a new method that simulates real evaluation situations to generate an image library based on EMPA standard photographs. The images generated were processed and a feature dataset produced with a sufficient number of data for training and testing the artificial neural network classifier. The ANN classifier shows robustness in handling actual fabric samples with different structures and colours. The system introduced is user friendly and does not depend on human experience of the process, which enables standardised evaluation for the pilling resistance of knitted fabrics.

Acknowledgment

This project was funded by the Deanship of Scientific Research (DSR), King Abdulaziz University, Jeddah, Saudi Arabia, under grant no. (186/364/1433). The authors, therefore, acknowledge with thanks the DSR technical and financial support.

References

1. Standard Terminology Relating to Textiles. ASTM International 2003, Active Standard ASTM D123, Developed by Subcommittee: D13.92.
2. Annis PA. Surface Wear Analysis of Fabrics. *ASTM Standardization News*, September 2005.
3. Paek SL. Pilling, Abrasion, and Tensile Properties of Fabrics from Open-End and Ring Spun Yarns 1. *Textile Research Journal* 1989; 59: 577-583.
4. Behera BK, Mohan TEM. Objective measurement of pilling by image processing technique. *International Journal of Clothing Science and Technology* 2005; 17: 279-291.
5. Konda A, Xin LC, Okoshi Y, Toriumi K. Evaluation of Pilling by Means of Computer Image Analysis Part 2 : Evaluation of Pilling Classes. *Sen'i Kikai Gakkaishi (Journal of the Textile Machinery Society of Japan)* 1988; 41: T152-T161.
6. Palmer S, Wang X. Objective classification of fabric pilling based on the two-dimensional discrete wavelet transform. *Textile Research Journal* 2003; 73: 713-720.
7. Palmer SR, Joud I, Wang X. Characterization and application of objective pilling classification to patterned fabrics. *Journal of the Textile Institute* 2005; 96: 423-430.
8. Kim SC, Kang TJ. Image analysis of standard pilling photographs using wavelet reconstruction. *Textile Research Journal* 2005; 75: 801-811.
9. Semnani D, Ghayoor H. Detecting and measuring fabric pills using digital image analysis. *World Academy of Science, Engineering and Technology* 2009; : 49: 897-900.
10. Yun SY, Kim S, Park CK. Development of an objective fabric pilling evaluation method. I. Characterization of pilling using image analysis. *Fibers and Polymers* 2013; 14: 832-837.
11. Torres Y, Navarro R. Automatic method based on image analysis for pilling evaluation in fabrics. *Optical Engineering* 1998; 37: 2937-2947.
12. Hsi CH, Breese RR, Annis PA. Characterizing fabric pilling by using image-analysis techniques. Part I: Pill detection and description. *Journal of the Textile Institute* 1998; 89: 80-95.
13. Xin B, Hu J, Yan H. Objective evaluation of fabric pilling using image analysis techniques. *Textile Research Journal* 2002; 72: 1057-1064.
14. Chen X, Huang XB. Evaluating fabric pilling with light-projected image analysis. *Textile Research Journal* 2004; 74: 977-981.
15. Jasińska J. Assessment of a Fabric Surface after the Pilling Process Based on Image Analysis. Fibres & Textiles in Eastern Europe 2009; 17, 2, 73: 55-58.
16. de Oliveira Mendes A, Fiadeiro PT, Miguel RAL, Lucas JM. Optical estimation of a set of pilling coefficients for textile fabrics. *Textile Research Journal* 2009; 79: 410-417.
17. de Oliveira Mendes A, Fiadeiro PT, Miguel RAL. Subjective and objective pilling evaluations of textile fabrics: a comparison. *Textile Research Journal* 2010; 80: 1887-1897.
18. de Oliveira Mendes A, Fiadeiro PT, Miguel RAL. Virtual subjective pilling evaluation: an alternative. *Textile Research Journal* 2011; 81: 892-901.
19. Kang TJ, Cho DH, Kim SM. Objective evaluation of fabric pilling using stereovision. *Textile Research Journal* 2004; 74: 1013-1017.
20. Palmer S, Zhang J, Wang X. New methods for objective evaluation of fabric pilling by frequency domain image processing. *Research Journal Of Textile And Apparel* 2009; 13: 11-23.
21. Zhang J, Wang X, Palmer S. Objective grading of fabric pilling with wavelet texture analysis. *Textile Research Journal* 2007; 77: 871-879.
22. Zhang J, Wang X, Palmer S. Objective pilling evaluation of wool fabrics. *Textile Research Journal* 2007; 77: 929-936.
23. Zhang J, Wang X, Palmer S. Objective pilling evaluation of nonwoven fabrics. *Fibers and Polymers* 2010; 11: 115-120.
24. Xiao Z-T, Yang H-W. Fabric Pilling Segmentation Based on Edgeflow Algorithm. In: *2007 International Conference on Machine Learning and Cybernetics (ICMLC)*. Hong Kong, China, 19-22 August, 2007. DOI: 10.1109/ICMLC.2007.4370429, pp. 1744-1748.
25. Xiaojun L. Segmentation for Fabric Pilling Images Based on Edge Flow. In: *2009 Second International Conference on Information and Computing Science*. 21-22 May 2009. DOI: 10.1109/ICIC.2009.204, pp. 369-372.

Received 10.02.2014 Reviewed 25.04.2014

PART II

Chapter 9

Adaptive Neuro-Fuzzy System For Quantitative Evaluation of Woven Fabrics' Pilling Resistance

Summary Sheet

- **Paper citation:**
  M. Eldessouki and M. Hassan, "Adaptive Neuro-Fuzzy System For Quantitative Evaluation of Woven Fabrics' Pilling Resistance," *Expert Systems with Applications,* vol. 42, no. 4, pp. 2098-2113, 2014, DOI:10.1016/j.eswa.2014.10.013.

- **Targeted problem:**
  Fabric pilling is measured according to ***subjective evaluation*** standards and while it is a ***surface property***, no research considered the ***textural features*** as descriptors and the classifications performed in the literature neglect the ***uncertainty*** during the ***decision making*** by the human operators

- **Objective(s):**
  - Develop an algorithm that considers the second-ordered statistical textural features of the fabric surface
  - Develop a method for creating a training dataset of a reasonable size suitable for the soft-computing classifier
  - Develop a classification system that counts for uncertainty in the decision making
  - Build an integrated system that combines these algorithms while being user-friendly

- **Materials scope:**
  - EMPA Standards (SN 198525) photographs were used as evaluation reference for training the artificial intelligence system
  - Fabrics produced with weaving technology of different structures and colors

- **Computation method:**
  - Second-order statistical and textural features as pills descriptors
  - Stochastic method for generating a dataset with a reasonable size
  - Adaptive neuro-fuzzy inference system (ANFIS) was used for the classification with some degree of uncertainity

- **Paper significance:**
  - Considered the *texture features* of the fabric images to quantize its pilling for the first time
  - Introduced a stochastic method for creating sampling dataset required in building the soft-computing classifier
  - Utilized the neuro-fuzzy classification system to approach the high level intelligence of human beings
  - Created a user-friendly GUI that integrates the main four stages of pilling evaluation

- **Software**
  A software program with a user-friendly GUI was developed for this paper. The software program for is included on the accompanied CD with a tutorial video demonstration. It also has example picture so the reader can test the program. The program's GUI is shown below:

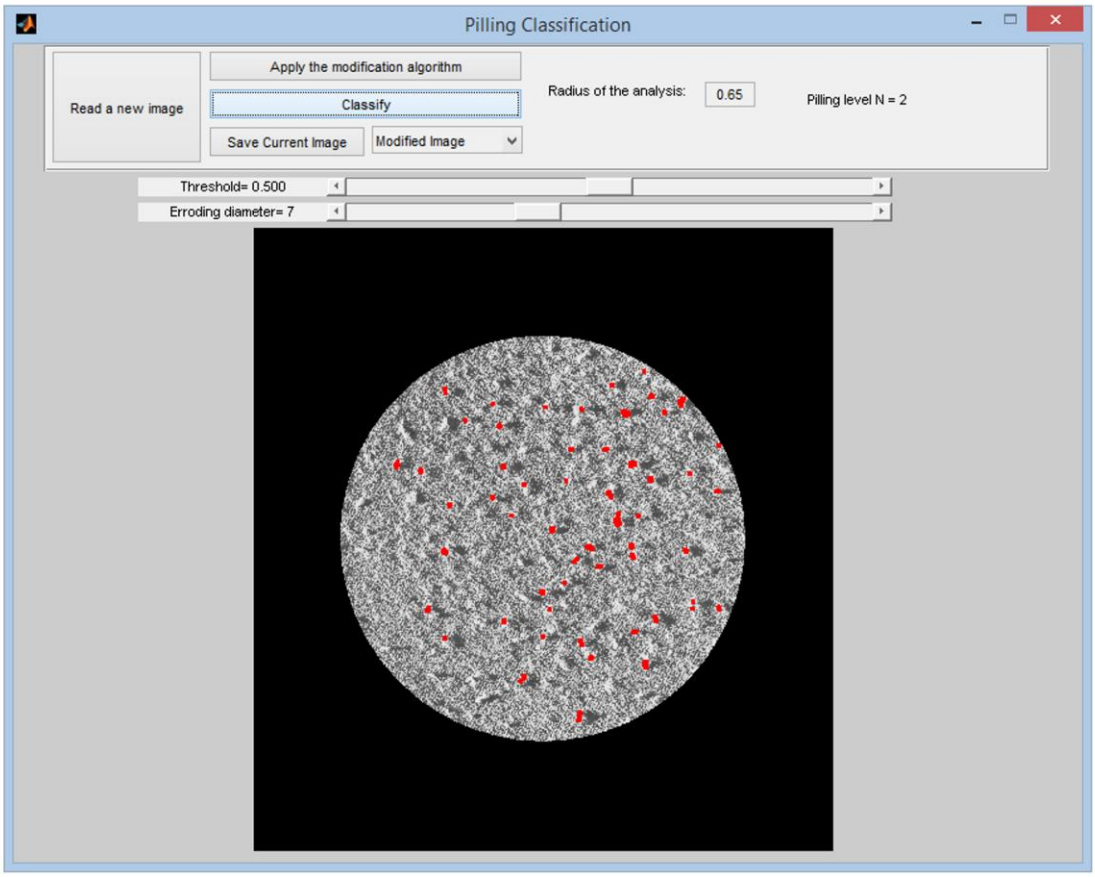
Pilling Classification
Read a new image
Apply the modification algorithm
Classify
Save Current Image
Modified Image
Radius of the analysis:
0.65
Pilling level N = 2
Threshold= 0.500
Erroding diameter= 7

Adaptive Neuro-Fuzzy System For Quantitative Evaluation of Woven Fabrics' Pilling Resistance

Mohamed Eldessouki[1,3*], Mounir Hassan[2,3]

[1] *Department of Materials Engineering, Technical University of Liberec, Czech Republic*

[2] *Faculty of Computing and Information Technology, King Abdulaziz University, Jeddah, Saudi Arabia*

[3] *Department of Textile Engineering, Faculty of Engineering, Mansoura University, Mansoura, Egypt*

* Corresponding author Email: eldesmo@auburn.edu

Abstract:

Fabric pilling is considered a performance and aesthetic property of the woven products that determine its quality. The subjective evaluation of the fabric pilling results in misleading values that depend on the measurement standard even for the same sample. This work utilizes some textural features extracted from the fabric's images to obtain better representative and quantitative values of the fabric's surface. An algorithm for creating features dataset for training and testing the soft-computing classifier was described where random noise was added to the limited number of fabric's pilling standard images. The objective pilling classification of the fabric samples was performed using an adaptive neuro-fuzzy system (ANFIS) which showed an ability to classify the noised standard images with a correct classification rate of 85.8%. The ANFIS was also able to classify actual fabric samples with a Spearman's coefficient of rank correlation at +0.985 when compared with the classification grades of the human operators. Results showed high efficiency of the system that is independent on the different fabric structure or color which suggests its availability to replace the currently applied subjective pilling evaluation.

1. Introduction

The quality control of the textile products is one of the major factors that determine the price, and therefore the profit, of these products. Among the important properties of fabrics are the *performance properties* which represent the response of the fabric to a certain force, exposure, or treatment. Performance properties of a fabric include the fabric strength, abrasion resistance, pilling, and color fastness. Fabric pilling is one of those properties that can be classified as performance or aesthetic properties of the fabric and, therefore, being critical phenomena for both the manufacturers and the consumers. According to the ASTM standard terminology related to textiles [1], pills can be defined as "bunches or balls of tangled fibers which are held to the surface of a fabric by one or more fibers". The fabric pilling is affected by a wide range of

parameters that may be related to: yarn parameters (e.g. twist, hairiness…etc), spinning technology (e.g. ring spinning, rotor, compact spinning…etc), fabric producing technology (e.g. weaving, knitting…etc), as well as other processing parameters [2].

Evaluating the fabric pilling during the quality control process depends in the majority of standard testing methods on accelerated fabric wear using laboratory devices that simulate the frictional mechanisms lead to surface wear and pilling formation. The available standards recommend comparing samples that gone under this accelerated wear process with standard photographs of different pilling grades where expert operators can judge the samples and assign a pilling grade to them. This results in a subjective evaluation of the fabric pilling with a great dependency on the human element. The majority of pilling standard evaluation methods assign a ranking system that ranges between 1 and 5 (where 1 is assigned to a sever pilling and 5 is assigned to no pilling). However, the existence of different standards (e.g. ASTM, SN, EN ISO,…etc) creates a lot of confusion as the same sample may be ranked with different pilling grades according to the standard that was used in the evaluation. This calls researchers for finding alternative objective evaluation methods that may help to standardize those standard methods [3].

Image analysis is a common technique in detecting textile faults [4] including their esthetic character as well as their irregularities [5]. The introduction of image analysis as a method for evaluating the fabric pilling started in the late 80's as a try to replace the applied subjective evaluation methods [6]. The application of the image processing and analysis in the evaluation of fabric pilling goes through four main stages as indicated in Figure 1 and the majority of the available literature on the topic tried to focus on one or more of these stages to modify the total outcome.

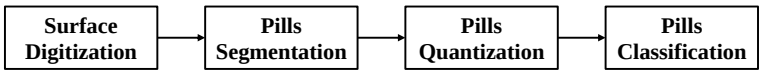

Figure 1. Stages of quantitative fabric pilling evaluation

The main four objective pilling evaluation stages can be explained as follow:

Fabric's surface digitization

The fabric surface digitization is the process of converting the fabric surface to a digital form that can be dealt with on computer systems. This process can be done using a digital scanner [7]–[11], a camera [3], [12]–[14], a light projected on camera [15], a camera attached to a microscope [16], optical triangulation topographic reconstruction of the fabric surface [17]–[19], a laser line

projected on the surface of the fabric specimen [20], or a stereovision surface reconstruction using two CCD cameras [20].

Pills detection and segmentation

Pills detection and segmentation is the process of separating the surface fuzz and pills from the complicated fabric structure background. This process was obtained using simple techniques such as the application of a binarization threshold on the fabric images [6], [20], or after processing the raw fabric images using spatial and spectral techniques. The raw image processing may include some filters for noise reduction or edge detection [10], a background dilation and erosion [13], [19], a fabric pattern detection and isolation using Fast Fourier Transform (FFT) [3], [11], [13], [14], [21] or the different techniques of wavelet transforms [8], [9], [21]–[24]. The pill detection was also performed using a template matching algorithm [14] and edge flow detection [25], [26]. For the colored images, pills were detected manually by blending the color channels of the fabric image [16].

Pills quantization

The pills quantization is the next stage after segmenting pills from the fabric image. The process focuses on extracting some features that numerically represent the pills population to allow a quantitative discrimination between the different images. The feature descriptors can be divided in two categories; one that depends on the final image of the segmented pills, and the second that utilizes the spectral decomposition and analysis that was performed during the pills segmentation. The first category of features includes simple features such as the number of pills, the total pixel area of pilling, mean area of pills, the relative area of the pills to the total surface area, the sum of the gray values of pill images, the total volume of pills, as well as the distributions of pills, their shape, orientation angle, contrast, and density or uniformity of pills spatial distribution on the fabric surface [3], [6], [7], [11], [13], [14], [16], [19], [20], [27]. The descriptor features can also be calculated from the gray-scale image of the processed surface or from the simulated fabric surface and includes roughness, skewness, as well as pills number, volume (total and average volumes), height (maximum and average), area (total and average), and fractal dimension [10], [15].

The second category of features includes the wavelet detail coefficients from the decomposition levels at the horizontal, the vertical and the diagonal orientations [24]. It can be defined also as the horizontal detailed coefficient (especially at scale close to the inter-yarn distances in the fabric) [9], as well as the energies of the reconstructed sub-images indifferent spatial orientations [22], [23]. Other statistical features can also be extracted from the wavelet decompositions such

as the range, the inter-quartile range, the variance, the standard deviation, the mean absolute deviation, the median absolute deviation, the standard error and the coefficient of variation [8].

Pills rating and classification

The classification stage is the ultimate goal of the whole process where a "successful" rating of images allows the trust in the method to replace the available subjective analysis. Classification models use the extracted set of features as inputs that can be used to generate the final rating of the image. The classification models may implement empirical and statistical methods such as the multi-variable linear regression [7], [14], [20] and discriminant analysis [8], [23], [24],or may implement artificial intelligent methods such as the application of different types of the artificial neural networks [15], [22], [28].

Based on this literature survey, three points can be highlighted:

- Although fabric wear and pilling are affecting the *texture* of the surface, there is no available publication that considers the image "textural parameters" during the pilling quantization.
- The classification methods based on artificial intelligence techniques require big databases for the system training and verification. However, the size of the dataset is limited because this dataset is based on photographs that are taken from standard images. Since the majority of standard methods utilize a rating system from 1 to 5, the standard images have a limited number that is not enough for creating a reasonable dataset size.
- There are few papers that consider the efficient techniques of each evaluation stage to create an integrated, robust, and effective evaluation process. On the other hand, the majority of these papers focus on enhancing one or more of these stages separately.

Therefore, this work tries to address these problems by:

- Considering the *texture features* of the images among the quantization parameters.
- Introducing a new method for creating sampling dataset that is large enough to suite the training and testing processes required in building the applied artificial intelligent classifier.
- Utilizing the neuro-fuzzy classification system to approach the high level of evaluation in human beings.

- Creating a user-friendly system that integrates the four evaluation stages. The system is semi-automatic in a way that classifies the pilling in the introduced sample automatically and allows the operator to change some of the detection parameters if not satisfied with the automatic detection.

2. Computation Theory:

2.1. Image preparation

The EMPA Standard (SN 198525) was used to obtain the standard images for pilling ranking. The EMPA standard has two series of photographs; the K-series for the knitted fabrics and the W-series for the woven fabrics. Among the W-series, there is the W1 category for evaluating the nonwoven fabrics while the W2 and W3 categories are used for evaluating the woven fabrics [3]. The W2 category is usually used in evaluating samples with big pill size while W3 is more suitable with samples of smaller pills. Within each category, there are four standard pictures used in the comparison and pills ranking on a scale of 1 (for the worst) to 5 (for the pill-free). To help the operators with their "fuzzy" and "subjective" evaluation, there are only four pictures for the five ranks where the first picture represents ranks 1-to-2, the second picture represents ranks 2-to-3,…etc. The standard photographs were scanned to the computer with a resolution of 600 x 600 dpi.

To generate a dataset with a suitable size out of these limited standard pictures, each standard image was duplicated many times where each copy had a random noise that was applied to it. To add noise to the pictures, different filter kernels were created with random parameters and each filter was convoluted with the picture to create a "noised" or "blurred" image. The applied filters are the "averaging", "disk", "Gaussian", "motion" filters, and the "partial spatial rearrangement". Representation of the original image and samples after the application of different noise filters are shown in Figure 2. The kernel for each filter was generated using random parameters that change each time of recalling the filter. The "partial spatial rearrangement" technique was applied by randomly selecting sub-image from the pilling region of the sample and having a size that represents 10% of the original image then placing the sub-image in a random way at a different position of the image.

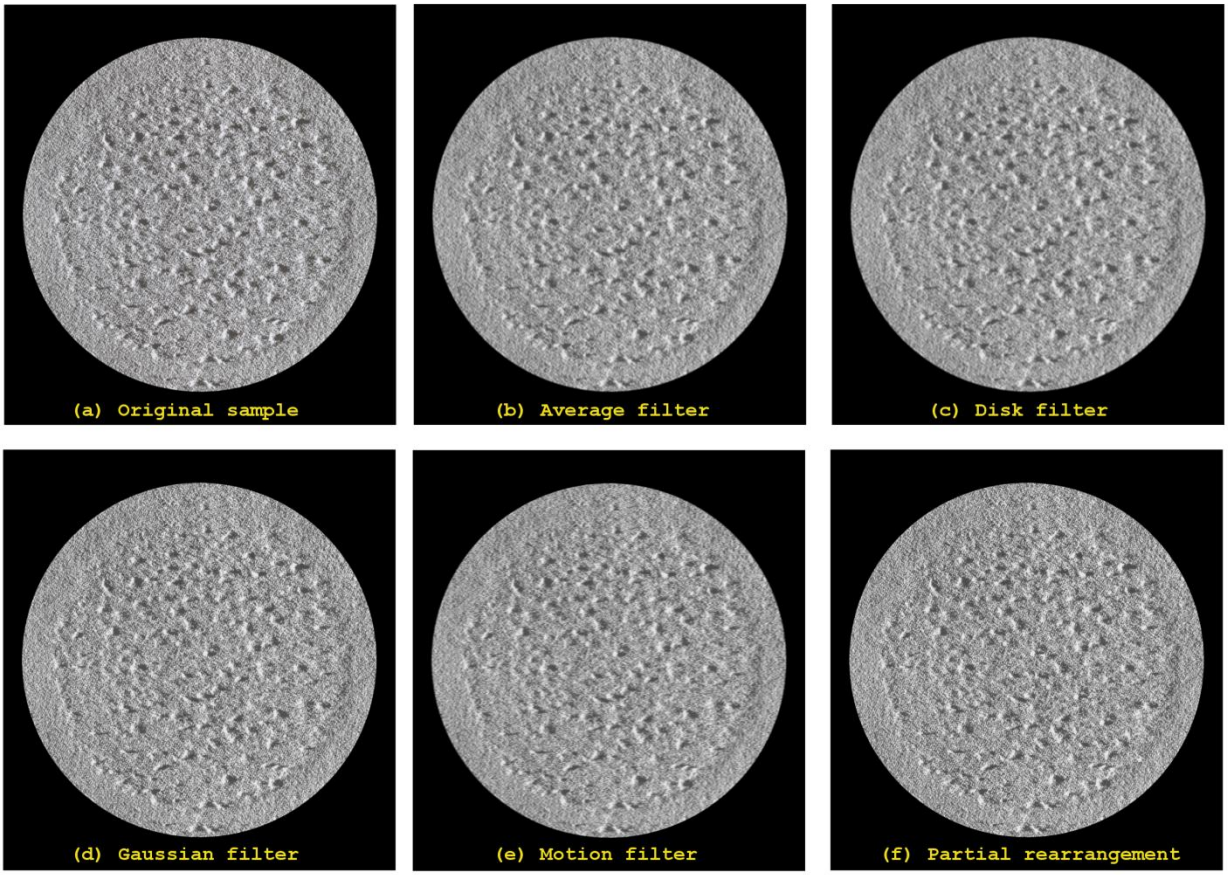

Figure 2. Examples for different shapes of the same fabric sample after applying random filters

These five types of noise generators were applied three times using random parameters to each standard picture which creates 15 noised copies of the original image. To avoid the system bias to the noised images, the features extracted from the original image were duplicated 35 times to create a features dataset with 30% representation of the noised images. The features dataset consists of the previously mentioned 4 features with 200 observations (50 observations for each standard image) of each standard category (W1, W2, and W3). The features dataset was then split randomly into a training dataset that represents 80% and a testing dataset that represents the remaining 20% of the data. The introduction of the noised images during the training of the classification system makes it more robust to classify different samples even with noised pictures.

2.2. Textural features

The basic statistics that are utilized in pilling quantization (the first order statistical features) extract data out of the gray-scale levels of the pixels in the digital image and does not reflect these surface features. On the other hand, the second order and textural features are more concerned about the spatial distribution of the gray-scale levels which reflects the roughness of the image and its texture. This gives the advantage of being close to the human awareness of the texture that describe surfaces as fine, coarse, smooth, rippled, irregular,...etc.

For an image with x and y representing the spatial coordinates, the gray-scale levels of that image can be expressed as $\boldsymbol{P}(x,y)$ and its gray level co-occurrence matrix (GLCM) can be calculated to determine the textural features of the image. The GLCM represents the joint probability density of the pairs of the gray levels occur at pairs of points separated by the vector $\boldsymbol{\delta}(\Delta x, \Delta y)$ [29]. The displacements Δx and Δy in the vector $\boldsymbol{\delta}$ determine the length (the running distance d) and the angel (direction θ) between the points of the required calculation. The calculated joint density takes the matrix form $\boldsymbol{C_\delta}$ with a size NxN where N is the maximum value of gray levels in the original image $\boldsymbol{P}$ and the value $\boldsymbol{C_\delta}(i,j)$ represents the probability of the pair of gray levels (i,j) occurring at separation $\boldsymbol{\delta}$. To illustrate the calculation of the GLCM, consider the example shown in Figure 3 for an image $\boldsymbol{P}(x,y)$ with N=4 gray levels values that range between 0 and 3. Therefore, the size of the co-occurrence matrix $\boldsymbol{C}$ is 4x4 and for a separation vector $\boldsymbol{\delta}(1,0)$ the entries $\boldsymbol{C_\delta}(i,j)$ are the number of times gray level i occur immediately (*i.e.* one pixel distance) to the left (*i.e.* in zero angel direction) of the gray level j.

Once the co-occurrence matrix was calculated the image texture can be analyzed based on the given parameters (d,θ) of the vector $\boldsymbol{\delta}$. If the image's texture is coarse and the displacement d is smaller than the size of the texture element, the pairs of points at separation $\boldsymbol{\delta}$ should have similar gray levels. Therefore, the high values in the co-occurrence matrix $\boldsymbol{C_\delta}$ should be concentrated at the main diagonal or its nearby. Similarly, for fine textured images with texture elements comparable in size to the separation $\boldsymbol{\delta}$, the values in $\boldsymbol{C_\delta}$ will be spread out. The same logic applies for the texture direction that might be directed to a certain angel and, therefore, the spread of the values about the main diagonal of $\boldsymbol{C_\delta}$ will depend on the selected angel (θ) of the vector $\boldsymbol{\delta}$. Therefore, an investigation of the image texture is required at different displacements (d) and directions (θ) then the scattering of values around the $\boldsymbol{C_\delta}$'s main diagonal should be measured.

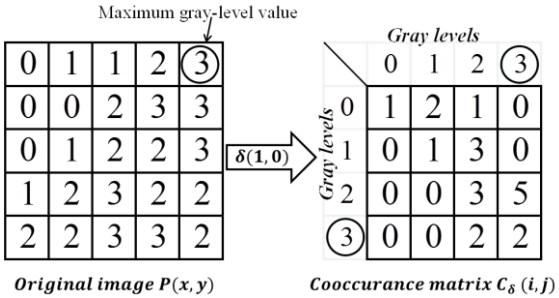

Figure 3. Demonstration for the construction of the GLCM for an image P(x,y)

To measure the spread of values in the co-occurrence matrix Haralick *et al* [30] suggested different features that represent the texture information of the image. The calculation of these features starts usually with the normalization of the matrix $\boldsymbol{C}$ by its total sum:

$$D_\delta(i,j) = \frac{C_\delta(i,j)}{\sum_{k=1}^{N}\sum_{l=1}^{N} C_\delta(k,l)}$$

Where *i*, *j*, *k*, and *l* are indices and $\boldsymbol{D_\delta}$ is the normalized matrix at a certain direction δ.

Among the features suggested by Haralick, four features were found to be more effective and will be tested in this study. These features are:

Contrast:

$$f_{1,\delta} = \sum_{i=1}^{N}\sum_{j=1}^{N}(i-j)^2 D_\delta(i,j)$$

The contrast is also known as the "*variance*", and the "*inertia*" and it is taken as a texture feature because it represents the moment of inertia of the matrix $\boldsymbol{D_\delta}$ around its main diagonal and it is a measure of the degree of its spread of values.

Correlation:

$$f_{2,\delta} = \sum_{i=1}^{N}\sum_{j=1}^{N}\frac{ijD_\delta(i,j) - \mu_i\mu_j}{\sigma_i\sigma_j}$$

Where μ_i, and σ_i are the mean and standard deviation, respectively, of the row sums and μ_j, and σ_j are the mean and standard deviation, respectively, of the column sums of the matrix $\boldsymbol{D_\delta}$. The correlation is a measure of the degree to which the rows (or columns) of the GLCM resemble each other and this value should be high when values are uniformly distributed in the matrix and low when the values off the diagonal are small.

Angular second moment (ASM):

$$f_{3,\delta} = \sum_{i=1}^{N}\sum_{j=1}^{N} D_\delta(i,j)^2$$

The angular second moment (ASM) is also known with different names such as the "*energy*", the "*uniformity*", and the "*uniformity of energy*". This value is small when $\boldsymbol{D_\delta(i,j)}$ are close in values and it increases when values largely varied as in the situation where values are clustered near the main diagonal.

Inverse difference moment (IDM):

$$f_{4,\delta} = \sum_{i=1}^{N}\sum_{j=1}^{N} \frac{D_\delta(i,j)}{1+(i-j)^2}$$

The inverse difference moment (IDM) can also be called the *homogeneity* and it measures the closeness of the distribution of elements in the GLCM to its diagonal and it reaches 1 for a diagonal matrix.

2.3. Adaptive Neuro-Fuzzy System

Fuzzy inference systems are useful in mapping data between two spaces while some degree of uncertainty is involved. The fuzzy system implements the membership functions, instead of the crisp-set functions, to imitate the human thinking and cognition without employing precise quantitative analyses [31]. This provides the opportunity to deal with imprecision and to represent the linguistic qualitative words such as "many", "low", "few"…etc. However, creating such fuzzy systems requires some understanding of the rules that govern the relations between the inputs and the outputs. Therefore, the adaptive neuro-fuzzy inference systems (ANFIS) were introduced to combine the natural language description of fuzzy systems and the learning properties of neural-networks. By using a hybrid learning algorithm, the ANFIS can construct an input-output mapping based on both human knowledge (in the form of fuzzy *if-then* rules) and stipulated input-output data pairs [31].

The initial model of the ANFIS was proposed by Jang [31], [32] who explained it using two inputs (x_1, x_2) and built the rule based system using two *if-then* rules, although the system can be generalized to any *N* number of inputs or *M* rules. The model with two inputs is demonstrated in Figure 4 with five layers that include two *adaptive* layers (layer #1 and layer #4, demonstrated by rectangles) and three *fixed* layers (layer #2, layer #3, and layer #5, demonstrated by circles). The two adaptive layers are distributed between the *premise* part, and the *consequent* part which

are the two basic components of all *logical statements*. The positioning of the adaptive layers at these two parts allows the adjustment of their parameters and consequently adjusting the performance of the whole system.

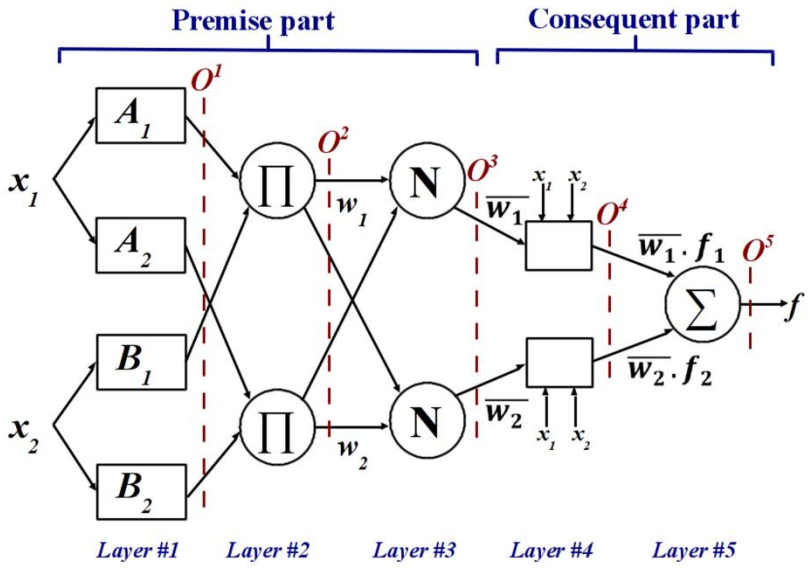

Figure 4. The ANFIS model

The two rules of Takagi and Sugeno were applied as:

Rule 1: If x_1 is A_1 and x_2 is B_1, then $f_1 = p_1x_1 + q_1 x_2 + r_1$

Rule 2: If x_1 is A_2 and x_2 is B_2, then $f_2 = p_2x_1 + q_2 x_2 + r_2$

The output of the k^{th} layer can be expressed with the vector O^k which can be stated for the first layer O^1 in the form:

$$O_i^1 = \begin{cases} \mu_{A_i}(x_1) \\ \mu_{B_i}(x_2) \end{cases}$$

Where μ_{A_i} and μ_{B_i} are the membership functions (MF) for the first and the second inputs, respectively. The membership function can take different shapes of any continuous and piecewise differentiable functions. The selected MF in this case is the Gaussian (bell shape) function with normalized output $\in [0,1]$ which can be written for the first input (x_1) in the following form (and a similar relation can be found for the second input):

$$\mu_{A_i}(x_1) = e^{-\left(\frac{x_1 - a_i}{b_i}\right)^2}$$

Where; the parameters {a_i and b_i} determine the shape and behavior of the membership function. These parameters will be called the *premise parameters* as they are the adjustable parameters in the premise part.

The neuron elements of the second layer are fixed with simple multiplication transfer function. The output of each neuron represents the *firing strength* of the rule. The output vector of this layer (O^2) can be calculated as:

$$O_i^2 = w_i = \mu_{A_i}(x_1).\mu_{B_i}(x_2)$$

The third layer is a fixed layer with the role of normalizing its inputs to produce the *normalized firing strength* which is the ratio of the firing strength of the i^{th} rule to the sum of the firing strength for all rules, that is:

$$O_i^3 = \overline{w_i} = \frac{w_i}{\sum_{j=1}^{N} w_j} = \frac{w_i}{w_1 + w_2}$$

Where, N is the number of the system inputs.

The fourth layer is the adaptive layer that multiplies the normalized firing strength by a first order polynomial for the first order Takagi and Sugeno model. The output vector of this layer O^4 can be expressed as:

$$O_i^4 = \overline{w_i} f_i = \overline{w_i}(p_i x_1 + q_i x_2 \ + \ r_i)$$

Where, the parameters {p_i, q_i, and r_i} are adjustable and can be used to tune the outputs of that layer. These parameters will be called the *consequent parameters* as they tune the output of the consequent part of the system.

The fifth layer has a single fixed neuron that sums up its inputs and produces the final result (f) of the system that can be represented as:

$$O_i^5 = f = \sum_{i=1}^{N} \overline{w_i} f_i = \frac{\sum_{i=1}^{N} w_i f_i}{\sum_{i=1}^{N} w_i}$$

2.4. Hybrid learning algorithm for the ANFIS

The goal of the learning of the ANFIS is to adjust all the tunable system parameters which includes both the premise parameters {a_i and b_i} and the consequent parameters {p_i, q_i, and r_i} to minimize the overall system's error. The hybrid learning algorithm utilizes two passes; the forward pass with fixed premise parameters and the backward pass with fixed consequent

parameters. To explain that, consider the forward pass with fixed premise parameters which results in an output that can be defined for the given two inputs ANFIS as:

$$f = \overline{w_1} f_1 + \overline{w_1} f_1 = \overline{w_1}(p_1 x_1 + q_1 x_2 + r_1) + \overline{w_2}(p_2 x_1 + q_2 x_2 + r_2)$$

That can be rearranged to:

$$f = (\overline{w_1} x_1) p_1 + (\overline{w_1} x_2) q_1 + (\overline{w_1}) r_1$$
$$+ (\overline{w_2} x_1) p_2 + (\overline{w_2} x_2) q_2 + (\overline{w_2}) r_2$$

It can be noticed from this equation that it represents a linear combination of the consequent parameters { p_1, q_1, r_1, p_2, q_2, and r_2 }. The least square method can be utilized to calculate those parameters. Therefore, the signal goes in the forward pass along the system until layer #4 then the least square method can be applied to allocate the consequent parameters and the whole system can be identified. The error rate of the system can be calculated after the system identification. The backward pass starts with fixing the consequent parameters and propagating the error rate backward through the system and the premise parameters {a_i and b_i} can be updated by the gradient descent method. This cycle continues until the desired performance is achieved as illustrated in Figure 5.

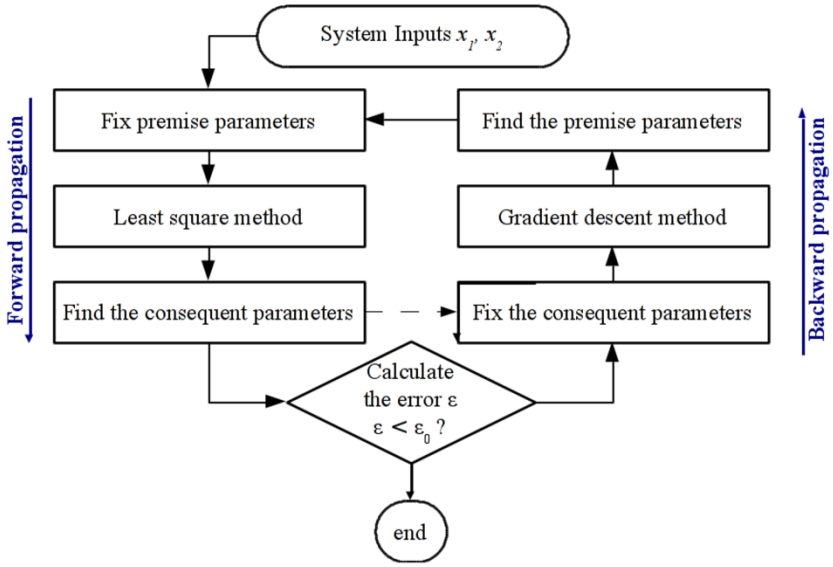

Figure 5. Hybrid ANFIS learning algorithm

3. Experimental Setup

Seven woven fabrics with different structures and colors are used and the specifications of these samples are listed in Table 1. To test the system ability in detecting the fabric pilling regardless

of the color shade, the tested samples were selected to have different colors. Samples were tested on Martindale instrument for pilling where two circular specimens of 140 mm diameters from each sample were placed on the machine head. The face of the lower specimen is up and the specimen is placed on the top of a standard felt of 140 mm diameter. The upper specimen is mounted on a holder of 90 mm diameter with a standard felt of the same size and fixed to the holder with an elastic ring. The upper holder is installed on the machine where the faces of the upper and lower specimens are in contact to each other. The samples were tested under 6.5 cN/cm^2 pressure for 10,000 cycles of Lissajous figure with 24 mm stroke.

Table 1. Tested knitted sample specifications

	Color	**Structure**	**Weight/Area (g/m^2)**	**Warp Density (threads/inch)**	**Weft Density (threads/inch)**	**Warp Count (tex)**	**Weft Count (tex)**
W1	White	1/6	128	71	70	21	21
W2	White	1/1	155	63	60	30	31
W3	Bright White	1/1	121	81	51	19	26
W4	Blue	1/3	145	86	56	21	32
W5	Blue	2/4	157	87	64	22	29
W6	Light Blue	1/3	167	88	55	21	38
W7	Paige	1/2	182	89	79	24	25

The measured samples were evaluated visually by seven different operators against the photographs of the EMPA Standards (SN 198525). The measured samples were then digitized using the setup shown in Figure 6 and processed using the developed software algorithm to obtain the pilling classes. The image acquisition system consists of a digital CCD camera that is equipped with a macro lenses to capture the sample surface details. The captured image resolution of 300 dpi and the image dimensions was 2048x1536 pixels. Lighting is critical for the imaging system and two light sources that equally distribute the light on the surface of the fabric were applied. The sample was tilted with a slight angel to the horizontal plane to allow contrasting the pills with their shadow.

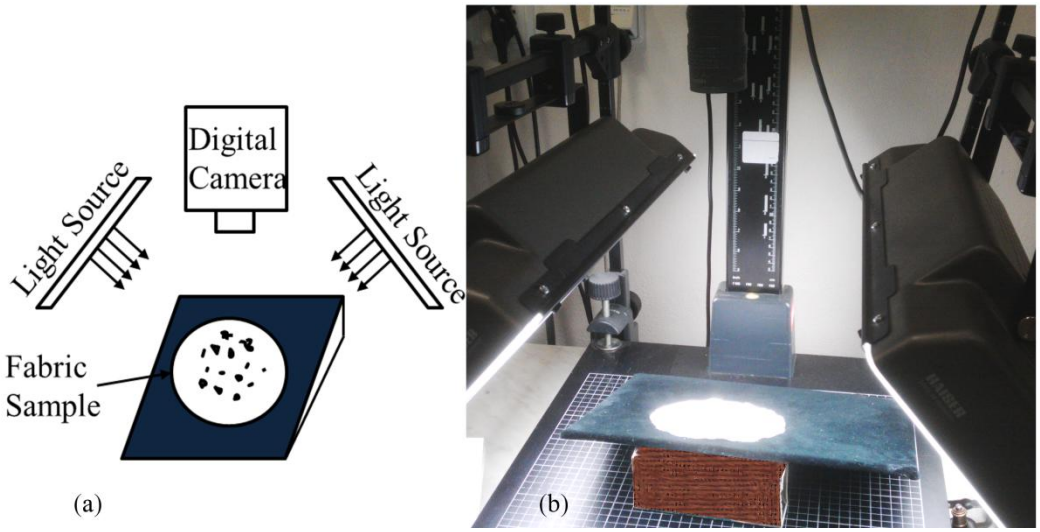

Figure 6. Image acquisition setup depicted schematically in (a) and photographed in (b)

4. Results and discussion:

Pre-investigation for the effective choice of the vector δ was performed by applying a distance sweep in the range of d = 0 to 50 with a step of one pixel. For long range investigations, another distance sweep in the range of 5 to 200 with a step of 5 pixels was also performed. In each case of the evaluation (the short term and the long term), a direction sweep was performed at four angles θ = 0°, 45°, 90°, and 135°. Results of the four extracted features for the short and long term distance sweeps are shown in Figure 7 to Figure 14 for the first sample of each standard category (i.e. W1_1-2, W2_1-2, and W3_1-2).

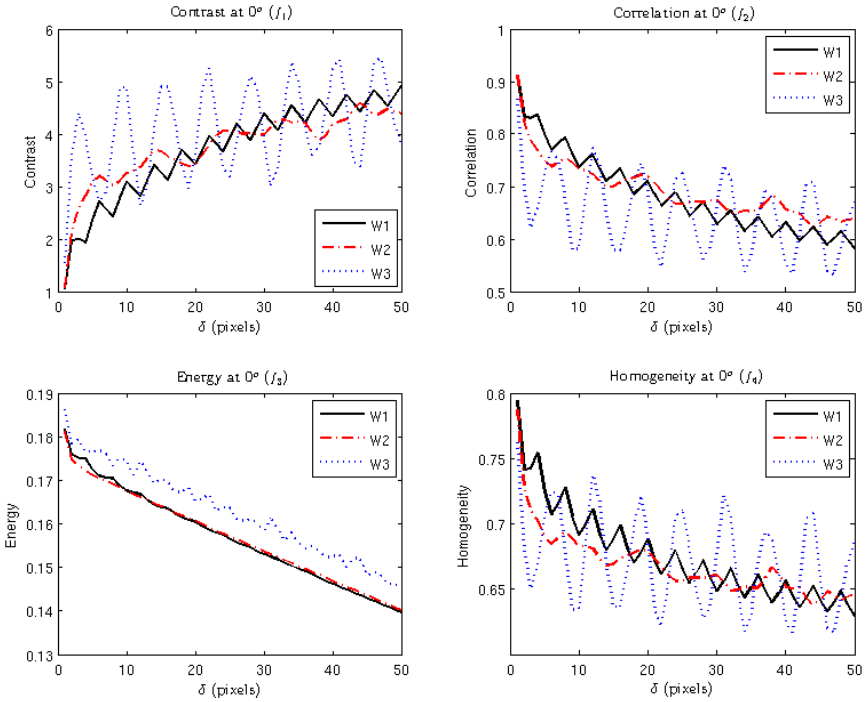

Figure 7. Features of the three categories at an angle of 0˚ and short term distance

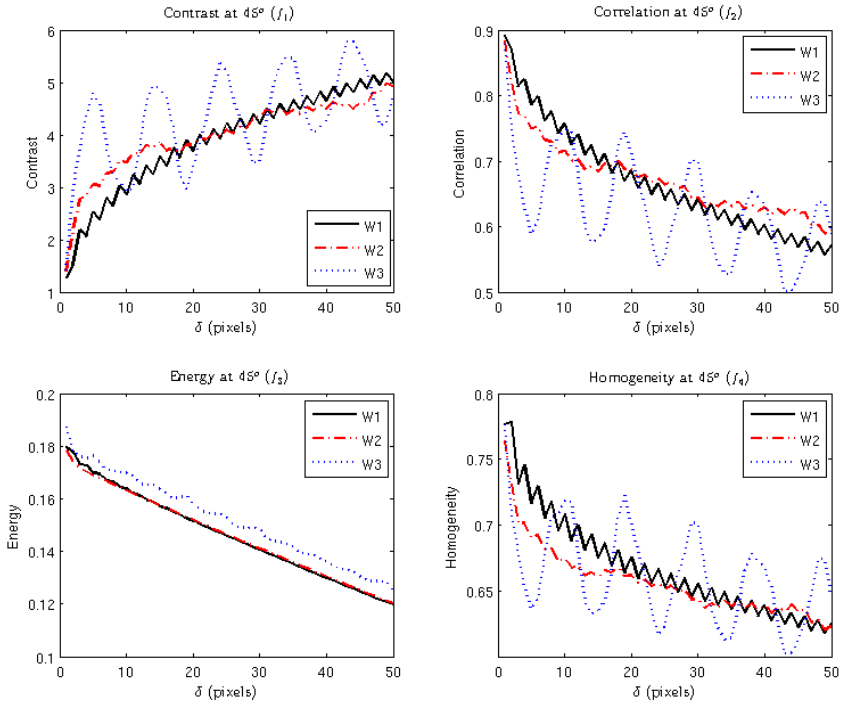

Figure 8. Features of the three categories at an angle of 45˚ and short term distance

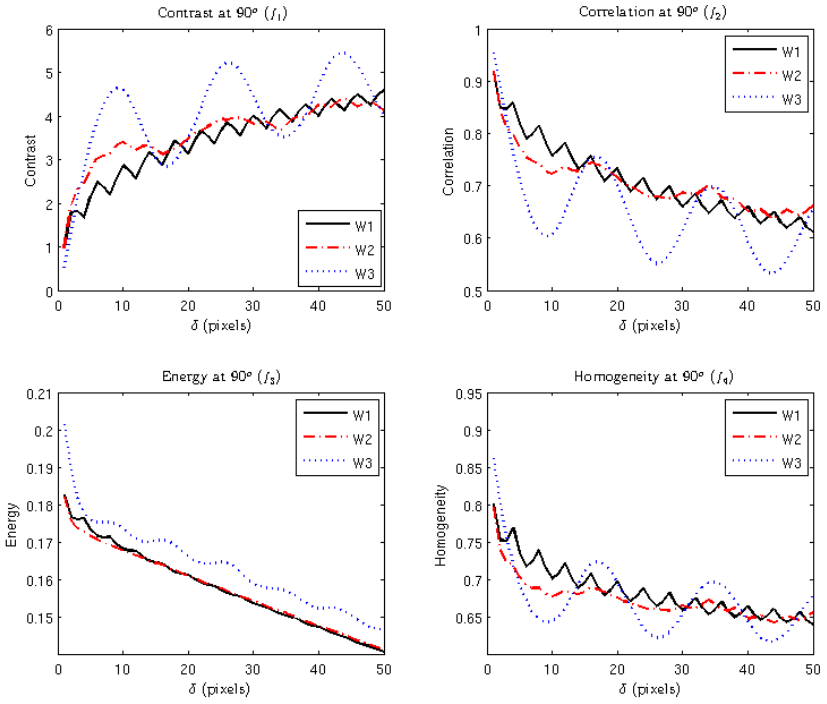

Figure 9. Features of the three categories at an angle of 90˚ and short term distance

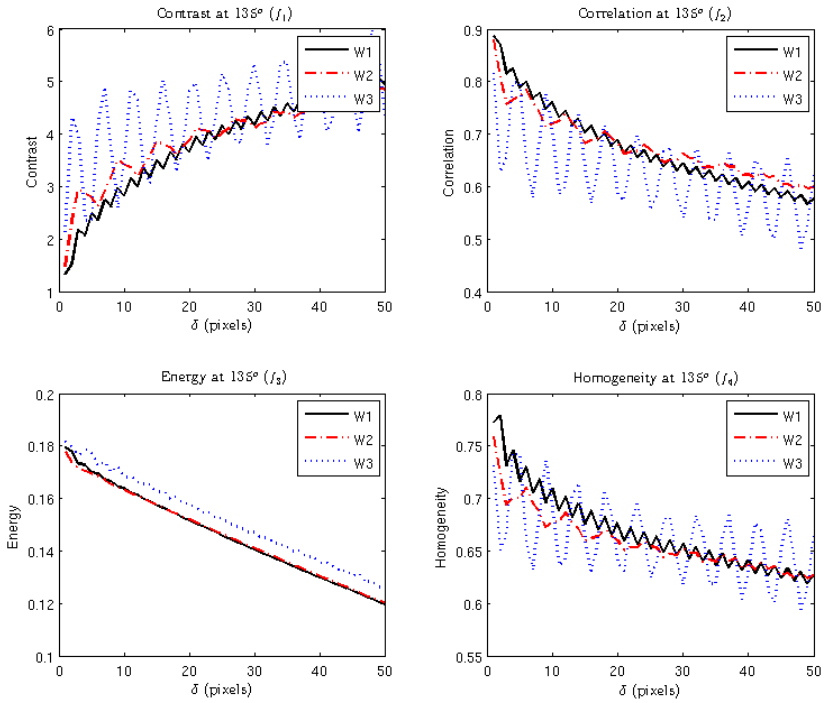

Figure 10. Features of the three categories at an angle of 135˚ and short term distance

Table 2. Features periodicity at short distance (values in pixels)

		f_1	f_2	f_3	f_4
Zero	W1	4	4	-	4
	W2	9*	-	-	9
	W3	6.5	6.5	-	6
45°	W1	4	4	-	4
	W2	9	9	-	9*
	W3	6	6	-	6
90°	W1	4	4	-	4
	W2	15	15*	-	9*
	W3	17	17	-	17
135°	W1	2	2	-	2
	W2	6.5	6.5	-	7
	W3	5	5	-	5

* Low correlation was observed at these values

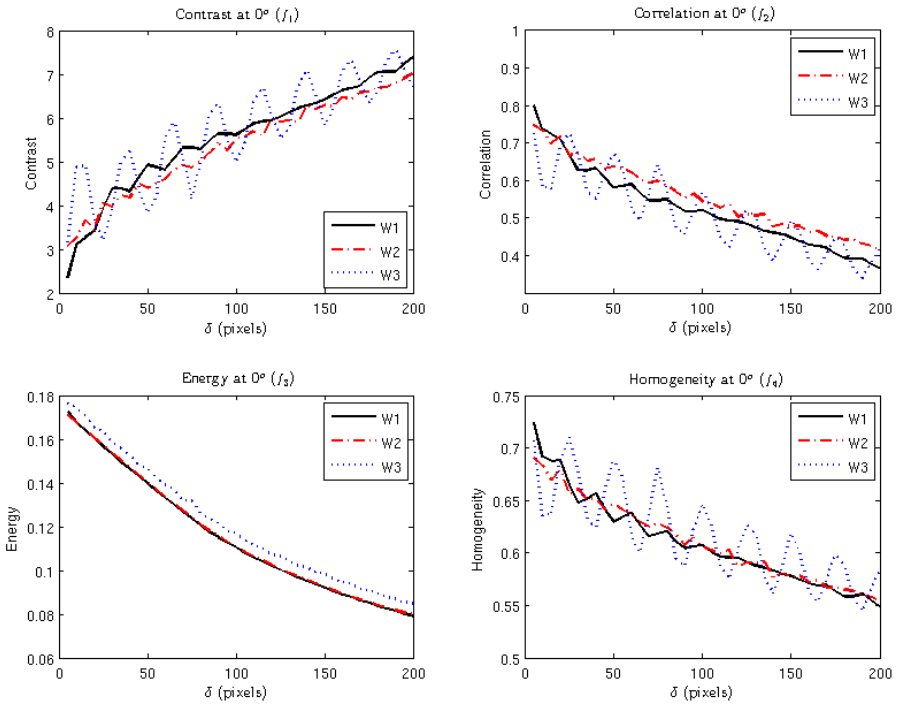

Figure 11. Features of the three categories at an angle of 0° and long term distance

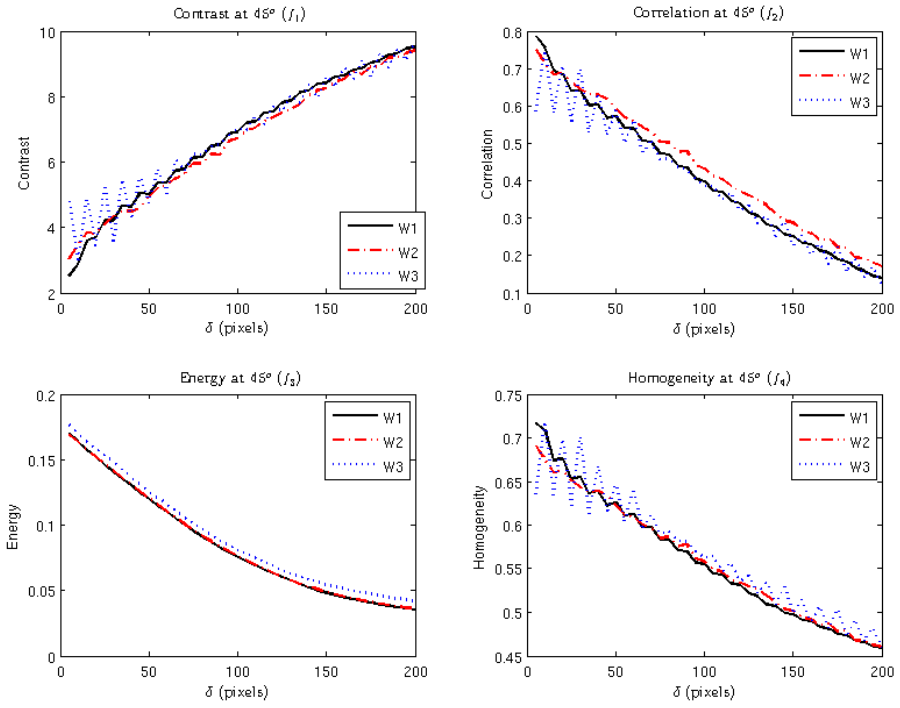

Figure 12. Features of the three categories at an angle of 45˚ and short term distance

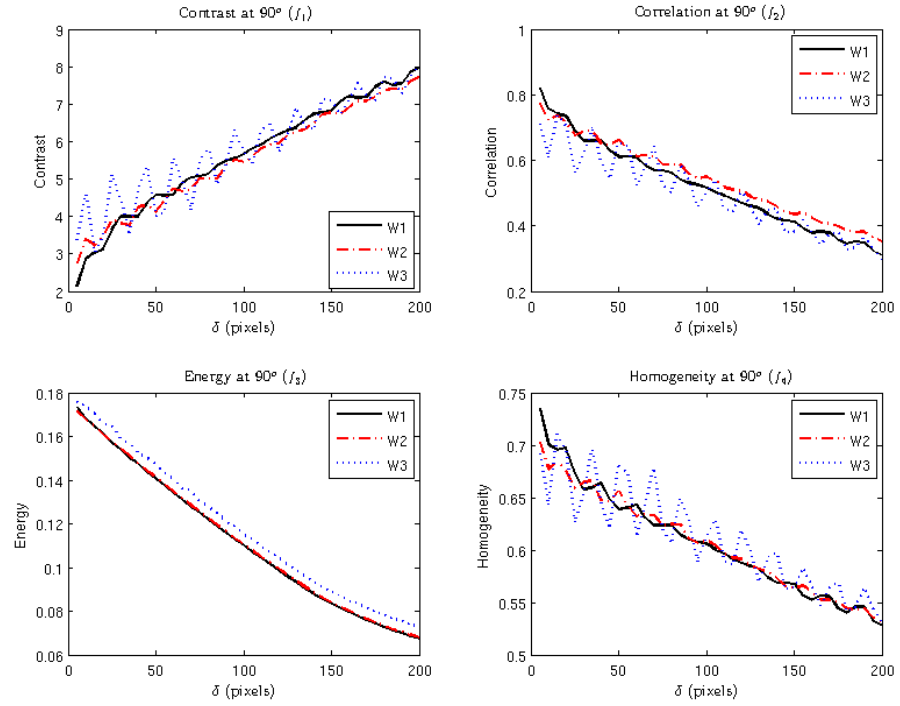

Figure 13. Features of the three categories at an angle of 90˚ and short term distance

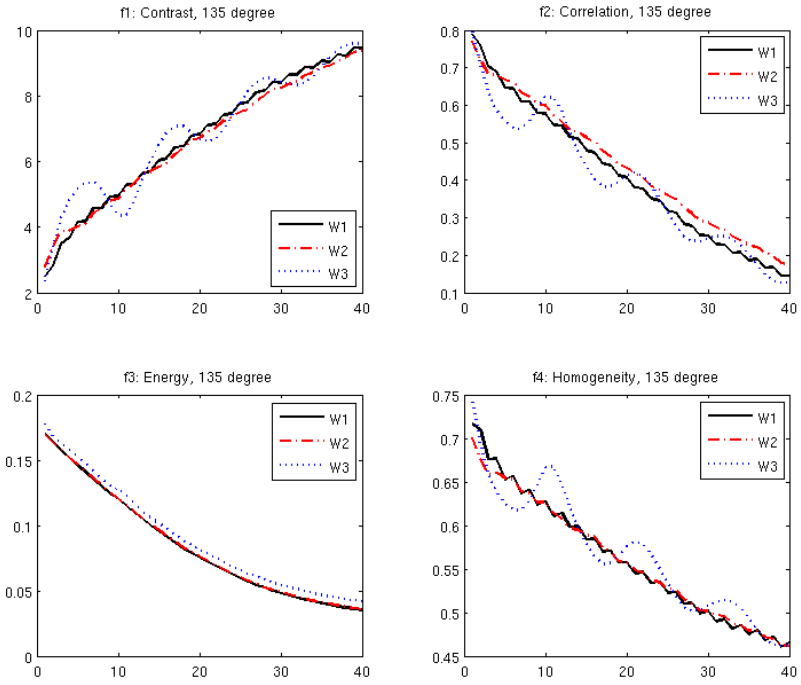

Figure 14. Features of the three categories at an angle of 135˚ and short term distance

Table 3. Features periodicity at long distance (values in pixels)

		f_1	f_2	f_3	f_4
Zero	W1	20	20	-	20
	W2	10	10	-	10
	W3	25	25	-	25
45˚	W1	-	10	-	10
	W2	-	25	-	25
	W3	10	10	-	10
90˚	W1	20	20	-	20
	W2	15	15	-	15
	W3	20	20	-	20
135˚	W1	10	10	-	10
	W2	-	-	-	-
	W3	55	55	-	55

From these figures some general notes can be observed on the fabric surface and its textural features:

- The behavior of the contrast feature (f_1) increases with increasing the calculation distance (δ) which is different from the other three features that decrease with distance.
- There is a form of periodicity in the behavior of most features, although this periodicity is not dominant in the energy feature (f_3) compared to the other features.
- The periodicity of the features can be considered as an indicator of the repeatability of objects on the fabric's surface at a certain distance. For example, by examining features f_1, f_2, f_4 at an angle of zero in Figure 7, a cyclic pattern can be observed with repeats of 4 pixels in category W1, 9 pixels in category W2, and 6 pixels in category W3. This indicates a repeatability of objects at these distances which might imply the repeatable pattern of the woven structure.
- The periodicity of features shown in Figure 7 to Figure 10 at short distances is summarized in Table 2 while the periodicity of the long distances shown in Figure 11 to Figure 14 is summarized in Table 3. Some features show periodicity although it might not be strong in some cases which were highlighted in the table with “low” and with the periodic interval, when available.
- Periodicity interval is almost constant when obtained from different features for the same fabric image.
- There is a small effect of the calculation angle on the periodicity of the features where similar intervals can be observed at different angles. The cases where a difference can be observed for the feature at different angles (e.g. f_1 at the angles 0° and 90°) might be attributed to the different warp and weft densities in the image.
- The repeat for a feature as observed at long distances is a multiplier of the repeat value for the same feature at short distance. For example the repeat of f_1 at 0° for W1 is 4 pixels (Table 2) while this value is 20 pixels (Table 3) when measured at long distance. This can be attributed to the different step size of evaluation during the short distance (1 pixel) and the long distance (5 pixels).
- Features that repeat at short distances were found to diminish after certain distance. For instance, the feature f_1 at 45° for W3 is found to have a strong repeating wave as observed in Figure 8 while this wave diminishes at long distances as shown in Figure 12. This

indicates the lack of correlation between the textural objects on the fabric's surface at long distances.

On the other hand, the change of the features at different directions at short distances is shown in Figure 15. There is a high similarity of the features' general trend at different angles with a coincidence allocation of the peaks at certain distances. The strength of the repeatable peak is decaying with distance and there is no significant repeatable behavior observed at longer distances (up to 200 pixels). The frequency of the peaks at 90° is almost double the frequency at 0° while a similar high frequency can be found at the angles 45° and 135°.

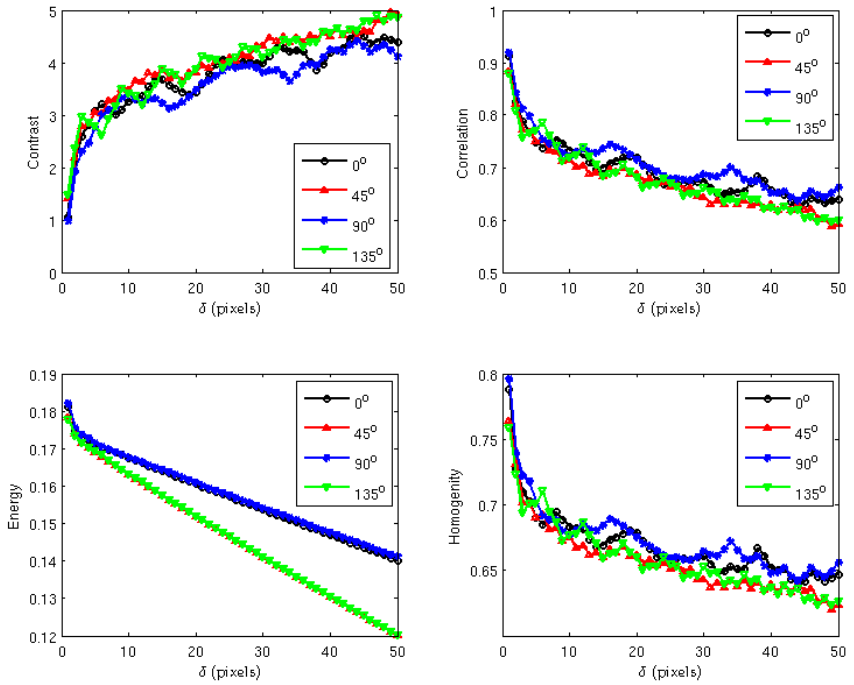

Figure 15. Features as calculated at different angles for sample W2_1-2

According to this pre-investigation, the actual samples are evaluated at an angle of 45° which should be a reasonable step that will coincide with angles of 0°, 90°, and 135° as indicated in the previously discussed figure. Features are also evaluated at a range of distance that covers the periods of peak maxima of the different features of the three categories. Based on the repeatability values listed in Table 2, the features are calculated in the distance interval from 4 to 10 pixels then values are summed up to be used as the characteristic features of the image during its evaluation. Also, due to the behavior similarity for the features, only the contrast and the correlation are used during the evaluation. These features are selected because they have a repeatable behavior and opposite trends. The other two features for evaluating the fabric pilling will be the number of pills and their relative area which is calculated as ratio between the pills area and the total area of interest in the studied sample.

Based on the described algorithm, an adaptive neruo-fuzzy system was constructed as shown in Figure 16 where the first adaptive layer consists of 3 neurons (3 membership functions) for each input. The premise parameters of this layer were calculated and the adjusted membership functions for the four inputs are shown in Figure 17. The multiplication and normalization were performed in the rule layer which is highlighted in Figure 16 with the blue color. The second adaptive layer is also shown in the same figure where the Takagi and Sugeno model applies and the consequent parameters are evaluated.

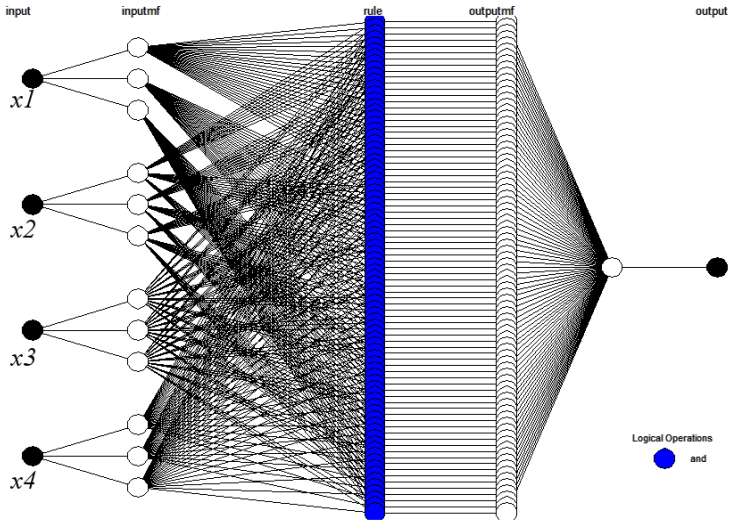

Figure 16. The ANFIS architecture for the given four inputs

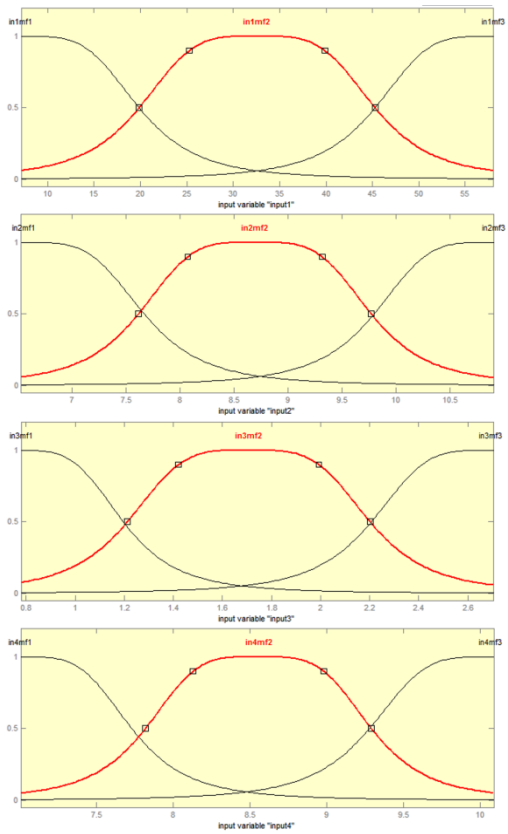

Figure 17. The adjusted membership functions for the four inputs (each input has two MFs)

The application of the ANFIS system is demonstrated in Figure 18 which includes the five basic steps of the calculation. The system starts with the *fuzzification* of the inputs where each input is processed in parallel through the membership functions. Second, the rules are applied using the *fuzzy operator* (AND) which results in the weighted firing strength to the third part of the *implication* and transfers data from the premise to the consequent. The fourth step is defined by the *aggregation* of the consequents across the rules and the final step is the *defuzzification* of the results to produce the final output.

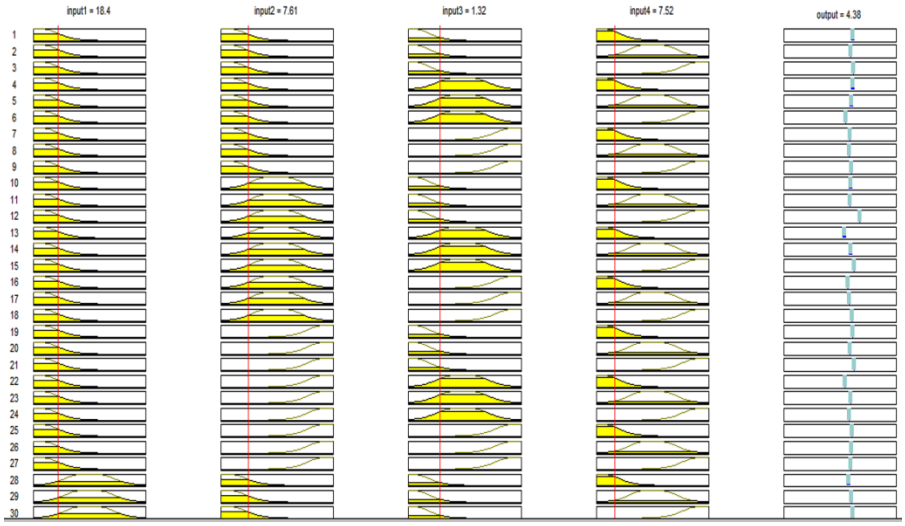

Figure 18. The application of the ANFIS

The given ANFIS structure was trained with the contrast, correlation, number of pills, and their relative areas as inputs and the standard pilling grades or ranks (1, 2, 3, 4 or 5) as outputs. The performance of the ANFIS systems is shown in Figure 19. For the 120 samples presented to the ANFIS systems, it can be seen that the ANFIS performed 85.8% in determining the pilling grade. Also, from these figures it can be observed that most of the samples that were miss-graded were deviated from the target class with only one degree which is acceptable in classifying such samples where the standards give two grades in the same picture.

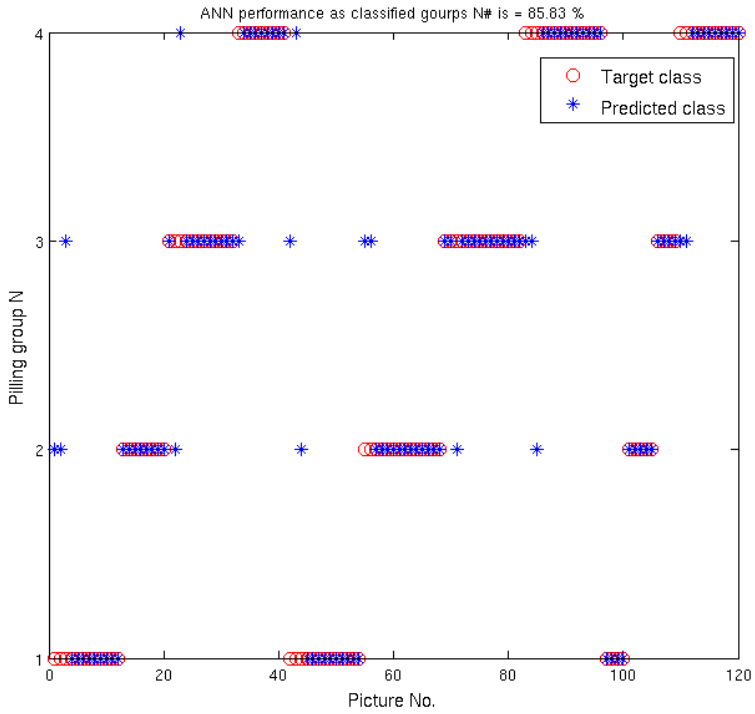

Figure 19. Performance of the ANFIS for the Nth grade

Although the relatively high performance of the ANFIS in detecting the correct pilling of the noised standard images, it is important to test the system on real fabric samples. Therefore, the developed algorithm was coded in a user-friendly graphical user interface (GUI) that is shown in Figure 20. The woven samples were introduced to seven human operators after their pilling test on Martindale to compare the samples with the standard pictures. The operators subjectively assigned a pilling rank for each sample as shown in Table 4 and the total pilling evaluation of the sample was calculated by the mode of the operator's ranks. The pictures of the woven samples were also introduced to the developed program that utilizes the ANFIS to rank the samples. The samples' pilling rank is listed in Table 4 and the Spearman's coefficient of rank correlation between the two categories of the human evaluation and the ANFIS evaluation is +0.982 which implies a good agreement between the two sets of results and a reliability of the system to be used in replacing the subjective evaluation of human operators.

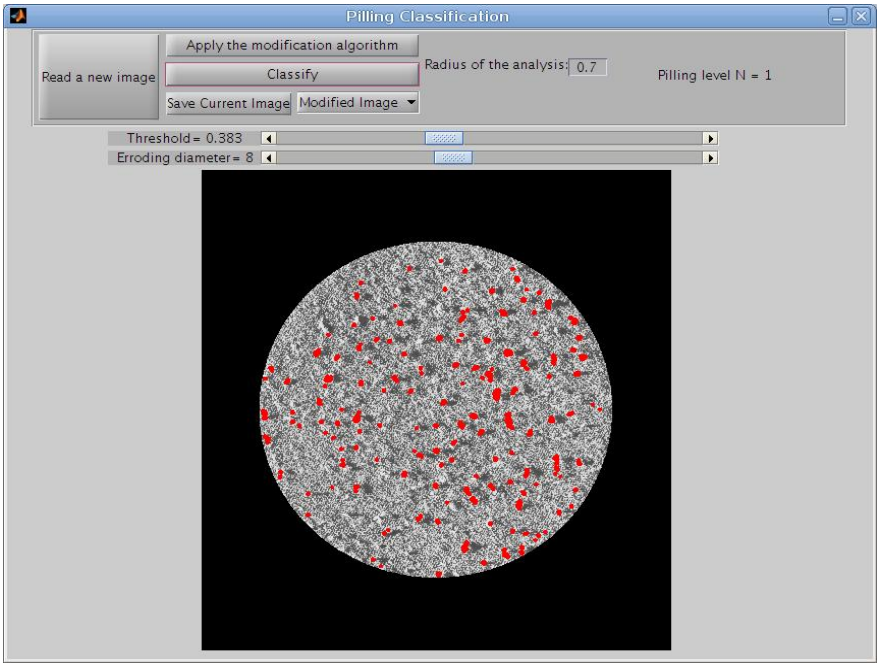

Figure 20. GUI of the developed software for fabric's pilling evaluation

Table 4. Human operators as compared to the ANFIS pilling evaluation

	OP.#1	OP.#2	OP.#3	OP.#4	OP.#5	OP.#6	OP.#7	Operators' evaluation	ANFIS evaluation
W1	3	3	1	2	2	2	2	2	2
W2	4	4	4	4	4	3	4	4	4
W3	3	2	2	1	4	2	2	2	2
W4	2	3	2	3	3	1	2	2	3
W5	2	1	1	1	3	2	1	1	1
W6	4	5	4	4	4	5	4	4	4
W7	3	3	3	3	4	2	5	3	3

Conclusion

This work introduces for the first time, to the best of the authors' knowledge, fabric's *image textural features* as measures for the fabric surface during the quantitative evaluation of pilling in woven fabrics. Creating a feature dataset from the available Standard images with enough size for training soft computing algorithms is challenging due to the limited number of those Standard images. To deal with this issue, a new approach was suggested to mimic the noise that interferes with the fabric surface during its digitization. Hence, a user-friendly pilling evaluation system

that integrates the processes of fabric surface digitization, pilling segmentation, quantization, and classification was implemented in this work. The system was able to classify woven fabric samples according to their surface texture with a high degree of correlation to the traditional methods of pilling evaluation.

Results of textural features show a trend similarity between the features which allows the reduction of the number of these features during the evaluation (contrast and correlation were only used in the final code). Selection of few features was not only to prevent redundancy in the system's inputs, but also to allow other pilling descriptors (such as the number of pills and their relative area) that represent pilling intensity to be considered. Taking more pilling descriptors into account during the pilling quantization might be useful; however the computational resources required for the ANFIS classifier increases exponentially with the increase in number of the system's inputs. This applies a constraint on the number of pilling descriptors that can be simultaneously used during the ANFIS classification which results in a "features optimization problem" due to the need of features that represent both the image texture as well as the pilling intensity quantifiers. A major part of the figures in the results section presented in this work was dedicated to investigate the texture features at different conditions and optimize their selection.

The application of random noise filters on the Standard images significantly affects the textural features while keeping a small effect on the pilling intensity features. The parameters of the applied filters were randomly selected; however the range of these parameters should extend to apply more "aggressive" noise to the pictures to allow the robustness of the system to deal with fabric images of different structures and textures. Also, more noise filters might be required to better resemble the image defects that might occur during the image acquisition, although the current filters were useful in increasing the amount of sampling datasets.

Success in digitizing the Standard samples in the same systematic fashion of real samples (rather than scanning Standard images) should increase the reliability of the suggested system and allows it to be standardized as a quantitative method that replaces the current subjective evaluation Standards. The relatively good results of the suggested system are promising for the methodology extension to cover fabrics that are produced using different technologies (knitted and nonwoven fabrics) as well as fabrics of different structures.

References

[1] D. Committee, "ASTM D123 - 13a Standard Terminology Relating to Textiles," *ASTM*. 2003.

[2] S. L. Paek, "Pilling, Abrasion, and Tensile Properties of Fabrics from Open-End and Ring Spun Yarns 1," *Text. Res. J.*, vol. 59, no. 10, pp. 577–583, 1989.

[3] B. K. Behera and T. E. M. Mohan, "Objective measurement of pilling by image processing technique," *Int. J. Cloth. Sci. Technol.*, vol. 17, no. 5, pp. 279–291, 2005.

[4] M. Eldessouki, M. Hassan, K. Qashqary, and E. Shady, "The Application of Principal Component Analysis to Boost The Performance of The Automated Fabric Fault Detector And Classifier," *FIBRES Text. East. Eur.*, vol. 22, no. 4(106), pp. 51–57, 2014.

[5] M. Eldessouki, S. Ibrahim, and J. Militky, "A Dynamic and Robust Image Processing Based Method for Measuring Yarn Diameter and Its Variation," *Text. Res. J.*, vol. 84, no. 18, pp. 1948–1960, 2014.

[6] A. Konda, L. C. Xin, Y. Okoshi, and K. Toriumi, "Evaluation of Pilling by Means of Computer Image Analysis Part 2 : Evaluation of Pilling Classes," *Sen'i Kikai Gakkaishi (Journal Text. Mach. Soc. Japan)*, vol. 41, no. 11, pp. T152–T161, 1988.

[7] S. C. Kim and T. J. Kang, "Image analysis of standard pilling photographs using wavelet reconstruction," *Text. Res. J.*, vol. 75, no. 12, pp. 801–811, 2005.

[8] S. R. Palmer, I. Joud, and X. Wang, "Characterization and application of objective pilling classification to patterned fabrics," *J. Text. Inst.*, vol. 96, no. 6, pp. 423–430, 2005.

[9] S. Palmer and X. Wang, "Objective classification of fabric pilling based on the two-dimensional discrete wavelet transform," *Text. Res. J.*, vol. 73, no. 8, pp. 713–720, 2003.

[10] D. Semnani and H. Ghayoor, "Detecting and measuring fabric pills using digital image analysis," *World Acad. Sci. Eng. Technol.*, vol. 49, pp. 897–900, 2009.

[11] S. Y. Yun, S. Kim, and C. K. Park, "Development of an objective fabric pilling evaluation method. I. Characterization of pilling using image analysis," *Fibers Polym.*, vol. 14, no. 5, pp. 832–837, 2013.

[12] C. H. Hsi, R. R. Bresee, and P. A. Annis, "Characterizing fabric pilling by using image-analysis techniques. Part I: Pill detection and description," *J. Text. Inst.*, vol. 89, no. 1, pp. 80–95, 1998.

[13] Y. Torres and R. Navarro, "Automatic method based on image analysis for pilling evaluation in fabrics," *Opt. Eng.*, vol. 37, no. 11, pp. 2937–2947, 1998.

[14] B. Xin, J. Hu, and H. Yan, "Objective evaluation of fabric pilling using image analysis techniques," *Text. Res. J.*, vol. 72, no. 12, pp. 1057–1064, 2002.

[15] X. Chen and X. B. Huang, "Evaluating fabric pilling with light-projected image analysis," *Text. Res. J.*, vol. 74, no. 11, pp. 977–981, 2004.

[16] J. Izabela, "Assessment of a Fabric Surface after the Pilling Process Based on Image Analysis," *Fibres Text. East. Eur.*, vol. 17, no. 2, p. 73, 2009.

[17] A. de Oliveira Mendes, P. T. Fiadeiro, and R. A. L. Miguel, "Subjective and objective pilling evaluations of textile fabrics: a comparison," *Text. Res. J.*, vol. 80, no. 18, pp. 1887–1897, 2010.

[18] A. de Oliveira Mendes, P. T. Fiadeiro, and R. A. L. Miguel, "Virtual subjective pilling evaluation: an alternative," *Text. Res. J.*, vol. 81, no. 9, pp. 892–901, 2011.

[19] A. de Oliveira Mendes, P. T. Fiadeiro, R. A. L. Miguel, and J. M. Lucas, "Optical estimation of a set of pilling coefficients for textile fabrics," *Text. Res. J.*, vol. 79, no. 5, pp. 410–417, 2009.

[20] T. J. Kang, D. H. Cho, and S. M. Kim, "Objective evaluation of fabric pilling using stereovision," *Text. Res. J.*, vol. 74, no. 11, pp. 1013–1017, 2004.

[21] S. Palmer, J. Zhang, and X. Wang, "New methods for objective evaluation of fabric pilling by frequency domain image processing," *Res. J. Text. Appar.*, vol. 13, no. 1, pp. 11–23, 2009.

[22] J. Zhang, X. Wang, and S. Palmer, "Objective pilling evaluation of nonwoven fabrics," *Fibers Polym.*, vol. 11, no. 1, pp. 115–120, 2010.

[23] J. Zhang, X. Wang, and S. Palmer, "Objective pilling evaluation of wool fabrics," *Text. Res. J.*, vol. 77, no. 12, pp. 929–936, 2007.

[24] J. Zhang, X. Wang, and S. Palmer, "Objective grading of fabric pilling with wavelet texture analysis," *Text. Res. J.*, vol. 77, no. 11, pp. 871–879, 2007.

[25] Z.-T. Xiao and H.-W. Yang, "Fabric Pilling Segmentation Based on Edgeflow Algorithm," in *Machine Learning and Cybernetics, 2007 International Conference on*, 2007, vol. 3, pp. 1744–1748.

[26] L. Xiaojun, "Segmentation for Fabric Pilling Images Based on Edge Flow," in *Information and Computing Science, 2009. ICIC'09. Second International Conference on*, 2009, vol. 2, pp. 369–372.

[27] C. H. Hsi, R. R. Bresee, and P. A. Annis, "Characterizing Fabric Pilling by Using Image-analysis Techniques. Part II: Comparison with Visual Pill Ratings," *J. Text. Inst.*, vol. 89, no. 1, pp. 96–105, 1998.

[28] M. Eldessouki, H. A. Bukhari, M. Hassan, and K. Qashqari, "Integrated Computer Vision and Soft Computing System For Classifying The Pilling Resistance of Knitted Fabrics," *(In Press. FIBERS Text. East. Eur.*, vol. 22, no. 6(108), pp. 106–112, 2014.

[29] J. S. Weszka, C. R. Dyer, and A. Rosenfeld, "A Comparative Study of Texture Measures for Terrain Classification," *IEEE Trans. Syst. Man. Cybern.*, vol. SMC-6, 1976.

[30] R. M. Haralick, K. Shanmugam, and I. Dinstein, "Textural Features for Image Classification," *IEEE Trans. Syst. Man. Cybern.*, vol. 3, 1973.

[31] J.-S. R. Jang, "ANFIS: adaptive-network-based fuzzy inference system," *IEEE Trans. Syst. Man. Cybern.*, vol. 23, 1993.

[32] J. R. Jang, "Self-learning fuzzy controllers based on temporal backpropagation.," *IEEE Trans. Neural Netw.*, vol. 3, pp. 714–723, 1992.

Expert Systems with Applications 42 (2015) 2098–2113

Contents lists available at ScienceDirect

Expert Systems with Applications

journal homepage: www.elsevier.com/locate/eswa

Adaptive neuro-fuzzy system for quantitative evaluation of woven fabrics' pilling resistance

Mohamed Eldessouki [a,c,*], Mounir Hassan [b,c,1]

[a] Department of Materials Engineering, Technical University of Liberec, Czech Republic
[b] Faculty of Computing and Information Technology, King Abdulaziz University, Jeddah, Saudi Arabia
[c] Department of Textile Engineering, Faculty of Engineering, Mansoura University, Mansoura, Egypt

ARTICLE INFO

Article history:
Available online 22 October 2014

Keywords:
Adaptive neuro-fuzzy system
Quantitative evaluation
Textural features
Woven fabric pilling

ABSTRACT

Fabric pilling is considered a performance and aesthetic property of the woven products that determine its quality. The subjective evaluation of the fabric pilling results in misleading values that depend on the measurement standard even for the same sample. This work utilizes some textural features extracted from the fabric's images to obtain better representative and quantitative values of the fabric's surface. An algorithm for creating features dataset for training and testing the soft-computing classifier was described where random noise was added to the limited number of fabric's pilling standard images. The objective pilling classification of the fabric samples was performed using an adaptive neuro-fuzzy system (ANFIS) which showed an ability to classify the noised standard images with a correct classification rate of 85.8%. The ANFIS was also able to classify actual fabric samples with a Spearman's coefficient of rank correlation at +0.985 when compared with the classification grades of the human operators. Results showed high efficiency of the system that is independent on the different fabric structure or color which suggests its availability to replace the currently applied subjective pilling evaluation.

1. Introduction

The quality control of the textile products is one of the major factors that determine the price, and therefore the profit, of these products. Among the important properties of fabrics are the *performance properties* which represent the response of the fabric to a certain force, exposure, or treatment. Performance properties of a fabric include the fabric strength, abrasion resistance, pilling, and color fastness. Fabric pilling is one of those properties that can be classified as performance or aesthetic properties of the fabric and, therefore, being critical phenomena for both the manufacturers and the consumers. According to the ASTM standard terminology related to textiles (Committee, 2003), pills can be defined as "bunches or balls of tangled fibers which are held to the surface of a fabric by one or more fibers". The fabric pilling is affected by a wide range of parameters that may be related to: yarn parameters (e.g. twist, hairiness…, etc), spinning technology (e.g. ring spinning, rotor, compact spinning…, etc), fabric producing technology (e.g. weaving, knitting…, etc), as well as other processing parameters (Paek, 1989).

Evaluating the fabric pilling during the quality control process depends in the majority of standard testing methods on accelerated fabric wear using laboratory devices that simulate the frictional mechanisms lead to surface wear and pilling formation. The available standards recommend comparing samples that gone under this accelerated wear process with standard photographs of different pilling grades where expert operators can judge the samples and assign a pilling grade to them. This results in a subjective evaluation of the fabric pilling with a great dependency on the human element. The majority of pilling standard evaluation methods assign a ranking system that ranges between 1 and 5 (where 1 is assigned to a sever pilling and 5 is assigned to no pilling). However, the existence of different standards (e.g. ASTM, SN, EN ISO…, etc) creates a lot of confusion as the same sample may be ranked with different pilling grades according to the standard that was used in the evaluation. This calls researchers for finding alternative objective evaluation methods that may help to standardize those standard methods (Behera & Mohan, 2005).

Image analysis is a common technique in detecting textile faults (Eldessouki, Hassan, Qashqary, & Shady, 2014) including their esthetic character as well as their irregularities (Eldessouki, Ibrahim, & Militky, 2014). The introduction of image analysis as a method for evaluating the fabric pilling started in the late 80s as a try to replace the applied subjective evaluation methods (Konda, Xin, Okoshi, & Toriumi, 1988). The application of the image processing and analysis in the evaluation of fabric pilling goes through four main stages as indicated in Fig. 1 and the majority of the available literature on the topic tried to focus on one or more of these stages to modify the total outcome.

The main four objective pilling evaluation stages can be explained as follow:

1.1. Fabric's surface digitization

The fabric surface digitization is the process of converting the fabric surface to a digital form that can be dealt with on computer systems. This process can be done using a digital scanner (Kim & Kang, 2005; Palmer, Joud, & Wang, 2005; Palmer & Wang, 2003; Semnani & Ghayoor, 2009; Yun, Kim, & Park, 2013), a camera (Behera & Mohan, 2005; Hsi, Bresee, & Annis, 1998a; Torres & Navarro, 1998; Xin, Hu, & Yan, 2002), a light projected on camera (Chen & Huang, 2004), a camera attached to a microscope (Izabela, 2009), optical triangulation topographic reconstruction of the fabric surface (De Oliveira Mendes, Fiadeiro, & Miguel, 2010, 2011; De Oliveira Mendes, Fiadeiro, Miguel, & Lucas, 2009), a laser line projected on the surface of the fabric specimen (Kang, Cho, & Kim, 2004), or a stereovision surface reconstruction using two CCD cameras (Kang et al., 2004).

1.2. Pills detection and segmentation

Pills detection and segmentation is the process of separating the surface fuzz and pills from the complicated fabric structure background. This process was obtained using simple techniques such as the application of a binarization threshold on the fabric images (Kang et al., 2004; Konda et al., 1988), or after processing the raw fabric images using spatial and spectral techniques. The raw image processing may include some filters for noise reduction or edge detection (Semnani & Ghayoor, 2009), a background dilation and erosion (de Oliveira Mendes et al., 2009; Torres & Navarro, 1998), a fabric pattern detection and isolation using Fast Fourier Transform (FFT) (Behera & Mohan, 2005; Palmer, Zhang, & Wang, 2009; Torres & Navarro, 1998; Xin et al., 2002; Yun et al., 2013) or the different techniques of wavelet transforms (Palmer & Wang, 2003; Palmer et al., 2005, 2009; Zhang, Wang, & Palmer, 2007a, 2007b; Zhang, Wang, & Palmer, 2010). The pill detection was also performed using a template matching algorithm (Xin et al., 2002) and edge flow detection (Xiaojun, 2009; Xiao & Yang, 2007). For the colored images, pills were detected manually by blending the color channels of the fabric image (Izabela, 2009).

1.3. Pills quantization

The pills quantization is the next stage after segmenting pills from the fabric image. The process focuses on extracting some features that numerically represent the pills population to allow a quantitative discrimination between the different images. The feature descriptors can be divided in two categories; one that depends on the final image of the segmented pills, and the second that utilizes the spectral decomposition and analysis that was performed during the pills segmentation. The first category of features includes simple features such as the number of pills, the total pixel area of pilling, mean area of pills, the relative area of the pills to the total surface area, the sum of the gray values of pill images, the total volume of pills, as well as the distributions of pills, their shape, orientation angle, contrast, and density or uniformity of pills spatial distribution on the fabric surface (Behera & Mohan, 2005; de Oliveira Mendes et al., 2009; Hsi, Bresee, & Annis, 1998b; Izabela, 2009; Kang et al., 2004; Kim & Kang, 2005; Konda et al., 1988; Torres & Navarro, 1998; Xin et al., 2002; Yun et al., 2013). The descriptor features can also be calculated from the gray-scale image of the processed surface or from the simulated fabric surface and includes roughness, skewness, as well as pills number, volume (total and average volumes), height (maximum and average), area (total and average), and fractal dimension (Chen & Huang, 2004; Semnani & Ghayoor, 2009).

The second category of features includes the wavelet detail coefficients from the decomposition levels at the horizontal, the vertical and the diagonal orientations (Zhang et al., 2007a). It can be defined also as the horizontal detailed coefficient (especially at scale close to the inter-yarn distances in the fabric) (Palmer & Wang, 2003), as well as the energies of the reconstructed sub-images indifferent spatial orientations (Zhang et al., 2007b, 2010). Other statistical features can also be extracted from the wavelet decompositions such as the range, the inter-quartile range, the variance, the standard deviation, the mean absolute deviation, the median absolute deviation, the standard error and the coefficient of variation (Palmer et al., 2005).

1.4. Pills rating and classification

The classification stage is the ultimate goal of the whole process where a "successful" rating of images allows the trust in the method to replace the available subjective analysis. Classification models use the extracted set of features as inputs that can be used to generate the final rating of the image. The classification models may implement empirical and statistical methods such as the multi-variable linear regression (Kang et al., 2004; Kim & Kang, 2005; Xin et al., 2002) and discriminant analysis (Palmer et al., 2005; Zhang et al., 2007a, 2007b),or may implement artificial intelligent methods such as the application of different types of the artificial neural networks (Chen & Huang, 2004; Eldessouki et al., 2014; Zhang et al., 2010).

Based on this literature survey, three points can be highlighted:

- Although fabric wear and pilling are affecting the *texture* of the surface, there is no available publication that considers the image "textural parameters" during the pilling quantization.
- The classification methods based on artificial intelligence techniques require big databases for the system training and verification. However, the size of the dataset is limited because this dataset is based on photographs that are taken from standard images. Since the majority of standard methods utilize a rating system from 1 to 5, the standard images have a limited number that is not enough for creating a reasonable dataset size.
- There are few papers that consider the efficient techniques of each evaluation stage to create an integrated, robust, and effective evaluation process. On the other hand, the majority of these papers focus on enhancing one or more of these stages separately.

Therefore, this work tries to address these problems by:

- Considering the *texture features* of the images among the quantization parameters.
- Introducing a new method for creating sampling dataset that is large enough to suite the training and testing processes required in building the applied artificial intelligent classifier.

Fig. 1. Stages of quantitative fabric pilling evaluation.

- Utilizing the neuro-fuzzy classification system to approach the high level of evaluation in human beings.
- Creating a user-friendly system that integrates the four evaluation stages. The system is semi-automatic in a way that classifies the pilling in the introduced sample automatically and allows the operator to change some of the detection parameters if not satisfied with the automatic detection.

2. Computation theory

2.1. Image preparation

The EMPA Standard (SN 198525) was used to obtain the standard images for pilling ranking. The EMPA standard has two series of photographs; the *K*-series for the knitted fabrics and the W-series for the woven fabrics. Among the W-series, there is the W1 category for evaluating the nonwoven fabrics while the W2 and W3 categories are used for evaluating the woven fabrics (Behera & Mohan, 2005). The W2 category is usually used in evaluating samples with big pill size while W3 is more suitable with samples of smaller pills. Within each category, there are four standard pictures used in the comparison and pills ranking on a scale of 1 (for the worst) to 5 (for the pill-free). To help the operators with their "fuzzy" and "subjective" evaluation, there are only four pictures for the five ranks where the first picture represents ranks 1-to-2, the second picture represents ranks 2-to-3, …, etc. The standard photographs were scanned to the computer with a resolution of 600 × 600 dpi.

To generate a dataset with a suitable size out of these limited standard pictures, each standard image was duplicated many times where each copy had a random noise that was applied to it. To add noise to the pictures, different filter kernels were created with random parameters and each filter was convoluted with the picture to create a "noised" or "blurred" image. The applied filters are the "averaging", "disk", "Gaussian", "motion" filters, and the "partial spatial rearrangement". Representation of the original image and samples after the application of different noise filters are shown in Fig. 2. The kernel for each filter was generated using random parameters that change each time of recalling the filter. The "partial spatial rearrangement" technique was applied by randomly selecting sub-image from the pilling region of the sample and having a size that represents 10% of the original image then placing the sub-image in a random way at a different position of the image.

These five types of noise generators were applied three times using random parameters to each standard picture which creates 15 noised copies of the original image. To avoid the system bias to the noised images, the features extracted from the original image were duplicated 35 times to create a features dataset with 30% representation of the noised images. The features dataset consists of the previously mentioned 4 features with 200 observations (50 observations for each standard image) of each standard category (W1, W2, and W3). The features dataset was then split randomly into a training dataset that represents 80% and a testing dataset that represents the remaining 20% of the data. The introduction of the noised images during the training of the classification system makes it more robust to classify different samples even with noised pictures.

2.2. Textural features

The basic statistics that are utilized in pilling quantization (the first order statistical features) extract data out of the gray-scale levels of the pixels in the digital image and does not reflect these surface features. On the other hand, the second order and textural features are more concerned about the spatial distribution of the gray-scale levels which reflects the roughness of the image and its texture. This gives the advantage of being close to the human awareness of the texture that describe surfaces as fine, coarse, smooth, rippled, irregular,… etc.

For an image with *x* and *y* representing the spatial coordinates, the gray-scale levels of that image can be expressed as $\boldsymbol{P}(x,y)$ and its gray level co-occurrence matrix (GLCM) can be calculated to determine the textural features of the image. The GLCM represents the joint probability density of the pairs of the gray levels occur at pairs of points separated by the vector $\delta(\Delta x,\Delta y)$ (Weszka, Dyer, & Rosenfeld, 1976). The displacements Δx and Δy in the vector δ determine the length (the running distance d) and the angel (direction θ) between the points of the required calculation. The calculated joint density takes the matrix form $\boldsymbol{C_\delta}$ with a size $N\delta N$ where N is the maximum value of gray levels in the original image $\boldsymbol{P}$ and the value $\boldsymbol{C_\delta}(i,j)$ represents the probability of the pair of gray levels (i,j) occurring at separation δ. To illustrate the calculation of the GLCM, consider the example shown in Fig. 3 for an image $\boldsymbol{P}(x,y)$ with $N = 4$ gray levels values that range between 0 and 3. Therefore, the size of the co-occurrence matrix $\boldsymbol{C}$ is 4×4 and for a separation vector $\delta(1,0)$ the entries $\boldsymbol{C_\delta}(i,j)$ are the number of times gray level i occur immediately (*i.e.* one pixel distance) to the left (*i.e.* in zero angel direction) of the gray level j.

Once the co-occurrence matrix was calculated the image texture can be analyzed based on the given parameters (d,θ) of the vector δ. If the image's texture is coarse and the displacement d is smaller than the size of the texture element, the pairs of points at separation δ should have similar gray levels. Therefore, the high values in the co-occurrence matrix $\boldsymbol{C_\delta}$ should be concentrated at the main diagonal or its nearby. Similarly, for fine textured images with texture elements comparable in size to the separation δ, the values in $\boldsymbol{C_\delta}$ will be spread out. The same logic applies for the texture direction that might be directed to a certain angel and, therefore, the spread of the values about the main diagonal of $\boldsymbol{C_\delta}$ will depend on the selected angel (θ) of the vector δ. Therefore, an investigation of the image texture is required at different displacements (d) and directions (θ) then the scattering of values around the $\boldsymbol{C_\delta}$'s main diagonal should be measured.

To measure the spread of values in the co-occurrence matrix Haralick, Shanmugam, and Dinstein (1973) suggested different features that represent the texture information of the image. The calculation of these features starts usually with the normalization of the matrix $\boldsymbol{C}$ by its total sum:

$$D_\delta(i,j) = \frac{\boldsymbol{C}_\delta(i,j)}{\sum_{i,j=0}^{N-1}\sum_{i,j=0}^{N-1}\boldsymbol{C}_\delta(k,l)}$$

where i, j, k, and l are indices and $\boldsymbol{D}_\delta$ is the normalized matrix at a certain direction δ.

Among the features suggested by Haralick, four features were found to be more effective and will be tested in this study. These features are:

Contrast:

$$f_{1,\delta} = \sum_{i=1}^{N}\sum_{j=1}^{N}(i-j)^2 D_\delta(i,j)$$

The contrast is also known as the "*variance*", and the "*inertia*" and it is taken as a texture feature because it represents the moment of inertia of the matrix $\boldsymbol{D}_\delta$ around its main diagonal and it is a measure of the degree of its spread of values.

Correlation:

$$f_{2,\delta} = \sum_{i=1}^{N}\sum_{j=1}^{N}\frac{ijD_\delta(i,j)-\mu_i\mu_j}{\sigma_i\sigma_j}$$

where μ_i and σ_i are the mean and standard deviation, respectively, of the row sums and μ_j, and σ_j are the mean and standard deviation, respectively, of the column sums of the matrix $\boldsymbol{D}_\delta$. The correlation is a measure of the degree to which the rows (or columns) of the GLCM resemble each other and this value should be high when values are uniformly distributed in the matrix and low when the values off the diagonal are small.

Angular second moment (ASM):

$$f_{3,\delta} = \sum_{i=1}^{N}\sum_{j=1}^{N}D_\delta(i,j)^2$$

The angular second moment (ASM) is also known with different names such as the "*energy*", the "*uniformity*", and the "*uniformity of energy*". This value is small when $\boldsymbol{D}_\delta(i,j)$ are close in values and it increases when values largely varied as in the situation where values are clustered near the main diagonal.

Inverse difference moment (IDM):

$$f_{4,\delta} = \sum_{i=1}^{N}\sum_{j=1}^{N}\frac{D_\delta(i,j)}{1+(i-j)^2}$$

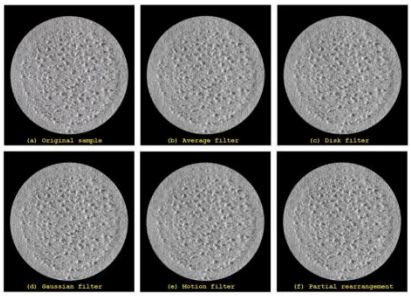

Fig. 2. Examples for different shapes of the same fabric sample after applying random filters.

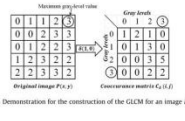

Fig. 3. Demonstration for the construction of the GLCM for an image $P(x,y)$.

The inverse difference moment (IDM) can also be called the *homogeneity* and it measures the closeness of the distribution of elements in the GLCM to its diagonal and it reaches 1 for a diagonal matrix.

2.3. Adaptive neuro-fuzzy system

Fuzzy inference systems are useful in mapping data between two spaces while some degree of uncertainty is involved. The fuzzy system implements the membership functions, instead of the crisp-set functions, to imitate the human thinking and cognition without employing precise quantitative analyses (Jang, 1993). This provides the opportunity to deal with imprecision and to represent the linguistic qualitative words such as "many", "low", "few"…, etc. However, creating such fuzzy systems requires some understanding of the rules that govern the relations between the inputs and the outputs. Therefore, the adaptive neuro-fuzzy inference systems (ANFIS) were introduced to combine the natural language description of fuzzy systems and the learning properties of neural-networks. By using a hybrid learning algorithm, the ANFIS can construct an input–output mapping based on both human knowledge (in the form of fuzzy *if–then* rules) and stipulated input–output data pairs (Jang, 1993).

The initial model of the ANFIS was proposed by Jang (1992, 1993) who explained it using two inputs (x_1, x_2) and built the rule based system using two *if-then* rules, although the system can be generalized to any *N* number of inputs or *M* rules. The model with two inputs is demonstrated in Fig. 4 with five layers that include two *adaptive* layers (layer #1 and layer #4, demonstrated by rectangles) and three *fixed* layers (layer #2, layer #3, and layer #5, demonstrated by circles). The two adaptive layers are distributed between the *premise* part, and the *consequent* part which are the two basic components of all *logical statements*. The positioning of

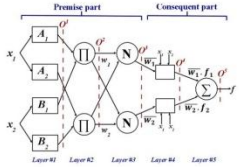

Fig. 4. The ANFIS model.

the adaptive layers at these two parts allows the adjustment of their parameters and consequently adjusting the performance of the whole system.

The two rules of Takagi and Sugeno were applied as:

Rule 1: If x_1 is A_1 and x_2 is B_1, then $f_1 = p_1x_1 + q_1x_2 + r_1$.
Rule 2: If x_1 is A_2 and x_2 is B_2, then $f_2 = p_2x_1 + q_2x_2 + r_2$

The output of the kth layer can be expressed with the vector O^k which can be stated for the first layer O^1 in the form:

$$O_i^1 = \begin{cases} \mu_{A_i}(x_1) \\ \mu_{B_i}(x_2) \end{cases}$$

where μ_{A_i} and μ_{B_i} are the membership functions (MF) for the first and the second inputs, respectively. The membership function can take different shapes of any continuous and piecewise differentiable functions. The selected MF in this case is the Gaussian (bell shape) function with normalized output ϵ [0, 1] which can be written for the first input (x_1) in the following form (and a similar relation can be found for the second input):

$$\mu_{A_i}(x_1) = e^{-\left(\frac{x_1 - a_i}{b_i}\right)^2}$$

where; the parameters {a_i and b_i} determine the shape and behavior of the membership function. These parameters will be called the *premise parameters* as they are the adjustable parameters in the premise part.

The neuron elements of the second layer are fixed with simple multiplication transfer function. The output of each neuron represents the *firing strength* of the rule. The output vector of this layer (O^2) can be calculated as:

$$O_i^2 = w_i = \mu_{A_i}(x_1) \cdot \mu_{B_i}(x_2)$$

The third layer is a fixed layer with the role of normalizing its inputs to produce the *normalized firing strength* which is the ratio of the firing strength of the ith rule to the sum of the firing strength for all rules, that is:

$$O_i^3 = \overline{w}_i = \frac{w_i}{\sum_{i=1}^{N} w_i} = \frac{w_i}{w_1 + w_2}$$

where, N is the number of the system inputs.

The fourth layer is the adaptive layer that multiplies the normalized firing strength by a first order polynomial for the first order Takagi and Sugeno model. The output vector of this layer O^4 can be expressed as:

$$O_i^4 = \overline{w}_i f_i = \overline{w}_i(p_i x_1 + q_i x_2 + r_i)$$

where, the parameters {p_i, q_i, and r_i} are adjustable and can be used to tune the outputs of that layer. These parameters will be called the *consequent parameters* as they tune the output of the consequent part of the system.

The fifth layer has a single fixed neuron that sums up its inputs and produces the final result (f) of the system that can be represented as:

$$O_i^5 = f = \sum_{i=1}^{N} \overline{w}_i f_i = \frac{\sum_{i=1}^{N} w_i f_i}{\sum_{i=1}^{N} w_i}$$

2.4. Hybrid learning algorithm for the ANFIS

The goal of the learning of the ANFIS is to adjust all the tunable system parameters which includes both the premise parameters (a_i and b_i) and the consequent parameters (p_i, q_i, and r_i) to minimize the overall system's error. The hybrid learning algorithm utilizes two passes: the forward pass with fixed premise parameters and the backward pass with fixed consequent parameters. To explain that, consider the forward pass with fixed premise

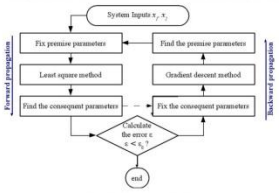

Fig. 5. Hybrid ANFIS learning algorithm.

Table 1
Tested knitted sample specifications.

	Color	Structure	Weight/area (g/m²)	Warp density (threads/inch)	Weft density (threads/inch)	Warp count (tex)	Weft count (tex)
W1	White	1/6	128	71	70	21	21
W2	White	1/1	155	63	60	30	31
W3	Bright white	1/1	121	81	51	19	26
W4	Blue	1/3	145	86	56	21	32
W5	Blue	2/4	157	87	64	22	29
W6	Light blue	1/3	167	88	55	21	38
W7	Paige	1/2	182	89	79	24	25

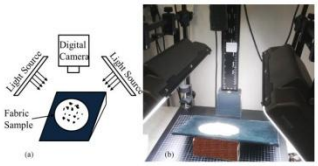

Fig. 6. Image acquisition setup depicted schematically in (a) and photographed in (b).

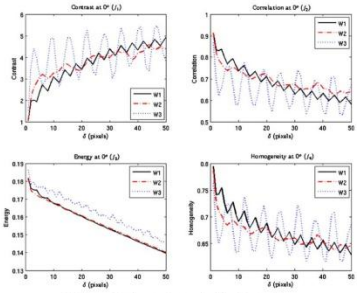

Fig. 7. Features of the three categories at an angle of 0° and short term distance.

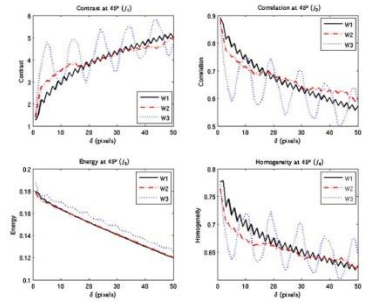

Fig. 8. Features of the three categories at an angle of 45° and short term distance.

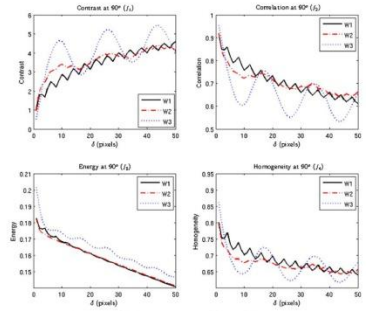

Fig. 9. Features of the three categories at an angle of 90° and short term distance.

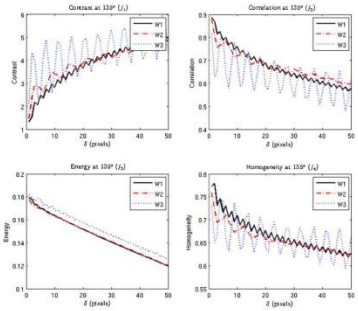

Fig. 10. Features of the three categories at an angle of 135° and short term distance.

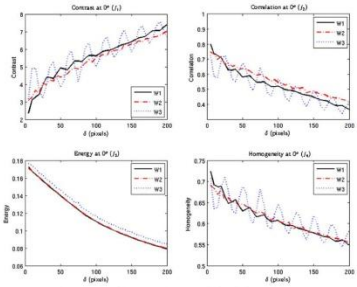

Fig. 11. Features of the three categories at an angle of 0° and long term distance.

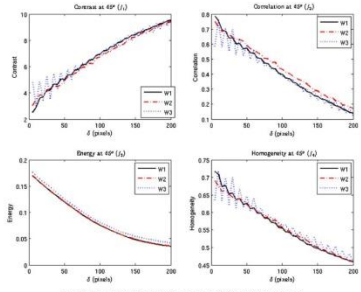

Fig. 12. Features of the three categories at an angle of 45° and long term distance.

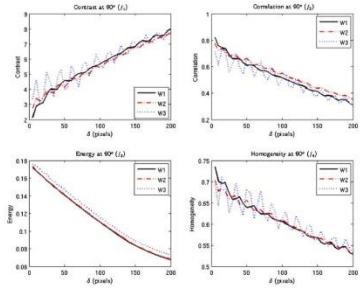

Fig. 13. Features of the three categories at an angle of 90° and long term distance.

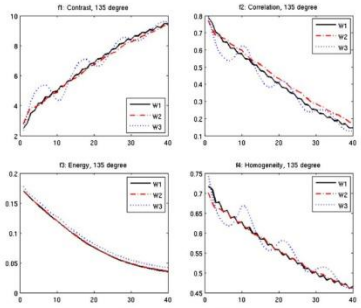

Fig. 14. Features of the three categories at an angle of 135° and long term distance.

Table 2
Features periodicity at short distance (values in pixels).

		f_1	f_2	f_3	f_4
Zero	W1	4	4	–	4
	W2	9	–	–	9
	W3	6.5	6.5	–	6
45°	W1	4	4	–	4
	W2	9	9	–	9
	W3	6	6	–	6
90°	W1	4	4	–	4
	W2	15	15*	–	9
	W3	17	17	–	17
135°	W1	2	2	–	2
	W2	6.5	6.5	–	7
	W3	5	5	–	5

* Low correlation was observed at these values.

parameters which results in an output that can be defined for the given two inputs ANFIS as:

$$f = \overline{W_1} f_1 + \overline{W_1} f_1 = \overline{W_1}(p_1 x_1 + q_1 x_2 + r_1) + \overline{W_2}(p_2 x_1 + q_2 x_2 + r_2)$$

That can be rearranged to:

$$f = (\overline{W_1} x_1) p_1 + (\overline{W_1} x_2) q_1 + (\overline{W_1}) r_1 + (\overline{W_2} x_1) p_2 + (\overline{W_2} x_2) q_2 + (\overline{W_2}) r_2$$

It can be noticed from this equation that it represents a linear combination of the consequent parameters $\{p_1, q_1, r_1, p_2, q_2,$ and $r_2\}$. The least square method can be utilized to calculate those parameters. Therefore, the signal goes in the forward pass along the system until layer #4 then the least square method can be applied to allocate the consequent parameters and the whole system can be identified. The error rate of the system can be calculated after the system identification. The backward pass starts with fixing the consequent parameters and propagating the error rate backward through the system and the premise parameters $\{a_i$ and $b_i\}$ can be updated by the gradient descent method. This cycle continues until the desired performance is achieved as illustrated in Fig. 5.

3. Experimental setup

Seven woven fabrics with different structures and colors are used and the specifications of these samples are listed in Table 1. To test the system ability in detecting the fabric pilling regardless of the color shade, the tested samples were selected to have different colors. Samples were tested on Martindale instrument for pilling where two circular specimens of 140 mm diameters

Table 3
Features periodicity at long distance (values in pixels).

		f_1	f_2	f_3	f_4
Zero	W1	20	20	–	20
	W2	10	10	–	10
	W3	25	25	–	25
45°	W1	–	10	–	10
	W2	–	25	–	25
	W3	10	10	–	10
90°	W1	20	20	–	20
	W2	15	15	–	15
	W3	20	20	–	20
135°	W1	10	10	–	10
	W2	–	–	–	–
	W3	55	55	–	55

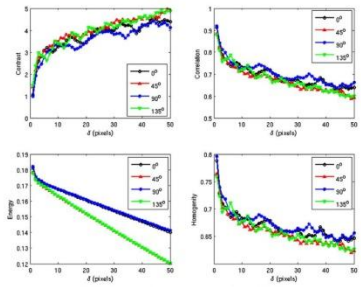

Fig. 15. Features as calculated at different angles for sample W2_1-2.

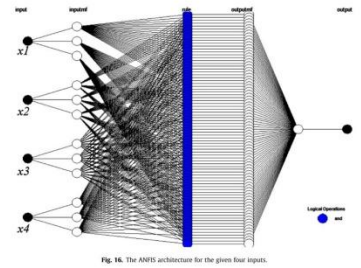

Fig. 16. The ANFIS architecture for the given four inputs.

from each sample were placed on the machine head. The face of the lower specimen is up and the specimen is placed on the top of a standard felt of 140 mm diameter. The upper specimen is mounted on a holder of 90 mm diameter with a standard felt of the same size and fixed to the holder with an elastic ring. The upper holder is installed on the machine where the faces of the upper and lower specimens are in contact to each other. The samples were tested under 6.5 cN/cm^2 pressure for 10,000 cycles of Lissajous figure with 24 mm stroke.

The measured samples were evaluated visually by seven different operators against the photographs of the EMPA Standards (SN 198525). The measured samples were then digitized using

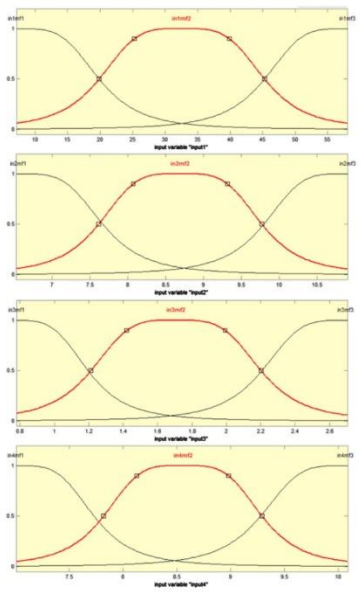

Fig. 17. The adjusted membership functions for the four inputs (each input has two MFs).

the setup shown in Fig. 6 and processed using the developed software algorithm to obtain the pilling classes. The image acquisition system consists of a digital CCD camera that is equipped with a macro lenses to capture the sample surface details. The captured image resolution of 300 dpi and the image dimensions was 2048 × 1536 pixels. Lighting is critical for the imaging system and two light sources that equally distribute the light on the surface of the fabric were applied. The sample was tilted with a slight angel to the horizontal plane to allow contrasting the pills with their shadow.

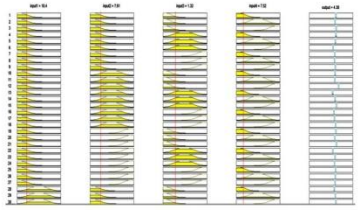

Fig. 18. The application of the ANFIS.

4. Results and discussion

Pre-investigation for the effective choice of the vector δ was performed by applying a distance sweep in the range of $d = 0$ to 50 with a step of one pixel. For long range investigations, another distance sweep in the range of 5 to 200 with a step of 5 pixels was also performed. In each case of the evaluation (the short term and the long term), a direction sweep was performed at four angles $\theta = 0°$, 45°, 90°, and 135°. Results of the four extracted features for the short and long term distance sweeps are shown in Figs. 7–14 for the first sample of each standard category (i.e. W1_1-2, W2_1-2, and W3_1-2).

From these figures some general notes can be observed on the fabric surface and its textural features:

- The behavior of the contrast feature (f_1) increases with increasing the calculation distance (δ) which is different from the other three features that decrease with distance.

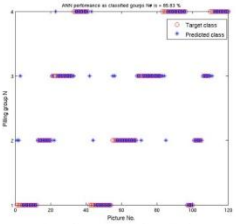

Fig. 19. Performance of the ANFIS for the Nth grade.

- There is a form of periodicity in the behavior of most features, although this periodicity is not dominant in the energy feature (f_3) compared to the other features.
- The periodicity of the features can be considered as an indicator of the repeatability of objects on the fabric's surface at a certain distance. For example, by examining features f_1, f_2, f_3, f_4 at an angle of zero in Fig. 7, a cyclic pattern can be observed with repeats of 4 pixels in category W1, 9 pixels in category W2, and 6 pixels in category W3. This indicates a repeatability of objects at these distances which might imply the repeatable pattern of the woven structure.
- The periodicity of features shown in Figs. 7–10 at short distances is summarized in Table 2 while the periodicity of the long distances shown in Figs. 11–14 is summarized in Table 3. Some features show periodicity although it might not be strong in some cases which were highlighted in the table with "low" and with the periodic interval, when available.
- Periodicity interval is almost constant when obtained from different features for the same fabric image.
- There is a small effect of the calculation angle on the periodicity of the features where similar intervals can be observed at different angles. The cases where a difference can be observed for the feature at different angles (e.g. f_1 at the angles 0° and 90°) might be attributed to the different warp and weft densities in the image.
- The repeat for a feature as observed at long distances is a multiplier of the repeat value for the same feature at short distance. For example the repeat of f_1 at 0° for W1 is 4 pixels (Table 2) while this value is 20 pixels (Table 3) when measured at long distance. This can be attributed to the different step size of evaluation during the short distance (1 pixel) and the long distance (5 pixels).
- Features that repeat at short distances were found to diminish after certain distance. For instance, the feature f_1 at 45° for W3 is found to have a strong repeating wave as observed in Fig. 8 while this wave diminishes at long distances as shown in Fig. 12. This indicates the lack of correlation between the textural objects on the fabric's surface at long distances.

On the other hand, the change of the features at different directions at short distances is shown in Fig. 15. There is a high similarity of the features' general trend at different angles with a coincidence allocation of the peaks at certain distances. The

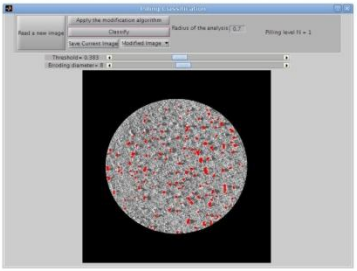

Fig. 20. GUI of the developed software for fabric's pilling evaluation.

strength of the repeatable peak is decaying with distance and there is no significant repeatable behavior observed at longer distances (up to 200 pixels). The frequency of the peaks at 90° is almost double the frequency at 0° while a similar high frequency can be found at the angles 45° and 135°.

According to this pre-investigation, the actual samples are evaluated at an angle of 45° which should be a reasonable step that will coincide with angles of 0°, 90°, and 135° as indicated in the previously discussed figure. Features are also evaluated at a range of distance that covers the periods of peak maxima of the different features of the three categories. Based on the repeatability values listed in Table 2, the features are calculated in the distance interval from 4 to 10 pixels then values are summed up to be used as the characteristic features of the image during its evaluation. Also, due to the behavior similarity for the features, only the contrast and the correlation are used during the evaluation. These features are selected because they have a repeatable behavior and opposite trends. The other two features for evaluating the fabric pilling will be the number of pills and their relative area which is calculated as ratio between the pills area and the total area of interest in the studied sample.

Based on the described algorithm, an adaptive neuro-fuzzy system was constructed as shown in Fig. 16 where the first adaptive layer consists of 3 neurons (3 membership functions) for each input. The premise parameters of this layer were calculated and the adjusted membership functions for the four inputs are shown in Fig. 17. The multiplication and normalization were performed in the rule layer which is highlighted in Fig. 16 with the blue color. The second adaptive layer is also shown in the same figure where the Takagi and Sugeno model applies and the consequent parameters are evaluated.

The application of the ANFIS system is demonstrated in Fig. 18 which includes the five basic steps of the calculation. The system starts with the *fuzzification* of the inputs where each input is processed in parallel through the membership functions. Second, the rules are applied using the *fuzzy operator* (AND) which results in the weighted firing strength to the third part of the *implication* and transfers data from the premise to the consequent. The fourth step is defined by the *aggregation* of the consequents across the rules and the final step is the *defuzzification* of the results to produce the final output.

The given ANFIS structure was trained with the contrast, correlation, number of pills, and their relative areas as inputs and the standard pilling grades or ranks (1, 2, 3, 4 or 5) as outputs. The performance of the ANFIS systems is shown in Fig. 19. For the 120 samples presented to the ANFIS systems, it can be seen that the ANFIS performed 85.8% in determining the pilling grade. Also, from these figures it can be observed that most of the samples that were

Table 4
Human operators as compared to the ANFIS pilling evaluation.

	OP.#1	OP.#2	OP.#3	OP.#4	OP.#5	OP.#6	OP.#7	Operators' evaluation	ANFIS evaluation
W1	3	3	1	2	2	2	2	2	2
W2	4	4	4	4	4	3	4	4	4
W3	3	2	2	1	4	2	2	2	2
W4	2	3	2	3	3	1	2	2	3
W5	2	1	1	1	3	2	1	1	1
W6	4	5	4	4	4	5	4	4	4
W7	3	3	3	3	4	2	5	3	3

miss-graded were deviated from the target class with only one degree which is acceptable in classifying such samples where the standards give two grades in the same picture.

Although the relatively high performance of the ANFIS in detecting the correct pilling of the noised standard images, it is important to test the system on real fabric samples. Therefore, the developed algorithm was coded in a user-friendly graphical user interface (GUI) that is shown in Fig. 20. The woven samples were introduced to seven human operators after their pilling test on Martindale to compare the samples with the standard pictures. The operators subjectively assigned a pilling rank for each sample as shown in Table 4 and the total pilling evaluation of the sample was calculated by the mode of the operator's ranks. The pictures of the woven samples were also introduced to the developed program that utilizes the ANFIS to rank the samples. The samples' pilling rank is listed in Table 4 and the Spearman's coefficient of rank correlation between the two categories of the human evaluation and the ANFIS evaluation is +0.982 which implies a good agreement between the two sets of results and a reliability of the system to be used in replacing the subjective evaluation of human operators.

5. Conclusion

This work introduces for the first time, to the best of the authors' knowledge, fabric's *image textural features* as measures for the fabric surface during the quantitative evaluation of pilling in woven fabrics. Creating a feature dataset from the available Standard images with enough size for training soft computing algorithms is challenging due to the limited number of those Standard images. To deal with this issue, a new approach was suggested to mimic the noise that interferes with the fabric surface during its digitization. Hence, a user-friendly pilling evaluation system that integrates the processes of fabric surface digitization, pilling segmentation, quantization, and classification was implemented in this work. The system was able to classify woven fabric samples according to their surface texture with a high degree of correlation to the traditional methods of pilling evaluation.

Results of textural features show a trend similarity between the features which allows the reduction of the number of these features during the evaluation (contrast and correlation were only used in the final code); Selection of few features was not only to prevent redundancy in the system's inputs, but also to allow other pilling descriptors (such as the number of pills and their relative area) that represent pilling intensity to be considered. Taking more pilling descriptors into account during the pilling quantization might be useful; however the computational resources required for the ANFIS classifier increases exponentially with the increase in number of the system's inputs. This applies a constraint on the number of pilling descriptors that can be simultaneously used during the ANFIS classification which results in a "features optimization problem" due to the need of features that represent both the image texture as well as the pilling intensity quantifiers. A major part of the figures in the results section presented in this work was dedicated to investigate the *texture features* at different conditions and optimize their selection.

The application of random noise filters on the Standard images significantly affects the textural features while keeping a small effect on the pilling intensity features. The parameters of the applied filters were randomly selected; however the range of these parameters should extend to apply more "aggressive" noise to the pictures to allow the robustness of the system to deal with fabric images of different structures and textures. Also, more noise filters might be required to better resemble the image defects that might occur during the image acquisition, although the current filters were useful in increasing the amount of sampling datasets.

Success in digitizing the Standard samples in the same systematic fashion of real samples (rather than scanning Standard images) should increase the reliability of the suggested system and allows it to be standardized as a quantitative method that replaces the current subjective evaluation Standards. The relatively good results of the suggested system are promising for the methodology extension to cover fabrics that are produced using different technologies (knitted and nonwoven fabrics) as well as fabrics of different structures.

References

Behera, B. K., & Mohan, T. E. M. (2005). Objective measurement of pilling by image processing technique. *International Journal of Clothing Science and Technology, 17*(5), 279–291.

Chen, X., & Huang, X. B. (2004). Evaluating fabric pilling with light-projected image analysis. *Textile Research Journal, 74*(11), 977–983.

Committee, D. (2003). ASTM D123-13a standard terminology relating to textiles. ASTM. Retrieved from <http://www.astm.org/Standards/D123.htm>.

De Oliveira Mendes, A., Fiadeiro, P. T., & Miguel, R. A. L. (2010). Subjective and objective pilling evaluations of textile fabrics: A comparison. *Textile Research Journal, 80*(18), 1887–1897.

De Oliveira Mendes, A., Fiadeiro, P. T., & Miguel, R. A. L. (2011). Virtual subjective pilling evaluation: An alternative. *Textile Research Journal, 81*(9), 892–901.

De Oliveira Mendes, A., Fiadeiro, P. T., Miguel, R. A. L., & Lucas, J. M. (2009). Optical estimation of a set of pilling coefficients for textile fabrics. *Textile Research Journal, 79*(5), 410–417.

Eldessouki, M., Bukhari, H. A., Hassan, M., & Qashqari, K. (2014). Integrated computer vision and soft computing system for classifying the pilling resistance of knitted fabrics. *FIBRES & TEXTILES in Eastern Europe, 22*(6(108)), 106–112.

Eldessouki, M., Ibrahim, S., & Militky, J. (2014). A dynamic and robust image processing based method for measuring yarn diameter and its variation. *Textile Research Journal, 84*(18), 1948–1960. http://dx.doi.org/10.1177/0040517514538032.

Eldessouki, M., Hassan, M., Qashqary, K., & Shady, E. (2014). The application of principal component analysis to boost the performance of the automated fabric fault detector and classifier. *FIBRES & TEXTILES in Eastern Europe, 22*(4(106)), 51–57.

Haralick, R. M., Shanmugam, K., & Dinstein, I. (1973). Textural features for image classification. *IEEE Transactions on Systems, Man, and Cybernetics*, 3. http://dx.doi.org/10.1109/TSMC.1973.4309314.

Hsi, C. H., Breese, R. R., & Annis, P. A. (1998a). Characterizing fabric pilling by using image-analysis techniques. Part I: Pill detection and description. *Journal of the Textile Institute, 89*(1), 80–95.

Hsi, C. H., Breese, R. R., & Annis, P. A. (1998b). Characterizing fabric pilling by using image-analysis techniques. Part II: Comparison with visual pill ratings. *Journal of the Textile Institute, 89*(1), 96–105.

Izabela, J. (2009). Assessment of a fabric surface after the pilling process based on image analysis. *FIBRES & TEXTILES in Eastern Europe, 17*(2), 73.

Jang, J. R. (1992). Self-learning fuzzy controllers based on temporal backpropagation. *IEEE Transactions on Neural NetworksA Publication of the IEEE Neural Networks Council, 3*, 714–723. http://dx.doi.org/10.1109/72.159060.

Jang, J.-S. R. (1993). ANFIS: Adaptive-network-based fuzzy inference system. *IEEE Transactions on Systems, Man, and Cybernetics, 23*. http://dx.doi.org/10.1109/21.256541.

Kang, T. J., Cho, D. H., & Kim, S. M. (2004). Objective evaluation of fabric pilling using stereovision. *Textile Research Journal, 74*(11), 1013–1017.

Kim, S. C., & Kang, T. J. (2005). Image analysis of standard pilling photographs using wavelet reconstruction. *Textile Research Journal, 75*(12), 801–811.

Konda, A., Xin, L. C., Okoshi, Y., & Toriumi, K. (1988). Evaluation of pilling by means of computer image analysis. Part 2: Evaluation of pilling classes. *Sen'i Kikai Gakkaishi (Journal of the Textile Machinery Society of Japan), 41*(11), T152–T161.

Paek, S. L. (1989). Pilling, abrasion, and tensile properties of fabrics from open-end and ring spun yarns 1. *Textile Research Journal, 59*(10), 577–583.

Palmer, S. R., Joud, L., & Wang, X. (2005). Characterization and application of objective pilling classification to patterned fabrics. *Journal of the Textile Institute, 96*(6), 423–430.

Palmer, S., & Wang, X. (2003). Objective classification of fabric pilling based on the two-dimensional discrete wavelet transform. *Textile Research Journal, 73*(8), 713–720.

Palmer, S., Zhang, J., & Wang, X. (2008). New methods for objective evaluation of fabric pilling by frequency domain image processing. *Research Journal of Textile and Apparel, 12*(1), 11–23.

Semnani, D., & Ghayoor, H. (2009). Detecting and measuring fabric pills using digital image analysis. *World Academy of Science, Engineering and Technology, 49*, 897–900.

Torres, Y., & Navarro, R. (1998). Automatic method based on image analysis for pilling evaluation in fabrics. *Optical Engineering, 37*(11), 2937–2947.

Weszka, J. S., Dyer, C. R., & Rosenfeld, A. (1976). A comparative study of texture measures for terrain classification. *IEEE Transactions on Systems, Man, and Cybernetics, SMC-6*. http://dx.doi.org/10.1109/TSMC.1976.5408777.

Xiao, Z.-f., & Yang, H.-W. (2007). Fabric pilling segmentation based on edgeflow algorithm. *2007 International conference on machine learning and cybernetics* (Vol. 3, pp. 1744–1748). IEEE.

Xiaojun, L. (2009). Segmentation for Fabric Pilling Images Based on Edge Flow. *Second international conference on information and computing science, 2009. ICIC'09* (Vol. 2, pp. 369–372). IEEE.

Xin, B., Hu, J., & Yan, H. (2002). Objective evaluation of fabric pilling using image analysis techniques. *Textile Research Journal, 72*(12), 1057–1064.

Yun, S. Y., Kim, S., & Park, C. K. (2013). Development of an objective fabric pilling evaluation method. I. Characterization of pilling using image analysis. *Fibers and Polymers, 14*(5), 832–837.

Zhang, J., Wang, X., & Palmer, S. (2007a). Objective grading of fabric pilling with wavelet texture analysis. *Textile Research Journal, 77*(11), 871–879.

Zhang, J., Wang, X., & Palmer, S. (2007b). Objective pilling evaluation of wool fabrics. *Textile Research Journal, 77*(12), 929–936.

Zhang, J., Wang, X., & Palmer, S. (2010). Objective pilling evaluation of nonwoven fabrics. *Fibers and Polymers, 11*(1), 115–120.

PART III

Chapter 10

Conclusion

Conclusion

The subjective evaluation of many fibrous structures is common and stands as a problem in the textile industry where it causes a great deal of dependency on the human operator and prevents the automation of the applied evaluation method. The lack of automation results in a heavy laborious work load that might affect the product at many levels:

- Quality *fluctuation* as a result of the dependence on the human element
- Lack in *understanding* the studied phenomenon; because of the lack of information about it which is usually collected through some measurement experiments. Once the measurement being automated, a lot of experiments can be carried out and enough information can be collected about the phenomenon of study
- Processing of information is usually performed in a *black-box system* with no clarity about the process

It is fortunate that the current advancement in computer science and technology, on the hardware and software levels, allow addressing these problems in a different way. Computer vision, for instance, allows the digitization of the physical objects and aims at understanding the digital model with a high level of intelligence. This level of intelligence can be achieved through the soft-computing algorithms which are based on the accumulation of different branches of science such as physiology, sociology, philosophy, mathematics…, etc. The work introduced in this thesis aimed at utilizing these tools in solving some of the current problems in fibrous materials at different levels; where yarns, fabrics at production, and fabrics at the end use were investigated.

Highlights of the work introduced in this study are summarized below:

- For the study of the yarn internal structure and geometry, the Chan-Vese (CV) model was utilized to detect the actual contours of both the yarn and its constituent fibers. The detected yarn contour allows the use of the actual yarn cross-sectional shape which differs from the approximated circular contours that are considered in the conventional methods for calculating the yarn packing density. By considering the actual yarn contour (rather than its circular approximation), the measured packing density using the introduced method is expected to be faster and more reproducible than the traditional methods of calculating the packing density. The method we suggested in this work is the first in literature to implement an active contour method (such as Chan-Vese) for studying the yarn internal structure and it significantly reduces the time for measuring the yarn packing density compared to the traditional methods of measurement. Also, the introduced method is not limited to studying the yarns but it can be extended to segment different fibrous structures and calculate their porosity and packing density.

- Our DiaLib® method introduced in this work is a new and simple method that is computationally inexpensive and can handle massive amount of images within a reasonable time. The data obtained from the applied algorithm were found to be significantly comparable to the commercial available instruments such as Uster evenness tester. The developed analysis was capable of detecting the short term, the long term, and the periodic variations of yarn diameter. To the best of our knowledge, this work is the first to process the images of continuous long length of yarns to allow its time-series treatment. The developed data-treatment algorithm is also powerful enough to handle data collected from the image analysis method or to handle the raw data that might be obtained from the commercial measuring instruments and standardize the results with a transparent explanation.
- Our introduced machine prototype for detecting and classifying the fabric faults was associated with computer vision algorithms at a high level of imitating the visual inspection of the human operators. The machine is capable of running at suitable speeds and the system was trained on identifying a relatively high number of fabric faults categories. A direct and hierarchical classification approaches were considered where the hierarchical approach aimed at reducing the processing time. Results introduced in this study are promising and may allow the application of the introduced techniques in real time fabric inspection systems because of the high successful classification rate and the relatively short processing time.
- The implementation of the principal component analysis (PCA) allows the dimensionality reduction of the input feature dataset without sacrificing the amount of information in the original dataset which enhanced the processing time. In this work on fabric fault detection, we considered a large set of features that composes of statistical as well as spectral features (using FFT). The performance of the network that was implemented after the application of the PCA surpasses the performance of the other network in all aspect of characterization.
- In our work on the objective fabric pilling evaluation, a comprehensive review of the available literature methods was done, for the first time, with a categorization of the published work. The literature survey showed some shortcomings of the current research in the field which led to the introduction of our two papers on fabric pilling. Our purpose was to introduce an integrated system that utilizes the best practices in the four main stages of the evaluation process and our suggested system was able to implement fast and efficient techniques for pills segmentation and quantization. The system also introduces a new stochastic method for creating sampling dataset that is large enough to suite the training and testing processes required in building the applied artificial intelligent classifiers.
- Similarly, the work on the objective pilling evaluation in woven fabrics introduces for the first time the *image textural features* as measures for the fabric surface. Creating a feature dataset from the available Standard images with enough size for training the soft

computing algorithms is challenging due to the limited number of those Standard images. To deal with this issue, a new approach was suggested to mimic the noise that interferes with the fabric surface during its digitization. Hence, a user-friendly pilling evaluation system that integrates the processes of fabric surface digitization, pilling segmentation, quantization, and classification was implemented. The system was able to classify woven fabric samples according to their surface texture with a high degree of correlation to the traditional methods of pilling evaluation.

Finally, the algorithms presented in this work are heading in the direction of *improving*, *simplifying*, *automating*, and *reducing* the time required for the current evaluation methods. Nevertheless, this work can only be considered as few steps in that direction and the future is full of opportunities for further development.

APPENDICES

Appendix I

The author's list of publications

LIST OF PUBLICATIONS

1. Books:

- M. Eldessouki, *Synthesis and Modeling of Poly(L-lysine) Based Biomaterials*: LAP LAMBERT Academic Publishing, Germany, 2011, ISBN: 978-3846535455

2. Book Chapter:

- M. Eldessouki, "Nanomaterials and Textiles," in *Progress in Fibrous Material Science*, 1st ed., D. Kremenakova, J. Militky, and R. Mishra, Eds. Liberec, Czech Republic: Technical University of Liberec, 2014, pp. 57–80, ISBN: 978-8087269404, DOI: 10.13140/2.1.1687.3769

3. Refereed (ISI) Journals:

3.1. Published Papers:

- M. Eldessouki, S. Ibrahim, and R. Farag, "Dynamic Properties of Air-Jet Yarns Compared to Rotor-Spun Yarns," *(in press) the Textile Research Journal*, 2015, DOI: 10.1177/0040517514563726
- M. Eldessouki, S. Ibrahim, "Chan-Vese Segmentation Model For Faster And Accurate Evaluation of Yarn Packing Density," *(in press) Textile Research Journal*, 2015, DOI: 10.1177/0040517514557314
- M. Eldessouki and M. Hassan, "Adaptive Neuro-Fuzzy System For Quantitative Evaluation of Woven Fabrics' Pilling Resistance," *Expert Systems with Applications*, vol. 42, no. 4, pp. 2098-2113, 2014, DOI:10.1016/j.eswa.2014.10.013
- M. Eldessouki, M. Hassan, H. A. Bukhari, and K. Qashqari, "Integrated Computer Vision and Soft Computing System For Classifying The Pilling Resistance of Knitted Fabrics," *FIBERS & TEXTILES in Eastern Europe*, vol. 22, no. 6(108), pp. 106–112, 2014
- M. Eldessouki, S. Ibrahim, and J. Militky, "A Dynamic and Robust Image Processing Based Method for Measuring Yarn Diameter and Its Variation," *Textile Research Journal*, vol. 84, no. 18, pp.1948-1960, 2014, DOI: 10.1177/0040517514530032

- M. Eldessouki, M. Hassan, K. Qashqary, and E. Shady, "The Application of Principal Component Analysis to Boost The Performance of The Automated Fabric Fault Detector And Classifier," *FIBERS & TEXTILES in Eastern Europe*, vol. 22, no. 4(106), pp. 51–57, 2014
- H. Eldeeb, M. Mohy, T. Elbagoury, K. Aboseda, E. Shady, and M. Eldessouki, "An Automated Fabric Fault Detection and Classification System Based on Computer Vision and Soft Computing," *ACC JOURNAL*, vol. XIX, issue A, pp. 16-24, 2013
- M. Eldessouki, G. Buschle-Diller, and Y. Gowayed, "Poly(L-lysine) / microcrystalline cellulose biocomposites for porous scaffolds," *Polymer Composites*, pp. 1937-1944, 2011
- T. Turel, E. Shady, R. Farag, M. Eldessouki, Y. Gowayed, O. Burtovyy, and I. Luzinov, "A probabilistic model for the permeation of gases through microporous membranes," *Journal of the Textile Institute*, vol. 101, pp. 583-594, 2010

3.2. Pending Papers (submitted to journals)

- M. Eldessouki and Y. Gowayed, "Multi-scale Modeling of Lactide Monomer And Its Polymer With Experimental Verification," *Under review at the journal of Fibers and Polymers*
- M. Eldessouki, Y. Gowayed, and G. Buschle-Diller, "A Novel Solution-based Method for Preparing Branched Poly(L-Lactide) in Different Architectures with a Study of their Effects on the Rheological Properties," *Under review at the journal of Polymer International*

4. Papers Published in International Conference Proceedings:

- M. Eldessouki and S. Ibrahim, "The Internal Structure Of Air-Jet Yarns As Observed By Computed Tomography," in *the 4th International Conference of Applied Arts*, Damietta, Egypt, 2015.
- M. Eldessouki and S. Ibrahim, "Computed Tomography Application For investigating The Internal Structure Of Air-Jet Yarns," in *the 20th International Conference: Structure and Structural Mechanics of Textiles*, Liberec, Czech Republic, 2014.
- M. Eldessouki, E. Shady, and Y. Gowayed, "Effect of Functionalized Carbon Nanotubes Proportions on Mechanical Properties of Epoxy Nanocomposites," in the *8th Aachen-Dresden International Textile Conference*, Dresden, Germany, 2014

- M. Eldessouki, Y. Gowayed, and O. Acevedo, "Ab-Initio and Density Functional Theory Simulation For Lactide Monomer," in *the 6th International Conference, NanoCon 2014*, Brno, Czech Republic, 2014.
- M. Eldessouki and M. Hassan, "A Computer Vision With Soft-Computing Classifier As Integrated System For Fabric Pilling Quantitative Analysis," presented at *the 14th AUTEX World Textile Conference*, Bursa, Turkey, 2014
- M. Eldessouki, S. Ibrahim, and B. Neckář, "A Method For More Accurate Evaluation Of Yarn Packing Density," presented at *the 14th AUTEX World Textile Conference*, Bursa, Turkey, 2014
- M. Eldessouki, G. Buschle-Diller, and Y. Gowayed, "A New Solution-Based Method to Synthesize Branched poly(L-lactide)," in *The Fiber Society, Fibers for Progress*, Liberec, Czech Republic, 2014
- M. Eldessouki, E. Shady, and Y. Gowayed, "Surface Activation of Carbon Nanotubes Generating a Chemical Interaction in Epoxy Nanocomposite," in *ICCN 2014: International Conference on Composites and Nanoengineering*, Paris, France, 2014
- M. Eldessouki, S. Ibrahim, and R. Farag, "Mechanical Properties of Air-Jet Yarns Spun on Different Systems," presented at *the 2014 Beltwide Cotton Conferences*, New Orleans, LA, USA, 2014
- M. Eldessouki, S. Ibrahim, and J. Militky, "Video Processing for Dynamic Evaluation of Yarn Diameter," presented at *the 2014 Beltwide Cotton Conferences*, New Orleans, LA, USA, 2014
- S. Ibrahim, M. Eldessouki, J. Militky, and D. Kremenakova, "Analysis of Air jet yarn diameter," in *12th Asian Textile Conference*, Shanghai, China, 2013
- M. Eldessouki, S. Ibrahim, and J. Militky, "A Robust Image Processing Algorithm for Measuring Yarn Diameter," in *8th International Conference Textile Science*, Liberec, Czech Republic, 2013
- S. Ibrahim, M. Eldessouki, J. Militky, D. Kremenakova, and E. Moučková, "Comparative Study of Yarn Diameter Measured by Means of a High Speed Camera, Uster Evenness Tester, CTT, and QQM," in *8th International Conference Textile Science*, Liberec, Czech Republic, 2013
- H. Eldeeb, M. Mohy, T. Elbagoury, K. Aboseda, E. Shady, and M. Eldessouki, "An Automated Fabric Fault Detection and Classification System Based on Computer Vision and Soft Computing " in *8th International Conference Textile Science*, Liberec, Czech Republic, 2013
- M. Eldessouki, G. Buschle-Diller, and Y. Gowayed, "Polypeptide/cellulose biocomposite for tissue engineering," in *The 241st ACS National Meeting & Exposition*, Anaheim, CA - USA, 2011

- M. Eldessouki, Y. Gowayed, and G. Buschle-Diller, "Biodegradable Interpenetrating Network Structures," in *the 239th ACS National Meeting & Exposition*, San Francisco, CA - USA, 2010
- T. Turel, Y. Gowayed, M. Eldessouki, E. Shady, G. Buschle-Diller, I. Luzinov, and O. Burtovyy, "Modeling of Gas Permeability Through Microporous Membranes," in *the 17th Annual National Textiles Center Forum*, Hilton Head, SC - USA, 2009
- M. Eldessouki, Y. Gowayed, and G. Buschle-Diller, "Effect of Secondary Structure of Polypeptides on Properties of Their Nanocomposites," in *the 237th ACS National Meeting & Exposition*, Salt Lake City, UT - USA, 2009
- T. Turel, E. Shady, M. Eldessouki, G. Buschle-Diller, Y. Gowayed, A. Karaaslan, R. Farag, P. Livant, I. Luzinov, and O. Burtovyy, "Surface Modification of PET Microporous Membranes for Toxins Blocking," in *the 16th Annual National Textiles Center Forum*, Greenville, SC - USA, 2008 (the *Director's Award*)
- T. Turel, Y. Gowayed, M. Eldessouki, E. Shady, G. Buschle-Diller, I. Luzinov, and O. Burtovyy, "Gas Transmission Rate Through Microporous Membranes," in *the Fiber Society Annual Meeting and Technical Conference*, Davis, CA - USA, 2007
- T. Turel, E. Shady, Y. Gowayed, G. Buschle-Diller, A. Karaaslan, I. Luzinov, M. Eldessouki, O. Burtovyy, and R. Farag, "Efficient Biological-Chemical Protective Materials," in *the 15th Annual National Textiles Center Forum*, Hilton Head, SC - USA, 2007
- M. Hassan and M. Eldessouki, "Image Analysis Method for Pilling Evaluation," *the 2nd International Material Conference TEXCO*, Ružomberok, Slovak Republic, 2006
- R. A. El-Bealy, F. F. El-Habiby, and M. Eldessouki, "Adopting a Model to Investigate Yarn Evenness and Imperfections Through Raw Material Qualities," *the 5th International Engineering Conference*, Sharm ElSheikh, Egypt, 2006

5. Invited Speaker:

- M. Eldessouki, "A Glance at The Applications of Nanotechnology in Textiles," *The Arab Forum 2011 entitled "Industrial Applications of Nanotechnolgy",* Hilton Dream - Dreamland, 6th of October City – Egypt, 27-29th December 2011